Comparative analysis of interactions of the RASSF family mediated by the Ras-association (RA) and SARAH domains

Jia Jia Chan

A thesis submitted to University College London (UCL) for the degree of Doctor of Philosophy

2014

University College London

Institute of Structural and Molecular Biology

Gower Street

London, WC1E 6BT

I, Jia Jia Chan confirm that the work presented in this thesis is my own. Where information has been derived from other sources, I confirm that this has been indicated in the thesis.

Abstract

Members of the RASSF family (RASSF1-10) have been identified as candidate tumour suppressors that are frequently downregulated by promoter hypermethylation in cancers. These adaptor proteins carry a common Ras-association (RA) and SARAH domain (RASSF1-6) that can potentially bind Ras oncoproteins and mediate protein-protein interactions with other SARAH domain proteins (e.g. MST kinase). However, there is a notable lack of comparative characterisation of the RASSF family, as well as of molecular and structural information that facilitate their tumour suppressive functions.

As part of our comparative analysis, we modelled the RA and SARAH domains of the RASSF members based on existing structures and predicted their potential interactions and the key residues involved. These *in silico* predictions were compared to *in vitro* studies and intracellular binding assays using Förster Resonance Energy Transfer (FRET). Several SARAH domain mutants were also investigated for their effects on RASSF interactions. Furthermore, we compared the interactions of the RASSF family with several key proteins involved in death and NFκB signalling.

Our biochemical data show a diversity of interactions within the RASSF family RA domain, whereas interactions between RASSF and MST correlate with the presence of the SARAH domain, which is supported by the FRET experiments. Mutations of specific non-polar residues in the dimerisation interface of the SARAH domain also prove detrimental to the interaction between selected RASSF members and MST. Moreover, we observed stimulation-dependent interactions between specific RASSF members and MOAP1, TNF-R1, DAPK and TBK1. These results suggest that different members, despite shared general architecture, may have distinct binding properties, but ultimately could share overlapping functions. Current data also support an interaction model where RASSF serves as an adaptor for the assembly of multiple protein complexes and further functional interactions, involving MST kinases and other interacting partners, which could be regulated by Ras.

Table of Contents

List of Figures and Tables

Chapter 1

Chapter 2

Chapter 3

Chapter 4

Chapter 5

Chapter 6

Chapter 7

Abbreviations

AJ	adhesion junction
Akt/PBK	protein kinase B
ALL	acute lymphoblastic leukaemia
ASA	solvent accessible surface area
ASPP	apoptosis stimulating protein of p53
ATM	ataxia telangiectasia mutated
Bax	Bcl-2-associated X protein
BH3	Bcl-2 homology domain 3
BRCA1	breast cancer 1, early onset
BSA	bovine serum albumin
C1	protein kinase C conserved region 1
CaM	calmodulin
cAMP	cyclic adenosine monophosphate
CC	coiled-coil
CDK	cyclin dependent kinase
CXCR4	C-X-C chemokine receptor type 4
DAPK	death-associated protein kinase
DMEM	Dulbecco's Modified Eagle's Medium
DMSO	dimethyl sulphoxide
DNA	deoxyribonucleic acid
dNTP	deoxyribonucleotide triphosphate
DTT	dithiothreitol
ECL	enhanced chemiluminescence
EDTA	ethylenediamine tetra-acetic acid
FADD	Fas-associated protein with death domain
FBS	foetal bovine serum
FL	full length
FLIM	fluorescence lifetime imaging microscopy
FRET	Förster Resonance Energy Transfer
GAP	GTPase activating protein
GAPDH	glyceraldehyde 3-phosphate dehydrogenase
GDI	guanine nucleotide dissociation inhibitor

GDP	guanosine diphosphate
GEF	guanine nucleotide exchange factor
GFP	green fluorescent protein
GST	glutathione S-transferase
GTP	guanosine triphosphate
HCC	hepatocellular carcinoma
HIPK1	homeodomain-interacting protein kinase 1
Hpo	Hippo
IFN	interferon
IKK	IκB kinase
IP	immunoprecipitation
IPTG	isopropyl 1-thio-β-D-galactopyranoside
ITC	isothermal titration calorimetry
JNK	c-Jun N-terminal kinase
K_D	dissociation constant
LB	lysogeny broth
Lck	lymphocyte-specific protein tyrosine kinase
LFA-1	lymphocyte function-associated antigen 1
LPS	lipopolysaccharide
MKK7	dual specificity mitogen-activated protein kinase kinase 7
MMTV	mouse mammary tumour virus
MOAP1	modulator of apoptosis 1
MS	mass spectrometry
MST	mammalian sterile 20-like kinase
MTOC	microtubule organising centre
NDR	nuclear dbf2-related
NES	nuclear export sequence
NFκB	nuclear factor kappa-light-chain-enhancer of activated B cells
NLS	nuclear localisation sequence
NMR	nuclear magnetic resonance
NSCLC	non-small-cell lung carcinoma
PAGE	polyacrylamide gel electrophoresis
PBS	phosphate buffered saline
PCR	polymerase chain reaction

PEI	polyethylenimine
PH	pleckstrin homology
PI3K	phosphoinositide 3-kinase
PKA	protein kinase A
PLC	phospholipase C
PP2A	protein phosphatase 2
PVDF	polyvinylidene difluoride
RA	Ras association
RalGDS	Ral guanine nucleotide dissociation stimulator
RASSF	Ras-association domain family
RBD	Ras binding domain
rms	root mean square
RNA	ribonucleic acid
RNAi	RNA interference
rpm	revolutions per minute
SARAH	Sav/Rassf/Hippo
Sav	Salvador
SDS	sodium dodecyl sulphate
SH2	Src homology 2
siRNA	small interfering RNA
SKAP1	Src kinase-associated phosphoprotein 1
SNP	single nucleotide polymorphism
SUMO	small ubiquitin-like modifier
TBK1	TANK-binding kinase 1
TBS	tris buffered saline
TCEP	tris(2-carboxyethyl)phosphine
TEV	Tobacco Etch Virus
TLR	toll-like receptor
TNF-R1	tumour necrosis factor receptor 1
TNFα	tumour necrosis factor α
TRADD	TNF-R1-associated death domain
TRAIL	TNF-related apoptosis-inducing ligand
TSG	tumour suppressor gene
WT	wild-type

1 Introduction

The topic of this thesis is the molecular and structural basis for the interactions of the Ras-association domain (RASSF) family members with their various binding partners. This introduction will first provide an overview of the RASSF family, their structural features and main interactions. This will be followed by a brief description of the main features of the signalling pathways in which the RASSF family are involved through their main interacting partners. The functions of the RASSF family in these signalling networks and their roles in diseases will also be discussed in more detail for each RASSF member. Finally, the aims of the project will be introduced.

1.1. The Ras-association domain (RASSF) family

1.1.1. Overview of the RASSF family

The RASSF family consists of 10 members, known as RASSF1 to RASSF10. Studies have revealed that at least eight of the RASSF members are downregulated by promoter hypermethylation in various types of cancer (Table 1.1). This epigenetic silencing is often linked to advanced or aggressive tumours, poor prognosis, disease progression and survival (Lee et al., 2010, Pfeifer and Dammann, 2005, Wen et al., 2011).

For the last decade since its identification, the RASSF family has been extensively studied. The RASSF proteins carry several characteristic domains and function as adaptor proteins in many important biological processes. Initial studies elucidated their interactions with various Ras GTPases and the MST kinases, as well as their tumour suppressor roles in apoptosis, the Hippo pathway, cell cycle and cytoskeleton regulation. Two of the main hallmarks of cancer are evasion of apoptosis and insensitivity to anti-growth signals during the cell cycle (Hanahan and Weinberg, 2000). Collectively, these mark the RASSF family as potential tumour suppressors and tumour diagnostic and prognostic markers, which have been comprehensively summarised in previous reviews (Richter et al., 2009, van der Weyden and Adams, 2007).

Since then, there has been increasing evidence of various RASSF members having more diverse functions than just tumour suppression (Del Re et al., 2010, Oceandy et al., 2009). A role in emerging pathways including the NFκB and

Table 1.1 Overview of the RASSF family

Gene	Chromosome location	Splice variants (described in literature)		Expression	Changes in expression in cancer	References
RASSF1	3p21.3 Loss of heterozygosity reported	Promoter 1:	**Rassf1A** Rassf1D Rassf1E Rassf1F Rassf1G	Ubiquitously Specifically in cardiac cells Specifically in pancreatic cells	Epigenetically silenced in at least 37 tumour types: bladder, brain, breast, cervical, colon, oesophageal, gastric, head and neck, hepatocellular (HCC), Hodgkin's lymphoma, kidney, lung, melanoma, nasopharyngeal, osteosarcoma, ovarian, pancreatic, prostate, childhood tumours	van der Weyden and Adams (2007)
		Promoter 2:	Rassf1B **Rassf1C**	Predominantly in haematopoietic cells Ubiquitously	Upregulated in pancreatic, breast cancer cell lines	Malpeli et al. (2011), Reeves et al. (2010)
RASSF2	20p13	Predicted:	**Rassf2A** Rassf2B, C	Widely expressed in most tissues, high levels in brain, peripheral blood, placenta, lung	Epigenetically silenced in various cancers: breast, colorectal, lung NSCLC, gastric, nasopharyngeal, HCC, thyroid, prostate, squamous cervical cancer	Calvisi et al. (2012), Guerrero-Setas et al. (2013), Liu et al. (2013), Richter et al. (2009), Schagdarsurengin et al. (2010)
RASSF3	12q14.1	Predicted:	**Rassf3A** Rassf3B, C	Widely expressed in all normal tissues	Epigenetically silenced in somatotroph adenomas	Peng et al. (2013), Tommasi et al. (2002)
RASSF4	10q11.21	Predicted:	**Rassf4A** Rassf4B-F	Widely expressed in most normal tissues (heart, brain, placenta, lung, liver, skeletal muscle, pancreas)	Epigenetically silenced in nasopharyngeal carcinoma, breast, lung, colorectal, kidney tumour cell lines	Chow et al. (2004), Eckfeld et al. (2004)

RASSF5	1q32.1	Promoter 1:	**Rassf5A** Rassf5B Rassf5D	Widely expressed in normal tissues	Epigenetically silenced in lung NSCLC, breast, kidney primary tumours, HCC, leukaemia, melanoma, neuroblastoma cell lines	Calvisi et al. (2009), Djos et al. (2012), Lee et al. (2010), Macheiner et al. (2006), (2009), van der Weyden and Adams (2007)
		Promoter 2:	**Rassf5C**	Widely expressed in normal tissues	Epigenetically silenced in colorectal carcinoma, HCC	
RASSF6	4q13.3	Predicted:	**Rassf6A** Rassf6B Rassf6C	Varying levels of expression in colon, thymus, kidney, small intestine, placenta, lung	Gene deletion and epigenetic silencing in 30-60% of breast, colon, kidney, liver, rectum, pancreas, stomach and thyroid primary tumours, many childhood leukaemias, neuroblastoma	Allen et al. (2007), Djos et al. (2012), Hesson et al. (2009)
RASSF7	11p15.5	Predicted:	**Rassf7A** Rassf7B, C	Varying levels of expression in normal tissues, high levels in lung and brain	Epigenetically silenced in neuroblastoma Upregulated in pancreatic ductal adecnocarcinoma, islet cell tumours, endometrial cancers due to hypoxia	Djos et al. (2012), Recino et al. (2010), Sherwood et al. (2008)
RASSF8	12p12.3	Predicted:	Rassf8A **Rassf8B** Rassf8C-G	Widely expressed in normal tissues	Downregulated in lung adenocarcinomas Epigenetically silenced in small subset of leukaemias	Falvella et al. (2006), Hesson et al. (2009)
RASSF9	12q21.31	No known splice variants		Testis, kidney, skeletal muscle, liver, lung, brain, heart, pituitary gland, adrenal gland, ovary	Not reported	Chen et al. (1998)
RASSF10	11p15.2	No known splice variants		Bone marrow, precursors of peripheral nervous system and sensory organs, salivary gland, testes, kidney, lung, brain	Epigenetically silenced in many childhood leukaemias, astrocytomas, primary glioblastomas, lung, head and neck, sarcoma, pancreatic, prostate, thyroid cancers, melanoma	Dansranjavin et al. (2012), Hesson et al. (2009), Hill et al. (2011), Richter et al. (2009), Schagdarsurengin et al. (2009)

Wnt signalling pathways, has been reported (Del Re et al., 2010, Lock et al., 2010, Song et al., 2012, Wei et al., 2013).

1.1.2. The RASSF structural features and main interactions

The ten members of the RASSF family are divided into the classical RASSF (RASSF1-6) and the new N-terminal RASSF (RASSF7-10) subgroups. They each have many splice variants and isoforms. Those that have been studied and shown to exhibit biological functions are illustrated in Figure 1.1.

All ten members share a common feature in the form of the Ras-association (RA) domain. This is located at the C-terminal region of the classical RASSF1-6 and the N-terminus of the N-terminal RASSF7-10. The presence of the RA domain implies potential Ras binding. Direct interactions with various Ras GTPases have been demonstrated for most classical RASSF members and RASSF7 of the N-terminal subgroup (Table 1.2). However, some of these reports appear to contradict each other in terms of the specificity of interaction and whether the interactions were direct or mediated by a third binding partner.

RASSF1A and RASSF5A also share the protein kinase C conserved region 1 (C1) domain at their N-terminal region. The C1 domain is essential for the association of RASSF1A with the TNF-R1/MOAP1 and TRAIL/MOAP1 complex (Foley et al., 2008). Additionally, following the C1 domain, RASSF1A carries an ATM domain, which is a putative ATM kinase phosphorylation motif. ATM kinase is known to regulate cell cycle checkpoints leading to DNA repair and apoptosis, thus implicating RASSF1A in the DNA damage and repair pathway, which was reviewed recently (Scrace and O'Neill, 2012).

Finally, the classical RASSF1-6 share an additional common feature known as the Sav/Rassf/Hippo (SARAH) domain. This is located at their C-terminus and is known to facilitate homotypic and heterotypic protein-protein interactions. All six classical RASSF members have been shown to heterodimerise with MST1 and MST2, whilst RASSF1 and RASSF5 can also form homodimers (Table 1.3). Furthermore, a motif within the SARAH domain is known to mediate the interaction between RASSF1A and MOAP1 from the death pathway (Baksh et al., 2005, Foley et al., 2008). Recent studies

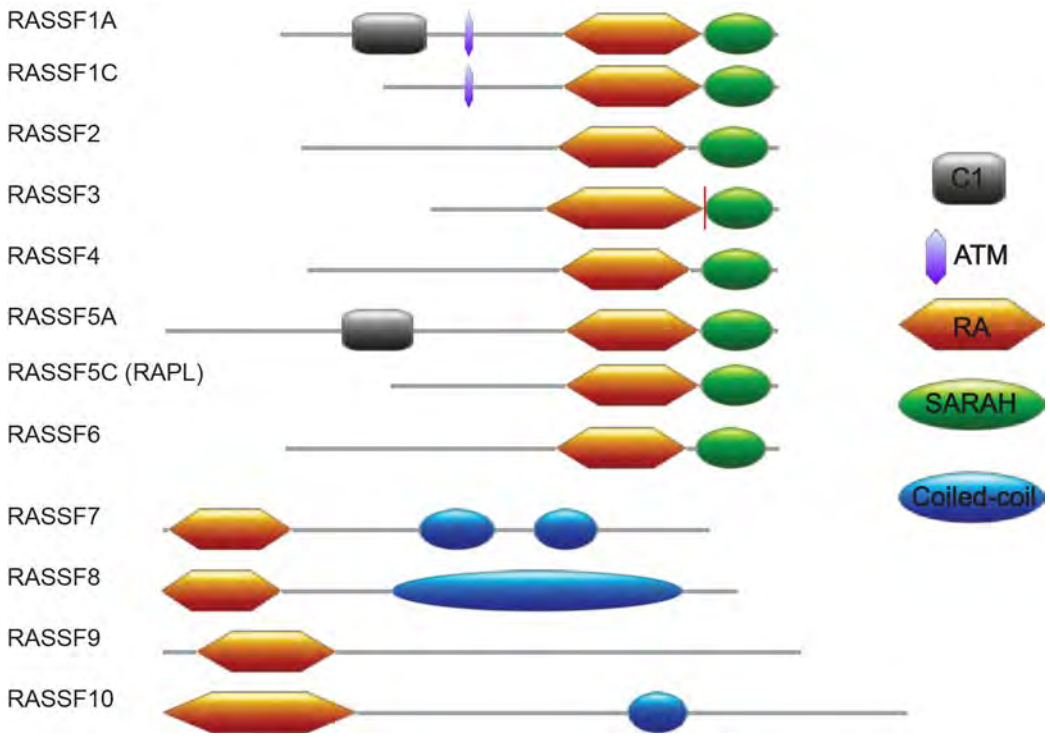

Figure 1.1 Schematic representations of the RASSF family members

One biologically relevant isoform is shown for each RASSF member, with two for RASSF1 (RASSF1A and RASSF1C) and RASSF5 (RASSF5A and RASSF5C, also known as RAPL). Characteristic domains shown are the protein kinase C conserved region (C1, grey), ATM kinase phosphorylation site (purple), Ras-association (RA, orange), Sav/Rassf/Hippo (SARAH, green) and coiled-coil motif (blue). The red line between the RA and SARAH domain in RASSF3 indicates an overlapping residue.

Table 1.2 Summary of the known interactions between the RASSF proteins and Ras family GTPases

The types of interaction assays performed to identify RAS binding are also shown.

RASSF protein	Binding to RAS GTPases	Experimental method	Comments	Reference
RASSF1				
aa1-340 (full length)	NRas, KRas, MRas	Pull-down from cell lysates		Rodriguez-Viciana et al. (2004)
	Ran	2D liquid-chromatography-tandem mass spectrometry (MS), pull-down		Dallol et al. (2009)
	Rap1A	Pull-down		Verma et al. (2011)
aa133-291 (RA)	HRas	Guanine nucleotide dissociation inhibitor (GDI) assay		Stieglitz et al. (2008)
RASSF2				
aa1-326 (full length)	KRas, MRas, NRas, RRas, TC21	Pull-down from cell lysates		Rodriguez-Viciana et al. (2004)
Endogenous	KRas	Co-immunoprecipitation (Co-IP)		Clark et al. (2012)
aa176-264 (RA)	KRasV12	Pull-down		Vos et al. (2003a)
RASSF4				
aa1-321 (full length)	Rap1, Rap2, KRas, MRas, NRas, RRas	Pull-down from cell lysates		Rodriguez-Viciana et al. (2004)
aa174-262 (RA)	KRas, KRasV12	Pull-down		Eckfeld et al. (2004)
RASSF5A				
aa1-417 (full length)	Rap1, Rap2, KRas, MRas, NRas, RRas, TC21	Pull-down from cell lysates		Rodriguez-Viciana et al. (2004)

RASSF protein	Binding to RAS GTPases	Experimental method	Comments	Reference
RASSF5C (RAPL)				
aa1-265 (full length)	Rap1	Pull-down		Katagiri et al. (2003)
aa42-265 (RA + SARAH)	HRasV12, MRasV22, Rap2BV12	Pull-down, isothermal titration calorimetry (ITC)	Mutations K154L, K155L and D160L abolish Ras-binding	Miertzschke et al. (2007)
mNORE1 (mouse)				
aa200-358 (RA)		GDI assay	Protein crystallised	Stieglitz et al. (2008)
aa203-363 (RA)	WT Ras, Ras D30E/E31K, Rap1	Co-IP	Mouse RA also binds tubulin	Bee et al. (2010)
aa203-363Δloop	HRasV12	Co-IP		
aa95-358 (C1 + RA)	HRasV12	ITC	RA binds C1 domain	Harjes et al. (2006)
RASSF6				
aa1-337 (full length)	KRas, KRasV12	Pull-down from cell lysates	Disputed by Ikeda et al. (2007), no binding detected	Allen et al. (2007)
aa186-274 (RA)	KRas	Pull-down		
RASSF7				
aa1-373 (full length)	NRas, NRasV12	Co-IP		Takahashi et al. (2011)
RASSF9				
aa1-435 (full length)	KRas, MRas, NRas	Pull-down		Rodriguez-Viciana et al. (2004)

have also revealed RASSF3 and RASSF6 as MOAP1 binding partners, possibly mediated by the same motif, which will be further discussed in Chapter 6 (Allen et al., 2007, Ikeda et al., 2007, Kudo et al., 2012). These interactions underpin the general role of the RASSF family in pro-apoptosis regulation, with increasing evidence of their involvement in both the Hippo and death receptor apoptotic pathways (Fausti et al., 2012).

1.2. Signalling networks and pathways involving the RASSF family

1.2.1. Ras signalling

The first *RAS* genes were discovered 30 years ago as a result of studies on cancer-causing viruses and since then have been implicated in a diverse range of biological functions and the regulation of many intracellular signalling pathways ranging from cell survival and proliferation to apoptosis (Cox and Der, 2003, Malumbres and Barbacid, 2003). To date, more than 150 members of the Ras small GTPase superfamily have been identified and are sub-classified into five individual families: Ras, Rho, Rab, Ran and Arf (Wennerberg et al., 2005). We will focus on the most prominent Ras subfamily as it undergoes interaction with the RASSF family (see Table 1.2).

The canonical Ras signalling pathway is the Raf/Mek/Erk protein kinase cascade downstream of Ras that regulates growth and development (Figure 1.2A). Various Ras effectors have also been identified and several of them have been implicated in Ras-mediated oncogenesis (Figure 1.2B). Ras mediates cell survival primarily through PI3K pathways that elicit strong anti-apoptotic effects via Akt/PKB, which activates NFκB signalling downstream (Cox and Der, 2003, Downward, 2003). On the other hand, it promotes cell proliferation mainly via the Raf/Mek/Erk signalling cascade, which activates transcription factors to upregulate key cell cycle regulatory proteins, thus promoting cell cycle progression (Downward, 2003). Interestingly, Ras can also both inhibit and promote apoptosis through the Raf/Mek/Erk pathway depending on the cellular homeostatic conditions (Figure 1.2B) (Cox and Der, 2003).

Table 1.3 Summary of the known interactions mediated by the SARAH domain of the RASSF proteins

The types of interaction assays performed to identify protein-protein interaction are also shown.

RASSF protein	Binding to other proteins	Experimental method	Comments	Reference
RASSF1A				
aa1-340 (full length/endogenous)	MST1, MST2	IP from KB cells, two-hybrid screen, 2D liquid-chromatography-tandem MS	Inhibits MST1 autoactivation through phosphorylation	Praskova et al. (2004) Khokhlatchev et al. (2002)
	RASSF5	Co-IP	Also forms homodimers	Ortiz-Vega et al. (2002)
aa1-320 (truncated SARAH)	MOAP1	Co-IP		Baksh et al. (2005)
RASSF1C				
aa220-270 (SARAH)	MST1	NMR titration, cross-linking		Hwang et al. (2007)
RASSF2				
aa1-326 (full length/endogenous)	MST1, MST2	Co-IP, MS, IP from KB cells, two-hybrid screen		Khokhlatchev et al. (2002) Schagdarsurengin et al. (2010)
	RASSF1, RASSF3, RASSF5	Co-IP, yeast two-hybrid		Hesson et al. (2005)
RASSF3				
aa1-238 (full length/endogenous)	MST1	Two-hybrid screen		Praskova et al. (2004)
	MST, MST2	Co-IP		Kudo et al. (2012)
RASSF4				
aa1-321 (full length)	MST1	(data not shown)		Eckfeld et al. (2004)

RASSF protein	Binding to other SARAH domains	Experimental method	Comments	Reference
RASSF5A				
aa1-413	MST1, MST2	Two-hybrid screen		Khokhlatchev et al. (2002)
aa266-413 (SARAH)	MST1	NMR titration, chemical shift perturbation	Crystallised as a homodimer Ras-binding to RASSF5 enhances MST1 activity to promote apoptosis	Hwang et al. (2007), Makbul et al. (2013)
RASSF5C (RAPL)				
aa1-265	MST1 SKAP1	Two-hybrid screen, co-IP Co-IP	Forms homodimers and oligomers (Miertzschke et al., 2007)	Katagiri et al. (2006) Raab et al. (2010)
RASSF6				
aa1-337 (full length)	MST2	Two-hybrid screen, pull-down	RASSF6 and MST2 mutually inhibit each other	Ikeda et al. (2009)

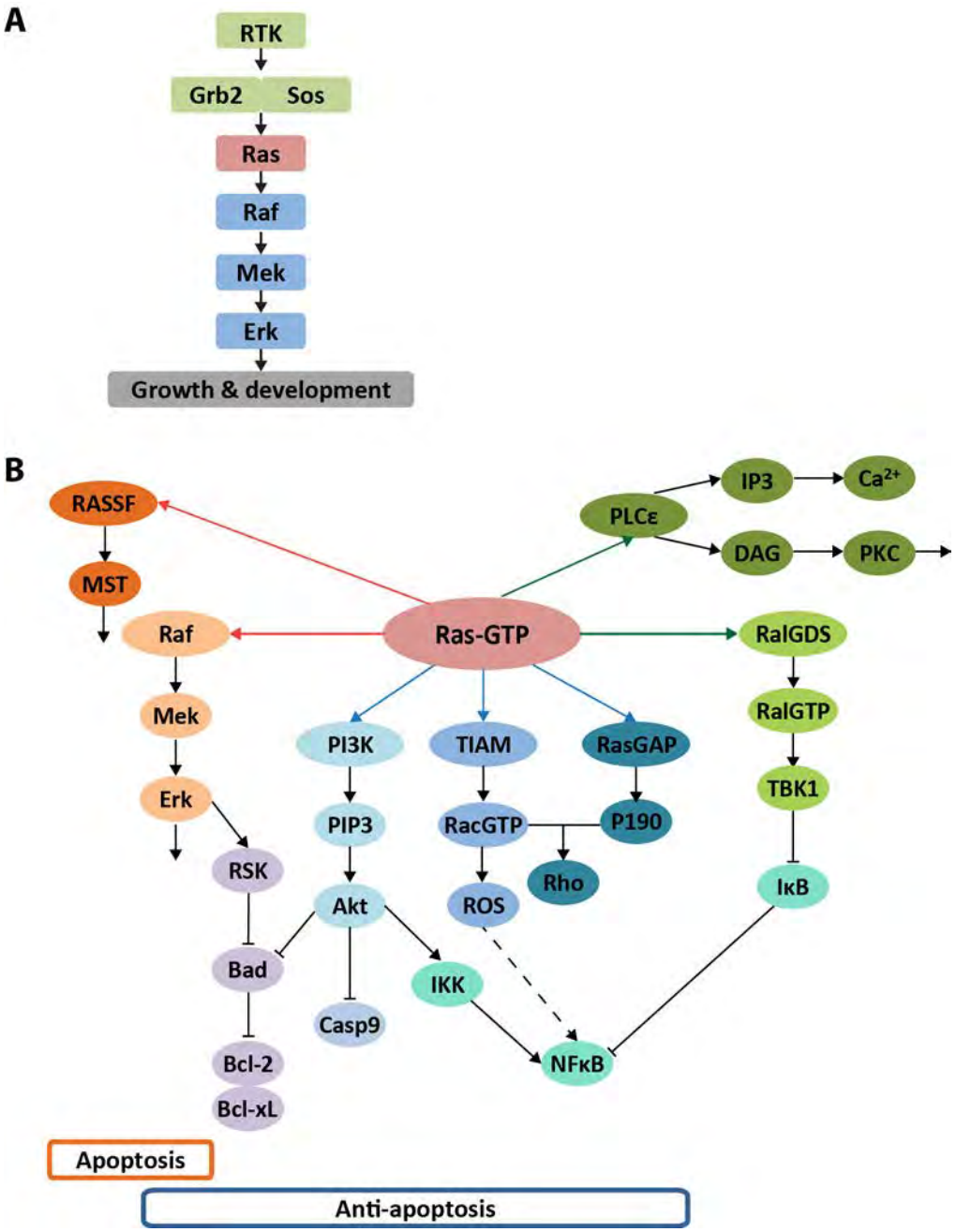

Figure 1.2 The Ras signalling network

(A) The canonical Ras signalling pathway through the Raf/Mek/Erk cascade.

(B) The Ras signalling network, adapted from Cox and Der (2003). Pro-apoptotic pathways are shown in orange, anti-apoptotic pathways in blue and pathways involved in other functions in green.

1.2.2. Hippo signalling

The Hippo signalling network was first elucidated in *Drosophila melanogaster* and plays an important role in controlling organ size in animals (Saucedo and Edgar, 2007). Recent studies have shown that many components and some regulatory aspects of this network are evolutionarily conserved in mammals and deregulation of the various pathways involved is linked to cancer (Table 1.4) (Harvey et al., 2013, Matallanas et al., 2008, Ribeiro et al., 2010). One major component is the mammalian sterile 20-like (MST) kinases, which are known to interact with several RASSF members (see Table 1.3), thus implicating the RASSF family in the regulation of Hippo signalling.

The Hippo signalling network consists of a core kinase cascade beginning with the activation of MST1/2 by various apoptotic and stress stimuli. The mechanisms of activation include caspase 3 cleavage, autophosophorylation and interaction with other proteins, such as WW45 and RASSF (Avruch et al., 2012). Activated MST then phosphorylates its substrates, such as WW45, LATS1/2, NDR1/2, FOXO, H2B and the kinases in the JNK signalling cascade, the latter of which is essential in facilitating MST-mediated chromatin condensation during apoptosis (Matallanas et al., 2008). These phosphorylation events lead to a cascade of further phosphorylation, including that of YAP transcription coactivator, and finally apoptosis. Additionally, MST-activated AGC-family kinases NDR1/2 and LATS1/2 also contribute to cell cycle arrest at G1/S and G2/M phases by reducing the levels of cyclin E and cyclins A/B respectively (O'Neill et al., 2005, Radu and Chernoff, 2009). The multiple apoptotic signalling pathways mediated by activated MST are summarised in Figure 1.3.

1.2.3. Death receptor apoptosis signalling

The interactions between several RASSF members and MOAP1 have linked them to death receptor signalling (Baksh et al., 2005, Ikeda et al., 2007, Kudo et al., 2012, Vos et al., 2006). The extrinsic death signal is activated by the ligation of membrane bound death receptors (Fas, TNF-R1 and TRAIL-R) to their cytokine ligands (FasL, TNFα and TRAIL). This leads to the recruitment of adaptor molecules, such as FADD and TRADD, followed by pro-caspase 8 to form the Death Inducing Signalling Complex (DISC). Subsequently, caspase 8 is activated upon its dimerisation and directly cleaves and activates caspase 3 and caspase 7, leading to apoptosis. Alternatively, crosstalk between

Table 1.4 Hippo pathway components and their links to cancer

Compiled from Harvey et al. (2013), Saucedo and Edgar (2007)

***D. melanogaster* gene**	**Human orthologue**	**Oncogene or TSG***	**Implications in cancer**
hippo (hpo)	MST1/2	TSG	None
salvador (sav)	SAV1 (WW45)	TSG	Mutations in cell lines derived from kidney cancer
warts (wts)	LATS1	TSG	None
	LATS2		Deleted
mats	MOB1A/B	TSG	Mutations in cancer cell lines
yorkie (yki)	YAP	Oncogene	Amplified
	TAZ		None
scalloped (sd)	TEAD1-4	Oncogene	None
fat	FAT1	TSG	Mutations in ovary, head and neck
	FAT2	TSG	Mutations in colorectum
	FAT3	TSG	None
	FAT4	TSG	Mutations in rectum
merlin (mer)	NF2	TSG	Somatic mutations, heritable cancer syndrome, inactivated in tumours of nerve tissue

* TSG, tumour suppressor gene

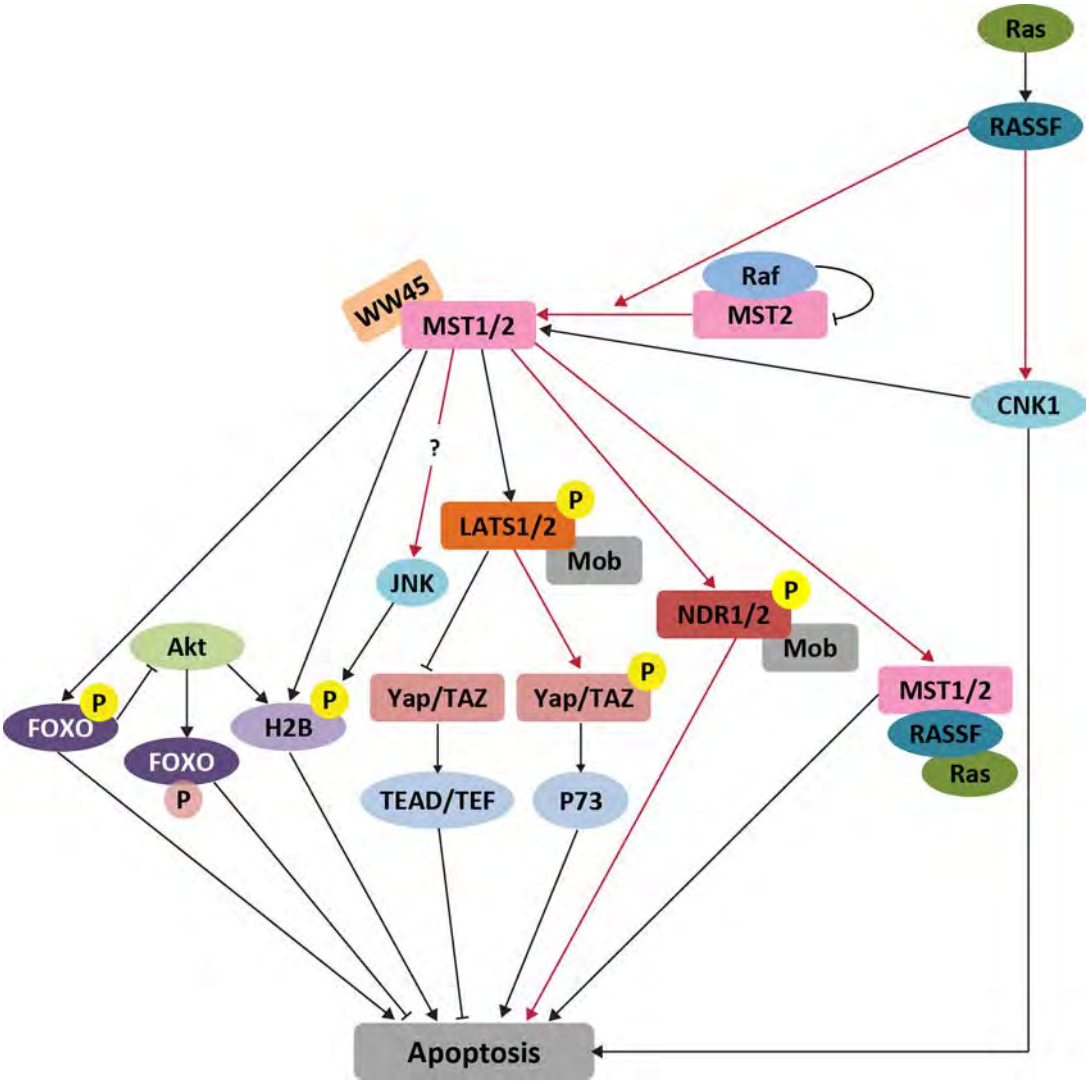

Figure 1.3 The Hippo signalling network in apoptosis

Multiple apoptotic signalling pathways are mediated by MST targets, adapted from Fausti et al. (2012), Radu and Chernoff (2009). The main Hippo pathway components are shown in rectangles and other components in ovals. Yellow and pink phosphates indicate activating and inhibitory phosphorylation respectively by MST. Red lines indicate RASSF-mediated activation.

intrinsic and extrinsic pathways through caspase 8 can activate executioner caspase 3 and caspase 7 via Bax and cytochrome c release from the mitochondria caused by mitochondrial outer membrane permeabilisation (MOMP) (Khosravi-Far and Esposti, 2004, Tait and Green, 2010). The latter is where RASSF and MOAP1 enter the picture. RASSF1A binds MOAP1/TNF-R1 to facilitate MOAP1 interaction with Bax, thus driving Bax activation and MOMP to cause apoptosis (Foley et al., 2008). This extrinsic signalling network and its crosstalk with the intrinsic pathway are summarised in Figure 1.4 and will be further discussed in Chapter 6.

1.2.4. NFκB signalling

The NFκB family consists of two structurally related subfamilies: the NFκB proteins (p100 and p105) and Rel proteins (RelA, RelB and RelC). All these proteins share a common DNA-binding domain known as the Rel homology domain (RHD) and are post-translationally modified (Perkins, 2007). NFκB is involved in cellular responses to a variety of stimuli and regulates physiological processes that include immune responses, apoptosis and inflammation. Deregulation of NFκB signalling has been associated with cancer, chronic inflammation, autoimmune diseases and viral infection (Courtois and Gilmore, 2006).

Under normal cellular conditions, the NFκB dimer, made up of the p50 and p65 subunits from NFκB p105 and RelA respectively, is present in its latent, inactive state and bound to inhibitory IκB proteins that mask its nuclear localisation sequence (NLS) and block DNA binding. In the presence of harmful stimuli, such as stress, cytokines and viral infections, the IκB kinase (IKK) complex, consisting of catalytic kinase subunits (IKKα and/or IKKβ) and a scaffold protein NFκB essential modulator (NEMO), is activated in the canonical pathway. This results in the phosphorylation-induced degradation of IκB, thus allowing active NFκB dimers to enter the nucleus and activate specific target genes. This general mechanism of activation is summarised in Figure 1.5. The regulation of NFκB signalling and its crosstalk with other signalling networks will be covered in greater detail in Chapter 6.

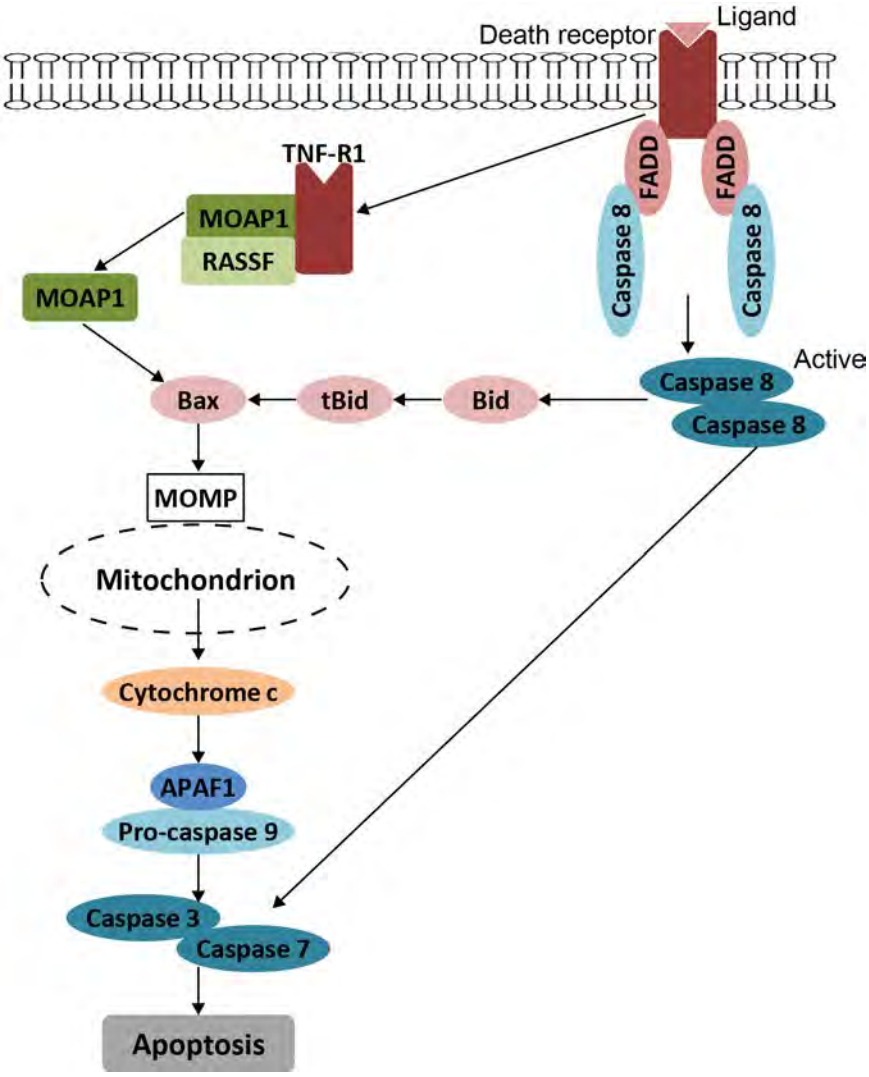

Figure 1.4 Death receptor signalling

RASSF is involved in a crosstalk between the intrinsic and extrinsic death pathway. The extrinsic pathway (right) is initiated by death receptor signalling, recruitment, dimerisation and activation of FADD and caspase 8, leading to the activation of caspase 3 and caspase 7. The crosstalk with the intrinsic pathway (left) occurs through caspase 8 or the RASSF/MOAP1/TNF-R1 complex following internalisation of TNF-R1 to cause mitochondrial outer membrane permeabilisation (MOMP) and apoptosis. Adapted from Tait and Green (2010).

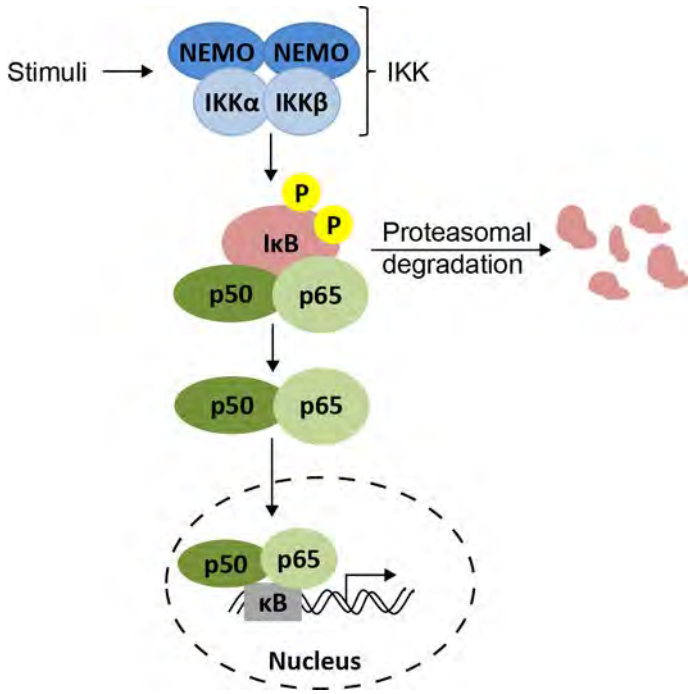

Figure 1.5 NFκB signalling

The canonical NFκB signalling pathway, adapted from Gilmore (2006). Harmful stimuli activate the IκB kinase (IKK) complex, leading to the phosphorylation and proteasomal degradation of the inhibitory IκB. This releases the active NFκB p50/p65 dimer, which enters the nucleus and activates specific target genes.

1.2.5. Wnt signalling

Wnt signalling is involved in various biological functions, mainly axis patterning, cell proliferation, differentiation, migration and stem cell control (Amin and Vincan, 2012, Nusse, 2008). Mutations of pathway components and abnormal signalling within the Wnt signalling network have been implicated in some diseases, most notably cancer (Clevers and Nusse, 2012).

There are three different Wnt signalling pathways: the canonical Wnt pathway and two non-canonical planar polarity and Wnt/calcium pathways (Moon et al., 2004). The canonical pathway is best-characterised and also the most functionally relevant with regards to the RASSF family. In the absence of Wnt ligands, β-catenin is recruited into the cytoplasmic "destruction complex" consisting of adenomatous polyposis coli (APC), AXIN, casein kinase 1 (CK1), glycogen synthase kinase 3 (GSK3) and ubiquitin ligase β-TrCP. AXIN facilitates β-catenin phosphorylation by CK1 then GSK3, targeting it for β-TrCP ubiquitination and proteosomal degradation (Figure 1.6A) (Clevers and Nusse, 2012). Recent studies have shown that the *AXIN* gene is mutated in several human cancers, which interferes with GSK3 binding and results in inappropriate activation and deregulation of the Wnt signalling pathways (Clevers, 2000, Lammi et al., 2004, Webster et al., 2000).

Wnt signalling is activated by the binding of WNT protein ligands to the receptors of the Frizzled (FZ) and LRP families on the cell surface. Upon activation, the complex associates with phosphorylated LRP to block the ubiquitination of β-catenin by β-TrCP. Newly synthesised β-catenin translocates to the nucleus where it binds to T-cell factor and lymphoid enhancer binding factor (TCF-LEF) family transcription factors to activate transcription of Wnt target genes (Figure 1.6B).

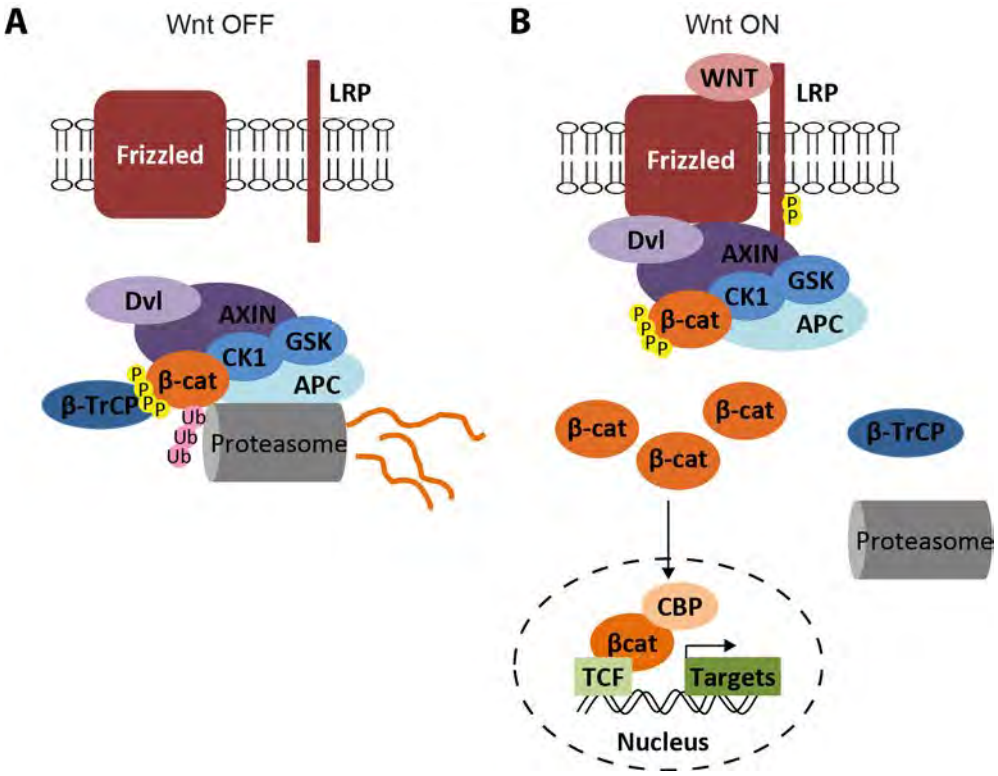

Figure 1.6 Wnt signalling

The canonical Wnt signalling pathway, adapted from Clevers and Nusse (2012).

(A) In the absence of WNT protein ligands, the signalling pathway is "off" as β-catenin is targeted for proteasomal degradation by the "destruction complex". The components of this complex are adenomatous polyposis coli (APC), AXIN, Dishevelled (Dvl), casein kinase 1 (CK1), glycogen synthase kinase 3 (GSK) and ubiquitin ligase β-TrCP.

(B) In the presence of WNT protein ligands, the pathway is "turned on". The "destruction complex" is recruited by the phosphorylated receptor LRP to block the degradation of β-catenin, which enters the nucleus to activate transcription of Wnt target genes via T-cell factor and lymphoid enhancer binding protein (TCF) and CREB-binding protein (CBP).

1.3. The functional characterisations of the RASSF family

1.3.1. RASSF1

1.3.1.1. RASSF1, a frequently downregulated tumour suppressor

RASSF1 is the first member of the RASSF family, identified using a yeast-two-hybrid screen via its interaction with XPA, a protein involved in DNA excision repair (Dammann et al., 2000). RASSF1 is also the most extensively studied member of the RASSF family in terms of its biological functions. It consists of at least seven different isoforms but there is evidence of biological functions for only RASSF1A and RASSF1C. These are expressed ubiquitously in normal tissues and cells but RASSF1A is often downregulated by promoter hypermethylation in various cancer cell lines and primary tumours (Table 1.1).

Previous studies have included *Rassf1a* knockout mouse models, overexpression of RASSF1A or silencing its expression using RNAi in cancer cell lines. The outcome of these studies are in agreement that the functions of RASSF1A include tumour growth inhibition through the promotion of different apoptotic pathways, microtubule stabilisation, subsequent regulation of the cell cycle and cell migration (Avruch et al., 2006, Dallol et al., 2005, Donninger et al., 2011, Guo et al., 2007, Matallanas et al., 2007, Oh et al., 2006, Praskova et al., 2004). The apoptotic pathways regulated by RASSF1 include KRas and death receptor-induced apoptosis, and the Hippo pathway through its SARAH domain-mediated interaction with MST1 and MST2, whilst it regulates the cell cycle at metaphase, G1, G2/M and prometaphase. RASSF1A is also involved in the DNA repair pathway and feedback loop activated by DNA damage, ATM kinase and p53 (Scrace and O'Neill, 2012). In addition, several polymorphisms have been found in RASSF1A. The polymorphism at codon 133 has been reported to disrupt its microtubule association and stabilisation domain, and is associated with tumour alterations and early onset of breast cancer in BRCA1/2 mutation carriers (Gao et al., 2008, Schagdarsurengin et al., 2005).

There have been fewer studies carried out on RASSF1C. It has been shown to interact with and stabilise microtubules, while inducing G2/M cell cycle arrest (Rong et al., 2004). Its overexpression also induces apoptosis, presumably by its translocation to microtubules upon stress and DNA damage, and its participation in the activation of

SAPK/JNK signalling pathway that regulates gene expression leading to apoptosis (Kitagawa et al., 2006).

1.3.1.2. Microtubule association, organisation and stabilisation

RASSF1A was recently shown to directly bind Ran GTPase via its RA domain and MST2 via its SARAH domain to control microtubule organisation and the integrity of the mitotic spindle (Dallol et al., 2009). MST2 cooperates with RASSF1A to increase Ran-GTP levels by phosphorylating RCC1, a Ran nucleotide guanine exchange factor (GEF), on S2 and S11, whilst RASSF1A regulates its localisation during interphase in mitotic cells. This pathway also includes a negative feedback loop in which Ran-GTP disrupts the RASSF1A/MST2 complex.

A different member of the large Ras GTPase family, Rap1A, is also involved in microtubule regulation by RASSF1A (Verma et al., 2011). Rap1A directly binds RASSF1A in a GTP-dependent manner and the complex is localised to the circular perinuclear network. Overexpression of either protein leads to the circularisation of microtubules around the nucleus and a loss of the microtubule organising centre (MTOC), whilst the complex induces bundling of the circularised microtubules around the nucleus. Consequently, this affects processes directly or indirectly dependent on microtubule organisation, such as vimentin retraction in perinuclear bundles, partial dispersal of the Golgi complex or complete fragmentation.

A recent study on the polymorphisms in RASSF1A has shed more light into its effects on microtubule association, which was first reported by Schagdarsurengin et al. (2005). The regions in RASSF1A required for microtubule association have been mapped to the ATM motif (^{131}SQAEI) and the SARAH domain (^{300}ELHNFL) (El-Kalla et al., 2010). The three polymorphisms found in RASSF1A include C65R, A133S and E264K, which are in the C1 domain, ATM motif and RA domain respectively. Each of these mutations exhibited distinctive defects in localisation, tubulin association and acetylation, resulting in microtubule instability and enhanced tumour formation in nude mice.

The SARAH domain of RASSF1A also plays a role in the MTOC stability as its deletion resulted in multipolar and monopolar spindles (Dittfeld et al., 2012). However,

it appears that this is not due to microtubule destabilisation and the mechanism behind the regulation of the MTOC in which the SARAH domain is involved is not known.

1.3.1.3. Regulation of the cell cycle

The role of RASSF1A in cell cycle regulation is well studied and often correlates with its ability to stabilise microtubules, which are a crucial component of the mitotic spindles. Dallol et al. (2009) showed the importance of MST2 in RASSF1A-mediated mitotic spindle stability as RNAi silencing of either RASSF1A or MST2 caused prometaphase delay during the cell cycle. Additionally, deletion of the SARAH domain leading to aberrant spindle formation resulted in unequal alignment of chromosomes between poles, abnormal mitoses and reduced mitotic rates (Dittfeld et al., 2012).

Earlier studies reported RASSF1A phosphorylation at S203 within the RA domain by mitotic kinase Aurora A during mitosis, interfering with RASSF1A association with microtubules and its ability to induce M phase cell cycle arrest (Rong et al., 2007). RASSF1A also interacts with CDC20 during early prometaphase to inhibit the formation of the APC/CDC20 complex, which is part of the ubiquitin-conjugation system that marks proteins for proteasomal degradation (Song et al., 2004). This inhibits APC activity and arrests the cell cycle. A more recent study illustrated a link between Aurora A, RASSF1A and the APC/CDC20 complex in cell cycle regulation whereby Aurora A inhibits the ability of RASSF1A to suppress the APC/CDC20 complex (Song et al., 2009). Aurora A phosphorylates RASSF1A at S203 at the spindle poles during early mitosis to induce its dissociation from CDC20. This leads to prometaphase progression after G2/M. Overexpression of Aurora A has also been shown to upregulate phosphorylation of RASSF1A, leading to tumourigenesis due to a lack of cell cycle arrest (Song et al., 2009). Despite these observations, the interaction between RASSF1A and CDC20 has been disputed by Liu et al. (2007).

RASSF1A was recently shown to regulate the Raf/Mek/Erk pathway to arrest the cell cycle in a p21-dependent manner (Thaler et al., 2009). It inhibits Akt signalling, leading to the upregulation of p21, a cyclin-dependent kinase (CDK) inhibitor, which reduces the level of cyclin A. This regulation is independent of p53 and results in the inhibition of S phase progression, thus an arrest at the G1 phase.

1.3.1.4. Regulation of apoptosis

Heterodimerisation between RASSF1A and the MST kinases, and its role in MST kinase-mediated apoptosis are well documented. The binding of RASSF1A to MST1 initially inhibits its kinase activity but recruitment of the complex to the membrane via Ras association with RASSF1A leads to its activation (Avruch et al., 2006, Oh et al., 2006, Praskova et al., 2004). Recently, RASSF1A was reported to prevent the dephosphorylation of MST1 and MST2 by phosphatase PP2A to keep the kinases in an active state to induce apoptosis (Guo et al., 2011). Interestingly, RASSF1A stabilises MST2 but has no effect on the level of MST1, thus implying that RASSF1A acts via MST2 for apoptosis, a concept that contradicts previous reports. This is also the first instance of a tumour suppressor protein acting as an inhibitor of the dephosphorylation pathway. Another study highlighted the importance of the SARAH domain and heterodimerisation in regulating apoptosis as deleting the SARAH domain led to aberrant apoptosis at a rate that is 39% higher than the wild-type (Dittfeld et al., 2012).

Previous studies have demonstrated the role of RASSF1A in the death receptor apoptotic pathway. It interacts with the TNF-R1/MOAP1 complex and its interaction with MOAP1 may be enhanced by the presence of KRas to induce Bax activation and cell death (Baksh et al., 2005, Foley et al., 2008, Vos et al., 2006). More recently, El-Kalla et al. (2010) showed that microtubule localisation of RASSF1A is crucial for RASSF1A-driven cell death. A lack of microtubule association by RASSF1A reduces RASSF1A-mediated cell death and PARP cleavage due to a slower rate of TNF-R1 internalisation. This was also observed for the polymorphism at codon C65 of RASSF1A, a mutation that inhibits microtubule localisation, thus is unable to prevent tumour growth in nude mice.

1.3.1.5. Regulation of the cardiac function

Traditionally, RASSF1A is known to be a major player in tumour suppression. However, it is now evident that it has a wider role as it is also involved in cardiac pathologies. Oceandy et al. (2009) first reported RASSF1A in the regulation of cardiac function and the mechanism involves the Ras/Raf/Erk pathway. RASSF1A was shown to interact with RASSF5 and indirectly form a complex with Ras. These interactions block the recruitment of Raf1 to active Ras, thus inhibiting the prohypertrophic Erk1/2 pathway in

the heart. RASSF1A expression was also reported to be lower in human heart failure patients. Taken together, this suggests a new role for RASSF1A in cardiac protection.

A second report demonstrated the importance of the RASSF1A/MST1 complex in the protection of cardiac fibroblasts against pressure overload (Del Re et al., 2010). Cardiac stress upregulates the expression of RASSF1A, which then interacts with and activates MST1. This series of events prevents proliferation and induces apoptosis via MST1 to suppress fibrosis following stress, thus improving cardiac function. RASSF1A, mediated by MST1, also inhibits the NFκB pathway as silencing RASSF1A resulted in the upregulation of TNFα and NFκB signalling, in turn causing hypertrophy through a paracrine mechanism and fibroblast proliferation. This was also observed when the RASSF1/MST1 complex was disrupted by a specific point mutation in the RASSF1 SARAH domain, thus demonstrating the importance of the synergistic properties of both proteins. These observations are in line with the first report and have added a new player in the form of MST1 in facilitating the RASSF1A function in cardiac protection.

RASSF1A plays a role in a diverse range of processes, including the regulation of apoptosis, genomic stability, microtubule organisation and the cell cycle. Now it is known that these functions are not limited to tumour suppression, but are also essential in cardiac function, thus RASSF1 may serve as a key adaptor to integrate various signalling pathways to control critical biological functions and provide a link between tumour development and heart failure (summarised in Figure 1.7).

1.3.1.6. RASSF1C, a potential oncogene

The role of RASSF1C is very ambiguous and reports concerning its functions have been contradictory as RASSF1C has been shown to exhibit both tumour suppressive as well as oncogenic properties (Richter et al., 2009). Recent reports include its upregulation in pancreatic endocrine tumours, primary epithelial cells and breast cancer cell lines (Malpeli et al., 2011, Reeves et al., 2010). Overexpression of RASSF1C downregulated pro-apoptotic genes, including Bax and caspase 3, whilst upregulating growth promoting genes, such as CXCR4 chemokine receptor. The combination of these effects led to an increase in cell proliferation and enhanced cell invasion, hence metastasis in breast cancer (Reeves et al., 2010).

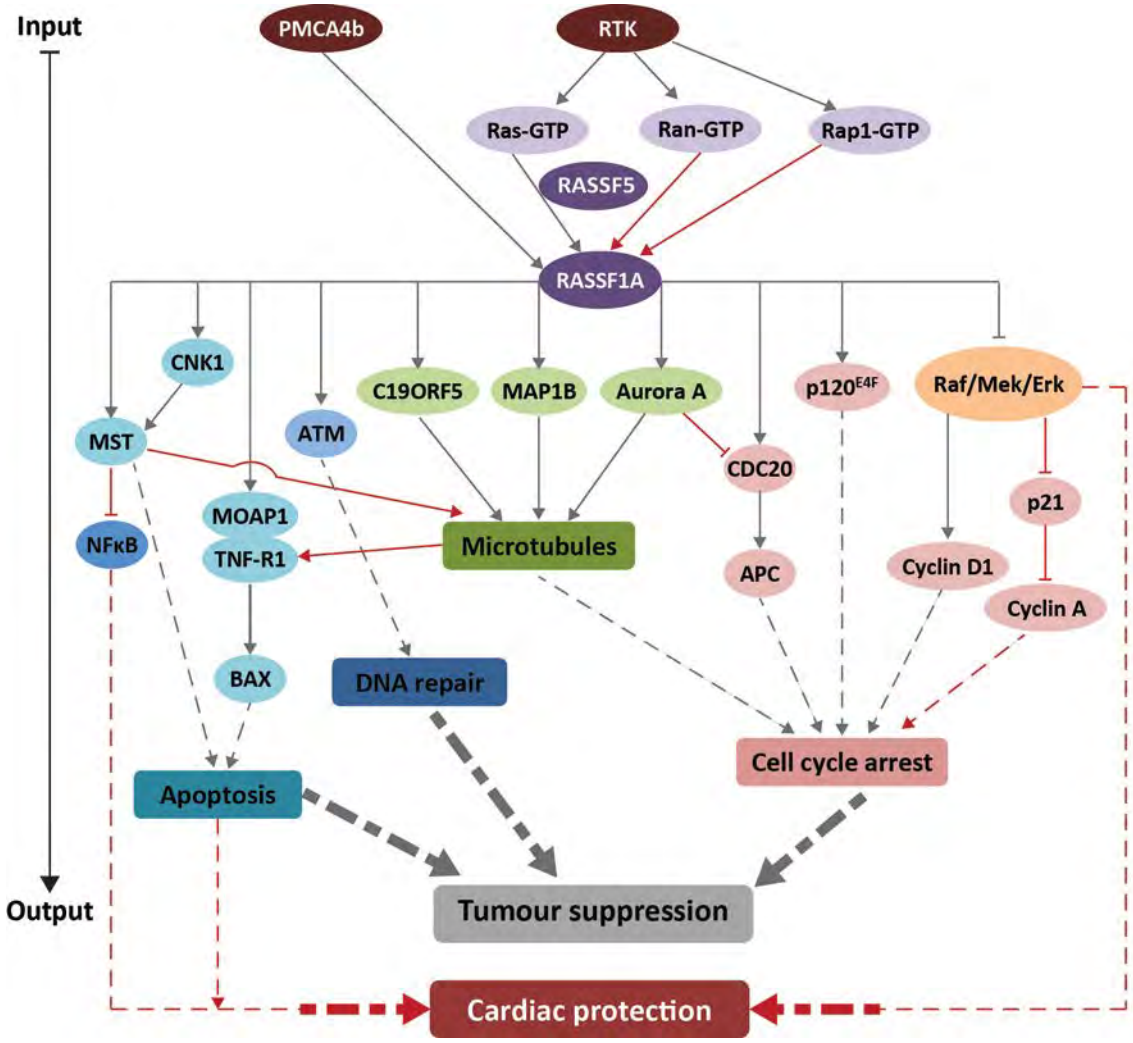

Figure 1.7 Summary of the network of interactions and functions of RASSF1A

The arrow on the left indicates the direction of the signalling cascades from signal inputs at the membrane level to the biological outputs. The proteins involved in signal inputs are shown in brown, Ras GTPases in lilac and RASSF in purple. The proteins that RASSF1A directly bind or inhibit are coloured according to the biological functions in which they are involved: apoptosis (light blue), DNA repair (dark blue), microtubule regulation (green) and cell cycle arrest (pink). Solid lines are part of the signalling cascades and dotted lines show the biological outcomes. The grey lines represent consolidated pathways and functions, and red lines represent emerging functions.

Previous studies have implicated RASSF1C in aiding the activation of SAPK/JNK signalling upon DNA damage (Kitagawa et al., 2006). In contrast, RASSF1C was recently reported to be targeted for degradation in response to DNA damage (Zhou et al., 2012). Under stress conditions, RASSF1C is phosphorylated by GSK3β, targeting it for polyubiquitination and degradation via Mule and $SCF^{\beta\text{-}TrCP}$. This process is negatively regulated by the PI3K/Akt pathway, which suggests that RASSF1C could function as an oncogene.

A different study also showed that RASSF1C upregulates genes involved in cell growth and proliferation, whilst downregulating pro-apoptotic genes (Reeves et al., 2012). RASSF1C induces phosphorylation of Erk1/2 and activates the Mek/Erk pathway to upregulate one of the identified target genes, stem cell renewal gene PIWIL. The expression of PIWIL is elevated in lung cancer cell lines and has been implicated in promoting cancer cell growth. Collectively, these recent studies point towards a more oncogenic role for RASSF1C as opposed to the tumour suppressor function of its isoform RASSF1A.

1.3.2. RASSF2

1.3.2.1. RASSF2, a potential tumour suppressor

RASSF2 is widely expressed in most tissues but is often downregulated by promoter hypermethylation and histone deacetylation in various cancer cell lines and primary tumours (Table 1.1). Its downregulation is also correlated with primary colorectal cancers with BRaf and KRas mutations (Akino et al., 2005). RASSF2 exhibits tumour suppressor properties by inhibiting cell growth, inducing apoptosis via its interaction with the MST kinases and arresting the cell cycle at G0/G1 and G2/M phase (Akino et al., 2005, Praskova et al., 2004, Vos et al., 2003a). It is also implicated in actin cytoskeleton organisation, as overexpressing RASSF2 disrupted the actin stress fibre network by suppressing the Ras/Rho pathway (Akino et al., 2005).

1.3.2.2. Regulation of apoptosis

The tumour suppressor function of RASSF2 lies mainly in its ability to regulate and promote apoptosis. Most studies on its apoptotic functions illustrated the significance of its interaction with either or both MST1 and MST2 (Cooper et al., 2009, Schagdarsurengin et al., 2010, Song et al., 2010). These reports highlighted the

importance of the SARAH domain in mediating this interaction and the apoptotic activities of the RASSF2/MST complex. Schagdarsurengin et al. (2010) showed that deletion of the SARAH domain and downregulation of RASSF2 by promoter hypermethylation in thyroid cancer significantly reduced apoptosis. Furthermore, RASSF2 is reported to be phosphorylated by MST1 and MST2 to maintain its stability and the complex maintains it in a phosphorylated state, which protects MST from degradation and turnover, thus mutually stabilising each other (Cooper et al., 2009, Song et al., 2010). The RASSF2/MST1 complex also greatly enhances MST1 activity and apoptosis by activating the JNK signalling pathway that is needed for MST-mediated apoptosis (see section 1.2.2) (Song et al., 2010). However, the same effect was also observed in the absence of MST1, leading to the speculation that MST1 activity can be compensated by MST2 or RASSF2-induced apoptosis may be independent of MST1.

RASSF2 was also reported to regulate death receptor-induced apoptosis via Prostate Apoptosis Response Protein 4 (PAR4) (Donninger et al., 2010). It forms a direct endogenous complex with PAR4 and this interaction is regulated and activated by KRas. PAR4 is involved in FAS and TRAIL-induced cell death (see section 1.2.3) and RASSF2 appears essential in TRAIL-induced PAR4 nuclear localisation and apoptosis in prostate cancer cells.

1.3.2.3. Other tumour suppressor activities of RASSF2

With the increasing number of studies on the functions of RASSF2, one study has revealed the role of nucleo-cytoplasmic shuttling of RASSF2 in facilitating its tumour suppressor functions (Kumari and Mahalingam, 2009). This process is regulated by Erk2 phosphorylation of RASSF2, which carries a nuclear export signal (NES) within residues 240-260 and interacts with export receptor CRM-1. The report also highlighted the importance of nuclear localisation of RASSF2 in promoting apoptosis and G1/S cell cycle arrest.

Apart from apoptosis, RASSF2 also regulates other biological activities to suppress tumourigenicity and may be a potential therapeutic target in lung cancer (Clark et al., 2012). RASSF2 was confirmed as a bona fide KRas effector. It appears to modulate the Ras signalling pathway, as the loss of its expression correlated with the increase of active, phosphorylated Akt. This increased the transforming potential of activated KRas, leading to a more aggressive phenotype with enhanced cell proliferation

and invasion, decreased cell adhesion and cell morphological changes, the latter of which was also observed in an earlier study (Akino et al., 2005). The study also showed for the first time, that the loss of RASSF2 expression resulted in resistance to known chemotherapeutic drugs, taxol and cisplatin; therefore it can potentially be used for epigenetic-based therapy in lung cancer.

1.3.2.4. Regulation of bone development and remodelling

A novel function of RASSF2 was elucidated in a recent study using the first *Rassf2* knockout mouse model. This study illustrated the RASSF2 regulation of postnatal bone development and remodelling and the significance of this in haematopoiesis (Song et al., 2012). In the mouse model, *Rassf2* knockout induced bone defects, which resulted in haematopoiesis anomalies and lymphopenia. To regulate this process, RASSF2 associates with and inhibits the IKK activity to suppress NFκB hyperactivation (see section 1.2.4), thus normalising osteoclast and osteoblast differentiation. Song et al. (2012) also reported the gradual increase in the expression of RASSF2 and the Hippo pathway components, MST1 and LATS1, during osteoclast and osteoblast differentiation. These observations suggest that RASSF2 may synergise with the Hippo signalling network to regulate bone development.

In general, RASSF2 exerts its tumour suppression function mainly by mediating different pro-apoptotic pathways. However, there is increasing evidence suggesting the functional diversity of RASSF2, which is summarised in Figure 1.8.

1.3.3. RASSF3

1.3.3.1. RASSF3, a RASSF member in need of further characterisation

RASSF3 is present in all normal tissues and does not harbour any inactivating mutations (Tommasi et al., 2002). When the RASSF family was last reviewed, it was only known to interact with MST1 from a yeast-two-hybrid screen with no further functional characterisation (Praskova et al., 2004).

1.3.3.2. The tumour suppressor activities of RASSF3

There has been a gradual increase in studies on RASSF3 in recent years. The first functional characterisation of RASSF3 comes from an interesting study performed on

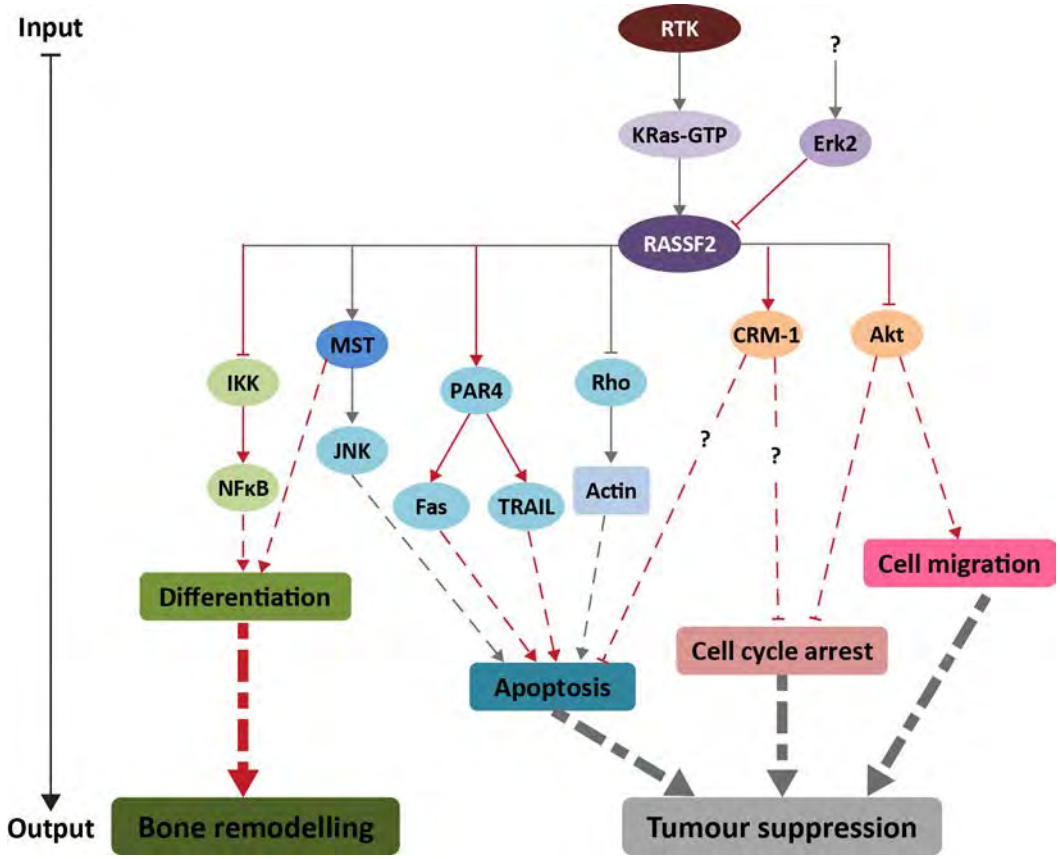

Figure 1.8 Summary of the network of interactions and functions of RASSF2

The arrow on the left indicates the direction of the signalling cascades from signal inputs at the membrane level to the biological outputs. The proteins involved in signal inputs are shown in brown, upstream proteins in lilac and RASSF in purple. The proteins that RASSF2 directly bind, regulate or inhibit are coloured according to the biological functions in which they are involved: differentiation (green) and apoptosis (blue). Proteins with dual functions are shown in orange. Other representations are as described in Figure 1.7.

MMTV/neu transgenic mice to screen for alterations in gene expression in the mammary gland. The study showed that RASSF3 is overexpressed in the mammary gland of tumour-resistant mice (Jacquemart et al., 2009). Its overexpression delays tumour formation and inhibits proliferation in breast cancer cell lines by inducing apoptosis.

In the latest report, RASSF3 was shown for the first time to be downregulated by promoter hypermethylation in approximately 80% of somatotroph adenomas cell lines (Table 1.1). New studies have also revealed its role in regulating apoptosis, the cell cycle and potentially also DNA repair in a p53-dependent manner (Kudo et al., 2012, Peng et al., 2013).

RASSF3 was shown to stabilise p53 by directly interacting with and facilitating the ubiquitination of Mdm2, the E3 ligase that targets p53 for degradation (Kudo et al., 2012). Although it interacts with MST1 and MST2, RASSF3-induced apoptosis does not appear to be MST-dependent as knocking down MST1/2 and LATS1/2 did not inhibit apoptosis. In contrast, p53 negative cells failed to induce apoptosis. Interestingly, RASSF3 also interacts with MOAP1 and knocking down MOAP1 partially inhibited apoptosis. Furthermore, RASSF3 induces cell cycle arrest at G1/S phase via p53, whilst its depletion impaired the G1/S checkpoint and led to genomic instability and an increase in polyploidy due to a compromise in DNA repair. In line with the observations from this study, Peng et al. (2013) also reported RASSF3-mediated increase in the expression of p53, Bax and caspase, leading to apoptosis.

Collectively, RASSF3 exhibits tumour suppressor properties as it promotes apoptosis possibly via the death receptor-induced pathway, regulates the cell cycle and may play a role in DNA repair and all these processes are p53-dependent.

1.3.4. RASSF4

1.3.4.1. The tumour suppressor functions of RASSF4

RASSF4 is widely expressed in most normal tissues but epigenetically silenced in various cancer cell lines (Table 1.1). The only functional study on RASSF4 demonstrated its direct interaction with KRas and that addition of a C-terminal CAAX motif enhanced apoptosis and growth inhibition (Eckfeld et al., 2004). RASSF4 was also shown to interact with both MST1 and MST2 via its SARAH domain and inhibits MST2 activity (Ikeda et al., 2009).

1.3.5. RASSF5

1.3.5.1. RASSF5, a structurally characterised and functionally diverse RASSF

RASSF5 is the closest homologue of RASSF1 and was first discovered in the form of mouse NORE1 (Vavvas et al., 1998). The two main isoforms of RASSF5 with known biological functions are RASSF5A and RASSF5C, which are also known as NORE1A and NORE1B (or RAPL) respectively. They differ mainly at the N-terminus, where RASSF5A carries a C1 domain that is absent in RASSF5C. Nevertheless, they share identical RA and SARAH domains. Both isoforms are widely expressed in normal tissues. However, there are mixed reports on their expressions in cancer with evidence suggesting epigenetic silencing of RASSF5A in specific tumour types whilst the expression of RASSF5C in tumours is more variable (Table 1.1) (van der Weyden and Adams, 2007, Vos et al., 2003b).

RASSF5 is the only member of the family that has been structurally characterised in terms of its RA and SARAH domains and it binds various Ras GTPases and both MST kinases (Makbul et al., 2013, Stieglitz et al., 2008). Previous studies highlighted the importance of Ras binding and SARAH domain-mediated heterodimerisation as the RASSF5A/MST1 complex is needed to mediate the apoptotic effect of KRasV12 whilst the RASSF5A/RASSF1A complex is essential for indirect Ras association with RASSF1A and its tumour suppressor function (Khokhlatchev et al., 2002, Ortiz-Vega et al., 2002).

Both RASSF5 isoforms also suppress tumour growth either in a HRas-dependent manner that induces apoptosis or through a mechanism independent of Ras and MST1/2 that induces cell cycle delay at the G1/S phase (Aoyama et al., 2004, Vos et al., 2003b). RASSF5A was also reported to be a centrosomal protein and its RA domain is required for microtubule association and its tumour suppressor activity of inhibiting the Erk signalling pathway (Moshnikova et al., 2006).

RASSF5C has a more specialised function in the immune system and cell migration. Its interactions with Rap1, Rap2 and MST1 facilitate its regulation of lymphocyte adhesion, T cell migration and T cell receptor activation, whilst its microtubule localisation contributes to directional vascular endothelial cell migration (Fujita et al., 2005, Katagiri et al., 2003, 2004, 2006).

1.3.5.2. Silencing of RASSF5A in cancer

Although the loss of RASSF5A expression has been previously reported for different types of cancer, a correlation between these observations and disease progression was never established. Recent reports showed that RASSF5A is downregulated by promoter hypermethylation in 70% of colorectal cancer cell lines, 38.8% of primary carcinoma tissues and 35% of hepatocellular carcinoma (HCC) tumour samples (Calvisi et al., 2009, Lee et al., 2010). Additionally, RASSF5A is also silenced by loss of heterozygosity in 15% of HCC. 85.7% of HCC displaying promoter hypermethylation were characterised with poor prognosis whilst RASSF5A reduction was significantly higher in stage III colorectal tumours (52.8%) compared to the early stage I and II tumours (26.9% and 27.8%). Therefore, the loss of RASSF5A expression contributes to poor prognosis and more aggressive tumour phenotypes, and is also associated with malignant progression.

1.3.5.3. Microtubule association and organisation

RASSF5A has previously been linked to the microtubule cytoskeleton but did not appear to require microtubule localisation for its growth suppression function (Moshnikova et al., 2008). In a more recent study, RASSF5A was shown to directly interact with tubulin via its RA domain and induce microtubule nucleation (Bee et al., 2010). This event is downregulated in a dual specific way: 1) RASSF5A interacts with and is phosphorylated by Aurora A within its RA domain at S277 or 2) RASSF5A binds to activated Ras. These two processes are mutually exclusive as Aurora A and Ras compete for overlapping binding sites within the RA domain, whilst binding to Ras restricts Aurora A phosphorylation.

1.3.5.4. Regulation involving E3 ubiquitin ligases

To date, two different E3 ubiquitin ligases have been shown to play a part in the RASSF5A-regulated processes. The first is Mdm2, a well-known negative regulator of p53. Similar to RASSF1A, RASSF5A directly interacts with Mdm2, possibly via the well-conserved C1 domain as is the case for RASSF1A (Lee et al., 2012, Song et al., 2008). However in this instance, the interaction induces the polyubiquitination and proteasomal degradation of oncoprotein HIPK1. The mechanism by which this occurs is through RASSF5A recruitment of HIPK1 and Mdm2 to nuclear dots to enhance their interaction. The consequence of HIPK1 degradation is reduced tumourigenicity by way of reduced proliferation, cell migration and anchorage-independent growth.

The second report involves a HECT class E3 ubiquitin ligase, Itch, which acts as a negative regulator of RASSF5A (Suryaraja et al., 2013). RASSF5A binds Itch via a PPxY motif, leading to its degradation by the polyubiquitination 26S proteasome pathway. The study also revealed acetylation as a regulatory mechanism for RASSF5A stability. RASSF5A is hyperacetylated in selected tumours, which restricts Itch binding and stabilises RASSF5A. However, both acetylation and Itch-mediated ubiquitination inhibit the growth suppressive functions of RASSF5A.

1.3.5.5. Regulation of the cell cycle

Earlier studies showed that RASSF5A induces growth suppression in A549 lung cancer cell line primarily by causing cell cycle delay rather than apoptosis. However, the mechanism involved has never been investigated (Aoyama et al., 2004). Recently, RASSF5A was reported to modulate p21 via p53 and it was found that their expression levels are closely correlated and often downregulated together in HCC (Calvisi et al., 2009). RASSF5A, facilitated by p53, activates p21 to inhibit CDK2, thus arresting the cell cycle at G1. It appears that RASSF5A also promotes the nuclear localisation of p53 possibly via post-translational modifications. Furthermore, the loss of p21 expression in cell systems impaired the growth inhibitory effects of RASSF5A, highlighting the importance of p21 and p53 in activating RASSF5A-mediated cell cycle regulation.

RASSF5A has also been reported as a nucleo-cytoplasmic shuttling protein, similar to RASSF2, and this plays an important role in facilitating its function in cell cycle regulation (Kumari et al., 2010). The study revealed a hydrophobic-rich NES (residues 260-300) and two NLSs at each end of RASSF5A. It was shown to interact with the SH2 domain of tyrosine kinase Lck via its C-terminus putative SH2 binding motif and its phosphorylation by Lck is critical for its nuclear translocation. Nuclear retention of RASSF5A is required for its regulation of the cell cycle, whereby it causes an arrest in the G1/S phase. Suryaraja et al. (2013) also showed that acetylation and ubiquitination negatively regulate RASSF5A and the incidence of these events is inversely correlated to the RASSF5A-induced cell cycle arrest.

1.3.5.6. Regulation of apoptosis

Calvisi et al. (2009) showed that suppression of RASSF5A reduces apoptosis, whilst in cells induced for its expression, several pro-apoptotic genes were upregulated, including

a target of p53. In addition, the inactivation of RASSF5A and p53 are mutually exclusive, thus implicating RASSF5A in the p53-induced apoptotic pathway. Conversely, restoration of both RASSF5A and RASSF5C showed significant growth suppression by apoptosis in mutant p53 colorectal cancer cell line Caco-2, thus the process is not dependent on p53 (Lee et al., 2010).

Kumari et al. (2010) reported that the RASSF5A-induced apoptosis occurs independently of cell cycle arrest, thus is regulated by a different pathway. Moreover, the apoptotic effect of RASSF5A is dependent on its nuclear localisation, an observation that contradicts previous findings that showed the importance of nuclear export and cytoplasmic localisation for RASSF5-mediated apoptosis (Kumari et al., 2010, Park et al., 2008). In addition, E3 ligase Itch negatively regulates RASSF5-mediated apoptosis (see section 1.3.5.4) (Suryaraja et al., 2013).

Lastly, RASSF5A was also shown for the first time to play a role in death receptor-mediated cell death (Park et al., 2010). It forms a complex with TNF-R1 and is needed for the oligomerisation and activation of Bax. Additionally, YAP1, a component of the Hippo pathway, interacts with TNF-R1 and is required for TNFα-induced apoptosis. RASSF5A also activates p38 kinase and JNK signalling that is known to facilitate MST1-mediated apoptosis, whilst the *Rassf5a* knockout mice failed to activate MST1 and were resistant to TNFα- and TRAIL-induced apoptosis. Collectively, these observations demonstrate that apart from RASSF1A, RASSF5A is also capable of mediating TNFα- and TRAIL-induced apoptosis, and does so via MST1. This also raises the possibility of overlapping functions between the two RASSF members, especially when taking into account their ability to form heterodimers.

In summary, recent studies have reinforced the pro-apoptotic and cell cycle regulatory functions of RASSF5A. It is able to regulate several different apoptotic pathways that are either death receptor-induced, dependent or independent of p53. RASSF5-induced apoptosis and cell cycle arrest may be separately regulated, but often occur simultaneously to promote its growth inhibitory effects (summarised in Figure 1.9).

1.3.5.7. The tumour suppressor properties of RASSF5C

Previous reports vary regarding the expression of RASSF5C in tumours, with some reporting downregulation in selected cancer cell lines whilst other reporting no evidence

of promoter methylation (van der Weyden and Adams, 2007). The potential tumour suppressor activities of RASSF5C were also never investigated until recently. It was found to be downregulated by promoter hypermethylation in 31.3% of primary colorectal carcinoma tissues and 40% of colorectal cancer cell lines; and 62% of HCC tumours (Lee et al., 2010, Macheiner et al., 2006, 2009).

Interestingly, the epigenetic silencing of RASSF5C in HCC is directly correlated with that of RASSF1A, with both downregulated in a combined 97% of HCC tumours (Macheiner et al., 2006). A follow-up study revealed that RASSF5C acts via RASSF1A to suppress replication and cell transformation in hepatocytes (Macheiner et al., 2009). This requires intact RA and SARAH domains to facilitate heterodimerisation of RASSF1A and RASSF5C, which allows them to synergise to induce cell cycle arrest at the G1 and G2/M phases. Furthermore, this complex is required to suppress c-Myc/HRas-induced cell transformation, thus exerting their tumour suppressor properties early in carcinogenesis. Additionally, *Rassf5c* knockout mice had a higher propensity in developing B cell lymphoma, HCC, and lung adenocarcinomas (Katagiri et al., 2011).

1.3.5.8. RASSF5C in the immune system

A recent study showed that RASSF5C-deficient mice developed lupus-like autoimmunity in addition to B cell lymphoma and other tumours (Katagiri et al., 2011). Further investigation revealed that RASSF5C serves as a G1/S phase checkpoint in the cell cycle to prevent lymphoproliferative disorder. It does so by regulating the localisation of p27, a major CDK2 inhibitor, in both B and T cells through the suppression of its S10 phosphorylation by Kinase Interacting Stathmin (KIS). This promotes nuclear localisation of p27 and reduces CDK2 activity to delay S phase entry, thus preventing hyperproliferation of lymphocytes.

A novel interaction partner of RASSF5C, SKAP1, has been identified recently (Raab et al., 2010). It forms a 1:1 complex with RASSF5C via the SARAH domain and competes with MST1 for binding to RASSF5C. The PH domain of SKAP1 is needed for the RASSF5C/Rap1 complex formation in T cells and the binding of this ternary complex to LFA-1 (Raab et al., 2011). This complex regulates T cell motility and interactions, thus mutations disrupting this interaction also disrupt component localisation in vesicles and T cell-dendritic cell conjugation. A later report showed that

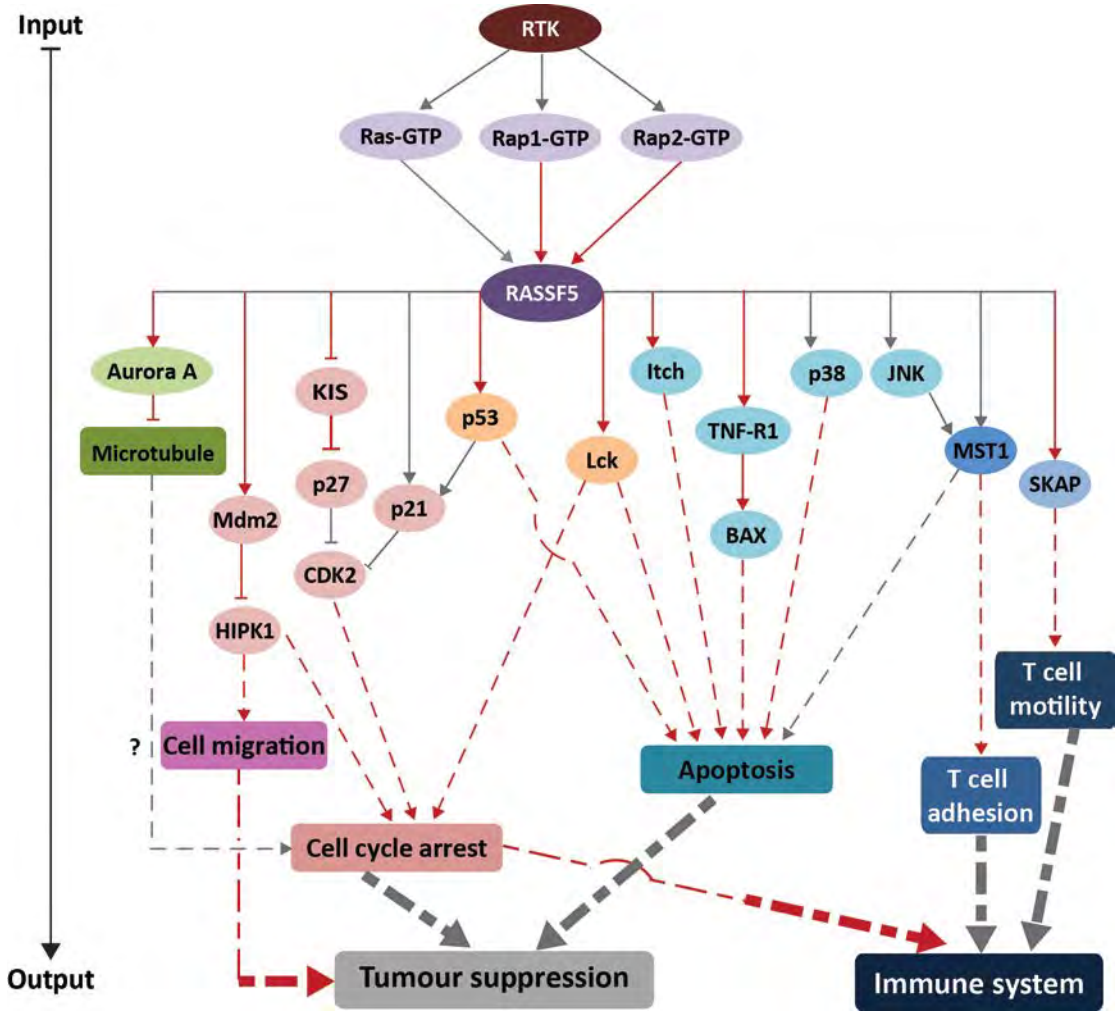

Figure 1.9 Summary of the network of interactions and functions of RASSF5

The arrow on the left indicates the direction of the signalling cascades from signal inputs at the membrane level to the biological outputs. The proteins involved in signal inputs are shown in brown, Ras GTPases in lilac and RASSF in purple. The proteins that RASSF5A directly bind, regulate or inhibit are coloured according to the biological functions in which they are involved: microtubule regulation (green), cell cycle arrest (light pink) and apoptosis (light blue). Proteins with dual functions are in orange. The proteins that interact with RASSF5C and are involved in regulation of the immune system are shown in dark blue. Other representations are as described in Figure 1.7.

the PH domain of SKAP1 and PI3K activity are also needed to facilitate the membrane localisation of RASSF5C/Rap1 in T cells for the T cell receptor "inside-out" signalling pathway (Raab et al., 2011).

1.3.6. RASSF6

1.3.6.1. RASSF6, a mainly pro-apoptotic protein

RASSF6 is expressed in most normal tissues at varying levels, but has been shown to be downregulated in various childhood leukaemias and 30-60% of different primary tumour tissues (Table 1.1). It exhibits growth inhibitory properties primarily by promoting apoptosis in synergy with MOAP1 in caspase-dependent and -independent pathways (Allen et al., 2007, Ikeda et al., 2007). RASSF6 is also genetically linked to Respiratory Syncytial Virus (RSV)-induced bronchiolitis and is able to suppress the NFκB pathway, thus it may potentially play a role in the inflammatory response to RSV (Allen et al., 2007).

1.3.6.2. Silencing of RASSF6 in cancer

Recent studies have highlighted the significance of epigenetic silencing of RASSF6 in prognostication and patient outcome. Complete silencing of RASSF6 was found in 71.6% of gastric cancer tissues and 86.5% of lymph node metastasis tissues (Wen et al., 2011). The study also found that patients with RASSF6-negative tumours have higher recurrence rates and poor survival after radical surgery, whilst the downregulation of RASSF6 is significantly associated with cancer invasion, lymph node and distal metastasis, and advanced tumour stage. Collectively, this makes RASSF6 a novel prognostic marker for gastric cancer patients and a biomarker for aggressive gastric cancer. Similar observations were reported for neuroblastoma, in which RASSF6 was downregulated in 67% of the cell lines tested (Djos et al., 2012). This was correlated to unfavourable outcome, chromosome 1p (short arm) deletion that increases the risk of neoplasia, and *MYCN* (proto-oncogene) amplification.

1.3.6.3. Regulation of apoptosis

RASSF6 has been shown to bind MST1 and MST2 via its SARAH domain (Ikeda et al., 2009). Through its interaction with MST2, it is involved in promoting both Hippo-dependent and -independent apoptotic pathways (Ikeda et al., 2009). Interestingly, the RASSF6/MST2 complex is mutually inhibitory to the apoptotic functions of both

proteins and antagonises the Hippo pathway. This complex appears to be a ternary complex including WW45. However, upon the activation of the Hippo pathway by other stimuli, the complex dissociates, presumably due to heavy phosphorylation of WW45 by MST2. Consequently, MST2 is free to mediate apoptosis via the canonical Hippo pathway, whilst RASSF6 induces apoptosis in an independent, parallel pathway, partially via MOAP1, which was also observed in a previous study (Ikeda et al., 2007).

1.3.6.4. RASSF6 and obesity

Recently, RASSF6 was shown to be downregulated at the mRNA level in adipocytes (Sanada et al., 2013). The expression of RASSF6 is negatively correlated with the level of macrophage infiltration into adipose tissues, an event associated with obesity. Downregulation of RASSF6 also enhances the expression of CD44 and high mobility group protein HMGA2. CD44 is an adhesion molecule and major receptor for a main component of the tumour extracellular matrix, whilst HMGA2 is related to mesenchymal tumour cell types, such as fat cell tumours lipomas. This latest study has revealed a novel role for RASSF6 in the regulation of obesity and its related physiological processes, such as white adipose tissue development and lipoma formation.

1.3.7. RASSF7

1.3.7.1. RASSF7, with unclear functions as a tumour suppressor or oncogene

RASSF7 was originally known as HRC1 and identified due to its close genetic proximity to the *HRAS* gene (Weitzel et al., 1992). Since then, several independent studies have found RASSF7 upregulated in different types of cancers, apparently due to hypoxia (Table 1.1). Additionally, the expression of RASSF7 could be inversely correlated to the tumour suppressor BRCA1 (Welcsh et al., 2002). Despite this, there is no evidence to suggest that RASSF7 could promote tumour formation. Nevertheless, RASSF7 has been linked to several biological functions, including the regulation of mitotic spindle formation, mitotic progression and necroptosis, a regulated form of necrosis distinct from apoptosis (Hitomi et al., 2008, Sherwood et al., 2008).

1.3.7.2. Regulation of the microtubule cytoskeleton and the cell cycle

Consistent with a previous study in *Xenopus*, Recino et al. (2010) showed that human RASSF7 localises to the centrosome and promotes mitotic progression (Recino et al., 2010, Sherwood et al., 2008). However, unlike in *Xenopus*, centrosomal localisation is

independent of microtubule association. Silencing RASSF7 led to defects in the microtubule cytoskeleton and spindle assembly, as well as a loss of Aurora B activation and localisation to the kinetochore, hence a failure in chromosomal congression. Therefore, RASSF7 is required for normal microtubule growth, completion of mitosis and cell growth.

1.3.7.3. Anti-apoptotic effects of RASSF7

A recent study has revealed the anti-apoptotic role of RASSF7, mediated by its binding to activated NRas (Takahashi et al., 2011). This was also the first report of a Ras interaction by RASSF7. The RASSF7/NRas complex binds to phosphorylated MKK7 to prevent its dephosphorylation, thus inhibiting downstream JNK phosphorylation by MKK7 and negatively regulating the pro-apoptotic JNK signalling pathway. However, in prolonged stress, RASSF7 stability is regulated by ubiquitination that targets it for degradation to allow cell death signalling to progress. The mechanism behind RASSF7 ubiquitination and the E3 ubiquitin ligase involved are yet to be identified.

1.3.7.4. Silencing of RASSF7 in cancer

To date, there is only one report of RASSF7 silencing by promoter hypermethylation in 89% of neuroblastoma cell lines tested (Djos et al., 2012). However, Recino et al. (2010) found no evidence of RASSF7 epigenetic silencing in the 57 cell lines screened, including 20 lung, 12 breast, eight colorectal, five glioma and four neuroblastoma.

Although reports on the expression levels of RASSF7 in cancers are conflicting, its anti-apoptotic, pro-mitosis and proliferation functions suggest a more oncogenic potential rather than a tumour suppressor role for RASSF7.

1.3.8. RASSF8

1.3.8.1. RASSF8 in lung carcinogenesis

RASSF8 was first known as HOJ-1 and C12ORF2 before joining the RASSF family (Sherwood et al., 2010). The *RASSF8* gene was found to be located in close proximity to the *KRAS2* gene and has been linked to lung tumourigenesis (Falvella et al., 2006). RASSF8 is ubiquitously expressed in normal tissues but downregulated in lung adenocarcinomas and leukaemias (Table 1.1). Overexpression of RASSF8 in lung cancer cell lines reduced anchorage-independent growth, a phenotype associated with tumour

progression and metastasis. Conversely, RNAi silencing of RASSF8 in NSCLC cell lines promoted anchorage-independent growth and *in vivo* tumourigenicity in severe combined immunodeficiency (SCID) mice, whilst morpholino-mediated knockdown in *Xenopus* increased cell proliferation (Falvella et al., 2006, Lock et al., 2010).

1.3.8.2. Regulation of cell-cell adhesions and tumour suppression

Recent studies have highlighted a new biological role of RASSF8 in the regulation of cell-cell adhesions (Langton et al., 2009, Lock et al., 2010). The RASSF8 homolog in *Drosophila*, dRASSF8 was first shown to interact with dASPP (Langton et al., 2009). The complex localises to adherens junctions (AJs) and regulate cell-cell adhesion during *Drosophila* retinal morphogenesis. It does so by promoting C-terminal Src kinase (CSK) activity, which inhibits the proto-oncogene Src, thus modulating the Src signalling pathway that is known to promote AJ remodelling in development and metastasis. Furthermore, dRASSF8 also promotes apoptosis of excess cells in the *Drosophila* eyes. Interestingly, the RASSF8/ASPP interaction is conserved in humans, whilst both ASSP and RASSF8 are potential tumour suppressors, with ASPP also involved in p53 pro-apoptotic function (Langton et al., 2009, Underhill-Day et al., 2011).

Similarly, Lock et al. (2010) showed that RASSF8 co-localises with adhesion junctions (AJs) components, β-catenin and E-cadherin, to regulate cell-cell adhesion. The loss of RASSF8 destabilised AJs through the mislocalisation of β-catenin and p65 from the site of cell-cell contact to the nucleus, whilst E-cadherin was lost from cell membrane, the latter was also observed by Langton et al. (2009). The relocalisation of β-catenin and the p65 subunit of the NFκB heterodimer to the nucleus increased Wnt signalling via its interaction with the TCF-LEF transcription factor and NFκB signalling respectively. In addition, RASSF8 was also shown to maintain the actin cytoskeleton with its knockdown resulting in an increase in cellular migration.

Taken together, these observations suggest that the tumour suppressor function of RASSF8 includes the regulation of cell-cell adhesion via the Src signalling pathway, which in turn modulates the Wnt and NFκB signalling pathways that are known to promote malignant transformation and inhibit apoptosis. RASSF8 could also promote apoptosis and regulate the actin cytoskeleton to prevent lung carcinogenesis and metastasis.

1.3.9. RASSF9

1.3.9.1. RASSF9, a potential Ras effector with unknown functions

RASSF9, formerly known as PAM C-terminal interactor-1 (P-CIP1) is widely expressed in multiple organs (Table 1.1). It interacts with peptidylglycine alpha-amidating monooxygenase (PAM) and recycling endosomes, thus may be involved in regulating vesicle trafficking (Sherwood et al., 2010, Underhill-Day et al., 2011). It was also reported to show preferential binding to KRas and NRas (Rodriguez-Viciana et al., 2004).

1.3.9.2. Regulation of epidermal homeostasis

A recent report finally shed some light into the function of RASSF9. It was shown to play a role in the maintenance of epidermal homeostasis (Lee et al., 2011). The study reported high levels of RASSF9 expression in epidermal keratinocytes of the skin. The *Rassf9* knockout mouse model exhibited a dramatic change in epithelial organisation of the skin, whilst displaying a phenotype that resembled human ageing with growth retardation, short lifespan, less subcutaneous adipose layer and alopecia. Furthermore, aberrant proliferation and differentiation in the skin were observed in the knockout mice. Therefore, RASSF9 negatively regulates cell proliferation through p21 during growth and early differentiation, and is required for normal differentiation of keratinocytes.

1.3.10. RASSF10

1.3.10.1. Epigenetic silencing of RASSF10 in cancer

RASSF10 was the last member to join the RASSF family and is widely expressed in various organs and tissues, with high levels of expression in several brain tissues (Table 1.1) (Underhill-Day et al., 2011). Epigenetic silencing of RASSF10 has also been observed in an increasing number of tumours; the most prominent ones include 100% of leukaemia cell lines, 88% of T cell ALL, 100% of thyroid cancer cell lines, 66% of primary thyroid carcinoma, 75% of gastric cancers, 80% pancreatic cancer cell lines, 60-70% lung, sarcoma and head and neck cancer cell lines and gliomas (Table 1.1). Furthermore, promoter hypermethylation of RASSF10 is a potential prognostic marker for secondary glioblastomas associated with worse progression-free survival and overall survival and early stage tumour development (Hill et al., 2011). Downregulation of

RASSF10 was also observed in 56% of neuroblastoma cell lines; however, promoter hypermethylation does not appear to be the cause in this case.

1.3.10.2. The tumour suppressor activities of RASSF10

The distribution of RASSF10 has recently been shown to be cell cycle-dependent (Hill et al., 2011). It relocates to the nucleus specifically during mitosis and associates with microtubules at developing centrosomes and spindle poles. Other functional tests showed that RASSF10 inhibited anchorage-independent growth and cell proliferation in glioma cells, potentially via cell cycle regulation at the G1/S and G2/M phases (Hill et al., 2011, Richter et al., 2012). The study also revealed putative NLS and NES on RASSF10, making it a potential nucleo-cytoplasmic shuttling protein, similar to RASSF2 and RASSF5, so its tumour suppressive functions could be dependent upon its cellular localisation.

RASSF10 was shown to inhibit growth and colony formation whilst inducing apoptosis in various cell lines (Richter et al., 2012, Wei et al., 2013). These tumour suppressive properties are facilitated by its inhibition of the Wnt signalling pathway, which is known to be aberrantly activated in gastric cancers (Wei et al., 2013). RASSF10 reduces nuclear localisation of β-catenin, resulting in lower levels of expression of the β-catenin downstream target genes, such as c-Myc, cyclin D1, CD44, that are required for cell proliferation. Interestingly, RASSF10 expression is upregulated upon contact inhibition. This is regulated at the promoter level and is controlled upstream by forksolin, protein kinase A (PKA) and activator Protein 1 (AP-1) member JunD, thus RASSF10 may activate cAMP and PKA signalling to upregulate p27 and halt cell cycle progression to inhibit tumour growth (Richter et al., 2012).

In summary, RASSF10 acts as a tumour suppressor potentially by inducing apoptosis and inhibiting cell cycle progression upon contact inhibition via its regulation of the Wnt, cAMP and PKA signalling pathways.

1.4. Aims of the project

As summarised in Figure 1.10, most of the RASSF family members are either established or potential tumour suppressors, with some members having wider biological roles. Many of the RASSF members are functionally well studied, with most studies highlighting the significance of the RA and SARAH domain-mediated interactions in the regulation of various signalling pathways and biological processes. However, there is a notable lack of systematic comparative characterisation of the RASSF family, as well as the molecular and structural information that facilitate their tumour suppressive functions.

The hypothesis is that all six classical RASSF members should display similar interaction behaviours due to their high homologies and protein interaction domains, whereas the interactions of the N-terminal RASSF members may vary as their interaction domains and sequences are more divergent.

The aim of this project was to characterise the RA and SARAH domains across the ten RASSF members and compare their interactions with several binding partners that facilitate their main functions. The experimental approaches included *in silico* structural predictions, as well as *in vitro* and cell based interaction and functional studies. Specific point mutations were introduced in the SARAH domain to assess their effect on interactions. Several other potential RASSF interacting partners were also investigated.

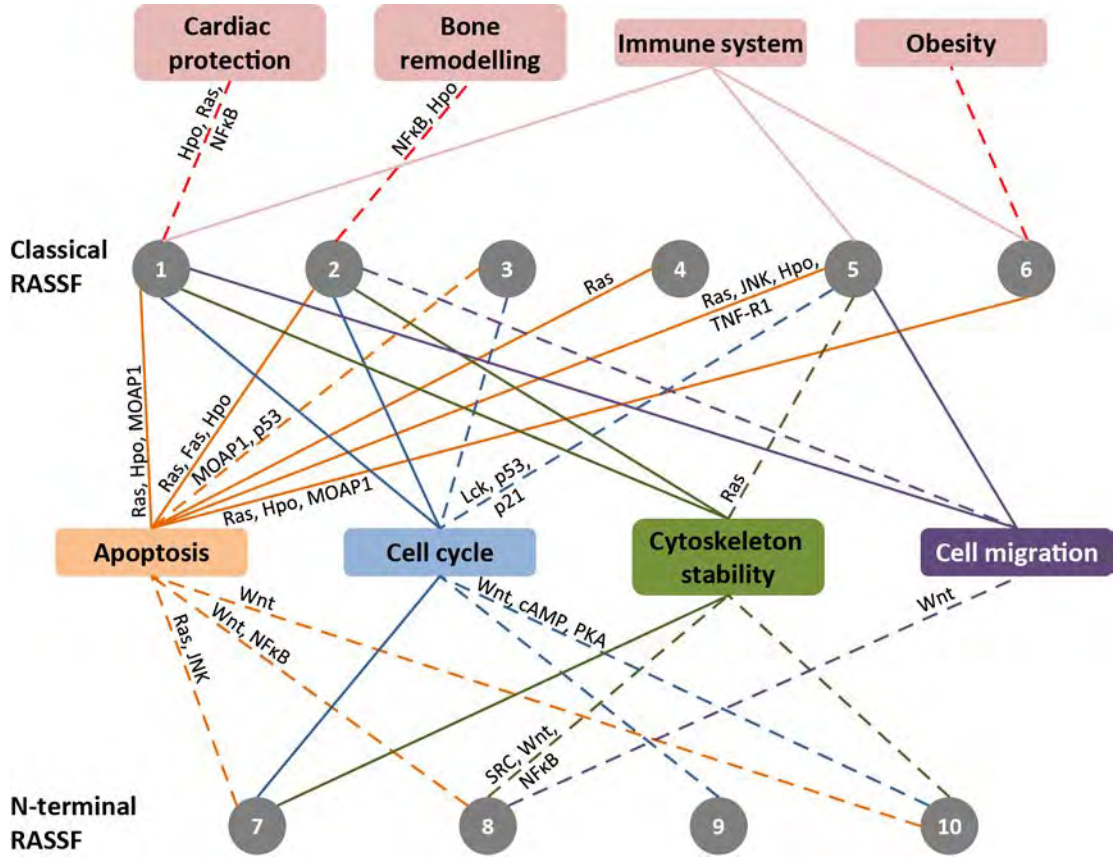

Figure 1.10 Summary of the multiple RASSF functions

The ten RASSF members are shown in grey and abbreviated 1-10. The biological functions involved in tumour suppression (or possible tumour formation for RASSF7) and the lines connecting them to the individual RASSF member are colour coded: apoptosis (orange), cell cycle (blue), cytoskeleton stability (green), cell migration (purple) and biological functions not associated with tumour suppression (pink). Solid lines depict well-established functions, and dotted lines represent new pathways and emerging functions. Major or new signalling pathways and interactions involved are labelled along the relevant lines.

2 Material and Methods

2.1. DNA Manipulation and Analysis

2.1.1. Isolation and purification of DNA

2.1.1.1. Preparation of plasmid DNA

For small scale plasmid preparations, the QIAprep Spin Miniprep Kit (Qiagen) was used. 5 ml of bacterial cultures were grown overnight at 37 °C in Luria Broth (LB) medium [10 g/L tryptone, 5 g/L yeast extract, 5 g/L NaCl] containing the appropriate antibiotic and harvested by centrifugation at 3,700 x*g* (Allegra® X-15R Centrifuge, Beckman Coulter). Bacterial pellets were then processed according to the manufacturer's instructions for the kit and DNA was eluted in 50 µl of elution buffer provided by the kit.

For large scale plasmid purification, 500 ml of LB bacterial cultures were grown overnight at 37 °C with the appropriate antibiotics (i.e. 100 µg/ml ampicillin, 50 µg/ml kanamycin, 34 µg/ml chloramphenicol or 10 µg/ml gentamicin). The overnight culture was harvested by centrifugation at 3,700 x*g* for 20 min at 4 °C (Allegra® X-15R Centrifuge, Beckman Coulter). All centrifugation steps were performed at 3,700 x*g* and 4 °C unless otherwise stated. The cell pellet was resuspended in 37 ml of Alkaline Lysis Buffer I [50 mM glucose, 25 mM Tris-HCl pH 8.0, 10 mM EDTA] and lysed by addition of 50 ml of Alkaline Lysis Buffer II [200 mM NaOH, 1% (v/v) SDS]. Lysis was stopped by addition of 37 ml of Alkaline Lysis Buffer III [3 M potassium acetate, 115 mM glacial acetic acid]. The lysate was centrifuged for 10 min and the supernatant was filtered through cheesecloth into a 250 ml centrifuge bottle then mixed with 0.7 volumes of isopropanol to precipitate the total amount of nucleic acids. This mixture was centrifuged for 15 min and the nucleic acid pellet was resuspended in 2 ml of TE buffer pH 8.0 [10 mM Tris-HCl pH 8.0, 1 mM EDTA] then transferred to a 15 ml Falcon tube. The RNA was precipitated by addition of an equal volume of 5 M LiCl (Sigma) and pelleted by centrifugation for 10 min. The supernatant was transferred to a fresh 15 ml Falcon tube and the DNA was precipitated by addition of 0.7 volumes of isopropanol. The DNA was pelleted by centrifugation for 10 min and the pellet resuspended in 0.5 ml TE buffer pH 8.0. To remove residual RNA, 5 µl of RNAse (Qiagen stock 100 mg/ml) was added and the mixture was incubated for 15 min at 37 °C. The DNA solution was

transferred to a 1.5 ml centrifuge tube and mixed with an equal volume of 13% PEG 8,000 (Sigma) and 1.6 M NaCl. This mixture was incubated on ice for 60 min and centrifuged at 21,000 x*g* for 15 min at 4°C (Centrifuge 5417R, Eppendorf). The pellet was resuspended in 200 µl TE buffer pH 8.0 and mixed with an equal volume of phenol:chloroform:isoamyl alcohol (Sigma) to precipitate residual proteins. After centrifugation at 21,000 x*g* for 5 min, the aqueous phase was transferred to a fresh microfuge tube. This phenol/chloroform extraction step was repeated twice. Finally, the DNA was precipitated by adding 0.1 volume of 3 M sodium acetate and 2.5 volumes of 100% ethanol, followed by centrifugation at 21,000 x*g* for 2 min. The pellet was washed once with 70% ethanol and air dried before resuspension in 100-200 µl of TE buffer pH 8.0.

The DNA concentration was determined by measurement of absorbance at 260 nm and 280 nm using a NanoDrop 2000c (Thermo Scientific). An $A_{260\ nm}$ value of 1.0 corresponds to approximately 50 µg/ml double stranded DNA. The ratio between $A_{260\ nm}$ and $A_{280\ nm}$ values provides an indication of the DNA purity.

2.1.1.2. Purification of DNA from agarose gels

Agarose gels were typically prepared at 0.8% agarose concentration by dissolving the appropriate amount of agarose (Sigma) in 1x TAE buffer [40 mM Tris-HCl pH 8.0, 20 mM glacial acetic acid, 1 mM EDTA] and run in the same buffer. Samples for running on the gel were prepared in 10x sample buffer [50% (v/v) glycerol, 0.1% (w/v) bromophenol blue]. A 1kb plus or 100bp DNA ladder (Invitrogen) was also run for reference. Gels were stained with GelRed™ (Biotium) and a G:BOX (Syngene) gel documentation system was used to obtain a digital image of the gel.

QIAEX II Gel Extraction Kit (Qiagen) was used to purify PCR products and restriction digest fragments. The DNA bands were excised from the gel using a clean scalpel and DNA was extracted and purified following the manufacturer's instructions.

2.1.2. Polymerase Chain Reaction (PCR)

PCR was used for the following applications: 1) amplification of DNA for cloning specific genes into expression vectors (section 2.1.2.1), 2) colony screening of clones (section 2.1.2.2) and 3) introduction of mutations using primers (section 2.1.2.3).

2.1.2.1. KOD Hot Start Polymerase

The high fidelity, proofreading KOD Hot Start Polymerase (Novagen, Merck) was used to amplify DNA that was subsequently used for cloning into pTriEx™-6 Ek/LIC, pENTR™ and pmCherry-C1 vectors (Table 2.1).

Reaction mixtures contained 1x Buffer, 0.16 mM dNTPs, 1 mM $MgSO_4$, 0.4 µM forward and reverse primers, 10 ng template DNA, 0.02 U/µl KOD Hot Start DNA Polymerase in a total volume of 25 µl. The PCR was carried out in a thermal cycler (GS1, G-Storm) using the following temperature cycles:

95 °C for 5 min
95 °C for 30 sec
50 °C for 30 sec
70 °C for 20 sec per kb of the plasmid DNA } 30 cycles
70 °C for 10 min

2.1.2.2. Taq DNA Polymerase

Taq DNA Polymerase (Qiagen) was used for insert verification of genetic constructs. PCR reactions were carried out using primer pairs, one of which bound the destination vector close to the cloning site and the second bound the inserted gene. Insertions were identified by the presence of a product of a predicted size. Reaction mixtures were prepared using 1x QIAGEN® CoralLoad PCR Buffer, 0.1 mM dNTPs, 1 µM forward and reverse primers and 0.05 U/µl Taq DNA Polymerase. A pipette tip was used to transfer bacteria directly from the colony to be verified into the reaction mix.

The PCR was carried out in a thermal cycler (GS1, G-Storm) using the following temperature cycles:

94 °C for 3 min
94 °C for 30 sec
50-68 °C for 30 sec } 30 cycles
72 °C for 1 min
72 °C for 10 min

Table 2.1 DNA constructs and primers used for cloning

Vector and construct name	Properties and protein encoded by DNA insert	Cloning method	Primers 5' → 3'
pTriEx™-6	All with N-terminal StrepII, SUMO*, myc tag	Ligation-independent cloning (LIC)	
MST1 FL	aa 1-487		2 step PCR Fwd1 Linker CAGGGACCCG GTTGGTCTCA TCCTCAATTT GAGAAAAGCG ATAGCGAAGT GAAC Rev1 Linker AACAACGATC TGTTCGCG Fwd GCGAACAGAT CGGTGGTGAA CAAAAACTCA TCTCAGAAGA GGATCTGGAG ACGGTACAGC TGAGG Rev GGCACCAGAG CGTTGAAGTT TTGTTGCCGT CTCTT
MST1 SARAH	aa 432-487		2 step PCR Fwd1 Linker CAGGGACCCG GTTGGTCTCA TCCTCAATTT GAGAAAAGCG ATAGCGAAGT GAAC Rev1 Linker AACAACGATC TGTTCGCG Fwd GCGAACAGAT CGGTGGTGAA CAAAAACTCA TCTCAGAAGA GGATCTGGAC TACGAGTTTC TTAAGAGTTG Rev GGCACCAGAG CGTTGAAGTT TTGTTGCCGT CTCTT
MST2 FL	aa 1-491		2 step PCR Fwd1 Linker CAGGGACCCG GTTGGTCTCA TCCTCAATTT GAGAAAAGCG ATAGCGAAGT GAAC Rev1 Linker AACAACGATC TGTTCGCG Fwd GCGAACAGAT CGGTGGTGAA CAAAAACTCA TCTCAGAAGA GGATCTGGAG CAGCCGCCGG CGCCT Rev GGCACCAGAG CGTTAAAGTT TTGCTGCCTT CTTTT
MST2 SARAH	aa 437-491		2 step PCR Fwd1 Linker CAGGGACCCG GTTGGTCTCA TCCTCAATTT GAGAAAAGCG ATAGCGAAGT GAAC Rev1 Linker AACAACGATC TGTTCGCG Fwd GCGAAGAGAT CGGTGGTGAA GAAAAAGTCA TCTCAGAAGA GGATCTGTTT GACTTTTTGA AAAATCTAAG Rev GGCACCAGAG CGTTAAAGTT TTGCTGCCTT CTTTT
pTriEx™-4		Gateway® ^	
MST1 SARAH	aa 432-487, N-terminal TEV-linker, C-terminal myc tag		Fwd ATGGAGAATC TTTATTTTCA GGGCGACTAC GAGTTTCTTA AGAGTTGGA Rev TTACAGATCC TCTTCTGAGA TGAGTTTTTG TTCGAAGTTT TGTTGCCGTC TCT
RASSF5 SARAH	aa 212-265, C-terminal myc tag		Fwd ATGGAGGTAG AGTGGGATGC CTTCTC Rev CAGATCCTCT TCTGAGATGA GTTTTTGTTC CCCAGGTTTG CCCTGGGATT

Vector and construct name	Properties and protein encoded by DNA insert	Cloning method	Primers 5' → 3'	
pEGFP-C1		Gateway® ^		
RASSF1 FL	aa 1-340		Fwd	ATGTCGGGGG AGCCTGAG
			Rev	TCACCCAAGG GGGCAGGC
RASSF2 FL	aa 1-326		Fwd	ATGGACTACA GCCACCAA
			Rev	TCAGATTGTT GCTGGGGT
RASSF3 FL	aa 1-238		Fwd	ATGAGCAGCG GCTACAGC
			Rev	CTTAATCAGG CTTCCACACC TC
RASSF4 FL	aa 1-321		Fwd	ATGAAGGAAG ACTGTCTGCC
			Rev	TTACTTGGCC TCCACCAC
RASSF5 FL	aa 1-265		Fwd	ATGACCGTGG ACAGCAGCAT
			Rev	TTACCCAGGT TTGCCCTGGG
RASSF5 ΔSARAH	aa 1-211		Fwd	ATGACCGTGG ACAGCAGCAT
			Rev	TTATCCAGTT TCATTCTCCT TTAGCACA
RASSF5 SARAH	aa 212-265		Fwd	ATGGAGGTAG AGTGGGATGC CTTCTC
			Rev	TTACCCAGGT TTGCCCTGGG
RASSF6 FL	aa 1-337		Fwd	ATGGCTCACC AGTACCCC
			Rev	CTAAACTGTT GTCTCTGTTT TTATT
RASSF7 FL	aa 1-373		Fwd	ATGTTGTTGG GACTGGCG
			Rev	TCACAGAGCC TGGGGCTG
RASSF7 RA	aa 6-89		Fwd	GCGGCCATGG AGCTGAAGGT
			Rev	TTAGGGCCCT GTGCGCCTCA G
RASSF8 FL	aa 1-392		Fwd	ATGGAACTTA AAGTATGG
			Rev	CTAATCTTTA CACTCCTGCT TATC
RASSF9 FL	aa 1-435		Fwd	ATGGCTCCCT TTGGAAGA
			Rev	CTATGTTGAC AACAGCACCA C
RASSF10 FL	aa 1-507		Fwd	ATGGATCCTT CGGAAAAGAA G
			Rev	CCACAAGGGA TTCGCACATG GG
MST1 FL	aa 1-487		Fwd	ATGGAGACGG TACAGCTGAG G
			Rev	TTACGAAGTT TTGTTGCCGT CTCTT
MST1 SARAH	aa 432-487		Fwd	ATGGAGGTAG AGTGGGATGC CTTCTC
			Rev	TTACGAAGTT TTGTTGCCGT CTCTT

Vector and construct name	Properties and protein encoded by DNA insert	Cloning method	Primers 5' → 3'	
pEGFP-C1		Gateway® ^		
MST2 FL	aa 1-491		Fwd	ATGGAGCAGC CGCCGGCGCC T
			Rev	TTACAAAGTT TTGCTGCCTT CTTTT
pTagRFP-T		Gateway® ^		
MST1 FL	aa 1-487		Fwd	ATGGAGACGG TACAGCTGAG G
			Rev	TTACGAAGTT TTGTTGCCGT CTCTT
MST1 SARAH	aa 432-487		Fwd	ATGGAGGTAG AGTGGGATGC CTTCTC
			Rev	TTACGAAGTT TTGTTGCCGT CTCTT
pmCherry-C1		Restriction digest and ligation		
MST1 FL	aa 1-487		Fwd	GAAGATCTAT GGAGACGGTA CAGCTGAGG
			Rev	CCCAAGCTTG TTAGAAGTTT TGTTGCCGTC TC
MST1 ΔSARAH	aa 1-431		Fwd	GAAGATCTAT GGAGACGGTA CAGCTGAGG
			Rev	CCCAAGCTTG TTATCCATCC TGTGGTATTT TCCAATC
MST1 SARAH	aa 432-487		Fwd	GAAGATCTGA CTACGAGTTT CTTAAGAGTT GGA
			Rev	CCCAAGCTTG TTAGAAGTTT TGTTGCCGTC TC

^ All Gateway® cloning primers start with the following sequences (5' → 3'):

Forward (Fwd) GGGGACAAGT TTGTACAAAA AAGCAGGCTC CACC

Reverse (Rev) GGGGACCACT TTGTACAAGA AAGCTGGGT

2.1.2.3. Mutagenesis PCR

QuickChange® Site-Directed Mutagenesis Kit (Stratagene), containing *PfuUltra*™ High-Fidelity DNA Polymerase, was used to introduce point mutations into plasmid constructs. Primers of at least 20 nucleotides in length were designed to incorporate the mutations (Table 2.2). The primers are extended around the whole plasmid by the polymerase, resulting in a nicked, mutated plasmid.

Each reaction mix contained 1x *PfuUltra*™ HF reaction buffer, 0.2 mM dNTPs, 0.05 U/µl *PfuUltra*™ HF DNA polymerase, 2.5 ng/µl forward and reverse primers, 6% DMSO and 10 ng template DNA in a total volume of 25 µl. The PCR was carried out in a thermal cycler (GS1, G-Storm) using the following temperature cycle:

95 ºC for 1 min
95 ºC for 50 sec
60 ºC for 50 sec
68 ºC for 1 min per kb of the plasmid DNA } 18 cycles
68 ºC for 7 min

The mutagenesis product was treated with 0.25 U/µl DpnI (New England Biolabs) at 37 ºC for 1 h, which digests the template DNA leaving the DNA containing the mutation. This was transformed into ultracompetent XL10 Gold cells (section 2.1.3.5) and the mutated DNA constructs were verified by sequencing (section 2.1.4).

2.1.3. Cloning of plasmid constructs

2.1.3.1. Cloning into pTriEx™-6 vector

MST1 and MST2 kinases and their respective SARAH domains were cloned into pTriEx™-6 (Novagen) using the pTriEx™ Ek/LIC vector kit. This method uses ligation independent cloning. The 3' to 5' exonuclease activity of T4 DNA polymerase is utilised in the presence of dATP so its activity is counteracted by the 5' to 3' polymerase activity when it reaches a dATP residue. This results in DNA with single strand overhangs. KOD polymerase (section 2.1.2.1) was used to produce insert fragments encoding a StrepII, SUMO* and myc tag in addition to the gene of interest with complementary sequences to the linearised pTriEx™-6 vector. The vector and gel purified gene fragment (section 2.1.1.2) were treated with T4 DNA polymerase following the manufacturer's instructions

Table 2.2 Mutagenesis of DNA constructs by point mutation(s)

Template construct	Mutation introduced	Primers with indicated mutated codon(s) 5' → 3'	
pTriEx™-6 Ek/LIC			
MST1 FL	AAG → AGG	Fwd	CCGGCCAGAT TGTTGCTATT AGGCAAGTTC CTGTGGAATC AGA
	K59R	Rev	TCTGATTCCA CAGGAACTTG CCTAATAGCA ACAATCTGGC CGG
MST2 FL	AAG → AGG	Fwd	CCGGTCAAGT TGTCGCAATT AGGCAAGTAC CTGTTGAATC AGA
	K56R	Rev	TCTGATTCAA CAGGTACTTG CCTAATTGCG ACAACTTGAC CGG
pEGFP-C1			
RASSF1 FL	CTA → CCC	Fwd	CCTTCAGCAT GCCTGAACCC CATAACTTCC TACG
	L301P	Rev	CGTAGGAAGT TATGGGGTTC AGGCATGCTG AAGG
RASSF1 FL	CTA → CCC	Fwd	GAACTACATA ACTTCCCCCG TATCCTGCAG C
	L305P	Rev	GCTGCAGGAT ACGGGGGAAG TTATGTAGTT C
RASSF1 FL	CTG → CCC	Fwd	CATAACTTCC TACGTATCCC CCAGCGGGAG GAGGAGGAGC AC
	L308P	Rev	GTGCTCCTCC TCCTCCCGCT GGGGGATACG TAGGAAGTTA TG
RASSF1 FL	CTA → CCC, CTA → CCC	Fwd	CCTTCAGCAT GCCTGAACCC CATAACTTCC CCCGTATCCT GCAGC
	L301P + L305P	Rev	GCTGCAGGAT ACGGGGGAAG TTATGGGGTT CAGGCATGCT GAAGG
RASSF1 L301P	(CTA → CCC)*, CTG → CCC	Fwd	CATAACTTCC TACGTATCCC CCAGCGGGAG GAGGAGGAGC AC
	(L301P)* + L308P	Rev	GTGCTCCTCC TCCTCCCGCT GGGGGATACG TAGGAAGTTA TG
RASSF1 FL	CTA → CCC, CTG → CCC	Fwd	CTACATAACT TCCCCCGTAT CCCCCAGCGG GAGGAG
	L305P + L308P	Rev	CTCCTCCCGC TGGGGGATAC GGGGGAAGTT ATGTAG
RASSF5 FL	CTT → CCC	Fwd	CTCCATCCCT GAACCCCAGA ACTTCC
	L224P	Rev	GGAAGTTCTG GGGTTCAGGG ATGGAG
RASSF5 FL	CTA → CCC	Fwd	CTTCAGAACT TCCCCACAAT CCTGG
	L228P	Rev	CCAGGATTGT GGGGAAGTTC TGAAG
RASSF5 FL	CTG → CCC	Fwd	CAGAACTTCC TAACAATCCC CGAAAAAGAG GAGCAGGACA AAA
	L231P	Rev	TTTTGTCCTG CTCCTCTTTT TCGGGGATTG TTAGGAAGTT CTG

Template construct	Mutation introduced	Primers with indicated mutated codon(s) 5' → 3'	
RASSF5 FL	CTT → CCC, CTA → CCC	Fwd	CTCCATCCCT GAACCCCAGA ACTTCCCCAC AATCCTGG
	L224P + L228P	Rev	CCAGGATTGT GGGGAAGTTC TGGGGTTCAG GGATGGAG
RASSF5 L224P	(CTT → CCC)*, CTG → CCC	Fwd	CAGAACTTCC TAACAATCCC CGAAAAAGAG GAGCAGGACA AAA
	(L224P)* + L231P	Rev	TTTTGTCCTG CTCCTCTTTT TCGGGGATTG TTAGGAAGTT CTG
RASSF5 FL	CTA → CCC, CTG → CCC	Fwd	CTTCAGAACTTCCCCACAATCCCCGAAAAAGAGGAG
	L228P + L231P	Rev	CTCCTCTTTTTCGGGGATTGTGGGGAAGTTCTGAAG
MST1 FL	CTT → CCC	Fwd	GAGTTGGACA GTGGAGGACC CCAGAAGAG GCTCTTGGCC CTG
	L444P	Rev	CAGGGCCAAG AGCCTCTTCT GGGGGTCCTC CACTGTCCAA CTC
MST1 FL	CTC → CCC	Fwd	CTTCAGAAGA GGCCCTTGGC CCTG
	L448P	Rev	CAGGGCCAAG GGCCTCTTCT GAAG
MST1 FL	CTG → CCC	Fwd	CTCTTGGCCC CCGACCCCAT G
	L451P	Rev	CATGGGGTCG GGGGCCAAGA G
MST1 FL	CTT → CCC, CTC → CCC	Fwd	GAGTTGGACA GTGGAGGACC CCCAGAAGAG GCCCTTGGCC CTG
	L444P + L448P	Rev	CAGGGCCAAG GGCCTCTTCT GGGGGTCCTC CACTGTCCAA CTC
MST1 L444P	(CTT → CCC)*, CTG → CCC	Fwd	CTCTTGGCCC CCGACCCCAT G
	(L444P)* + L451P	Rev	CATGGGGTCG GGGGCCAAGA G
MST1 FL	CTC → CCC, CTG → CCC	Fwd	CTTCAGAAGA GGCCCTTGGC CCCCGACCCC ATG
	L448P + L451P	Rev	CATGGGGTCG GGGGCCAAGG GCCTCTTCTG AAG

* Brackets indicate existing mutation in template DNA and codons mutated are highlighted in blue in the primer sequence.

to insert the fragment into pTriEx™-6. The final reaction mix was transformed into ultracompetent XL10 Gold cells (section 2.1.3.5).

2.1.3.2. Gateway® cloning

GATEWAY® cloning technology (Invitrogen) is a reversible two-step strategy. First, a pENTR™ entry clone with the gene of interest is constructed. The gene can be subsequently shuttled into any destination vectors that carry a different antibiotic resistance gene and are compatible with the GATEWAY® system in a single recombination reaction to produce an expression clone.

To generate an entry clone, pDONR207 was the entry vector of choice. KOD polymerase (section 2.1.2.1) was used to produce insert fragments encoding the gene of interest between two *attB* recombination sites (Table 2.1). The reaction mix was set up using BP Clonase™ II following the manufacturer's instructions. The final product was transformed into ultracompetent DH5α cells (section 2.1.3.5).

Gene inserts in sequence verified entry clones were transferred into destination vectors using LR Clonase™ II following the manufacturer's instructions. pEGFP-C1 (Clontech) and pTriEx™-4 (Novagen) were the main destination vector used. These have previously been converted to GATEWAY® compatible vectors by inserting a GATEWAY® RfC.1 reading frame cassette in the original multiple cloning site of each vector. Newly made GATEWAY® compatible vectors were grown and selected in *E. coli* DB3.1 strain that carries a special resistance to the toxic *ccdB* gene present in the reading frame cassette. Gene inserts for pTriEx™-4 also contained an additional TEV protease recognition site linker at the N-terminus and a C-terminus myc tag. The final reaction mix was transformed into ultracompetent DH5α cells (section 2.1.3.5).

2.1.3.3. Cloning by restriction digest and ligation

pmCherry-C1 gene constructs (Table 2.1) were cloned using the traditional method of restriction digest and ligation. KOD polymerase (section 2.1.2.1) was used to generate insert fragments with specific restriction site sequences at the 5' (BglII) and 3' (HindIII) ends. The gel purified DNA and vector were cut with BglII and HindIII (New England Biolabs) in double digest reactions to generate complementary overhangs. The digested DNA was gel purified (section 2.1.1.2).

Vector and insert were then ligated using T4 DNA ligase (New England Biolabs) in a 1:4 molar ratio of vector to insert. The ligation reaction was prepared following the manufacturer's instructions and incubated overnight at 16 °C. The final reaction mix was diluted 5x with sterile water before transformation into ultracompetent XL10 Gold cells. The constructs were verified by sequencing (section 2.1.4).

2.1.3.4. In-Fusion™ cloning

pOPINs (Oxford Protein Production Facility) gene constructs (Table 3.2) were cloned using In-Fusion™ technology (Clontech). This is a high throughput and universal method that joins any DNA fragments with 15 bases of homology at their linear ends. Vectors were linearised using the appropriate restriction enzymes and DNA inserts with compatible ends were generated using KOD polymerase (section 2.1.2.1). These were mixed with the In-Fusion™ enzyme according to the manufacturer's instructions. The final reaction mix was transformed into ultracompetent XL10 Gold cells (section 2.1.3.5).

Table 2.3 Competent cells

Strains *E. coli*	Purpose	Genotype
DH5α	Gateway® cloning	F^- endA1 glnV44 thi-1 recA1 relA1 gyrA96 deoR nupG Φ80d*lacZ*ΔM15 Δ(*lacZYA-argF*)U169, hsdR17(r_K^- m_K^+), λ–
DB3.1	Propagate Gateway® vectors	F- gyrA462 endA1 glnV44 Δ(sr1-recA) mcrB mrr hsdS20(r_B^-, m_B^-) ara14 galK2 lacY1 proA2 rpsL20(Sm^r) xyl5 Δleu mtl1
XL10 Gold	DNA amplification for plasmid preparation General cloning	endA1 glnV44 recA1 thi-1 gyrA96 relA1 lac Hte Δ(mcrA)183 Δ(mcrCB-hsdSMR-mrr)173 tet^R F'[proAB $lacI^qZ$ΔM15 Tn10(Tet^R Amy Cm^R)]
C41(DE3)	Protein expression by IPTG induction	F^- ompT gal dcm $hsdS_B$(r_B^- m_B^-)(DE3) derived from BL21(DE3) with at least one unidentified mutation

2.1.3.5. Transformation of competent cells

1-2 µl of plasmid or reaction mix was added to 25 µl ultra competent cells (Table 2.3) and incubated on ice for 30 min. Competent cells were heat shocked for 30 sec at 42 °C in a water bath then chilled on ice for 2 min. 250 µl of SOC medium [20 g/L tryptone, 5 g/L yeast extract 0.5 g/L NaCl, 20 mM glucose, 10 mM $MgCl_2$, 2.5 mM $CaCl_2$] was

added to the cells and incubated at 37 °C for 1 h in a shaking incubator. 100 µl aliquots were plated on L agar plates containing appropriate antibiotics and incubated overnight at 37 °C.

2.1.4. Verification of constructs by sequencing

Following cloning and transformation, the resulting colonies were first checked for inserted genes by PCR (section 2.1.2.2). Once the insertions were verified, the specific clones were picked and grown in 5 ml cultures for DNA purification and sequencing. For mutagenesis products, individual clones were directly picked, cultured and sequenced. Sequencing was carried out to identify mutants and to ensure no additional mutations, insertions or deletions were introduced.

Each sequencing reaction contained 3 µl BigDye sequencing buffer, 2 µl BigDye Terminator v3.1 sequencing mix (ABI Prism), 1.6 µM forward or reverse primer and 150-500 ng plasmid DNA in a final volume of 12 µl. The temperature cycle was as follows:

96 °C for 1 min
96 °C for 10 sec
50 °C for 5 sec
60 °C for 4 min
} 25 cycles

Free fluorescent nucleotides were removed from the PCR products using the DyeEx™ 2.0 Spin Kit (Qiagen) following the manufacturer's instructions. The purified PCR products were dried on a heat block and the samples were sent to the sequencing laboratory at Source BioScience. DNA sequence alignments were performed using ClustalW2 (http://www.ebi.ac.uk/Tools/msa/clustalw2/) to confirm that the sequence was correct.

All constructs are of human origin and all RASSF5 constructs were derived from the RASSF5C isoform unless otherwise stated (Table 2.1 and 2.2). Other constructs used in this study were available in the lab, these included pTriEx™-4 constructs: RASSF5Δ41myc (aa42-265), RASSF5 SARAH (aa212-265) (Miertzschke et al., 2007), HRasV12, KRasV12, MRasV22, NRasV12 and Rap2BV12 (Bunney et al., 2006). The expression plasmids pXJ40 mycMOAP1 and pcDNA3 HA-DAPK were obtained from Dr Shairaz Baksh (University of Alberta, Edmonton) for a collaborative study.

2.2. Protein expression, purification and analysis

2.2.1. Production of recombinant protein from *E. coli*

2.2.1.1. Expression of recombinant protein

RASSF5 RA, RASSF5 SARAH, MST1 SARAHmyc and the various Ras GTPases were expressed from the pTriEx™-4 vector. Several colonies of freshly transformed C41(DE3) cells were grown in 500 ml pre-warmed 2xYT broth [16 g/L tryptone, 10 g/L yeast extract, 5 g/L NaCl] cultures at 37 °C and 250 rpm until an OD_{595nm} of 0.4. The temperature was lowered to 20 °C and protein expression was induced by addition of 100μM isopropyl 1-thio-β-D-galactopyranoside (IPTG) between OD_{595nm} 0.6 and 1.0. The cultures were grown overnight at 20 °C then pelleted at 3,700 x*g* for 30 min at 4 °C (Allegra® X-15R Centrifuge, Beckman Coulter). Pellets were stored at -20 °C until further processing.

2.2.1.2. Purification of His/S-tagged recombinant proteins

Bacterial pellets from 500 ml cultures were lysed in 25 ml Bacterial Lysis Buffer [25 mM Tris-HCl pH 8.0, 250 mM NaCl, 40 mM imidazole, 10 mM Benzamidine, 100 μg/ml lysozyme] at 4 °C for 30 min with shaking at 100 rpm. Lysis was continued for 1 h following the addition of 1 Kunit of DNase I and 5 ml of 10% (v/v) Triton-X100. The lysate was centrifuged at 4 °C for 1 h at 18,000 rpm in an SS34 rotor (Sorvall) and the supernatant containing the soluble proteins was further processed.

An ÄKTApurifier (GE Healthcare) was used for protein purification. The chromatography was performed at 5 ml/min flow. A 5 ml HisTrap HP column (GE Healthcare) was used to purify His-tagged proteins. The semi-automated purification program included column equilibration with 2 column volumes (CV) of His Buffer A [25 mM Tris-HCl pH 8.0, 500 mM NaCl, 40 mM imidazole, 1 mM Tris(2-carboxyethyl)phosphine (TCEP)] prior to the injection of the supernatant using a 50 ml Superloop. This was followed by 10 CVs of His Buffer A washes and elution of bound proteins with a linear gradient from His Buffer A to His Buffer B [25 mM Tris-HCl pH 8.0, 500 mM NaCl, 500 mM imidazole, 1 mM TCEP] over 5 CVs.

The proteins collected were either immediately further purified by gel filtration chromatography or subjected to TEV protease cleavage to remove the N-terminal His

and S tags (Table 2.5). For the latter, 10-15 ml of eluted protein were mixed with 100 µl of 8 mg/ml TEV protease in SnakeSkin Dialysis tubing (Thermo Scientific) with the appropriate molecular weight cut off. The tubing was placed in Dialysis Buffer [25 mM Tris-HCl pH 8.0, 150 mM NaCl, 10 mM imidazole, 1 mM TCEP] and stirred at 4 °C for 16-72 h.

A 5 ml HisTrap HP column was used to remove the TEV protease, cleaved His and S tags and any proteins that bound non-specifically to the column. It was equilibrated in Dialysis Buffer and the dialysed sample was loaded. The program used for this purification step is similar to the first step with the exception that the cleaved protein flowing through the column was collected whilst His Buffer B was used to elute the waste. The collected flow-through was purified in a final step of gel filtration (section 2.2.1.3).

2.2.1.3. Gel filtration chromatography

Gel filtration was used as a final step of purification for all proteins expressed in this study. Proteins are separated based on their sizes and polypeptide aggregates are also removed. Superdex 200 26/60 columns (GE Healthcare) were used to purify proteins expressed in *E. coli* and Freestyle™ 293F (section 2.2.2.1).

The chromatography was performed at a 4 ml/min flow. The column was equilibrated with 1 CV of Gel Filtration Buffer [25 mM Tris-HCl pH 8.0, 150 mM NaCl, 1 mM TCEP] before injecting the protein sample, which was eluted in 1 CV of the same buffer. The protein was collected based on peak fractionation monitored by A_{280nm} and was concentrated to 10-20 mg/ml using Vivaspin 20 centrifugal concentrators (Sartorius Stedim Biotech) with the appropriate molecular weight cut off. Protein concentrations were measured using NanoDrop 2000c (Thermo Scientific) by inputting the theoretical protein molecular weight and molar extinction coefficient. Aliquots of protein were snap frozen in liquid nitrogen and stored at -80 °C.

2.2.1.4. Buffer exchange of purified protein

Proteins used for mass spectrometry (MS) were buffer exchanged into MS buffer [150 mM sodium acetate, 0.5 mM dithiothreitol (DTT), pH 8.0]. These included TEV-cleaved RASSF5 RA, RASSF5 SARAH and MST1 SARAHmyc. Two methods were used for the buffer exchange step.

For quick buffer exchanges, Micro Bio-Spin® 6 chromatography columns (BioRad) were used. The columns were equilibrated and washed using the MS buffer and protein samples were loaded and eluted following the manufacturer's instructions.

An Ettan™ LC system (GE Healthcare) was used for a more efficient buffer exchange and to remove any aggregates from freeze-thaw cycles. This step is in essence a small scale gel filtration. The chromatography was performed at a 0.1 ml/min flow rate. A Superdex 200 10/300 GL column was equilibrated with 1 CV of MS buffer. 40 µl of concentrated protein samples were injected consecutively into the system from a 96-well plate using the autosampler. Each sample was eluted in 1 CV of MS buffer and collected as in gel filtration. The appropriate peak fractions were combined and concentrated to approximately 10-20 µM as described (section 2.2.1.3). Protein concentrations were measured and the samples were used immediately for MS.

2.2.2. Production of recombinant protein from mammalian cells

2.2.2.1. Expression of recombinant protein in Freestyle™ 293F

Freestyle™ 293F cells were the eukaryotic system of choice for expression of full length MST1 and MST2 and their respective kinase domain mutants K59R and K56R in the pTriEx™-6 vector (Table 2.1 and 2.2). Cells were grown and maintained as described in section 2.4.2, and transfected as described in section 2.5.1.3. A total volume of 1 L culture was used to express each recombinant protein. 72 h after transfection, the cells were pelleted by centrifugation at 2000 x*g* for 15 min. The pellets were snap frozen in liquid nitrogen and stored at -80 °C until further processing.

2.2.2.2. Purification of His/StrepII-tagged proteins

Cell pellets from a total of 1L cultures were resuspended in 25 ml of 293F Lysis Buffer [25 mM Tris-HCl pH 8.0, 250 mM NaCl, 40 mM imidazole, 10 mM benzamidine, 1 EDTA free protease inhibitor tablet (Roche)]. Cells were lysed by constant agitation on a rotating wheel at 4 °C for 30 min. Lysis was continued for 1 h following the addition of 1 Kunit of DNaseI and 5 ml of 10% Triton-X100 (v/v). Lysed material was clarified by centrifugation at 4°C for 1 h at 18,000 rpm in an SS34 rotor (Sorvall).

The supernatant was first processed by His affinity chromatography as described in section 2.2.1.2. The N-terminus 2xStrepII, SUMO*, myc tags and C-terminus 10xHis

tag were left intact and the eluted proteins were immediately applied to a 5 ml StrepTactin column (GE Healthcare). The column was washed with Streptactin Buffer A [50 mM Tris-HCl pH 8.0, 150 mM NaCl] to remove non-specifically bound contaminants. The recombinant proteins were eluted from the column using Streptactin Buffer B [50 mM Tris-HCl pH 8.0, 150 mM NaCl, 5 mM d-Desthiobiotin (Sigma)]. Eluted proteins were further purified by gel filtration using the standard Gel Filtration Buffer, concentrated, quantified and stored (section 2.2.1.3).

2.2.3. Protein analysis

2.2.3.1. SDS-PAGE and Coomassie staining

Discontinuous polyacrylamide gels were made according to the method of Laemmli (Laemmli, 1970). Polymerised gels were placed in running tanks (BioRad Miniprotean 3) with running buffer [25 mM Tris-HCl, 192 mM glycine, 0.1% SDS, pH 8.3]. Protein samples were mixed with 4x sample buffer [62.5 mM Tris-HCl pH 6.8, 2% SDS, 25% glycerol, 0.01% bromophenol blue, 0.72 M β-mercaptoethanol] in ratios between 1:1 and 3:1. These were incubated on a 95 °C heat block for 5 min. Between 10 and 50 µg of each sample were loaded and electrophoresis carried out between 150 and 200 V. Electrophoresis was stopped when the dye front reached the end of the gel.

Quick Coomassie Stain (Generon) was used to stain acrylamide gels following SDS-PAGE. The gels were rinsed in water then covered in 25 ml of the stain and left incubating on a rocker for 1 h at room temperature. These were destained in water for 30 min then photographed using a G:BOX (Syngene).

2.2.3.2. Western blotting

Proteins were analysed by western blotting according to the method of Towbin et al. (1979). Proteins resolved by SDS-PAGE were transferred to a PVDF membrane (Hybond-P, GE Healthcare) overnight at 30 V, 4 °C in transfer buffer [25 mM Tris-HCl, 192 mM glycine, 20% methanol, pH 8.3]. Following the transfer, non-specific binding to the membrane was blocked by incubation in blocking buffer [25 mM Tris-HCl pH 7.5, 144 mM NaCl, 0.2% Tween 20, 5% (w/v) non-fat milk (Sigma)] for 30 min at room temperature. Primary antibodies were diluted in blocking buffer (Table 2.4) and incubated with the membrane for 2 h at room temperature. The membrane was washed twice for 10 min in TBS-Tween [25 mM Tris-HCl, 144 mM NaCl, 0.1% Tween, pH 7.5]

before the addition of horseradish peroxidase-conjugated secondary antibody (GE Healthcare) diluted 1:4000 in blocking buffer. Following 1 h of incubation, the membrane was washed twice for 10 min in TBS-Tween then once for 10 min in TBS. ECL Prime Western Blotting Detection Reagent (GE Healthcare) was used for detection of immunoreactive proteins with BioMax XAR (Kodak) or RX (FujiFilm) films.

Table 2.4 Primary antibodies used for western blotting

Antibody	Antibody type	Company	Dilution
GAPDH (D-6)	Mouse monoclonal	Santa Cruz	1:25,000
GFP (B-2)	Mouse monoclonal	Santa Cruz	1:2,500
HA (12CA5)	Mouse monoclonal	In-house hybridoma provided by Dr Shairaz Baksh	1:400
Myc (9E10/12)	Mouse monoclonal	In-house	1:2,500
TBK1 (M-375)	Rabbit polyclonal	Santa Cruz	1:1,000
TNF-R1 (H-271)	Rabbit polyclonal	Santa Cruz	1:500
tRFP	Rabbit polyclonal	Evrogen	1:2,000

2.3. Specific protein constructs

Table 2.5 shows all the protein constructs used in this study. The table also includes notes about their specific purification and further application purposes. All proteins were shock frozen in liquid nitrogen in the same buffer they were purified by gel filtration indicated in the table and stored at -80 °C. Proteins used in this study that were already available in the laboratory were c-Raf RBD, RalGDS RA, PLCε RA2 and RASSF5Δ52.

2.4. Cell culture and cell lines

2.4.1. Adherent cells

COS-7 monkey kidney fibroblast-like cells, human A549 lung adenocarcinoma and HCT116 colon carcinoma cells were cultured in Dulbecco's Modified Eagle's Medium (DMEM) (Invitrogen) supplemented with 10% foetal bovine serum (FBS) and 0.5 mM L-glutamine. Cells were grown as a monolayer at 37 °C in 5% CO_2. When confluent, the cells were removed from the flask using 0.05% trypsin-EDTA (Invitrogen) and split 1:10.

Table 2.5 Recombinant proteins and their purification

Plasmid	Purification	Protein	Gel Filtration	Application
pTriEx™-6				
MST1 FL	His affinity, StrepTactin purification, gel filtration	2xStrepII/SUMO*/myc MST1-10xHis	25mM Tris-HCl pH8.0, 150mM NaCl, 1mM TCEP	Immunoprecipitation
MST1 K59R	His affinity, Streptactin purification, gel filtration	2xStrepII/SUMO*/mycMST1 K59R-10xHis	25mM Tris-HCl pH8.0, 150mM NaCl, 1mM TCEP	Immunoprecipitation
MST2 FL	His affinity, Streptactin purification, gel filtration	2xStrepII/SUMO*/mycMST2-10xHis	25mM Tris-HCl pH8.0, 150mM NaCl, 1mM TCEP	Immunoprecipitation
MST2 K56R	His affinity, Streptactin purification, gel filtration	2xStrepII/SUMO*/mycMST2 K56R-10xHis	25mM Tris-HCl pH8.0, 150mM NaCl, 1mM TCEP	Immunoprecipitation
pTriEx™-4				
RASSF5 RA (mouse NORE1A_199-358)	His affinity purification, gel filtration	6xHis/S-RASSF5 RA	25mM Tris-HCl pH8.0, 150mM NaCl, 1mM TCEP	*In vitro* pull-down
	His affinity purification. TEV cleavage, gel filtration	RASSF5 RA	150mM Sodium Acetate, 0.5mM DTT	Mass spectrometry
RASSF5 SARAH	His affinity purification, gel filtration	6xHis/S-RASSF5 SARAH	25mM Tris-HCl pH8.0, 150mM NaCl, 1mM TCEP	*In vitro* pull-down
	His affinity purification. TEV cleavage, gel filtration	RASSF5 SARAH	150mM Sodium Acetate, 0.5mM DTT	Mass spectrometry
MST1 SARAH	His affinity purification, gel filtration	6xHis/S-MST1SARAHmyc	25mM Tris-HCl pH8.0, 150mM NaCl, 1mM TCEP	*In vitro* pull-down
	His affinity purification, TEV cleavage, gel filtration	MST1 SARAHmyc	150mM Sodium Acetate, 0.5mM DTT	Mass spectrometry
HRasV12	His affinity purification, gel filtration	6xHis/S-HRasV12	25mM Tris-HCl pH8.0, 150mM NaCl, 1mM TCEP	*In vitro* pull-down
KRasV12	His affinity purification, gel filtration	6xHis/S-KRasV12	25mM Tris-HCl pH8.0, 150mM NaCl, 1mM TCEP	*In vitro* pull-down
MRasV22	His affinity purification, gel filtration	6xHis/S-KRasV12	25mM Tris-HCl pH8.0, 150mM NaCl, 1mM TCEP	*In vitro* pull-down
NRasV12	His affinity purification, gel filtration	6xHis/S-NRasV12	25mM Tris-HCl pH8.0, 150mM NaCl, 1mM TCEP	*In vitro* pull-down
Rap2BV12	His affinity purification, gel filtration	6xHis/S-Rap2BV12	25mM Tris-HCl pH8.0, 150mM NaCl, 1mM TCEP	*In vitro* pull-down

2.4.2. Suspension cells

Freestyle™ 293F cells were grown in suspension on a platform shaker in a humidified 37 °C CO_2 incubator (Infors) with rotation at 130 rpm. The cells were maintained between 4 x 10^5 and 3 x 10^6 cells/ml in a volume of 250 ml in 1 L culture flasks using Freestyle™ 293F Expression Medium (Invitrogen).

2.4.3. Frozen stocks

Adherent and suspension cells were frozen at a concentration of 1 x 10^6 in DMEM containing 5% DMSO and 1 x 10^7 cells/ml in Freestyle 293F Expression Medium containing 5% DMSO respectively. Cells were frozen slowly in cryo-vials in a freezing box at -80 °C overnight and transferred to liquid nitrogen.

2.5. Expression of exogenous DNA in mammalian cells

2.5.1. Transient transfection

2.5.1.1. Electroporation

COS-7 cells were transfected by electroporation using the Nucleofector™ 2b Device (Lonza). For each transfection, 100 µl of electroporation buffer [140 mM KCl, 8 mM NaCl, 0.88 mM $MgSO_4$, 2.97 mM Na_2HPO_4, 1.06 mM NaH_2PO_4, 0.5% BSA, pH 7.4] were mixed with 4-5 µg of DNA construct or a total of 8 µg of two DNA constructs for co-transfection. 1.2 x 10^6 cells were pelleted and resuspended in the buffer:DNA mix. The cell suspension was transferred to an electroporation cuvette and electroporated following the manufacturer's instructions. This was diluted with 500 µl normal medium (DMEM, 10% FBS, 0.5 mM L-Glutamine) and 3 x 10^4 cells were seeded per well in a 96-well glass-bottom plate.

2.5.1.2. Polyethylenimine (PEI)

For large scale protein expression, 250 ml of 293F cells were seeded at around 0.6 - 0.7 x 10^6 cells/ml a day prior to transfection for the cell density to reach 1.0 x 10^6 cells/ml at the time of transfection. At a smaller scale, 20 ml or 30 ml of 293F cells were seeded as described above. For transfection, the cells were mixed with plasmid DNA:PEI (~25kDa branched) (Sigma) complexes prepared as follows. 10 ml of OptiPRO SFM™

(Invitrogen) supplemented with 4 mM L-Glutamine were mixed with 312 µg DNA and a volume of PEI (1 mg/ml stock in deionised water) that is 1.5 times the mass ratio of the amount of DNA. 1.2 ml or 800 µl of supplemented OptiPRO SFM™ and a total of 37.5 µg or 25 µg DNA were used for small scale 30 ml and 20 ml transfections respectively. The transfection mix was incubated for 15 min at room temperature before it was added to the 293F cells. The cells were incubated at 37 °C for 72 h with shaking and then pelleted as described in section 2.2.2.1.

2.5.1.3. DharmaFECT

siRNA studies were performed by transfecting A549 and HCT116 using the reverse transfection method in a 96-well plate format. The cells were cultured to 90% confluency on the day of transfection and harvested using trypsin. Mix A contained 25 nM siRNA in a total volume of 15 µl Hank's Balanced Salt Solution (HBSS). Mix B contained 0.45 µl DharmaFECT (Thermo Scientific) diluted in a total volume of 45 µl HBSS. Mix A was added to Mix B and transferred onto a black 96-well plate. This was incubated for 30 min at room temperature and 7 x 10^3 cells were added to the siRNA:DharmaFECT complex in a total volume of 100 µl DMEM. Each set of transfections was performed in triplicates. The cells were incubated at 37 °C for 72 h before further treatment.

2.5.2. Protein analysis of cell lysates

For 1 L transfected 293F cultures, 1 ml aliquots were pelleted as described in section 2.2.2.1, washed in PBS and transferred into a 1.5 ml centrifuge tube before a final centrifugation step at 2,000 x*g* for 10 mins. The cells were lysed directly in 100 µl 4x sample buffer and prepared as described in section 2.2.3.1 for SDS-PAGE. For small scale transfected 293F cells, the cell pellets were lysed as described in section 2.6.1.2 and 2.6.2. A sample of each lysate was mixed 1:1 with 4x sample buffer. All samples were subjected to SDS-PAGE and western blotting.

2.6. Characterisation of protein-protein interaction

2.6.1. *In vitro* pull-down using pure proteins or cell lysates

The *in vitro* pull-down assay was used to test protein interactions between RASSF and different Ras small GTPase family members (section 2.6.1.1 and 2.6.1.2) and MST kinases (section 2.6.1.2).

2.6.1.1. Interaction between Ras small GTPases and isolated RA domains

Pull-down assays were performed using two slightly different approaches. The first method used immobilised S-tagged Ras GTPase and the second method used immobilised GST-tagged RA domains.

For pull-downs using S-tagged Ras GTPases, 40 µl of S-protein agarose (Novagen) were washed once in 0.5 ml Nucleotide Loading Buffer (NLB) [50 mM Tris-HCl pH 8.0, 15 mM EDTA, 1 mM TCEP] and loaded with 50 µg of purified S-tagged Ras small GTPases (Table 2.5). This was incubated for 30 min at room temperature and the beads were washed once with 0.5 ml NLB to remove unbound small GTPase. In order to force the GTPases into their respective active (GTP-bound) or inactive (GDP-bound) state, 0.5 ml NLB containing 1 mM GTP or GDP respectively was added to the beads and incubated for 10 min at room temperature. The reaction was stopped by addition of 20 mM $MgCl_2$ and excess nucleotides were removed. The beads were then incubated with 100 µg of purified RASSF5 RA (Table 2.5) and existing RA domain proteins in the lab (section 2.3) in 0.5 ml Binding Buffer (BB) [50 mM Tris-HCl pH 8.0, 150 mM NaCl, 1 mM TCEP, 1% (v/v) Triton X-100, 10 mg/ml BSA] for 30 min at room temperature. The beads were then washed in 0.5 ml Wash Buffer [25 mM Tris-HCl pH 8.0, 150 mM NaCl, 1 mM TCEP, 1% (v/v) Triton X-100].

For pull-downs between purified GST-tagged RA domain and untagged Rap2BV12 proteins, 40 µl of prewashed Glutathione Sepharose™ 4B beads (GE Healthcare) were used to immobilise the RA domain proteins in 0.5 ml NLB. This was incubated for 30 min at room temperature. The beads were washed in 0.5 ml NLB to remove unbound RA domain proteins. Purified Rap2BV12 was loaded with GDP or GTP as described above in a separate reaction and added to the RA domain-loaded beads in 0.5 ml BB. These were incubated for 30 min at room temperature and washed as above.

Finally, the beads were mixed with 20 µl 4x sample buffer and the eluted samples were subjected to SDS-PAGE and western blotting.

2.6.1.2. Interaction between Ras small GTPases and full length RASSF

Full length RASSFs, which could not be purified, were each expressed in 30 ml of 293F cell cultures transfected with 37.5 µg of pEGFP-C1 RASSF constructs and harvested as described in sections 2.2.2.1 and 2.5.1.3. The cell pellets were lysed in Lysis Buffer [25 mM Tris-HCl pH 7.5, 150 mM NaCl, 0.1% (v/v) NP-40, 1 mM TCEP, 1 EDTA free protease inhibitor tablet (Roche)]. Cell lysates were clarified by centrifugation at 21,000 x*g* for 15 min.

Various S-tagged Ras GTPases were immobilised and loaded with GDP or GTP as described in section 2.6.1.1. The beads were then incubated with 2 mg of each cell lysate in a total volume of 0.5 ml modified Binding Buffer [50 mM Tris-HCl pH 8.0, 150 mM NaCl, 1 mM TCEP, 0.1% (v/v) Triton X-100, 10 mg/ml BSA]. Following 1 h incubation at 4 °C, the beads were washed three times in 0.5 ml Lysis Buffer. The samples were then eluted in 20 µl 4x sample buffer and subjected to SDS-PAGE and western blotting.

2.6.1.3. Dimerisation between RASSF and MST kinases

Fifty µg of purified S-tagged RASSF5 SARAH were immobilised on 40 µl of S-protein agarose in 0.5 ml PBS. This was then incubated with 50 µg of purified MST1 SARAHmyc for 1 h with constant agitation at room temperature. The beads were washed three times in PBS and the bound proteins were eluted in 20 µl 4x sample buffer and subjected to SDS-PAGE.

2.6.2. Co-immunoprecipitation (Co-IP)

20 ml of 293F cell cultures were transfected with a total of 25 µg of DNA constructs as described in section 2.5.1.3. These were either single transfections of pEGFP-C1 RASSF, co-transfections of equal concentrations of pEGFP-C1 RASSF5 SARAHmyc with pTgFRP-T MST1 or MST1 SARAH, or various combinations of pEGFP-C1 RASSF with other constructs (Table 2.6).

Table 2.6 DNA constructs and concentrations for co-transfection of 293F cells

pEGFP-C1 RASSF1-10	12 µg	14 µg	14 µg	12.5 µg	12 µg
pTriEx™-4 RASSF5Δ41myc	13 µg	-	-	-	-
pTriEx™-6 mycMST1 K59R	-	11 µg	-	-	-
pTriEx™-6 mycMST2 K56R	-	-	11 µg	-	-
pXJ40 mycMOAP1	-	-	-	12.5 µg	-
pcDNA3 HA-DAPK	-	-	-	-	13 µg

72 h post-transfection, 20 ml cultures of cells co-transfected with pXJ40 mycMOAP1 and pEGFP-C1 RASSF or only pEGFP-C1 RASSF were split into two 10 ml aliquots. One set of the co-transfected cultures was treated with TNFα (PeproTech) at a final concentration of 50 ng/ml. One set of the singly transfected cultures was treated with either TNFα as above or lipopolysaccharide (LPS) from *Salmonella minnesota* R595 (Re) (Enzo Life Sciences) at a final concentration of 2 µg/ml. The cells were harvested 3 h after treatment. Cell pellets were lysed in 0.8 ml CellLytic™ M Lysis Reagent (Sigma) and clarified by centrifugation at 21,000 x*g* for 15 min at 4 °C.

Co-IP of myc-tagged proteins was performed using the Anti-c-Myc Immunoprecipitation kit (Sigma). In co-IP assays using purified proteins of full length or kinase-dead myc-tagged MST (see Table 2.5), 50 µg of each purified protein were immobilised on 20 µl of anti-c-myc agarose affinity gel antibody in SigmaPrep™ spin columns (Sigma) and incubated with 2 mg of cell lysate for 1 h at 4 °C with constant agitation. For co-IP assays using only cell lysates, 2 mg of each cell lysate were directly added to 20 µl of anti-c-myc agarose affinity gel antibody and incubated as above.

For co-IP of other proteins, 2 µg of anti-TNF-R1, anti-TBK1 or anti-HA antibody (see Table 2.4) were mixed with 1 mg of cell lysate in a SigmaPrep™ spin column (Sigma). Following overnight mixing at 4 °C, 25 µl of protein A (for polyclonal antibodies) or protein G (for monoclonal antibodies) agarose (Roche) were added to the antibody-lysate mixture and incubated with constant agitation for a further 2 h at 4 °C.

For all reactions, the beads were washed three times with PBS or PBS containing 0.01% (v/v) Triton-X100 and bound proteins were eluted in 80 µl 4x sample buffer then subjected to SDS-PAGE and western blotting.

2.6.3. Förster Resonance Energy Transfer (FRET)

FRET was used as a means of measuring protein-protein interactions. It entails exciting the "donor" fluorophore, resulting in a transfer of the excitation energy to an appropriate "acceptor" fluorophore. This transfer of energy is non-radiative and occurs over an extremely small radius; therefore, FRET efficiency is dependent on several factors. First, the distance between the donor and acceptor has to be within a 10 nm range to facilitate the short distance non-radiative energy transfer (Jares-Erijman and Jovin, 2006). This also requires the spectral overlap of the donor emission and acceptor excitation spectra, and the correct relative orientations of their respective dipole moments. In the presence of an acceptor and where the above conditions are fulfilled, FRET causes a decay in the donor lifetime, which is the signal being measured. This allows for the detection of interaction between the appropriately labelled proteins.

The FRET data are obtained using a high throughput fluorescence lifetime imaging (FLIM) automated multiwell plate reader developed in-house by our collaborators in the Photonics Group at Imperial College London (Figure 2.1A) (Alibhai et al., 2013, Kumar et al., 2011). A wide-field time-gated imaging and laser scanning TCSPC (Time-Correlated Single Photon Counting) microscope is linked to the automated Nipkow FLIM multiwell plate reader, which is based on a commercial plate reader (IN Cell Analyser 1000, GE Healthcare). The GOI (gated optical image intensifier) produces intensity images acquired at different precise time points for a few seconds (Figure 2.1B). These are used to reconstruct the fluorescence decay of the donor fluorophore, which is analysed with exponential decay functions. The technical details of the microscope set up and image acquisition are described by Kumar et al. (2011).

In this study, the proteins of interest were tagged with the "donor" GFP or "acceptor" mCherry by cloning their gene encoding DNA into the vectors pEGFP-C1 and pmCherry-C1 respectively (sections 2.1.3.2 and 2.1.3.3). COS-7 cells were transfected with 4-5 µg of pEGFP-C1 RASSF plasmids alone or together with 3.8 µg of pmCherry-C1 MST1 or MST1 SARAH or 3.5 µg of unlabelled KRasV12 by electroporation and seeded on 96-well glass-bottom plates as described in section 2.5.1.1. Following overnight incubation in a 37 °C incubator, transfected cells were washed in PBS, fixed in 4% formaldehyde in PBS for 15 min and washed twice in PBS to remove the formaldehyde.

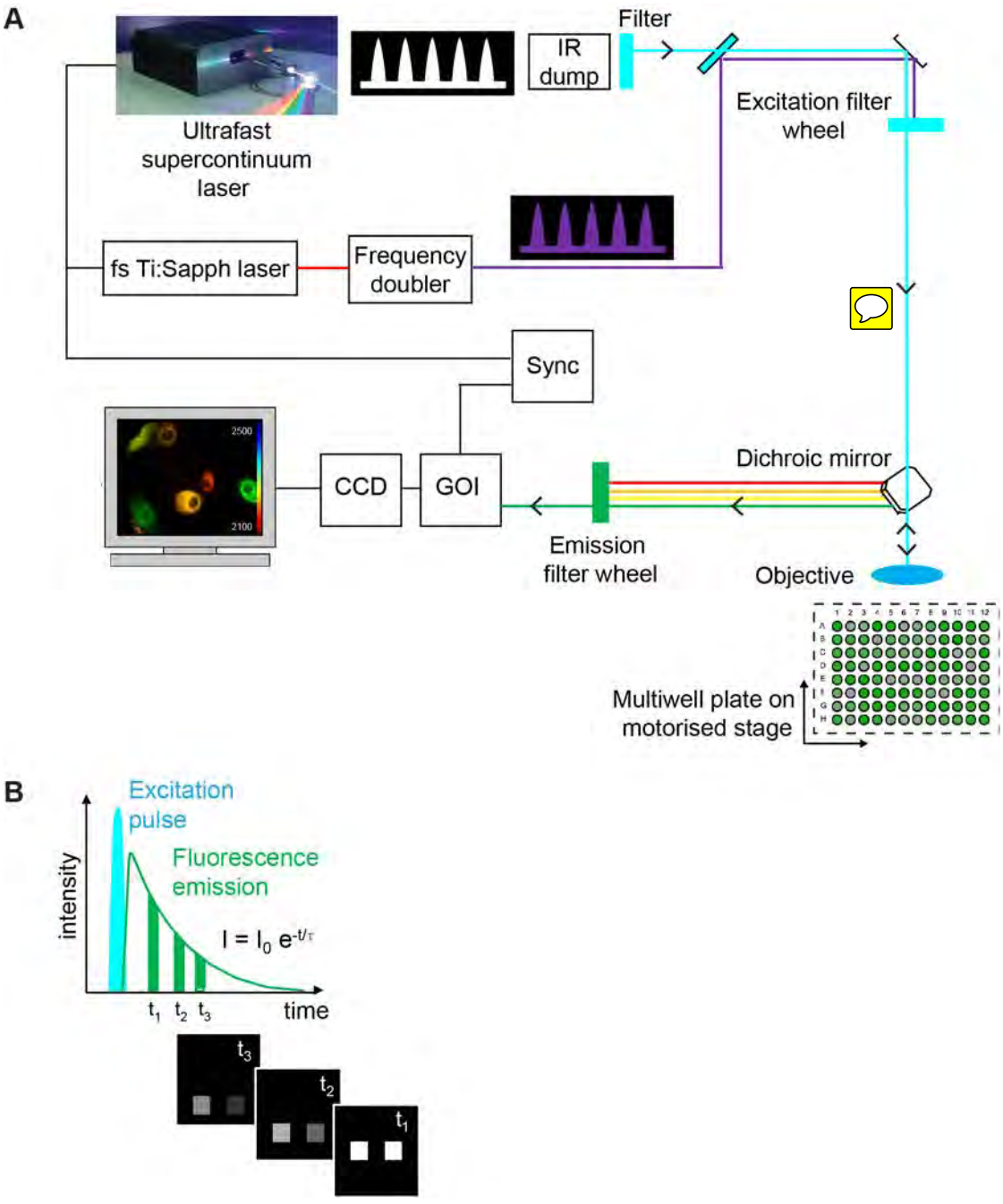

Figure 2.1 The FLIM system

(A) Schematic of the high throughput automated FLIM multiwell plate reader and microscope setup. Adapted from Alibhai et al. (2013) and Kumar et al. (2011). (GOI, gated optical image intensifier; CCD, camera; Sapph, sapphire laser)

(B) The GOI acts as a very fast electronic shutter that is synchronized with the laser pulses and opens at various delays after excitation to produce a series of different intensity images.

The cells were imaged in PBS by our collaborator, Dr Anca Margineanu (Photonics Group, Imperial College), using the FLIM multiwell plate reader and microscope described above and a 10x objective. Ten fields of view (FOV) per well, each consisting at least five cells, were acquired with five time gates and an exposuretime of typically 1 s per gate for the donor (GFP). The data were then analysed by Dr Anca Margineanu using an in-house segmentation and global fitting software, FLIMfit (Warren et al., 2013), whereby convolution and background correction were applied in the monoexponential analysis of the GFP donor lifetime.

2.6.4. Mass spectrometry (MS)

Protein samples (RASSF5 SARAH and MST1 SARAHmyc) were buffer exchanged into 150 mM ammonium acetate as described in section 2.2.1.4. For the mixing experiment, equimolar MST1 SARAHmyc and RASSF5 SARAH were incubated for 1 h at 4 °C prior to MS analysis. The protein samples were given to Jun Yan (Thalassinos Lab, ISMB, UCL) for MS analysis. Mass spectrometry experiments were carried out on a first-generation Synapt HDMS (Waters Corp., Manchester, UK) Quadrupole-TOF (time of flight) mass spectrometer (Pringle et al., 2007). 2.5 µl aliquots of the protein sample of 15 µM in concentration were introduced to the mass spectrometer by means of nano-electrospray ionisation using gold-coated capillaries prepared in-house. The instrument was mass calibrated using a 33 mM solution of Cesium Iodide in 250 mM ammonium acetate. Typical instrumental parameters were as follows: capillary voltage 1.0 kV, cone voltage 50 V, trap energy 6 V, transfer energy 4 V, bias voltage 2.0 V, and trap pressure 8.6e^-3 mbar.

2.7. Cell viability assay

Cell viability assays were performed using CellTitre-Blue® (Promega), which provides a fluorometric method to estimate the number of viable cells present in a multiwell plate. The metabolic capacity of cells, an indicator of cell viability, is measured using the indicator dye resazurin, which is reduced by viable cells into highly fluorescent resorufin. This change is detected by measuring absorbance using excitation and emission wavelengths of 560 nm and 590 nm respectively.

A549 cells were transfected with different siRNAs in black 96-well plates as described in section 2.5.1.3. After 72 h, 20 µl of CellTitre-Blue® (Promega) were added to each well of cells and incubated at 37 °C for 3 h. Absorbance readings were taken using a FLUOstar OPTIMA (BMG Labtech) with the wavelengths above.

2.8. Protein modelling

The sequences encoding the RA domain and SARAH domain were predicted using Prosite. For RASSF1-4 and RASSF6, the RA domain sequences were aligned to the template of RASSF5 RA domain (PDB: 3DDC) excluding the N-terminal subdomain (residues 274−358). The sequences of the predicted RA domain for RASSF7-9 were aligned to c-Raf RBD (PDB: 1GUA). A multiple alignment was first performed for all RA domain sequences using clustalW2 (http://www.ebi.ac.uk/Tools/msa/clustalw2/). Subsequently, the alignments were manually adjusted for each RA domain sequence using Swiss-PdbViewer 4.01 to take into account secondary structural elements of the ubiquitin fold and conserved residues important for interaction with small GTPases. Secondary structure predictions were performed using Psipred secondary structure prediction algorithm (http://bioinf.cs.ucl.ac.uk/psipred/). 3D models generated using the project mode of the Swissmodel server (http://swissmodel.expasy.org/) and their stereochemical quality were evaluated with Procheck (Laskowski et al., 1993).

The SARAH domains of RASSF1-6 were aligned to the template of MST1 kinase SARAH (PDB: 2JO8) using Prosite multiple sequence alignment. The 3D models were constructed using Modeller v9.8 (Eswar et al., 2006). 100 dimer models were calculated and the chosen model for each RASSF represents the best model with the lowest objective function. The models were evaluated and validated as described above and analysis was performed using PyMol and Swiss-PdbViewer.

SARAH domain heterodimer models were generated using the docking approach by our collaborators, Dr Delphine Flatters and Dr Fernando Rodriguez-Lima (Université Paris Diderot). Docking programs Hex (http://hexserver.loria.fr/index.php) and ClusPro (http://nrc.bu.edu/cluster) were used for rigid body docking and to run simulations of the heterodimers consisting of the monomer structures of MST1 (PDB: 2JO8) and the RASSF SARAH homology models from above (Comeau et al., 2004, Kozakov et al.,

2010, Macindoe et al., 2010, Ritchie and Kemp, 2000). Each run generated 100 or more solutions that were ranked by cluster sizes and the top two ranked models were selected. The results were analysed using naccess (http://www.bioinf.manchester.ac.uk/naccess/), which calculated the size of the dimer interfaces (Equation 1) and the difference in solvent accessibility per residue (ΔASA) in the dimeric structure and in each individual monomer (Equation 2 and 3).

Equation (1)

$$\text{Interface size} = [ASA_{tot}\ (\text{chA monomer}) + ASA_{tot}\ (\text{chB monomer})] - ASA_{tot}\ (\text{dimer})$$

Equation (2)

$$\Delta ASA_A = ASA_{res\_i}\ (\text{chA free monomer}) - ASA_{res\_i}\ (\text{chA in dimer})$$

Equation (3)

$$\Delta ASA_B = ASA_{res\_i}\ (\text{chB free monomer}) - ASA_{res\_i}\ (\text{chB in dimer})$$

where ASA_{tot} is total ASA and ASA_{res_i} is ASA of residues involved in interaction. The differences in ASA are indications of the involvement of specific residues in the dimerisation interface.

3 The RASSF RA domain and Ras interaction

3.1. Introduction

As mentioned in the Introduction chapter, all ten members of the RASSF family share a common RA domain, which makes them potential Ras effectors that could be involved in various biological pathways regulated by Ras. As the *RAS* genes are mutated in up to 30% of human tumours (Pylayeva-Gupta et al., 2011), the RASSF RA domain and its ability to interact with Ras GTPases carry particular importance in determining the role of the various RASSF members in cancer.

Structures of HRas in both GDP- and GTP-bound forms were first described more than 20 years ago (Wittinghofer and Pai, 1991). These provided significant insights into the biochemistry and molecular properties of Ras and the principles that define all regulatory GTPases. Various other Ras-related GTPases have also since been structurally characterised. These small GTPases consist mainly of the 20-25 kDa G domain, in which variations exist in different subfamilies, including insertions and extensions at the amino or carboxy termini. The Ras proteins have an additional CAAX motif at the C-terminal region, which is post-translationally processed by prenylation, typically farnesylation, and further modifications (Hancock, 2003) (Figure 3.1A). These lipid modifications are important for Ras subcellular membrane targeting and its biological functions (Magee and Seabra, 2005).

The G domain is the core active site in Ras that carries out its function of nucleotide and effector binding, as well as GTP hydrolysis. It has an α/β fold containing a six-stranded β-sheet and five helices located on both sides (Wittinghofer and Pai, 1991), a well-conserved canonical structure with a universal switch mechanism. The main regions of the G domain involved in Ras effector binding are the dynamic switch I and II regions, which cover residues 32-38 and 59-67 respectively (Karnoub and Weinberg, 2008) (Figure 3.1A). Upon GTP hydrolysis, switch I and II undergo conformational changes (Figure 3.1Bi), best described as a loaded-spring mechanism, which consequently results in the dissociation of the effector complex (Wittinghofer and Nassar, 1996). Ras in its GDP-bound state is incompatible with complex formation; therefore,

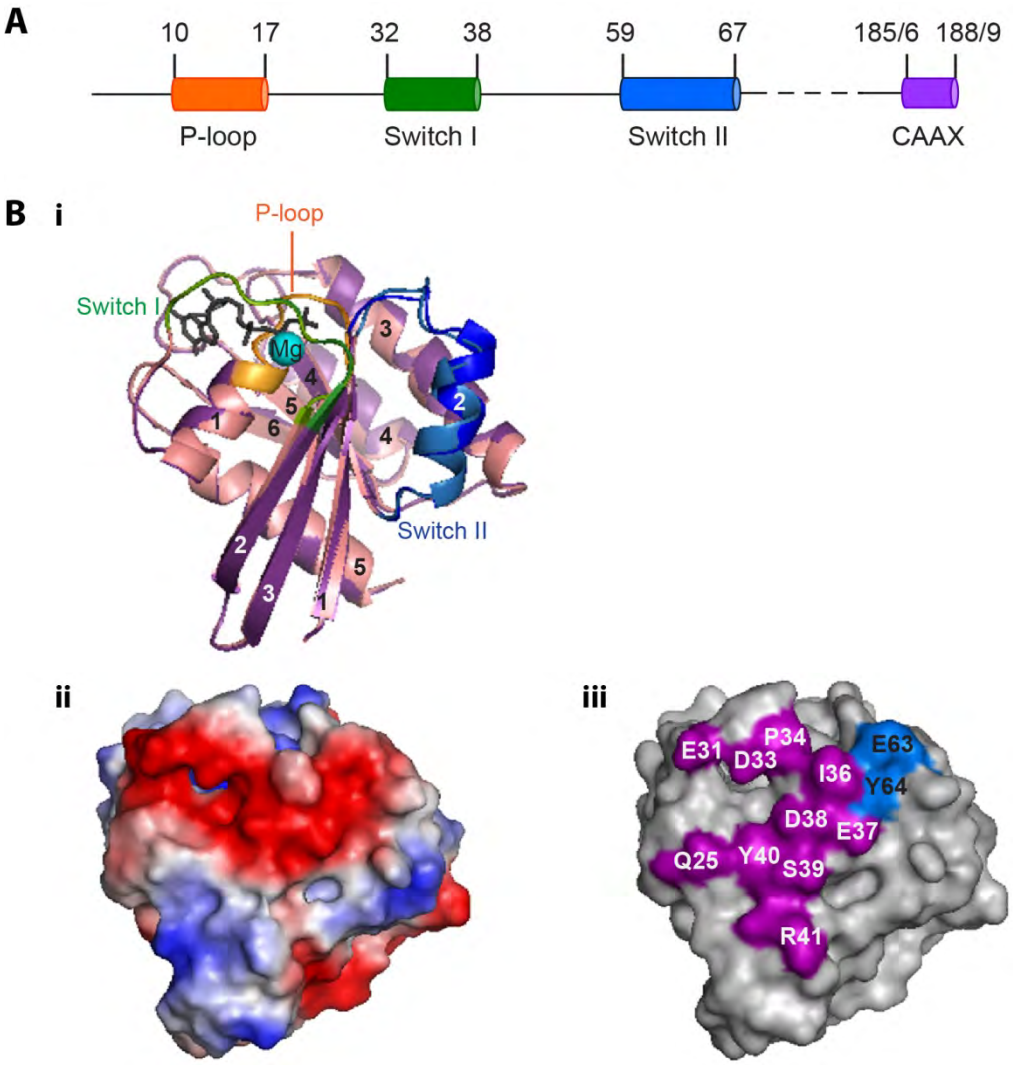

Figure 3.1 Common structural features of the Ras family GTPases

(A) Schematic representation of Ras. The regions important for nucleotide and effector binding are shown and the residue positions are indicated on top.

(B) Crystal structure of HRas. (i) Ribbon representations of HRas in complex with GDP (PDB: 1WQ1, pink) or GTP (PDB: 5P21, purple). Switch I (green) and switch II (blue) for the GDP- and GTP-bound forms are differentiated by light and dark colours respectively. (ii) Surface electrostatic potentials of the Ras effector binding interface, with positive charges in blue and negative charges in red. (iii) The specific residues on the effector binding interface that form direct contact with its effectors. Regions around switch I are in purple, switch II in blue.

only proteins that exhibit GTP-dependent tight binding to Ras are considered true Ras effectors.

The majority of Ras effectors share a common structural feature in the form of the Ras-binding domain (RBD) or RA domain. Both belong to the ubiquitin fold superfamily and there are no structural differences between RA and RBD, which are merely different names used for protein domains with the same ubiquitin fold (Wohlgemuth et al., 2005). From this point onwards they will both be referred to as RA domains. These names imply that the proteins carrying such domain bind to Ras GTPases. However, it has been shown that not all RA domains are true Ras binders and their interaction with Ras has to be determined empirically (Bunney et al., 2006, Kalhammer et al., 1997).

c-Raf was the first identified Ras effector with a putative RA domain. Amongst all the known RA domains to date, the c-Raf, RalGDS, PI3Kγ, PLCε and RASSF5 RA domains are best-characterised (Bunney et al., 2006, Huang et al., 1998, Nassar et al., 1996, Pacold et al., 2000, Stieglitz et al., 2008). They all display the conserved ubiquitin superfold, which is an α/β-roll consisting of five-stranded β-sheet and two helices. The Ras/effector complex is formed via an antiparallel intermolecular β-sheet between switch I of Ras and β2 strand of the canonical ubiquitin fold, a binding mode shared by most Ras effectors (Figure 3.2A) (Herrmann, 2003). Due to this common structural feature, most Ras/effector complexes show very similar binding kinetics with short lifetimes and dissociation constants (K_D) of 20 nM-2 μM (Wohlgemuth et al., 2005). Initial structural analyses only show interaction with Ras switch I (Figure 3.2Bi); however, subsequent structures of full-length PI3Kγ and PLCε RA2 illustrate the involvement of switch II, which appears to have a regulatory effect on the enzymatic functions of PI3Kγ and PLCε (Bunney et al., 2006, Pacold et al., 2000).

RASSF5 RA also makes contact with Ras switch II (Figure 3.2Bii) (Stieglitz et al., 2008). However, this contact is facilitated by a N-terminal subdomain of the canonical RA domain. The subdomain consists of a helix and β-strand (Figure 3.2Aii). It establishes a hydrophobic interface with Ras switch II and is indispensable for Ras interaction. This extension essentially doubles the size of the RASSF5 RA to about 160 residues, making it a unique RA domain. As RASSF5 is a non-enzymatic Ras effector,

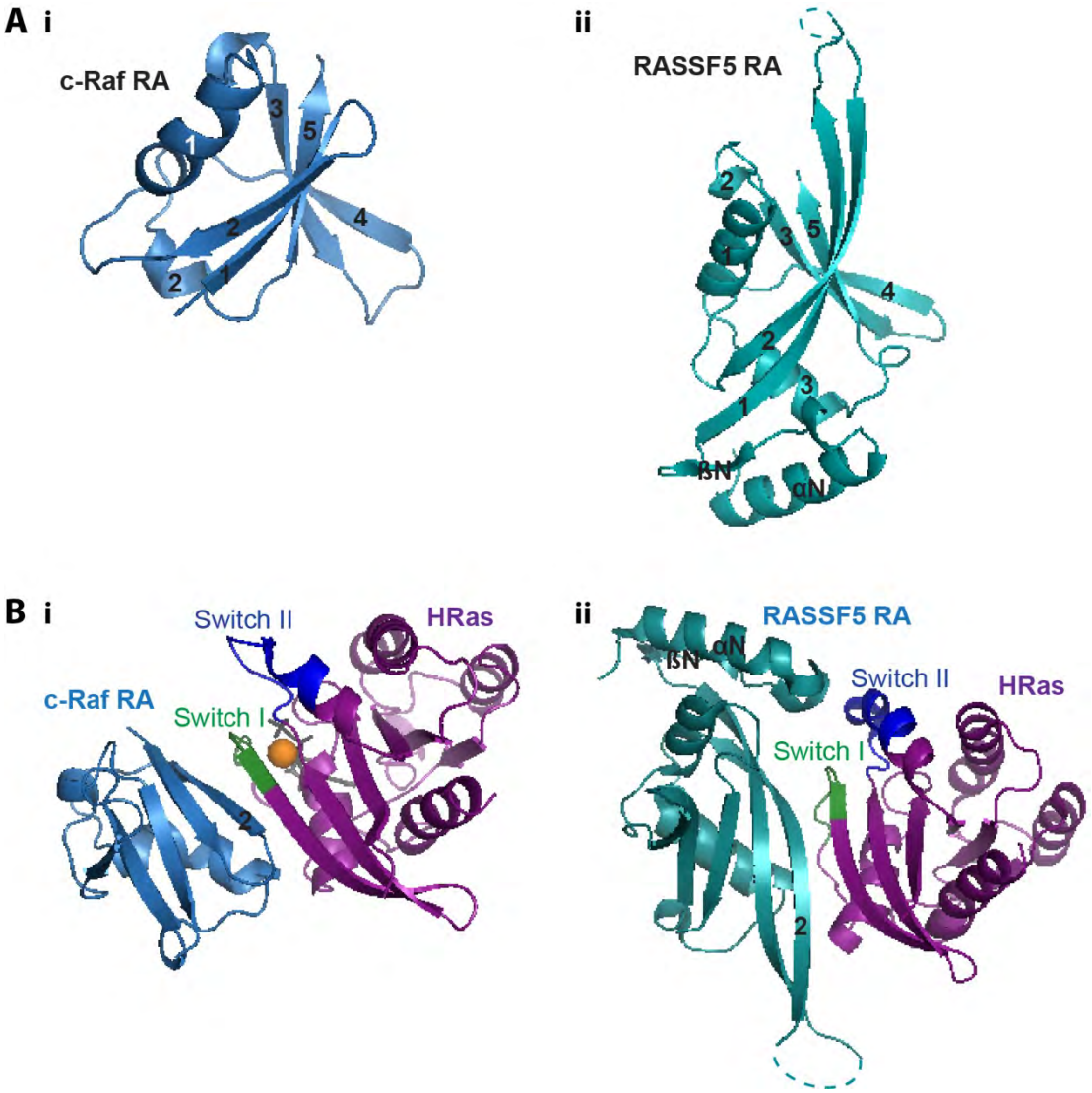

Figure 3.2 The RA domain and its binding to Ras family GTPases

(A) Ribbon representation of the RA domain ubiquitin fold of (i) c-Raf (PDB: 1GUA) and (ii) RASSF5 (PDB: 3DDC). The secondary elements of the ubiquitin fold are labelled in numerical order, those in the N-terminal subdomain of RASSF5 are labelled 'N'.

(B) Ribbon representation of the complex structures for the binding of HRas to (i) c-Raf RA domain and (ii) RASSF5 RA domain and N-terminal subdomain. Ras is shown in purple and RA domains in light blue or cyan. The secondary structures involved in Ras interaction are labelled as above. Ras switch I (green) and switch II (blue) are highlighted.

its distinctive kinetics of an average 10 s complex lifetime and a K_D of 0.08 μM point towards the characteristics of an adaptor protein.

Previous studies have highlighted the importance of general electrostatic interactions in Ras/effector binding in stabilising the intermolecular β-sheet (Kiel et al., 2004, Nassar et al., 1996). This was demonstrated by the clear difference in binding affinities to Ras between c-Raf and RalGDS. The strong electrostatic complementarity between Ras and c-Raf produces a strong, nanomolar affinity, whereas the poorer complementarity between Ras and RalGDS accounts for their lower affinity. Other characterised RA domains also display similar positively charged Ras binding interface (Figure 3.3). As the surfaces of Ras switch I and II are highly negatively charged (Figure 3.1Bii), an overall positive charge of the RA domain interacting surface suggests that one of the key criteria for Ras interaction is fulfilled.

Apart from electrostatic attraction, there are also specific residues on the surface of both Ras and its effectors that are involved in direct interaction. The residues on the Ras effector binding region known to form direct contact with the effector are generally well-conserved (Figure 3.1Biii). However, those on the effector surface are unique to each effector and cannot be predicted (Figure 3.3), therefore it is necessary to understand individual structures of these effectors to gain further insight into the mechanisms involved in Ras interaction. Nevertheless, there is a further complication that in some instances, these individual RA domain structures can provide only one part of the binding domain and cannot be analysed in isolation.

Although Ras interaction with several classical RASSF members has been reported, many of these observations are inconclusive and the methods used to show interaction were also widely different. In recent years, homology modelling using existing structural information, coupled with protein design algorithms have been used to predict new protein interactions. In particular, Kiel et al. (2007) have adopted this approach to draw a fairly accurate network of interactions between Ras and putative RA domains of various GEFs, GAPs and downstream effectors; the latter includes the RASSF family and are summarised in Figure 3.4. This method provides a platform for *in silico* predictions of Ras interaction with the RASSF family RA domains using the key criteria mentioned above and these can then be confirmed experimentally.

Figure 3.3 Surface representations of structurally known Ras effector RA domains

Surface representation of the Ras binding interface of the effector RA domains. (Top) Regions of key interacting residues are in cyan. Each residue and its position are labelled. (Bottom) Electrostatic potentials of the Ras binding interface are represented by positive (blue) and negative (red) charges. (A) c-Raf (PDB: 1GUA), (B) RalGDS (PDB: 1LFD), (C) PI3Kγ (PDB: 1HE8), (D) PLCε RA2 (PDB: 2C5L) and (E) RASSF5 (PDB: 3DDC). Images created in PyMol.

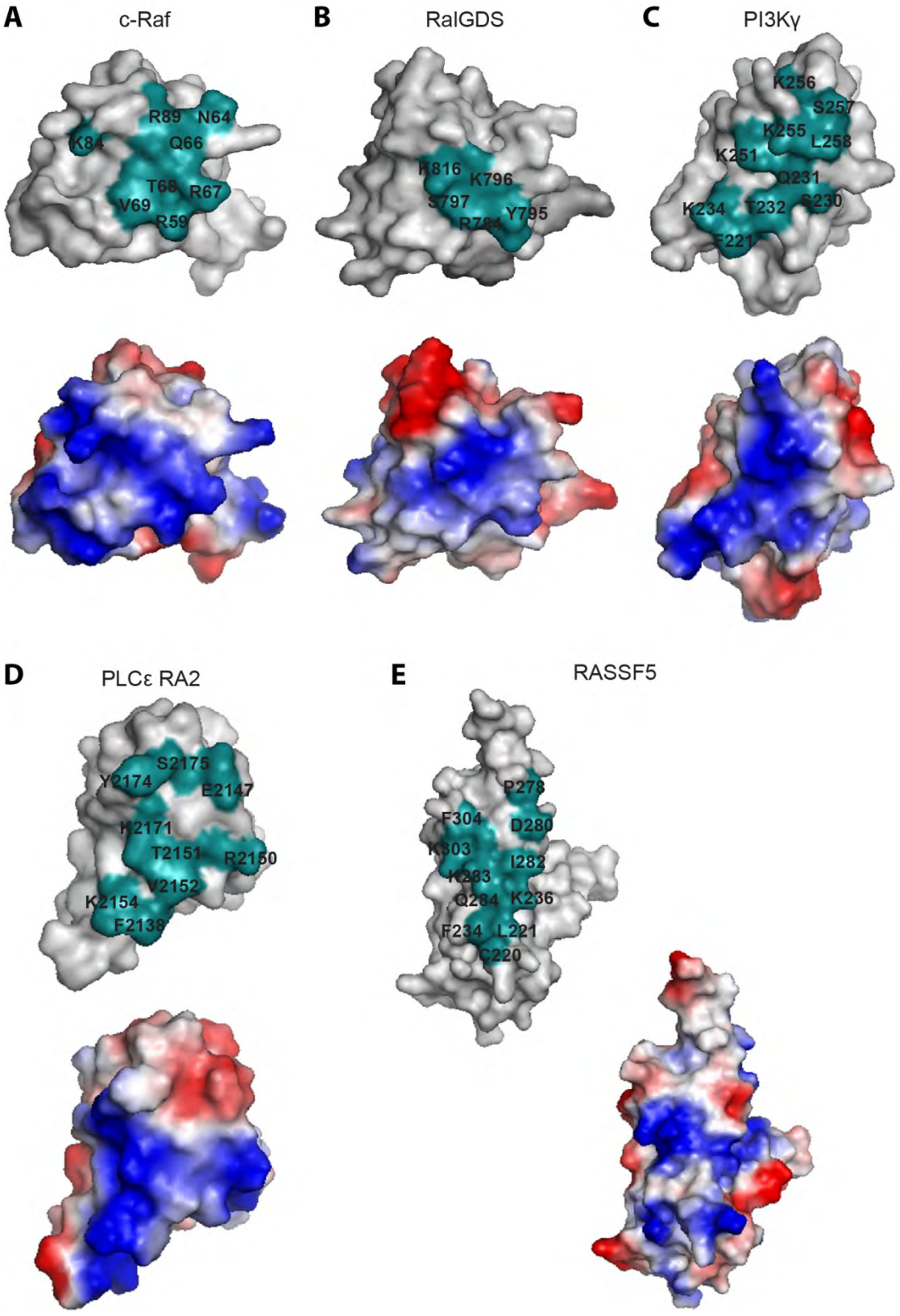
A
c-Raf
R89
N64
K84
Q66
T68
R67
V69
R59
B
RalGDS
H816
K796
S797
Y795
R724
C
PI3Kγ
K256
S257
K255
L258
K251
Q231
K234
T232
S230
F221
D
PLCε RA2
S2175
Y2174
E2147
K2171
T2151
R2150
Y2152
K2154
F2138
E
RASSF5
P278
F304
D280
K303
I282
K283
Q284
K236
F234
L221
C220

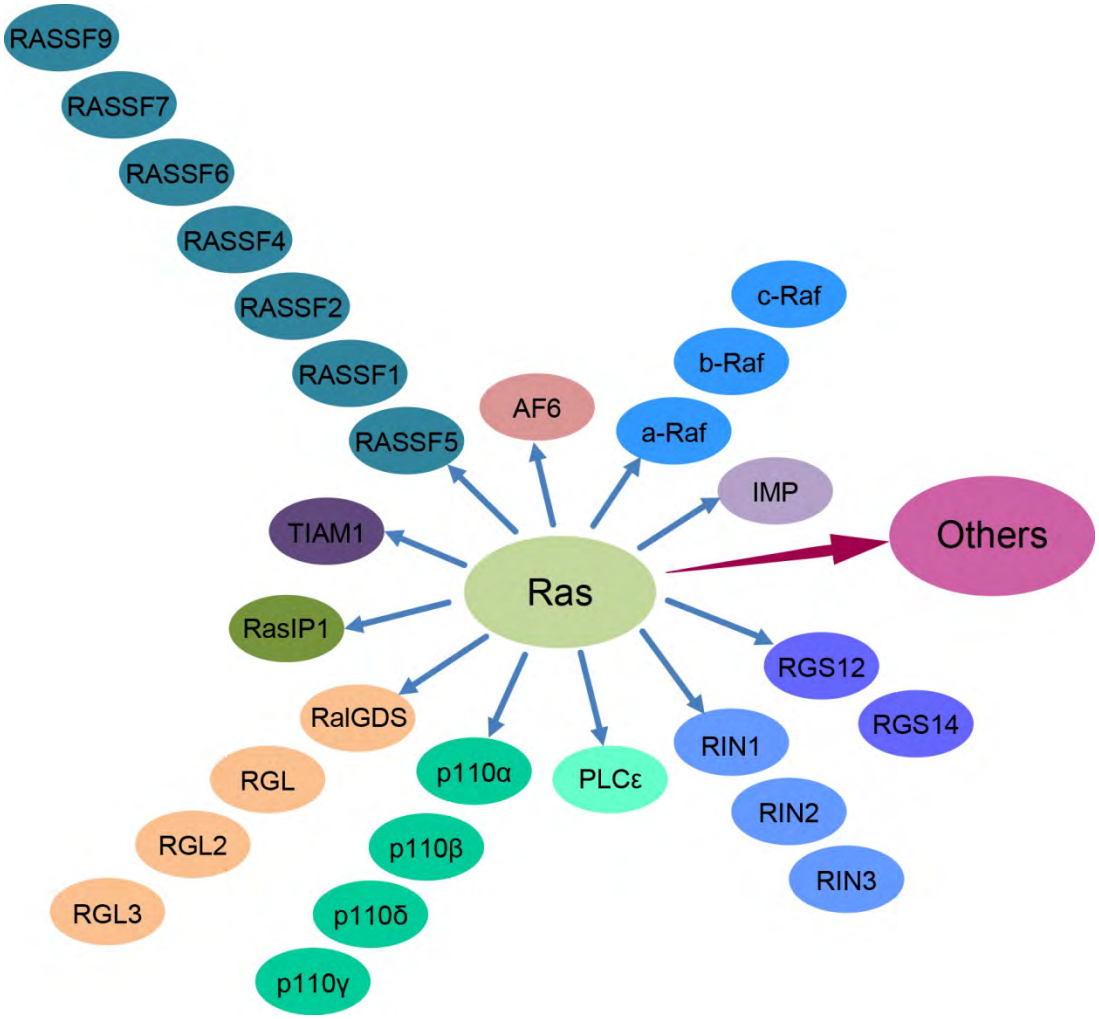

Figure 3.4 Ras interactome

This Ras network chart focuses on RA domain-containing proteins that act as immediate downstream effectors as shown. Other Ras binding proteins, such as GEF, GAP, CAAX modification and post-translational enzymes are grouped as “others”. Adapted from Cox and Der (2010).

The aim of this work was to compare the RA domains of all ten RASSF members, in terms of structure and their interaction with Ras GTPases, using RASSF5 as a benchmark and positive control. Here we observe differences between the *in silico* predictions and *in vitro* studies. The RASSF members also showed differential binding characteristics and affinities to Ras.

3.2. Results

3.2.1. Modelling the RASSF RA domain and predicting its interactions

First, we compared the homologies of the RA domains amongst the ten RASSF members by generating a phylogenetic tree (Figure 3.5). The classical RASSF1-6 and the N-terminal RASSF7-10 are clearly separated into two branches, which are both further split into two sub-branches. The homology scores for each RASSF pair are summarised in Table 3.1. RASSF1, 3 and 5 are 40-60% identical, whilst RASSF2, 4 and 6 share a 50-70% homology. In contrast, the RA domains of the classical RASSF and N-terminal RASSF appear to have little in common, with homologies mostly below 15%. However, within the N-terminal RASSF subgroup, RASSF7 and RASSF8 RA domains are 67% identical, whilst RASSF9 and RASSF10 share a 58% homology.

3.2.1.1. The classical RASSFs

Due to the high homology amongst the classical RASSF members, we performed homology modelling of their RA domains using RASSF5 as the structural template. However, the template was modified by removing the N-terminal subdomain and the β1 strand due to the unstructured loop region connecting β1 and β2, which makes it impossible to model the N-terminal extension and the canonical RA domain as a single unit. The sequences for the regions not modelled (Figure 3.6A) were aligned separately from the Prosite predicted RA domain sequences (Figure 3.6B) to compare the conservation pattern of the key interacting residues. In the N-terminal subdomain and β1 regions, only residues aligning to L226 and K241 are relatively conserved. However, interestingly, the residues in RASSF2, 4 and 6 aligning to K241 are oppositely charged. The main residues involved in electrostatic interactions are found in β2 and the C-terminus of α1. Several key residues, such as P283, K308 and F309 are

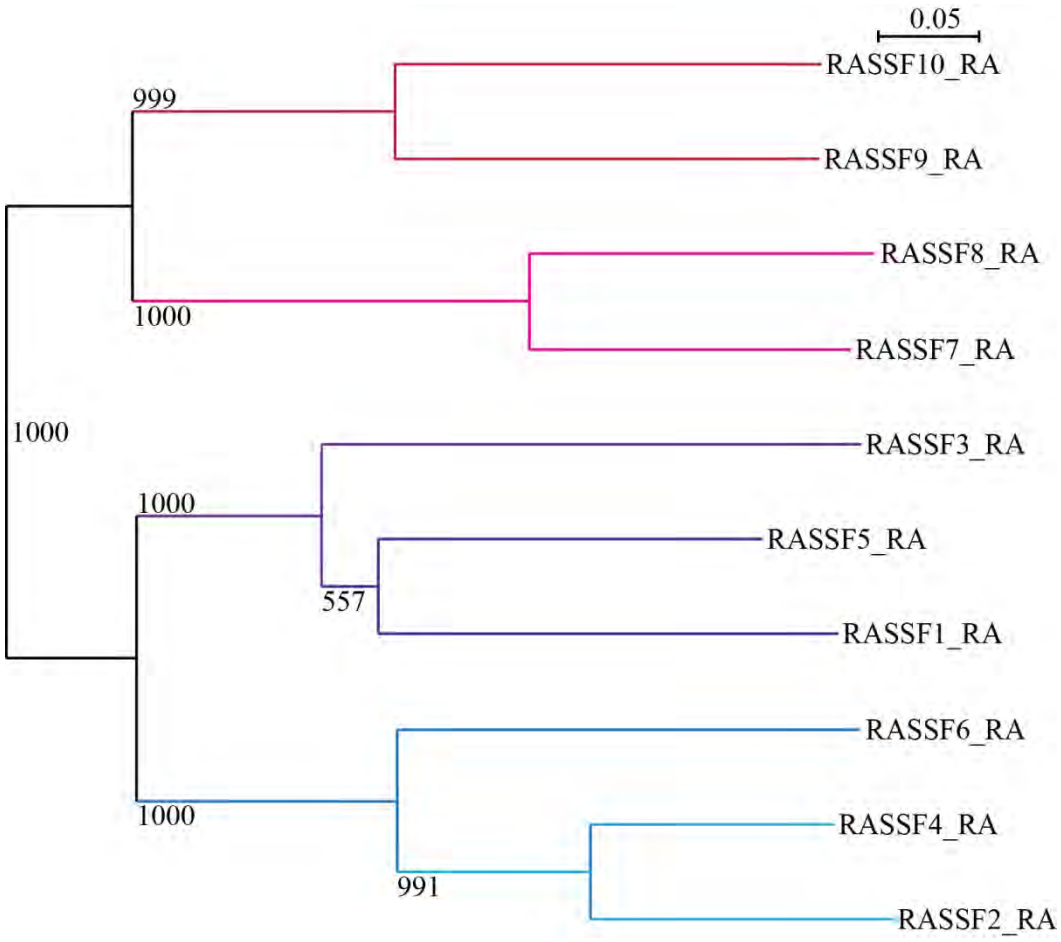

Figure 3.5 Phylogenetic tree of the RASSF family RA domain

Multiple sequence alignments were performed as described in section 2.8. The phylogenetic tree was built in njplot using the sequence alignments. Bootstrap figures are shown to represent the confidence level of each node, with 1000 being the maximum. The 0.05 scale bar refers to the branch length, which is a measure of the amount of divergence between two nodes in a tree. The tree is split into two branches, which are colour-coded: blue for classical RASSF1-6 and red for N-terminal RASSF7-10.

Table 3.1 Homology scores for each pair of RASSF members

RASSF	RASSF	Score (%)
1	2	24.72
1	3	44.21
1	4	33.71
1	5	58.24
1	6	32.58
1	7	15.48
1	8	7.32
1	9	18.95
1	10	17.89
2	3	26.97
2	4	73.03
2	5	29.21
2	6	55.06
2	7	2.38
2	8	3.66
2	9	6.74
2	10	3.37
3	4	29.21
3	5	51.65
3	6	24.72
3	7	14.29
3	8	10.98
3	9	9.47
3	10	13.76
4	5	29.21
4	6	52.81
4	7	4.76
4	8	13.41
4	9	7.87
4	10	3.37
5	6	28.09
5	7	10.71
5	8	4.88
5	9	12.09
5	10	25.27
6	7	5.95
6	8	6.10
6	9	7.87
6	10	4.49
7	8	67.07
7	9	27.38
7	10	28.57
8	9	34.15
8	10	30.49
9	10	57.89

fully conserved. However, other important residues in β2 aligning to D285, I287, K288 and Q289 are not as well conserved, with RASSF1 sharing the most conserved residues with RASSF5.

In the remodelled RASSSF5 template, β2 is not seen as a strand due to its anti-parallel position with β1, which was removed from the original template (Figure 3.6C). This is also the case for all the classical RASSF RA domain models (Figure 3.6D). Interestingly, the RA domain sequences predicted by Prosite for all six classical RASSF members do not include the β1 strand, which traditionally is part of the canonical RA domain. In the RASSF2, 4 and 6 models, β4 is also missing due to the gap aligning to that region (Figure 3.6B). Despite this minor structural variation and some differences in the key interacting residues, there are no major changes in the electrostatic surfaces for all models in the main interacting regions of β2 and α1, with the exception of RASSF3, which appears to have a more neutral surface around the β2 region (Figure 3.6Diii). However, theoretically, these changes should not affect Ras interaction for most of the classical RASSFs as they are not within the interacting surfaces.

3.2.1.2. The N-terminal RASSFs

The RA domains of the N-terminal RASSFs were modelled using c-Raf as a template due to its higher percentage of sequence identity (11.69%, 7.79% and 6.49% for RASSF7, 8 and 9 respectively) and better alignments (Figure 3.7A). There is a good alignment between c-Raf and RASSF7 and RASSF8 where most key interacting residues in β1 and β2, such as R59, Q66, R67 and V69 are 100% conserved. In contrast, the RASSF9 residues in these positions are not as well conserved, with only a conserved residue aligning to V69 and a semi-conserved residue at R67. Unlike the classical RASSFs, the residues aligning to K84 and R89 in the α1 region are not well conserved.

The differences observed in the sequence alignments are evident in the structural models. The template c-Raf has a highly positively charged surface around the β1, β2 and α1 regions (Figure 3.7B). Whilst there are no major electrostatic surface changes in the β1 and β2 regions of RASSF7 and RASSF8, their α1 region is neutral (Figure 3.7Ci, ii). This change is more significant in RASSF9, where the large negatively charged patch in the β2 region is a stark contrast to the template (Figure 3.7Ciii). The slight differences in the electrostatic potential in RASSF7 and RASSF8 interacting surfaces should not

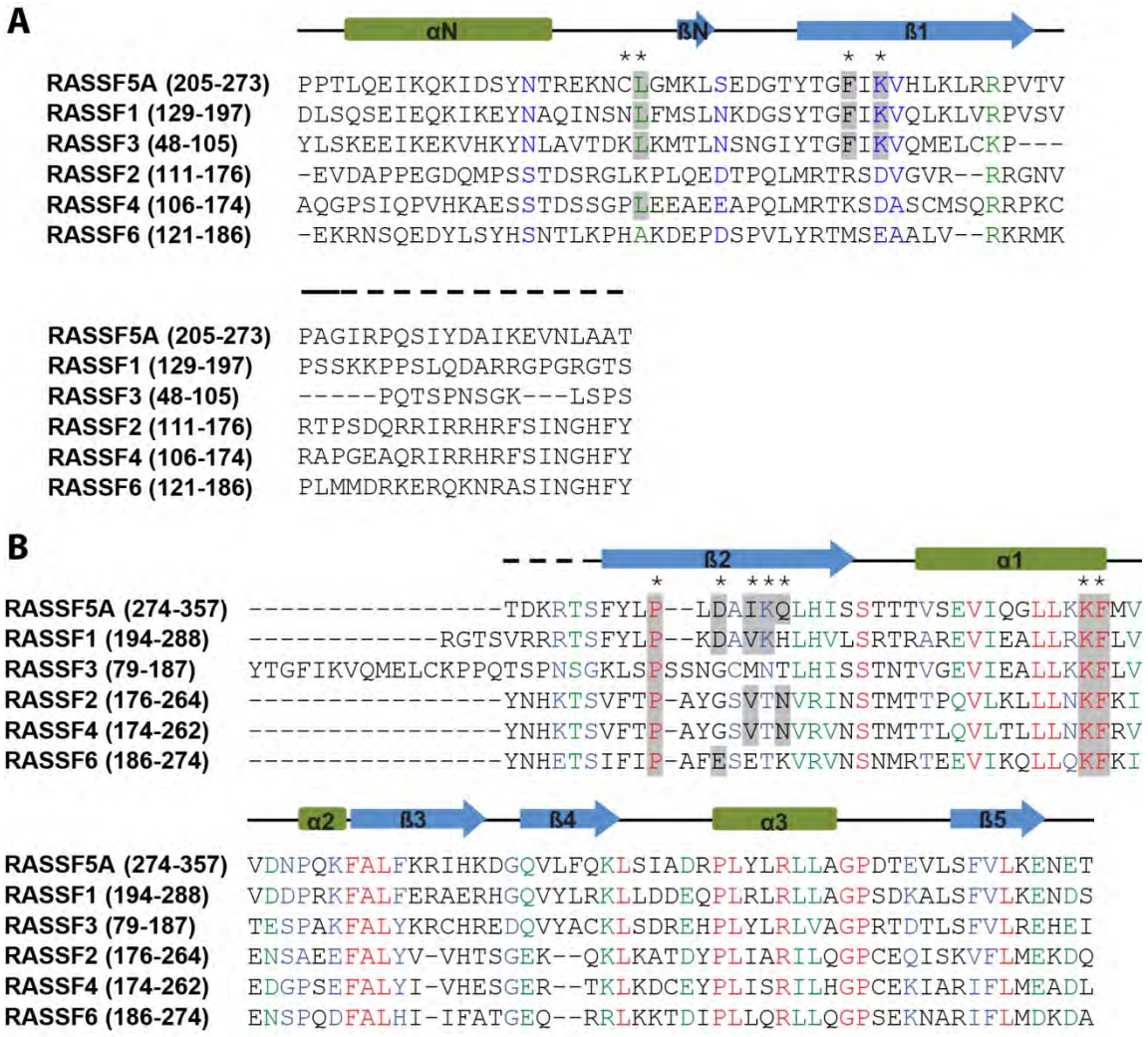

Figure 3.6 Modelling the classical RASSF RA domain

Multiple sequence alignments with secondary structural elements indicated above. The residues in RASSF5 involved in Ras interaction are marked with an asterisk (*) above and the conserved residues aligning to those positions are highlighted in grey. Other residues are coloured according to their similarity, fully conserved residues in red, highly similar residues in green and weakly similar residues in blue.

(A) RASSF1-6 sequences aligning to the RASSF5 N-terminal subdomain

(B) RASSF1-6 RA domain sequences predicted by Prosite

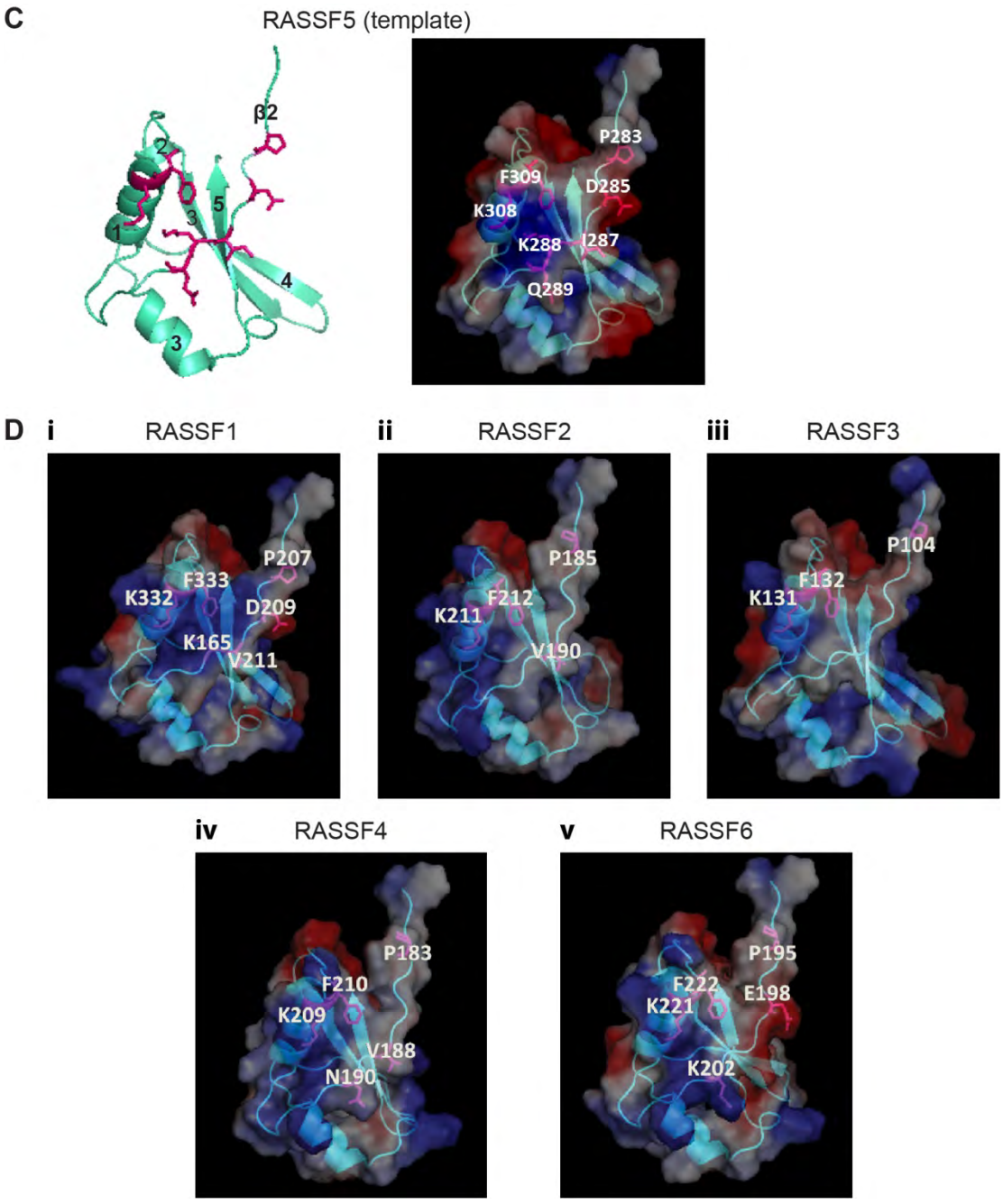

(C) The remodelled RASSF5 template without the N-terminal subdomain. (Left) Ribbon representation with the side chains of the key interacting residues in pink and labelled. (Right) Surface electrostatic potentials are represented as in Figure 3.3.

(D) Ribbon representation of the RA domain structural models of (i) RASSF1, (ii) RASSF2, (iii) RASSF3, (iv) RASSF4 and (v) RASSF6. Side chains of residues aligning to the conserved residues of RASSF5 are shown in pink. Surface electrostatic potential is superimposed as represented as above.

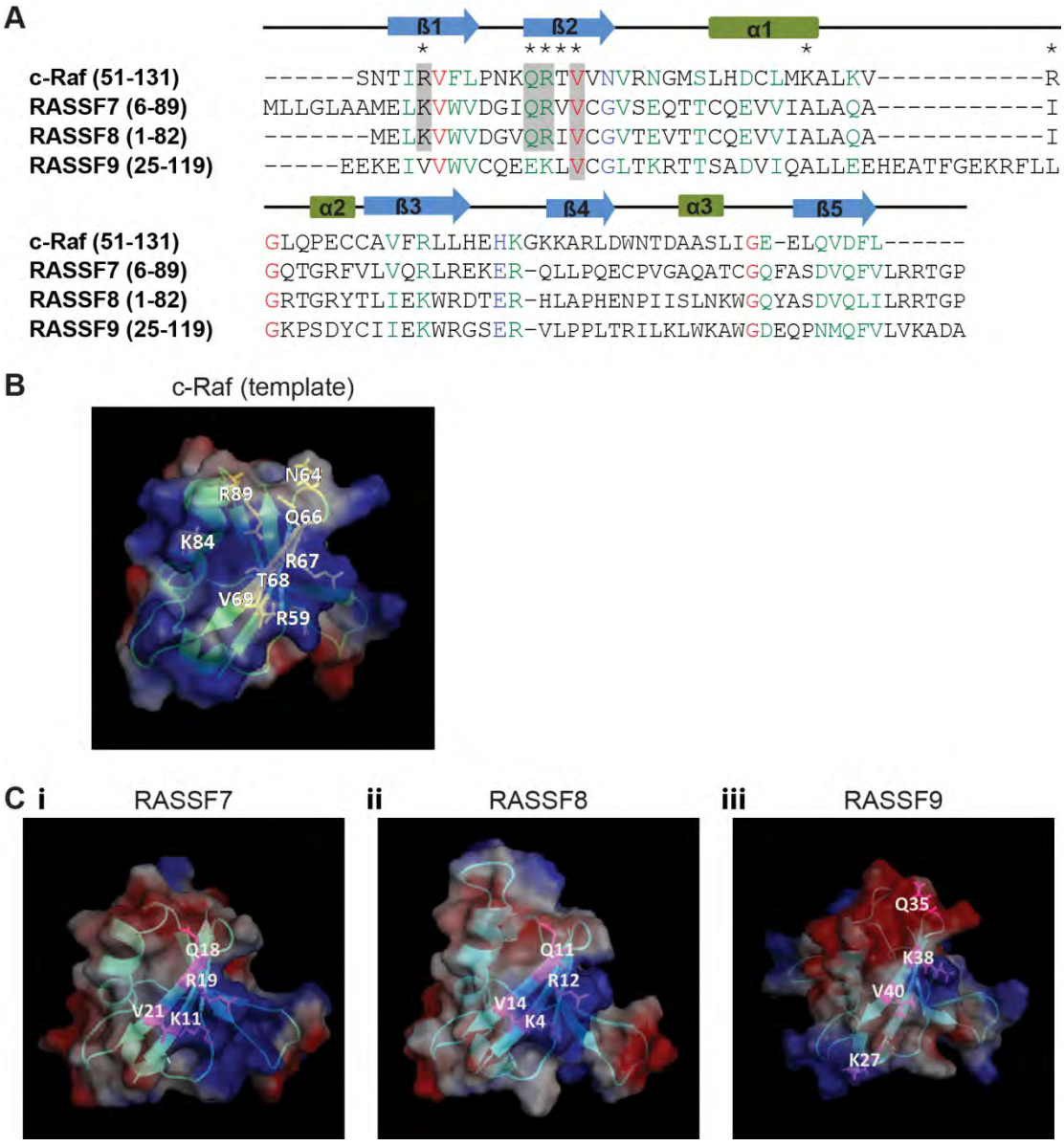

Figure 3.7 Modelling the N-terminal RASSF RA domain

(A) Multiple sequence alignments of RASSF7-10 and c-Raf RA domain sequences predicted by Prosite. The representations are as described in Figure 3.6A.

(B) The c-Raf RA domain template. The ribbon representation and surface electrostatic potential are superimposed. The side chains of key interacting residues are labelled and shown in yellow.

(C) RA domain structural models of (i) RASSF7, (ii) RASSF8 and (iii) RASSF9 represented as described in Figure 3.6D.

eliminate their ability to interact with Ras, but may serve to weaken this interaction.

Overall, in addition to the bona fide Ras effector RASSF5, we predict that RASSF1, 2, 4, 6, 7 and 8 are also potential Ras effectors. With a more neutral surface, the ability of RASSF3 to bind Ras can only be determined empirically, whereas RASSF9 with its large surface of negative charge is a clear non-binder.

3.2.2. RA domain of RASSF1-10 shows differential Ras interactions

In order to validate the *in silico* predictions and determine whether the predicted RASSF RA domains are able to bind Ras with a relatively high affinity, we performed an *in vitro* pull-down assay for the whole panel of full-length RASSF family members using purified proteins of activated HRasV12, KRasV12, MRasV22, NRasV12 and Rap2BV12. The pull-down method used in this study typically detects binding affinities of up to a K_D of 10 μM (Bunney et al., 2006). Therefore, protein interactions with a low affinity (high K_D) or fast off rate (high k_{off}) will not be detected using such a method.

A first set of pull-downs were conducted using purified proteins of structurally characterised RA domains to confirm detection and relative affinities using such technique (Figure 3.8A). Sequence alignments of the RA domains of c-Raf, RalGDS, PLCε, PI3Kγ and RASSF5 showed that whilst there is little sequence identity, their secondary structural elements are very well-conserved and all the key interacting residues are found within the β1, β2 and α1 region (Figure 3.8B). RASSF5 and PI3Kγ also share the common feature of having an additional helix after α1. As the isolated RA domain of PI3Kγ cannot be expressed, it was not included as a control in the pull-down assay. However, those of c-Raf, RalGDS, PLCε and RASSF5 were all detected at comparable levels with HRasV12 (Figure 3.8C). Whereas only RalGDS and RASSF5 were detected in complex with Rap2BV12, with RalGDS being the stronger binder (Figure 3.8D).

In many effectors, it has been shown that the isolated RA domain is a stronger Ras binder compared to their longer or full-length protein, and whilst they show less selectivity for lipid-modified Ras, they still preserve their specificity for GTP-bound Ras, for example c-Raf and PLCε (Bunney et al., 2006, Fischer et al., 2007, Stang et al., 1997). Therefore, our initial efforts were to express and purify isolated RA domains for the remaining nine RASSF members as these will allow us to first identify GTP-dependent

Figure 3.8 Interaction between Ras GTPases and isolated RA domain proteins

(A) Schematic outline of *in vitro* pull-down assay as described in section 2.6.1.1.

(B) Sequence alignments of ubiquitin folds from RASSF5, c-Raf, RalGDS, PLCε RA2 and PI3Kγ. Secondary structural elements are indicated above and the amino acid residues in those regions are coloured accordingly. Key Ras interacting residues are underlined.

(C) Amino acid residue boundaries for the purified RA domain proteins of c-Raf, RalGDS, PLCε RA2 and RASSF5Δ52 used in *in vitro* pull-down assays.

(D) Pull-down assay to show interaction between purified proteins of Ras GTPases and isolated RA domains listed in Figure 3.8C. Each set of pull-down experiment was repeated three times and a representative is shown here. (i) Immobilised HRasV12 in GDP (D) or GTP (T) bound form was used to pull-down GST-tagged RA domains. (ii) Immobilised GST-tagged RA domains were used to pull down untagged Rap2BV12 in (D) or (T) form.

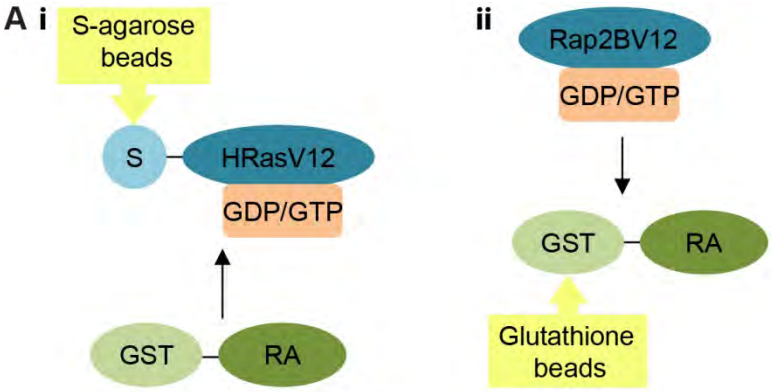

B

```
                    ß1                  ß2                  α1          (α2)
RASSF5 (83-209)  -YTGFIKVHLKLRRPVTVPSFYLPLD--AIKQMHISSTTTVSEVIQGLLDKFM-------V
c-Raf (55-131)   --SNTIRVFLP-------------NKQRTVVNVRNGMSLHDCLMKALKVRGL---------
RalGDS (779-864) --DCCIIRVSLDV---------DNGN-MYKSILVTSQDKAPTVIRKAMDKHNL-------D
PLCε (2132-2236) -SEEESFFVQVHDV----------SPEQPRTVIKAPRVSTAQDVIQQTLCKAKYSLS---I
PI3Kγ (217-310)  NNCIFIKIHRS---------------TTSQTIKVSPDDTPGAILQSFFTKMAKKKSLMDI

                 (α2)  ß3                  ß4          α2 (α3)          ß5
RASSF5 (83-209)  VDN--PQKFALFKRIHKDG--------QVLFQKLSIADYPLYLRLLAGPDTDVLSFVLKEN
c-Raf (55-131)   ----QPECCAVFRLLHEH---------KGKKARLDWNTDAASLIG--------EELQVDFL
RalGDS (779-864) EDE--PEDYELLQIIS-----------EDHKLKIPENANVFYAMNSAA----NYDFILKKR
PLCε (2132-2236) LSNPNPSDYVLLEEVVKDTTNKKTTTPKSSQRVLLDQECVFQAQSKWK---GAGKFILKLK
PI3Kγ (217-310)  PESQSEQDFVLRVC-----------GRDEYLVGETPIKNFQWVRHCLKNGEEIHVVLDTP
```

C

Protein	RA boundary	Comment
c-Raf	55-131	
RalGDS	779-864	
PLCε	2132-2236	RA2 domain
RASSF5Δ52	52-212	Includes N-terminal subdomain

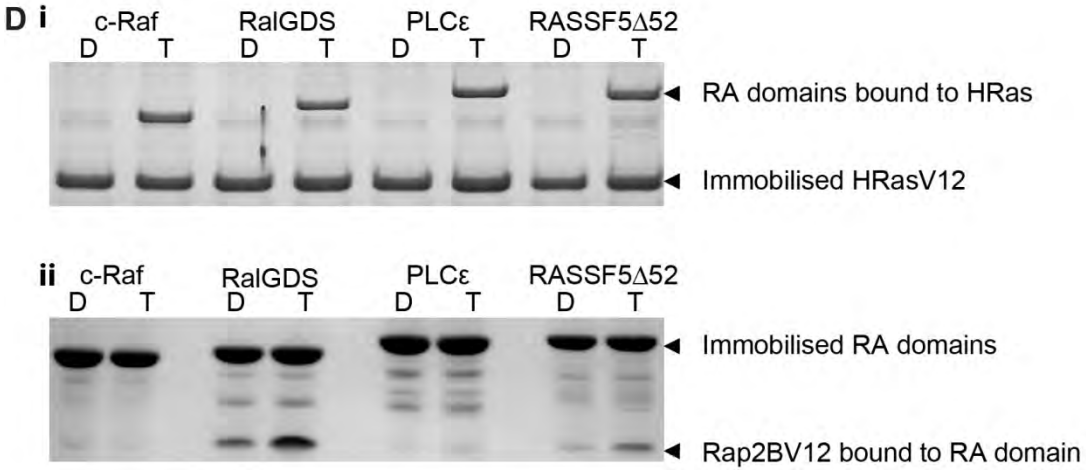

binders in a more definitive manner. However, most of these RA domains, regardless of the tags added to aid expression and solubility, either could not be expressed or produced very low yield, thus cannot be purified (Table 3.2). The few isolated RA domains that were successfully purified included those for RASSF3, 7, 8 and 9, which were subsequently tested for interaction with HRasV12 but no binding was detected (data not shown). This set of data provided the first indication that RASSF5 may in fact be quite a distinct member despite predicted similarities. The differences in inter-domain interactions and their integration into the overall structure could be one possible reason.

It has been shown in some cases that Ras interaction is influenced by other regions outside of the RA domain. For instance, RASSF5 which makes contacts with Ras switch II via its N-terminal subdomain (Stieglitz et al., 2008); and PI3Kγ, in which a loop insertion in the RA domain changes the binding orientation of Ras to establish switch II contacts with the PI3Kγ catalytic domain (Pacold et al., 2000). In the case of PI3Kγ, it is only possible to express an almost full-length protein but not its isolated RA domain. We considered that this might be a possibility for the RASSF proteins in bacterial expression systems. Thus, we attempted to express them as full-length proteins attached to a SUMO tag, which is the most efficient fusion technology to date in terms of aiding expression (Marblestone et al., 2006). Some expression was detected using the bacterial system; however, none of the proteins were expressed to a level that can be efficiently purified (Table 3.2).

Due to the extreme difficulty in purifying any form of the RASSF proteins and the negative results for the isolated RA domains tested, we resorted to using mammalian cell lysates containing full-length recombinant GFP-RASSF and purified Ras GTPases in a slightly modified pull-down assay (Figure 3.9Bi). In subsequent pull-down experiments, full-length RASSF5 served as a positive control and consistently showed GTP-dependent strong binding to all Ras GTPases tested (Figure 3.9Bii). The most striking observation was that no other RASSF member displayed as strong binding, if at all, as RASSF5. It is important to note here, we cannot confirm that the different RA domains are well folded in the *E. coli* or mammalian expression systems. It is possible that some of the RASSF1-10 RA domains fold incorrectly when overexpressed and thus cannot bind Ras. Nevertheless, RASSF1 showed GTP-dependent binding, although weaker and only to KRasV12 and NRasV12. The RASSF1 bands detected in MRasV22

Table 3.2 Summary of protein expression for the RASSF RA domain and full length proteins

Vector and tags	Constructs	Boundaries (aa)	Purification method	Yield (mg/L culture)	Pull-down assay
pTriEx™-6 (StrepII, 10xHis)	RASSF1 RA1	133-291	Section 2.2.1.2 No cleavage	No yield	-
	RASSF1 RA2	129-287		No yield	-
	RASSF2 RA	113-263		No yield	-
	RASSF3 RA1	48-186		No yield	-
	RASSF3 RA2	79-186		0.76	Performed, negative
	RASSF4 RA	108-261		No yield	-
	RASSF6 RA	120-236		No yield	-
	RASSF7 RA	1-89		No yield	-
	RASSF8 RA	1-82		No yield	-
	RASSF9 RA	22-119		No yield	-
	RASSF10 RA	1-133		No yield	-
pDEST565 (6xHis, GST)	RASSF1 RA1	133-291	3c protease cleaved	No yield	-
	RASSF1 RA2	129-287		No yield	-
	RASSF2 RA	113-263		No yield	-
	RASSF3 RA1	48-186		No yield	-
	RASSF3 RA2	79-186			-
	RASSF4 RA	108-261		No yield	-
	RASSF6 RA	120-236		No yield	-
	RASSF7 RA	1-89		No yield	-
	RASSF8 RA	1-82		No yield	-
	RASSF9 RA	22-119		No yield	-
	RASSF10 RA	1-133		No yield	-
pOPINS (6xHis, SUMO)	RASSF1 RA1	133-291	Ulp1 protease cleaved	No yield	-
	RASSF1 RA2	129-287		No yield	-
	RASSF2 RA	113-263		No yield	-
	RASSF3 RA1	48-186		No yield	-
	RASSF3 RA2	79-186		Very poor	-
	RASSF4 RA	108-261		No yield	-
	RASSF6 RA	120-236		No yield	-
	RASSF7 RA	6-89		3.3	Performed, negative
	RASSF7 RA99	6-99		3.5	
	RASSF7 RA109	6-109		3.5	
	RASSF7 RA119	6-119		5	
	RASSF7 RA129	6-129		Aggregate	
	RASSF7 RA139	6-139		5.3	
	RASSF7 RA149	6-149		5.3	
	RASSF7 RA159	6-159		5.4	
	RASSF7 RA176	6-176		11.2	

Vector	Constructs	Boundaries (aa)	Purification method	Yield (mg/L culture)	Pull-down assay
pOPINS (6xHis, SUMO)	RASSF8 RA	1-82	Section 2.2.1.2 Ulp1-cleaved	9.9	Performed, negative
	RASSF8 RA92	1-92		12.8	
	RASSF8 RA102	1-102		13.7	
	RASSF8 RA112	1-112		10.4	
	RASSF8 RA122	1-122		5.4	
	RASSF8 RA132	1-132		10.5	
	RASSF8 RA142	1-142		13.2	
	RASSF8 RA157	1-157		8.3	
	RASSF9 RA	22-119		3.4	
	RASSF10 RA	1-133		No yield	-
	RASSF1	1-340		No yield	-
	RASSF2	1-326		No yield	-
	RASSF3	1-238		No yield	-
	RASSF4	1-321		No yield	-
	RASSF5	1-265		Very poor	-
	RASSF6	1-337		No yield	-
	RASSF7	1-373		No yield	-
	RASSF8	1-392		Very poor	-
	RASSF9	1-435		No yield	-
	RASSF10	1-507		No yield	-

Figure 3.9 Interaction between Ras GTPases and full length RASSF

(A) Schematic outline of *in vitro* pull-down assay as described in section 2.6.1.2.

(B) Pull-down assay to show interaction between purified Ras GTPases and full length RASSF in whole cell lysates. Each set of pull-down experiment was repeated three times and a representative is shown here. (i) RASSF1-10 were expressed as full length GFP fusion proteins in the mammalian 293F expression system as described in sections 2.5.1.3 and 2.6.1.2. The expression of these proteins was detected by western blotting using the anti-GFP antibody and GAPDH was used as a loading control (top panel). Purified S-tagged Ras GTPases as described Table 2.5 (bottom panel). (ii) The indicated immobilised Ras GTPase in GDP (D) or GTP (T) bound form (bottom panels) was used to pull down GFP-tagged RASSF. The bound proteins were analysed by western blotting (top panels).

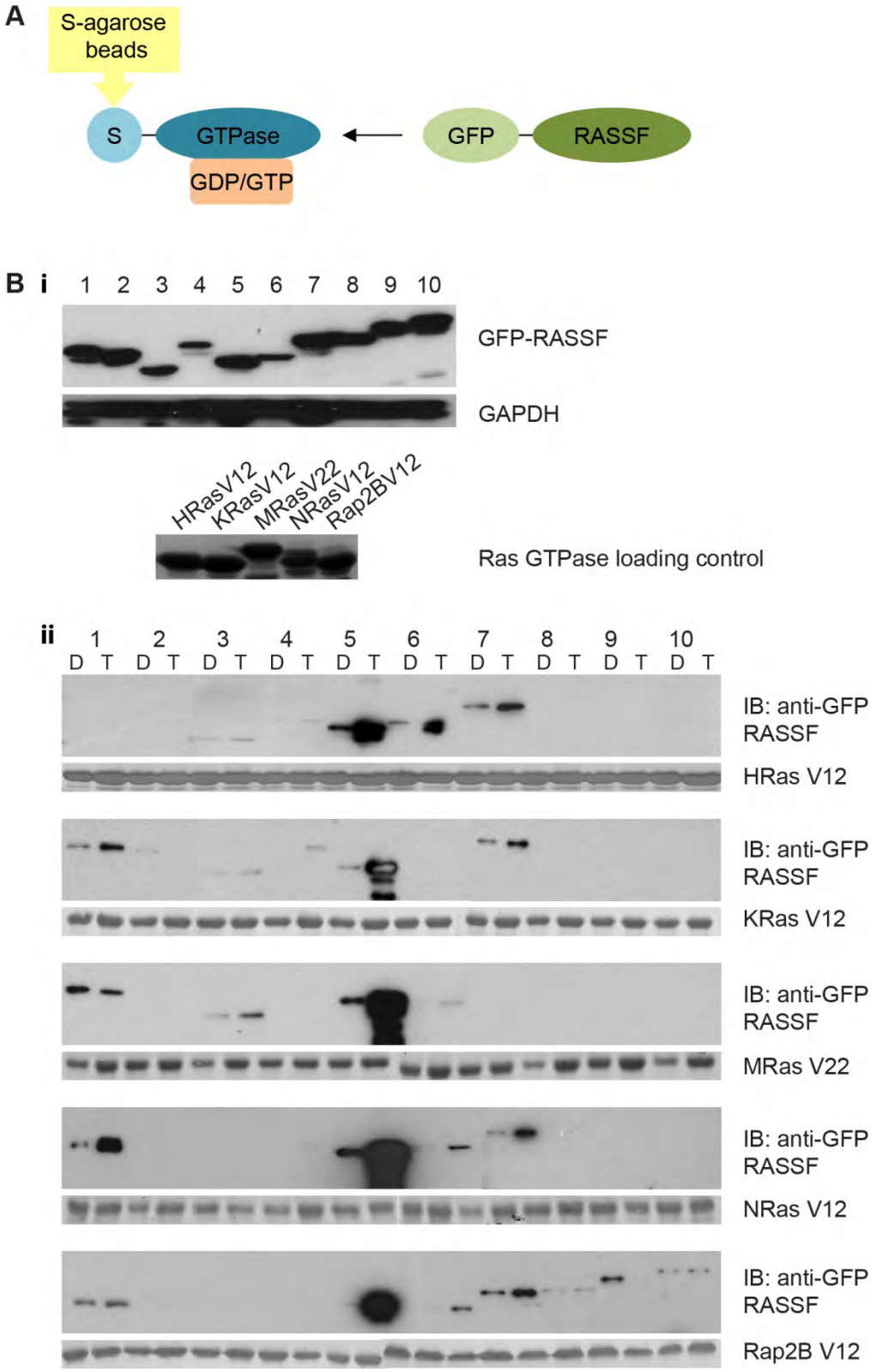
A
S-agarose beads
S
GTPase
GDP/GTP
GFP
RASSF
B i
1 2 3 4 5 6 7 8 9 10
GFP-RASSF
GAPDH
HRasV12
KRasV12
MRasV22
NRasV12
Rap2BV12
Ras GTPase loading control
ii
1 2 3 4 5 6 7 8 9 10
D T D T D T D T D T D T D T D T D T D T
IB: anti-GFP
RASSF
HRas V12
IB: anti-GFP
RASSF
KRas V12
IB: anti-GFP
RASSF
MRas V22
IB: anti-GFP
RASSF
NRas V12
IB: anti-GFP
RASSF
Rap2B V12

and Rap2BV12 pull-downs are likely the result of non-specific binding. RASSF3 and RASSF4 are much weaker binders, both binding HRasV12 and KRasV12, with RASSF3 also weakly interacting with MRasV22. On the other hand, RASSF6 displayed more consistency, binding relatively strongly to HRasV12, but very weakly to MRasV22 and NRasV12 and is the only other classical RASSF to bind to Rap2BV12. RASSF7 is the only N-terminal RASSF to show GTP-dependent binding to all Ras GTPases tested except MRasV22. In all cases binding was considerably weaker when compared to RASSF5. No binding was observed for RASSF2 and the rest of the N-terminal RASSFs.

3.2.3. Possible roles for RASSF proteins in Ras-dependent cellular functions

There are various reports implicating the RASSF family as tumour suppressors in many important biological pathways that could be regulated by Ras, including apoptosis and cell cycle arrest (Richter et al., 2009). In order to comparatively assess the importance of the RASSF proteins in relation to Ras in a physiological setting, we used siRNA to knockdown the individual RASSF members in cell lines carrying mutant KRas. These were human A549 lung adenocarcinoma and HCT116 colon carcinoma cell lines. Cell viability was used as a measure of phenotypic change as a result of these knockdowns.

Different responses were observed between the two cell lines (Figure 3.10). KRas knockdown was used as a positive control and as expected, caused a significant reduction in cell viability in HCT116. However, this change was much smaller in A549. Likewise, no significant changes were observed for all knockdowns in A549, with the exception of RASSF9, the loss of which resulted in an increased viability. In contrast, in HCT116, the loss of RASSF2, 4 and 7 caused a small but statistically significant reduction in viability. These observations are in line with the controls, whereby greater effects were observed in HCT116.

As a comparison to other potential or known Ras effectors, we also performed a siRNA screen on a panel of 46 other RA domain-containing proteins using the same cell lines (Table 3.3). Again, we observed differences between the two cell lines. However, we also identified a few positive hits after multiple repeats. These are the knockdowns that repeatedly produced significant decrease in cell viability in both A549 and HCT116, and they include PIK3C2α, b-Raf, TIAM2 and RIAM.

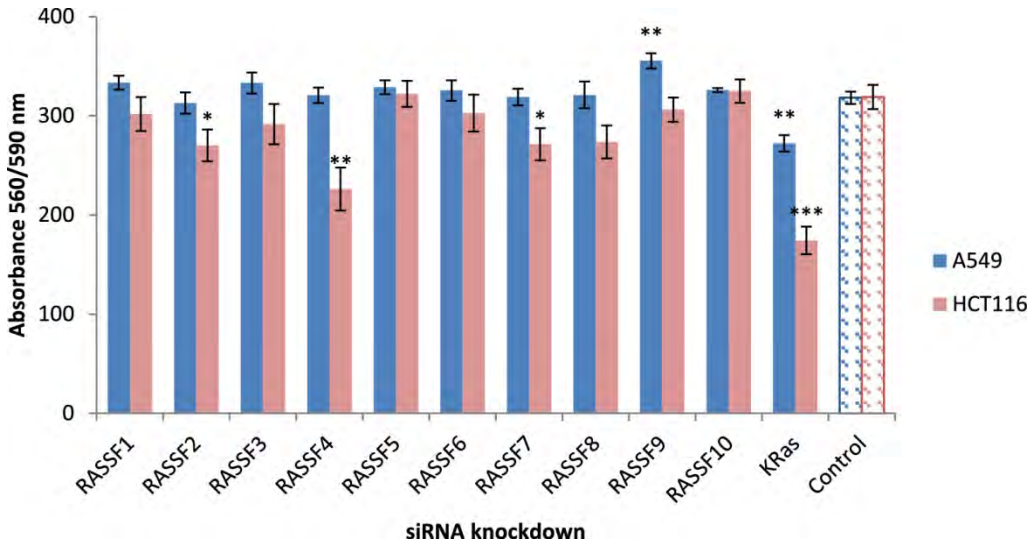

Figure 3.10 siRNA knockdown of RASSF1-10 in KRas mutant cell lines

A549 and HCT116 cell lines were transfected with siRNA and cell viability was used as a measure of phenotypic change as described in sections 2.5.1.3 and 2.7. Untransfected cells were used as a negative control and KRas knockdown a positive control. Higher absorbance indicates greater viability and vice versa. The levels of statistical significance are shown as $p \leq 0.05$ (*), $p \leq 0.01$ (**), $p \leq 0.001$ (***). These were calculated using the Student's t-test for each individual knockdown against the negative control. The experiments were repeated three times and each was performed in triplicates.

Table 3.3 Summary of the siRNA screen of a panel of Ras effectors

The screens were performed in A549 lung adenocarcinoma and HCT116 colon carcinoma cell lines. ✓ denotes significant decrease in viability in either cell line, ✓✓ in both cell lines and × no effect.

Genes	Viability inhibition	Genes	Viability inhibition	Genes	Viability inhibition
RALGDS	×	RAPGEF4	×	ARHGAP13	×
RGL1	×	RAPGEF6	✓	ARHGAP14	×
RGL2	×	SOS1	×	ARHGAP19	×
RIN1	×	SOS2	×	ARHGAP20	×
RIN2	×	a-Raf	×	KRIT 1	×
RIN3	×	b-Raf	✓✓	RIAM	✓✓
ARAP1	×	c-Raf	×	Raf pool*	✓
ARAP2	×	RGS12	×	PIK3C pool*	✓
ARAP3	×	SNX27	✓	RASSF1	×
PLCε1	×	RGS14	×	RASSF2	✓
DGKQ	✓	TIAM1	×	RASSF3	×
MAP3K1	✓	TIAM2	✓✓	RASSF4	✓
PIK3Cα	✓	MLLT4	×	RASSF5	×
PIK3Cβ	×	MYO9A	×	RASSF6	×
PIK3Cγ	×	MYO9B	×	RASSF7	✓
PIK3C2α	✓✓	MYO10	✓	RASSF8	×
PIK3C2β	×	GRB7	×	RASSF9	×
PIK3C2γ	×	GRB10	✓	RASSF10	×
RAPGEF2	×	GRB14	✓		
RAPGEF3	✓	ARHGAP4	×		

* Raf pool contains a-Raf, b-Raf and c-Raf, and PIK3C pool contains PIK3Cα, PIK3Cβ and PIK3Cγ.

3.3. Discussion

The comparison between *in silico* predictions and *in vitro* data clearly demonstrates the deficiencies in electrostatic surface predictions to determine Ras binding. The predicted Ras-binders were RASSF1, 2, 4, 6, 7 and 8 compared to the observed binders RASSF1, 3, 4, 6 and 7. Whilst no binding for RASSF9 and RASSF10 was observed as expected, there are some definite discrepancies between the predicted and observed binders for other RASSF members. For instance, RASSF1, which shares the highest sequence and surface homology with RASSF5, even outside the canonical RA domain, showed limited and much weaker interactions with different Ras GTPases. RASSF2, which also has a similar surface potential, did not interact with any Ras GTPases tested. Furthermore, despite both having similar electrostatic surfaces, RASSF4 proved to be a much weaker binder, if at all, compared to RASSF6. The clearest example is the discrepancy observed for RASSF7 and RASSF8. Both their RA domains share a high level of sequence identity and have almost identical electrostatic surfaces yet showed completely opposite binding behaviours in the *in vitro* studies. These observations highlight the two main limitations in predicting binding based on electrostatic interaction: 1) important specific residues within the surfaces and 2) other parts of the protein can be important in RASSF/ GTPase interaction. Furthermore, the experimental data revealed that only RASSF5 has clear, strong binding for Ras GTPases either as a full-length protein or isolated binding domain.

In the context of existing reports of Ras interaction with the RASSF family, several RASSF members have been shown to interact with various Ras isoforms. However, some of these reports appear contradictory, whilst comparison with our observations is also inconsistent.

Apart from RASSF5, the most studied RASSF member is RASSF1. It was first shown to directly bind HRas (Vos et al., 2000), only to be refuted by a report of indirect association via the RASSF5 RA domain when the two RASSF proteins heterodimerise in mammalian cells (Ortiz-Vega et al., 2002). Interestingly, RASSF1 has also been shown to interact with Ran-GTP from the Ran GTPases subfamily, which is the first report of RASSF interaction with a Ras-related small GTPase outside the Ras subfamily. Furthermore, this interaction is crucial in maintaining microtubule stability. Most recently, RASSF1 was shown to interact with Rap1A but not Rap2 and HRas, an

interaction which also appears to affect microtubule organisation (Verma et al., 2011). Our inability to detect any interaction between HRas and RASSF1 contrasts with these two reports. We also never tested for the presence of endogenous RASSF5 in the cell system we used to overexpress RASSF1. However, if RASSF1 interacted with Ras via RASSF5 as reported, then it should have shown GTP-dependent binding by RASSF1 for either all or none of the Ras GTPases tested, instead of the few that were observed. The last report is in agreement with our data as we did not observe specific interaction between RASSF1 and Rap2B or HRas, although both share an identical core effector region with Rap1 (Verma et al., 2011). Based on a previous study by Miertzschke et al. (2007) showing opposite binding behaviours by RASSF5 to Rap1 and Rap2, coupled with the high homology between RASSF1 and RASSF5, it is likely that we would also observe interaction between RASSF1 and Rap1 if tested.

Reports of Ras interaction with other members of the RASSF family are scarce, with only one or two reports each for RASSF2, 4, 6, 7 and 9. RASSF2, 4 and 6, which we have established as being the most closely related within the classical RASSF subgroup, were all shown to interact specifically and directly with GTP-loaded farnesylated KRas with rather high affinities and the canonical RA domain is sufficient for interaction (Allen et al., 2007, Clark et al., 2012, Eckfeld et al., 2004, Vos et al., 2003a). These interactions seem to have similar consequences in promoting apoptosis and cell cycle arrest in tumour cell lines. However, these observations of Ras interactions are in direct contrast with our data in which interaction between KRas and RASSF2 and RASSF6 was never detected whilst RASSF4 was barely detectable. This difference could be the result of farnesylation on the KRas CAAX box, which may contribute to effector recognition and specificity (Hancock, 2003).

Takahashi et al. (2011) was the first to demonstrate GTP-dependent interaction between farnesylated NRas and RASSF7, with a functional consequence in the JNK signalling pathway. However, they did not observe interaction with other Ras isoforms, including HRas and KRas. This is puzzling as our data indicate that RASSF7 is one of the more promiscuous Ras binders in the family, even in the absence of lipid modifications on the CAAX box.

Lastly, RASSF9 has also been shown to bind strongly to NRas and KRas, and weakly to MRas (Rodriguez-Viciana et al., 2004). As this study was performed using

cells co-overexpressing Ras and RASSF9, it is not clear whether these interactions are direct and stimulation- or GTP-dependent. They also contradict our findings where our *in silico* model greatly disfavoured binding, which was supported by our *in vitro* observation.

The work presented here shows that whilst the predictions made of Ras interactions using structural information and surface charge distributions are informative and true to a certain extent, they are insufficient to determine definite strong binding to different Ras GTPases. This could in part, be due to the specificities that different Ras GTPases have for their effectors, which are defined by such subtle differences in residue conservation and structure, making them difficult to differentiate using our *in silico* approach. Examples of this include the reversal in binding affinities between Ras and Rap1 (Herrmann, 2003) and Rap1 and Rap2 (Miertzschke et al., 2007), although they are all highly related and belong to the Ras subfamily. Comparison of our observations with existing reports suggests that the reverse could also apply to these potential Ras effectors, whereby they have different affinities and specificities for different small GTPases dictated by the minor differences on their interaction surfaces. Additionally, a strongly positively charged surface does not always signify a strong binder, as demonstrated by our *in vitro* data. Therefore, these *in silico* predictions cannot be universally applied to define general Ras association for any specific effector. Further analysis using more advanced bioinformatics and computational tools will likely increase the accuracy of such predictions, as has been shown previously (Kiel et al., 2007, 2008). Ultimately, these predictions must always be confirmed through *in vitro* and finally *in vivo* experimentation.

Besides differential specificities and affinities, the experimental settings, in the case of such sensitive interactions, could play a significant role in the differences between earlier studies and our data. These include the assay conditions, such as the stringency of wash cycles, cellular versus *in vitro* systems and in particular, the isoforms and lengths of Ras GTPases and effectors used. The majority of previously shown RASSF interactions that contradicted our data involve farnesylated Ras. While it has been shown that farnesylation of the CAAX motif is crucial for Ras trafficking and localisation in cells (Magee and Seabra, 2005), it is interesting to note that, though not always the case, this lipid modification also plays an important role in specific effector binding. Another point of interest is the N-terminal subdomain in the classical RASSF

members. Previous studies suggest that it is not required for Ras binding in the case of RASSF2, 4 and 6; however, this has not been tested for RASSF1 and RASSF3, which are the two members most similar to RASSF5.

In terms of the physiological functions of the RASSF family, theoretically, tumour suppressors such as the RASSF members should reduce cell viability. Thus, siRNA knockdown of their expression should result in an increase in viability and the reverse applies to oncogenes. The lack of response to the knockdowns in A549 cells could be due to the already low levels of expression or absence of these targeted proteins due to epigenetic silencing, which is a phenomenon that is well documented for many of the RASSF members, for example RASSF1 is known to be downregulated in A549 cells (Dammann et al., 2000). It could also be due to the KRas-independent phenotype of A549. However, some of our observations from the KRas-dependent cell line HCT116 appear to oppose the hypothesis. RASSF2 and RASSF4, which have been reported as potential tumour suppressors (Eckfeld et al., 2004, Vos et al., 2003a), appear to be important for cell viability. Interestingly, several recent studies, including a comprehensive siRNA study of tumour suppressor genes also reported similar observations whereby established tumour suppressors also exhibited oncogenic properties and vice versa under different assay conditions (Bric et al., 2009, Lamouille and Derynck, 2009, Negrini et al., 2013, Oleksiewicz et al., 2013, Pierce et al., 1999). Together, these suggest that some tumour suppressors may function in a context-dependent manner based on the genetic background and tumour microenvironment, and may exhibit pro-oncogenic properties under certain circumstances.

Due to the limitations of our RNAi approach, the siRNA screen is inconclusive in determining the functional connection between Ras and the RASSF family. The caveats include the lack of information on the endogenous expression levels of all the targets in the cell lines used, as well as the validation of effective siRNA-mediated gene knockdown and off-target effects. Due to a lack of robust RASSF antibodies, possible optimisations for future RNAi studies include screening for endogenous target protein expression and efficient knockdowns at the RNA level using RT-PCR. Further validations should also be performed to eliminate off-target effects and confirm on-target effects for potential hits.

Despite the limitations of the siRNA screen, it does serve as a useful gateway to investigate the Ras network. In order to improve our understanding on the link between Ras specificity and the potentially different physiological functions of the RASSF family members, more diverse and exhaustive biological assays and screens are needed. Cell viability could be scored in parallel with apoptosis and cell cycle arrests during siRNA screens. These screens could also be performed in more cell lines harbouring different mutant Ras isoforms, cell lines with different genetic backgrounds, different tumour models and microenvironments, all of which may help to shed more light on the specific functions and possible context-dependent tumour suppressor properties of the RASSF members.

Further work is also required to better characterise and compare the RA domains of the RASSF family and their interactions with different Ras GTPases. Various point mutations of critical interacting residues, especially those predicted to make contact with specific residues in Ras and Rap1 that may have opposite properties, may also be useful in determining Ras specificity.

4 The C-terminal SARAH domain and coiled-coil

4.1. Introduction

Although the ten RASSF members all share a common RA domain, their C-terminal domains differ between the classical RASSF1-6 and the N-terminal RASSF7-10. The classical RASSF members share a common SARAH domain. However, this is absent in the N-terminal RASSF. Instead, three of these RASSF members (RASSF7, 8 and 10) have predicted coiled-coil motifs at various positions towards their C-terminal region (see Chapter 1, Figure 1.1).

The name of the C-terminal domain, SARAH, is derived from the three proteins that share this common feature at their extreme C-terminal region: Salvador, RASSF, Hippo (Scheel and Hofmann, 2003). As mentioned in the Introduction chapter, the Hippo signalling pathway and many of its major components, including Salvador (Sav, human homologue WW45), RASSF and Hippo (Hpo, human homologues MST1 and MST2) are well conserved between *Drosophila melanogaster* and mammals. In the MST/Hippo pathway, the SARAH domain is a key feature that facilitates the interactions between MST1/2, WW45 and RASSF, all of which act in conjunction to promote apoptosis and restrict cell proliferation to suppress tumourigenesis (Guo et al., 2007, Khokhlatchev et al., 2002, Praskova et al., 2004, Scheel and Hofmann, 2003). MST1 and MST2 can also synergise with different RASSF members outside the Hippo pathway to induce apoptosis (Ikeda et al., 2007, 2009, Oh et al., 2006). Additionally, KRas has been shown to promote apoptosis via the RASSF1/MST1 and RASSF5/MST1 complexes (Khokhlatchev et al., 2002, Praskova et al., 2004). More recently, RASSF1 and MST1 have also been linked to cardiac physiology and disease, whereby their interaction facilitated by the SARAH domain greatly influences the cardiac function in response to stress (Del Re et al., 2010).

MST kinases consist of a N-terminal kinase domain, an inhibitory domain and a SARAH domain (Figure 4.1A) The MST1 SARAH domain was the first to be structurally characterised using Nuclear Magnetic Resonance (NMR) spectroscopy and has since been studied quite intensively (Hwang et al., 2007). The structure was solved

Figure 4.1 Comparison of the MST1 kinase and RASSF5 SARAH domain

(A) Schematic representation of MST1 kinase. The main structural features are shown and the residue positions are indicated above.

(B) The homodimer structure of the MST1 SARAH domain (PDB: 2JO8). (i) Ribbon representation of the SARAH homodimer. (ii) Surface representation of the SARAH domain in the same orientation (left) and the 180° rotated orientation. Basic residues are in blue, acidic in red, polar in white and hydrophobic in yellow. Side chains of hydrophobic residues involved in dimer stability are shown in yellow and labelled. Basic and acidic residues involved in electrostatic interactions are in blue and red respectively.

(C) The homodimer structure of the murine RASSF5 SARAH domain (PDB: 2YMY). (i) Ribbon representation of the SARAH homodimer. (ii) Surface representation of the SARAH domain in two orientations as described above. The residues and side chains are also coloured and labelled as above.

(D) Sequence alignment of the MST1 and murine RASSF5 SARAH domain. Fully conserved residues are marked by asterisks (*), highly conserved residues by colons (:) and moderately conserved residues by periods (.). Conserved hydrophobic residues involved in the dimer interface are highlighted in yellow, acidic residues in red and basic residues in blue. The top line indicates the heptad repeats within the SARAH domain and the stutters are shown in red text.

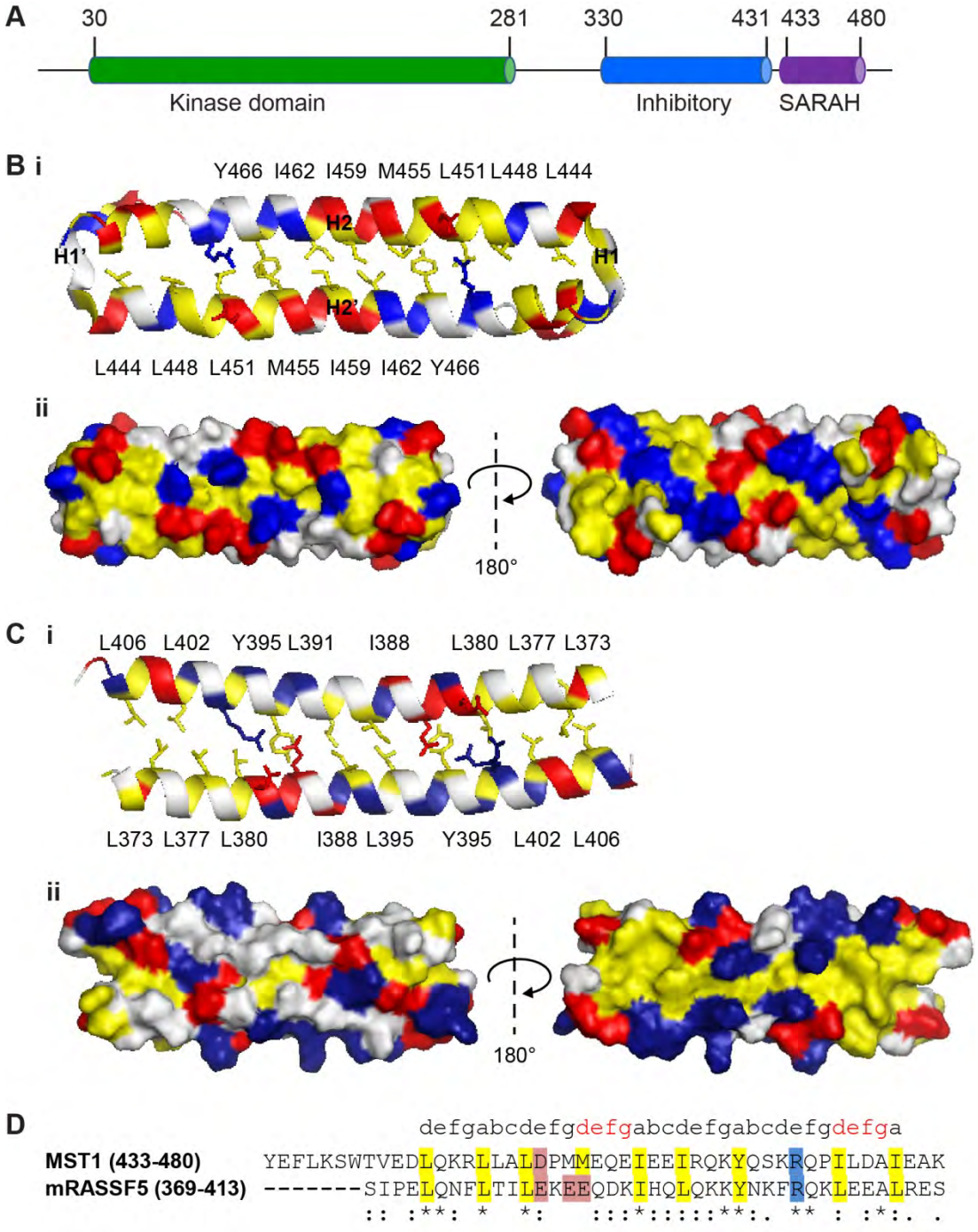
A
30
281
330
431
433
480
Kinase domain
Inhibitory
SARAH
B i
Y466 I462 I459 M455 L451 L448 L444
H1'
H2
H2'
H1
L444 L448 L451 M455 I459 I462 Y466
ii
180°
C i
L406 L402 Y395 L391 I388 L380 L377 L373
L373 L377 L380 I388 L395 Y395 L402 L406
ii
180°
D
defgabcdefgdefgabcdefgabcdefgdefga
MST1 (433-480) YEFLKSWTVEDLQKRLLALDPMMEQEIEEIRQKYQSKRQPILDAIEAK
mRASSF5 (369-413) -------SIPELQNFLTILEKEEQDKIHQLQKKYNKFRQKLEEALRES

as a homodimer, with each monomer consisting of two helices (Figure 4.1Bi). The first helix, H1 is a short 3_{10} helix folded toward the corresponding helix H1' of the other monomer. It also brings the two kinase domains into close proximity to allow their autophosphorylation, an event that is important for the activation of its kinase activity and downstream signalling (Anand et al., 2008, Praskova et al., 2004). The second long helix, H2 constitutes the rest of the SARAH domain and exhibits coiled-coil properties (Constantinescu Aruxandei et al., 2011). The monomers form a dimer via a head-to-tail interaction of the two long helices in an antiparallel arrangement. This dimer interface is largely stabilised by hydrophobic interactions from the aliphatic side chains of the residues in H2 (Figure 4.1B). Additional intermolecular electrostatic interactions and bifurcated hydrogen bonds also contribute to the dimer stability.

Initial structural studies revealed a higher propensity for the isolated MST1 SARAH domain to form heterodimers, rather than homodimers, with the RASSF5 SARAH domain with a K_D in the nanomolar range (Hwang et al., 2007). However, later studies have shown that the isolated SARAH domain behaves differently compared to its longer construct, which is more reflective of its physiological state. When the MST1 SARAH domain is expressed with its N-terminal inhibitory region that connects it to the kinase domain (Figure 4.1A), it has a higher homodimer affinity within the low micromolar (average 1 μM) K_D range (Constantinescu Aruxandei et al., 2011). The inhibitory domain also contributes extra thermodynamic stability to the dimeric state of the SARAH domain, whereas the monomer is less stable and dimer dissociation is coupled to partial unfolding. This structural plasticity appears necessary in facilitating the switch from one complex to another, in the case of MST1, from a homodimer to a heterodimer.

More recently, the RASSF5 SARAH domain was crystallised, the first example of a crystal structure of a RASSF SARAH domain (Makbul et al., 2013). However, this crystal structure consists only of the long helix H2 of the predicted SARAH domain (Figure 4.1C). Nevertheless, the RASSF5 SARAH domain also forms an antiparallel homodimer via its long helix and the dimer interface consists of inter-helical interactions of hydrophobic residues, electrostatic and water-mediated ionic interactions.

The MST1 and RASSF5 SARAH domains share many similarities. They display the same coiled-coil characteristics in the form of a seven-residue (heptad) repeat,

although both are disrupted by two stutters at the same positions (Figure 4.1D). The RASSF5 SARAH domain homodimer also undergoes simultaneous dissociation and unfolding previously described for MST1 (Makbul et al., 2013). Interestingly, the C-terminal end of the SARAH domain is flexible, which mirrors the inhibitory domain of MST1, and this may facilitate its dimerisation with different interaction partners. Despite this, a few distinctive characteristics were observed for the RASSF5 SARAH domain. Its homodimer is much less stable at physiological temperatures, with a K_D of only 25 μM; whereas its monomer is slightly more stable. Additionally, this equilibrium between the monomeric and dimeric states could be dependent on the total protein concentration, which may in turn affect its activity.

In terms of the SARAH domain heterodimers, only the interactions between MST1 and RASSF5 or WW45 have been touched upon (Hwang et al., 2007). The MST1 and RASSF5 SARAH heterodimer are formed in a 1:1 stoichiometry and involve hydrophobic residues from the dimer interface of the MST1 helical domain. The formation of this heterodimer also appears to induce a conformational change in MST1. Whereas, WW45 binds to a different surface on the MST1 SARAH domain and its binding affinity is much weaker and insufficient to dissociate the MST1 homodimer. In contrast, the *Drosophila* homologues dRASSF and Hpo appear to form a weaker complex that is easily displaced by increasing Sav concentrations (Polesello et al., 2006). Despite the different binding surfaces, a ternary complex of MST1/WW45/RASSF5 is thought to be unlikely (Hwang et al., 2007), which is consistent with the biochemical data on dRASSF (Polesello et al., 2006). However, RASSF6, WW45 and MST2 have been shown to form a tripartite complex (Ikeda et al., 2009). Apart from this, not much is known about the molecular mechanisms involved in these interactions.

The SARAH domain is absent in the N-terminal RASSF members. However, alternative coiled-coil structures have been predicted for RASSF7, 8 and 10. The coiled-coil was first described in 1953 as the main structural element of many fibrous proteins and is essentially a bundle of three to four α-helices wound into a superhelix (Ciani et al., 2010, Lupas, 1996). This motif has been described to form different numbers of oligomers, including dimers, trimers, tetramers and other higher-order complexes, the actual number being determined by the distribution of the hydrophobic core residues (Ciani et al., 2010, Moutevelis and Woolfson, 2009). Given that hydrophobic interactions play a major role in SARAH domain dimerisation, the coiled-coil could

potentially also function similarly to the SARAH domain and facilitate homo- and hetero-dimerisation involving the N-terminal RASSF members.

Multiple studies have illustrated the importance of the SARAH domain and its dimerisation. It is now widely recognised that these interactions play a significant role, not only in the Hippo signalling network, but also in other emerging novel pathways and functions as described in the Introduction chapter. The consequences involve tumour suppression and possibly also protection against heart failures and bone development. It is therefore imperative to further investigate the SARAH domain and the C-terminal coiled-coil to gain a better understanding of the mechanisms of their interaction and the possible functional consequences.

The aim of this study was to compare the SARAH domain structure of the classical RASSF1-6 and the ability of the ten RASSF members to homo- and hetero-dimerise within the family and with MST kinase via the SARAH domain or coiled-coil motif. The results strongly suggest that the SARAH domain is required for dimerisation, whereas the coiled-coil is insufficient to facilitate any dimerisation between the proteins analysed here.

4.2. Results

4.2.1. Modelling the RASSF SARAH domain and predicting its interactions

We first built a phylogenetic tree for the SARAH domain of the classical RASSF1-6 and MST1 to compare their homologies and evolutionary links (Figure 4.2). There is a distinctive pattern similar to that observed for the RA domain (see Chapter 3, Figure 3.5). RASSF1, 3, 5 and RASSF2, 4, 6 are separated into two sub-branches, with MST1 grouped together with the former. The homology scores for each RASSF pair and RASSF/MST pair are summarised in Table 4.1. RASSF1, 3 and 5 share 50-60% homology, but less than 30% similarity with RASSF2, 4 and 6. In this second subgroup, RASSF2 and RASSF4 are 65% identical, but RASSF6 appears quite different, sharing less than 40% sequence identity with both members. With regards to the MST1 SARAH domain, it shares 17-27% homology with the RASSF SARAH domains. Interestingly, it has exactly the same sequence identity scores for RASSF4, 5 and 6, which amongst

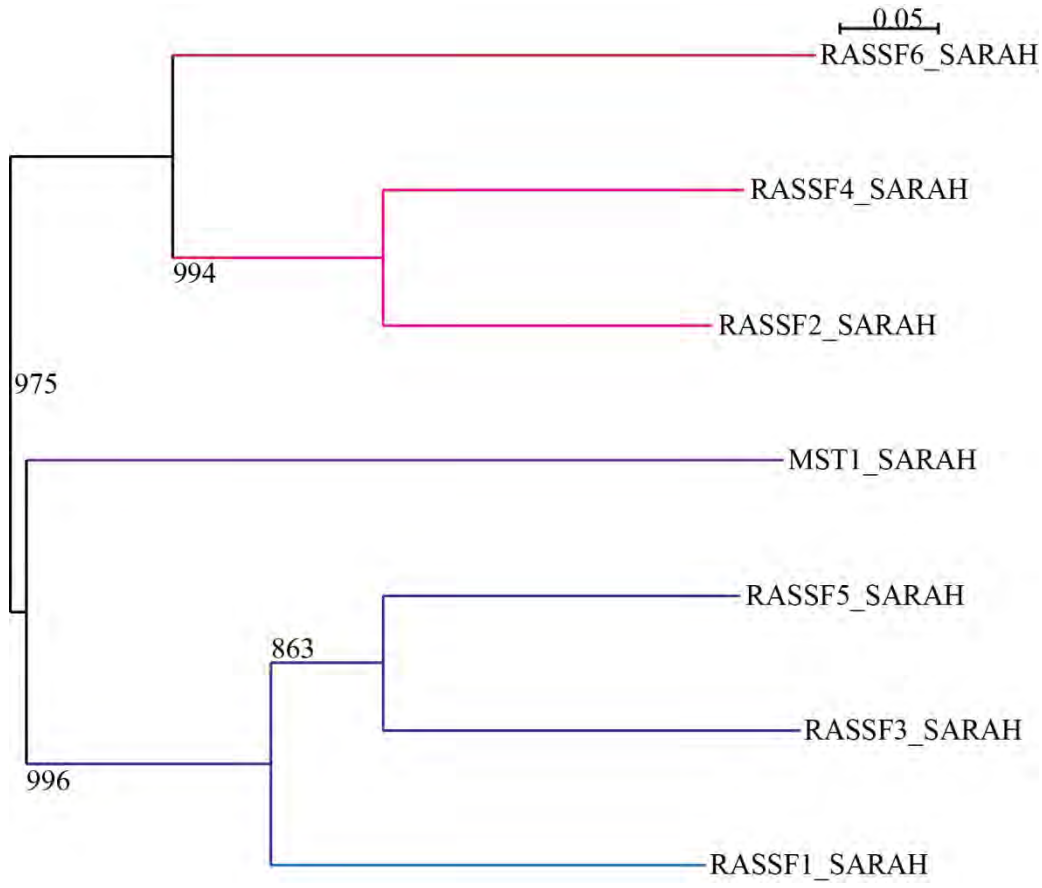

Figure 4.2 Phylogenetic tree of the MST1 and RASSF family SARAH domain

Multiple sequence alignments were performed as described in section 2.8. The phylogenetic tree was built in njplot using the sequence alignments. Bootstrap figures are shown to represent the confidence level of each node, with 1000 being the maximum. The 0.05 scale bar refers to the branch length, which is a measure of the amount of divergence between two nodes in a tree. The tree is split into two branches, which are colour-coded: blue for MST1 and RASSF1, 3 and 5, and red for RASSF2, 4 and 6.

Table 4.1 Homology scores for the RASSF and MST1 SARAH domains

RASSF	RASSF	Score (%)
1	2	29.17
1	3	50.0
1	4	25.0
1	5	54.17
1	6	20.83
2	3	31.25
2	4	64.58
2	5	25.0

RASSF	RASSF	Score (%)
2	6	37.5
3	4	22.92
3	5	60.42
3	6	16.67
4	5	22.92
4	6	39.58
5	6	22.92

MST	RASSF	Score (%)
1	1	27.08
1	2	16.67
1	3	18.75
1	4	20.83
1	5	20.83
1	6	20.83

themselves share rather low homologies. Thus, the phylogenetic tree is more reflective than the individual identity scores of the overall similarities and differences amongst the SARAH domains.

At the time of our study, the MST1 SARAH domain was the only structurally characterised SARAH domain. Therefore, we used MST1 as the structural template for the homology modelling of the RASSF SARAH domains. Although the homology scores between MST1 and the classical RASSF members are not high, their sequence alignments show that many of the key residues involved in maintaining dimer stability are remarkably well conserved (Figure 4.3A). Most residues involved in hydrophobic interactions (L444, L448, L451, I459, I462 and Y466 from MST1) are highly conserved except M455. The two residues involved in electrostatic interaction are D452 and R470; the first is only conserved in RASSF3 and RASSF5, whilst the latter appears very well conserved across all six RASSF members. The physico-chemical properties of the residues aligning to those involved in stabilising the H1 and H2 helices in the MST1 monomer (L436, W439, V441, L444, I473 and I477) are generally conserved, thus still allowing for hydrophobic interactions.

The homodimeric SARAH domain models for all six RASSF members are very similar in terms of the distribution of the hydrophobic residues along helix H2 (Figure 4.3B). They are also comparable to that of the MST1 and RASSF5 structures (Figure 4.1Bi and Ci). Despite the poor conservation of residues aligning to D452, the models suggest electrostatic interactions with the second helix H2 are still possible due to the presence of a stretch of acidic residues between the regions aligning to L451 and I459 of MST1. Based on the conservation of the main features involved in dimerisation, we predict that all six classical RASSF members will be able to form homodimers and heterodimers within the RASSF family and with MST kinases.

Modelling of the N-terminal RASSF coiled-coil motifs was not performed due to a lack of available template structures and the widely variable sequence length of the motif. Due to these limitations, it is only possible to determine their interaction capabilities empirically.

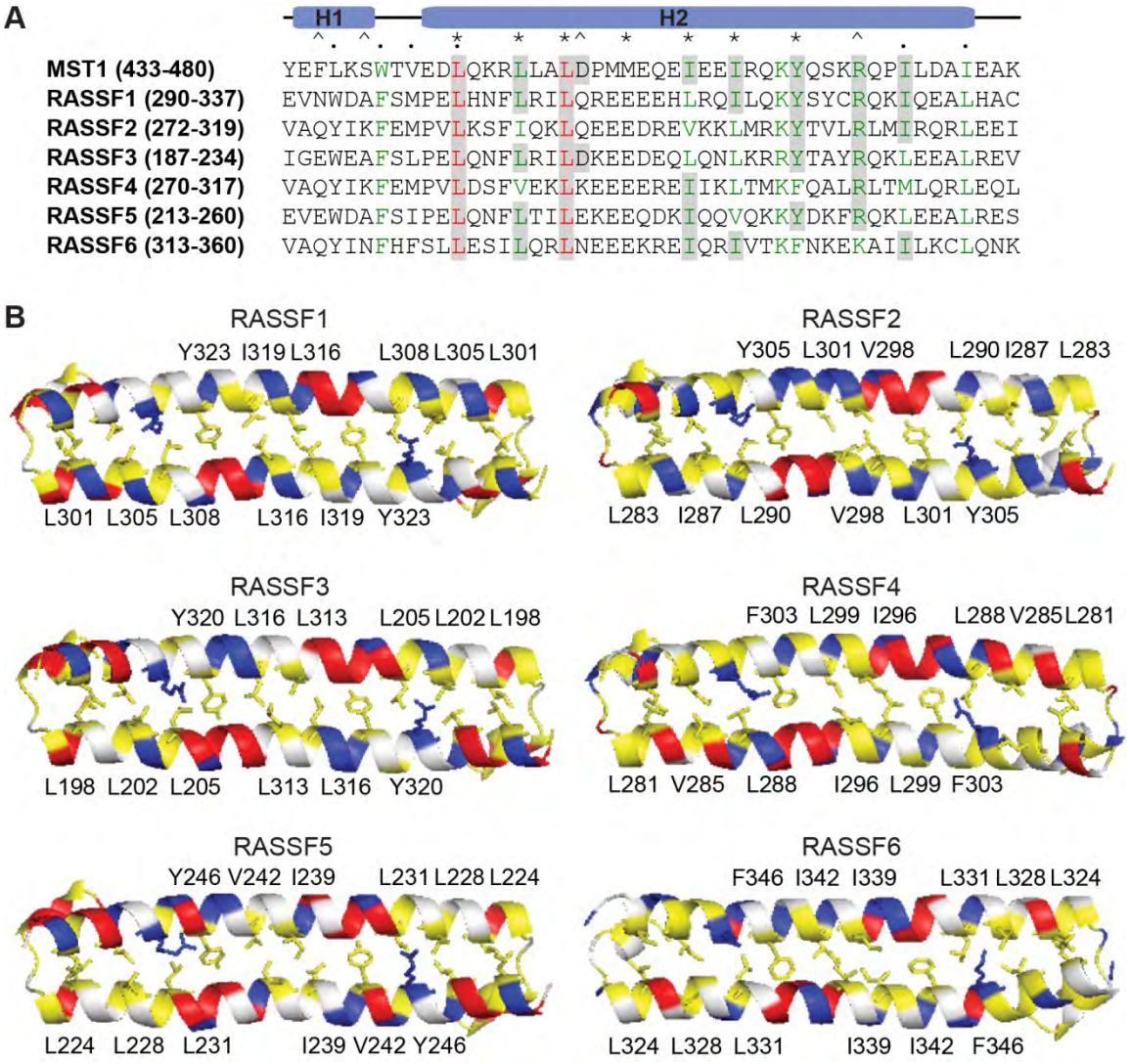

Figure 4.3 Modelling the RASSF SARAH domain

(A) Multiple sequence alignments of the Prosite predicted SARAH domain. The secondary structural elements are indicated as helix 1 (H1) and helix 2 (H2). Residues in MST1 involved in electrostatic interactions are marked with arrow heads (^), hydrophobic interactions for monomer stability with periods (.) and for dimer stability with asterisks (*). Fully conserved interacting residues are highlighted in grey. Other residues are coloured according to their similarity: fully conserved residues in red and highly similar residues in green.

(B) Ribbon representation of the classical RASSF SARAH domain modelled against MST1 (PDB: 2JO8). Basic residues are in blue, acidic in red, polar in white and hydrophobic in yellow. Side chains of hydrophobic residues involved in dimer stability are labelled and shown in yellow; the major basic residue involved in electrostatic interaction is in blue.

4.2.2. *In vitro* interaction studies of the SARAH domain and coiled-coil

In order to validate the *in silico* predictions, we used a few different experimental approaches to determine whether the predicted RASSF SARAH domains and coiled-coil motifs are able to form homodimers or heterodimers under different *in vitro* experimental settings.

4.2.2.1. Dimerisation of isolated SARAH domain "*in vitro*" versus "in cells"

As *in vitro* biochemical characterisation has never been done for the isolated RASSF5 and MST1 SARAH domain, which are the only two SARAH domain proteins that can be feasibly expressed and purified (see Table 2.5), we performed a pull-down assay using these proteins. Unexpectedly, no binding was detected between the RASSF5 and MST1 SARAH domain (Figure 4.4A). This observation was further confirmed by our mass spectrometry analysis, in which no heterodimers were detected when the proteins were mixed (Figure 4.4Biii). Conversely, monomers and homodimers were detected with sizes identical to those for the individual MST1 and RASSF5 SARAH domains (Figure 4.4Bi, ii). Surprisingly, these *in vitro* data contradicted the data obtained under cellular settings as the co-IP analysis using co-transfected cell lysates showed that the RASSF5 SARAH domain was able to heterodimerise with both full length MST1 and the MST1 SARAH domain in a cell context (Figure 4.4C).

Due to the differential preference for homodimerisation and heterodimeristion in a completely *in vitro* setting, we did not pursue any further studies on the kinetics and binding dynamics of the isolated RASSF SARAH domains under these conditions. Instead, we focused on their interactions under cellular conditions.

4.2.2.2. Dimerisation within the RASSF family

First, we performed a set of co-IPs using the myc epitope tag to show dimerisation within the RASSF family, specifically with RASSF5 (Figure 4.5Ai). This is a partial *in vitro* method using cell lysates containing overexpressed proteins, which may be in a pre-formed complex when immunoprecipitated. The myc-tagged RASSF5 DNA construct used for co-expression was RASSF5Δ41 as it co-expresses very well in cellular systems. This construct was generated by a previous member of the laboratory and has a deletion of the first 41 amino acid residues (Figure 4.5Aii).

Figure 4.4 Interaction between isolated SARAH domains "*in vitro*" and "in cells"

(A) Pull-down analysis of purified proteins of MST1 SARAHmyc and immobilised S-RASSF5 SARAH as described in section 2.6.1.3. This is a representative of the three repeats performed for this experiment.

(B) Mass spectra of MST1 SARAHmyc and RASSF5 SARAH under native MS conditions, performed by Jun Yan as described in section 2.6.4. Experimental conditions are described in section 2.6.4. (i) Mass spectrum of MST1 SARAHmyc, (ii) RASSF5 SARAH and (iii) MST1 SARAHmyc mixed with RASSF5 SARAH in a 1:1 stoichiometry. Charge states corresponding to MST1 SARAHmyc monomer and dimer, and RASSF5 SARAH monomer and dimer, are indicated and coloured in red and blue, green and cyan, respectively. The table below compares the protein monomeric and dimeric mass measurements to the theoretical masses. The low error confirms the accuracy of the experimental results.

(C) Co-IP analysis of TagRFPT-MST1 SARAH and myc-RASSF5 SARAH, in which full length (FL) MST1 and TagRFPT (tRFP) served as a positive and negative control respectively. The DNA constructs were co-transfected in equal concentrations and co-IP were performed as described in section 2.6.2. IP and IB indicate immunoprecipitates and imunoblots respectively. This assay was repeated three times and a representative is shown here.

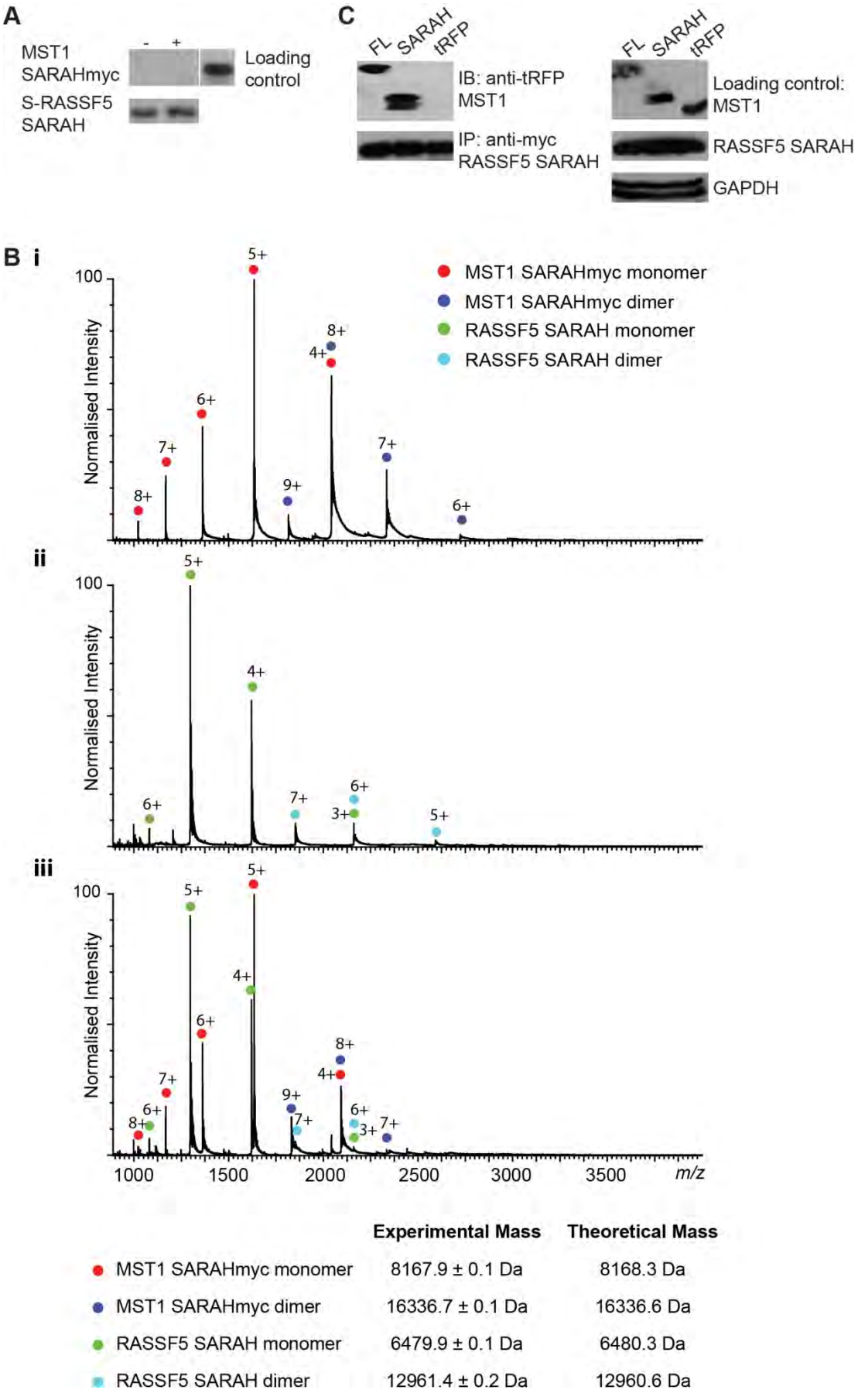
A
MST1 SARAHmyc
S-RASSF5 SARAH
- +
Loading control
C
FL SARAH tRFP
IB: anti-tRFP MST1
IP: anti-myc RASSF5 SARAH
FL SARAH tRFP
Loading control: MST1
RASSF5 SARAH
GAPDH
B i
ii
iii
Normalised Intensity
100
MST1 SARAHmyc monomer
MST1 SARAHmyc dimer
RASSF5 SARAH monomer
RASSF5 SARAH dimer
1000 1500 2000 2500 3000 3500 m/z
Experimental Mass
Theoretical Mass
MST1 SARAHmyc monomer 8167.9 ± 0.1 Da 8168.3 Da
MST1 SARAHmyc dimer 16336.7 ± 0.1 Da 16336.6 Da
RASSF5 SARAH monomer 6479.9 ± 0.1 Da 6480.3 Da
RASSF5 SARAH dimer 12961.4 ± 0.2 Da 12960.6 Da

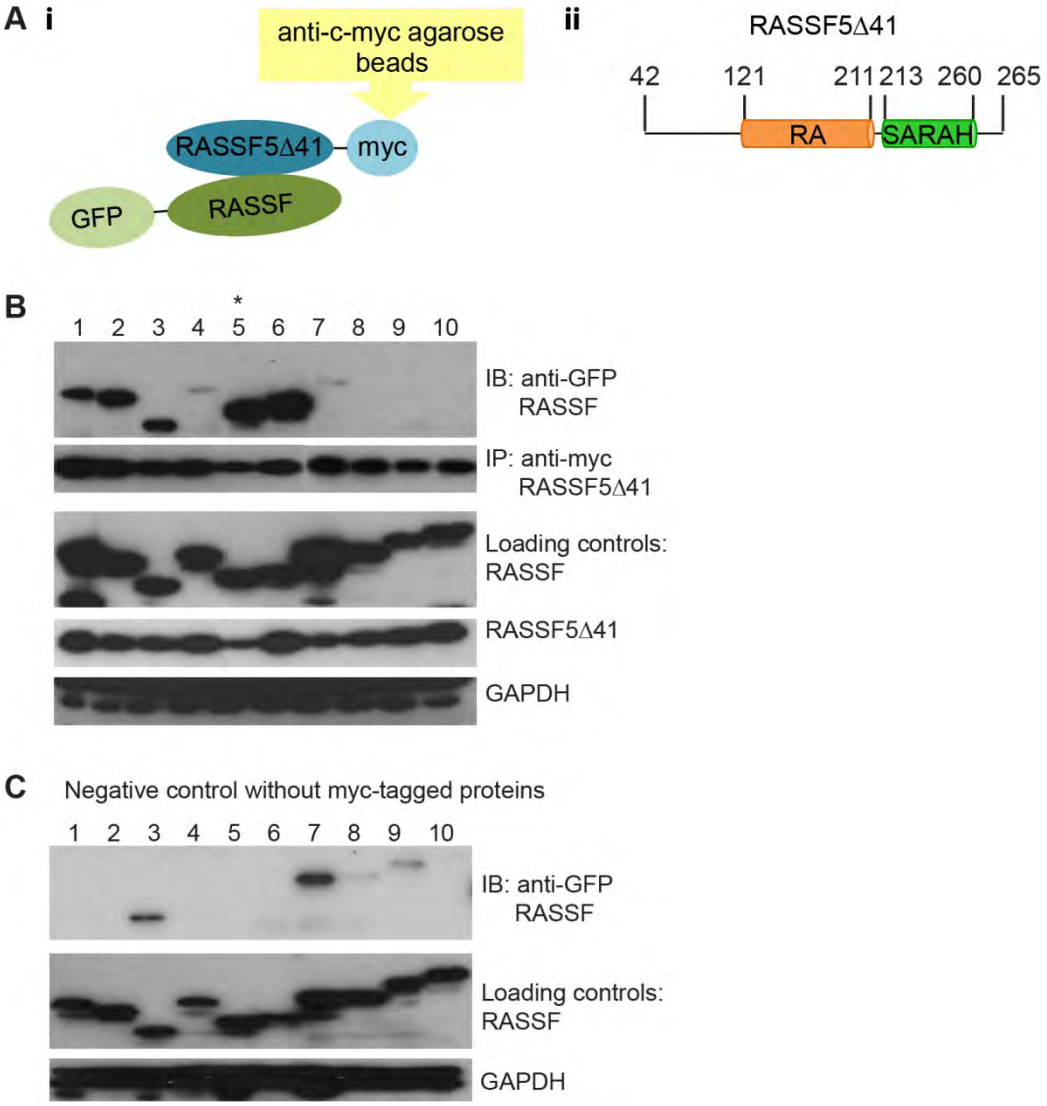

Figure 4.5 Dimerisation within the RASSF family

(A) (i) Schematic outline of the co-IP assay as described in section 2.6.2. (ii) Schematic representation of the myc-tagged RASSF5Δ41 construct used. The residue positions are indicated above. All co-IP assays were repeated three times and a representative is shown here.

(B) Co-IP assay to show interaction between GFP-RASSF1-10 and myc-RASSF5Δ41. The RASSF loading controls and GAPDH endogenous control are shown below the co-IP panels for each cell lysate. The RASSF5 homodimer is marked with an asterisk above the panel.

(C) Co-IP assay of the negative controls performed using cell lysates consisting only GFP-RASSF. The loading controls are shown below.

All six classical RASSF members were detected in the immunoprecipitates at varying levels, which confirmed that RASSF1, 2, 3, 4 and 6 could form heterodimers with RASSF5 and possibly with different affinities; whereas RASSF5 is also able to homodimerise (Figure 4.5B). A very weak signal was also detected for RASSF7. However, a further negative control experiment performed without the myc-tagged protein showed that RASSF7 has a propensity to bind non-specifically to the anti-c-myc-agarose, with weak non-specific binding also detected for RASSF3, 8 and 9 (Figure 4.5C). Therefore, the RASSF7 band from the co-IP experiment is likely a false positive, whereas the non-specific binding of RASSF3 should have minimal significance as the positive band detected in the dimerisation experiment was much stronger and comparable with the loading control.

It is possible to repeat these experiments with other RASSF members in analogous settings. However, heterodimerisation or homodimerisation with other RASSF members were not tested in this study as the other myc-tagged RASSF proteins co-expressed very poorly and inconsistently with the GFP-tagged RASSF proteins. Nevertheless, based on this set of data and the highly similar homology models, it is likely that the remaining classical RASSF members can also form different combinations of heterodimers amongst themselves.

4.2.2.3. Heterodimerisation between the RASSF family and MST kinases

Next, we looked at heterotypic interactions between the RASSF family and the MST kinases using the same technique and full length myc-tagged MST. As wild-type MST1 and MST2 did not express very well or in a consistent manner (data not shown), we generated their respective kinase-dead mutants K59R and K56R that are known to improve expression levels and consistency. We attempted to express and purify these proteins, which were used for the initial experiments (Figure 4.6A). However, the yield of the purified proteins from large scale purifications was not sufficient to carry out all the experiments. Additionally, we could not obtain a purity of above 90% (data not shown). Therefore, all further experiments were performed using cell lysates co-expressing RASSF and MST unless otherwise stated (Figure 4.6Aii).

For the initial experiments, we compared RASSF5 dimerisation with purified proteins of wild-type and kinase-dead MST1 and MST2. RASSF5 co-

Figure 4.6 Heterodimerisation between the RASSF family and MST kinases

(A) Schematic outline of co-IP assays using (i) purified proteins of myc-MST or (ii) co-transfected cell lysates containing pre-formed complexes as described in section 2.6.2. All co-IP assays were repeated three times and a representative is shown here.

(B) Co-IP assay to show interaction between GFP-RASSF5 and purified proteins of wild-type (WT) myc-MST1 and MST2 or their respective kinase-dead mutants, K59R and K56R. The RASSF loading controls and GAPDH endogenous control are shown below.

(C) Co-IP assay to show interaction between wild-type (WT) RASSF5 or truncated RASSF5Δ213-265, lacking the SARAH domain, and MST1 K59R and MST2 K56R (left). The loading controls are shown on the right.

(D) Co-IP assay to show interaction between GFP-RASSF1-10 and MST1 K59R (left) or MST2 K56R (right). The loading controls are shown below.

(E) Sequence alignment of the MST1 and MST2 SARAH domain. Fully conserved residues are marked by asterisks (*), highly conserved residues by colons (:) and moderately conserved residues by periods (.). The conserved key interacting residues are highlighted: hydrophobic, acidic and basic residues are in yellow, red and blue respectively.

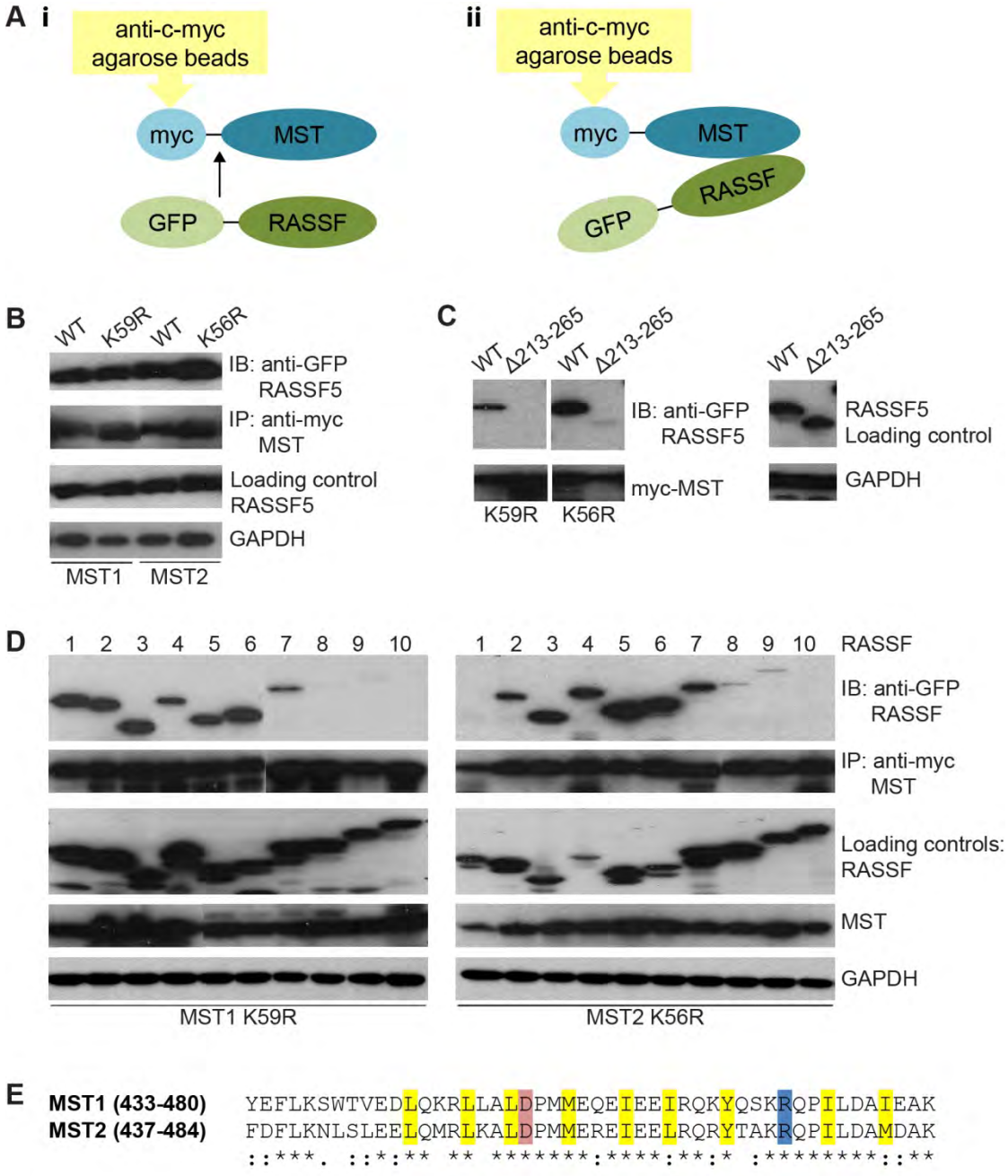
A i
anti-c-myc agarose beads
myc
MST
GFP
RASSF
ii
anti-c-myc agarose beads
myc
MST
RASSF
GFP
B
WT
K59R
WT
K56R
IB: anti-GFP RASSF5
IP: anti-myc MST
Loading control RASSF5
GAPDH
MST1
MST2
C
WT
Δ213-265
WT
Δ213-265
IB: anti-GFP RASSF5
myc-MST
K59R
K56R
WT
Δ213-265
RASSF5 Loading control
GAPDH
D
1 2 3 4 5 6 7 8 9 10
1 2 3 4 5 6 7 8 9 10
RASSF
IB: anti-GFP RASSF
IP: anti-myc MST
Loading controls: RASSF
MST
GAPDH
MST1 K59R
MST2 K56R
E
MST1 (433-480) YEFLKSWTVEDLQKRLLALDPMMEQEIEEIRQKYQSKRQPILDAIEAK
MST2 (437-484) FDFLKNLSLEELQMRLKALDPMMEREIEELRQRYTAKRQPILDAMDAK

immunoprecipitated equally with all four types of MST kinases tested (Figure 4.6B). Subsequently, we also tested a truncated RASSF5Δ213-265 lacking the SARAH domain and no binding was detected (Figure 4.6C). This confirmed that the kinase activity does not interfere with heterodimerisation and the RASSF SARAH domain is crucial for interaction.

For all subsequent interaction assays involving MST1 and MST2, their kinase-dead mutants were used unless otherwise stated. In the following co-IP assay, the complete panel of all ten RASSF members were tested for their interaction with MST1 and MST2. All classical RASSF members were detected in complex with MST1 (Figure 4.6D, left). RASSF7 was also detected in the immunoprecipitate. However, this could again be a false positive due to its non-specific interaction with the resin (see section 4.2.2.1). A similar interaction pattern was observed with MST2, with the exception of RASSF1 (Figure 4.6D, right). As both MST kinases have a 67% sequence identity and almost 100% conservation in their key interacting residues (Figure 4.6E), this varied detection of RASSF1 between the two MST kinases could be due to the lower expression levels of both RASSF1 and MST2 when co-expressed rather than a difference in its interaction with MST1 and MST2.

4.2.3. Using intracellular FRET to study heterodimerisation

To date, all approaches used to demonstrate heterodimerisation between the RASSF family and MST kinases have been either *in vitro* or non-quantitative. Therefore, we next attempted to study these interactions in a cellular system using quantitative FRET measurements. This study was performed in collaboration with Dr Anca Margineanu from the Photonics Group at Imperial College London using their in-house FLIM automated multiwell plate reader and analysis software as described in section 2.6.3. Schematics of all the fluorescent constructs used in this study are shown in Figure 4.7.

4.2.3.1. Heterodimerisation between the RASSF family and MST1

First, we compared the interactions of the ten full length RASSF proteins with the isolated MST1 SARAH domain. The negative controls used were cells expressing only GFP-RASSF or both GFP-RASSF and mCherry-MST1ΔSARAH, a MST1 construct lacking the SARAH domain. These should give the maximum or close to the maximum

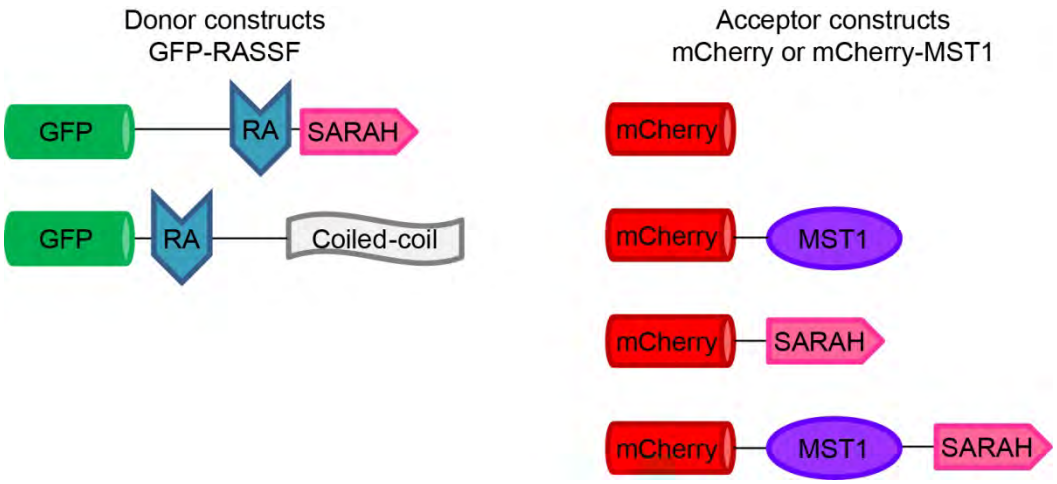

Figure 4.7 Schematic representations of the fluorescence FRET constructs

The GFP-tagged (green) full length RASSF constructs are used as the FRET donors (left). The mCherry-tagged (red) constructs are used as the FRET acceptors (right). From top to bottom for the mCherry constructs: mCherry only, MST1ΔSARAH (SARAH domain deletion), MST1 SARAH (kinase domain deletion) and full length MST1. FRET experiments were performed and data were analysed as described in section 2.6.3.

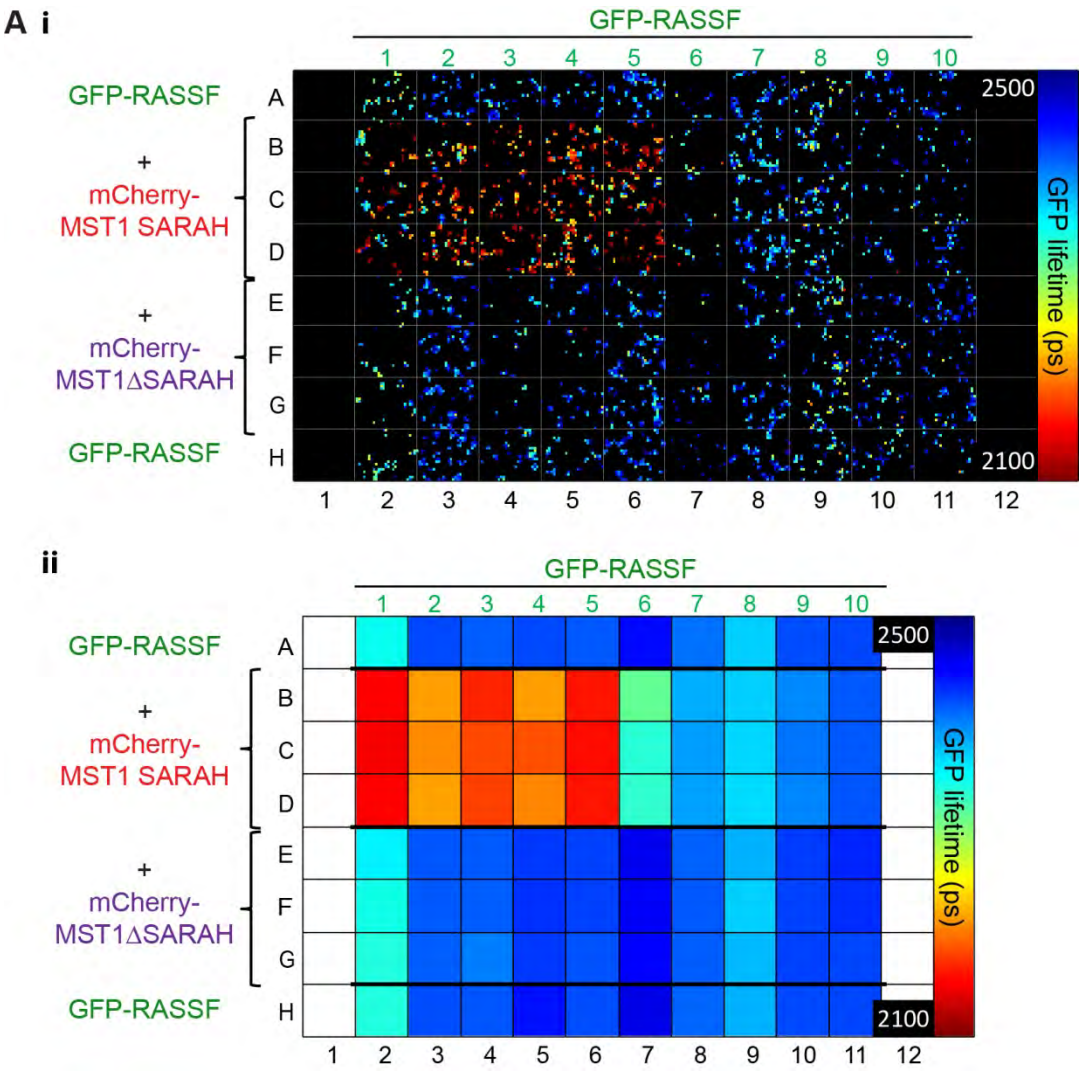

Figure 4.8 FRET studies on RASSF and the isolated MST1 SARAH domain

(A) Plate maps of the 96-well plate setup for GFP-RASSF and mCherry-MST1 or the negative control mCherry-MST1ΔSARAH. Image acquisitions and data processing were performed by Dr Anca Margineanu as described in section 2.6.3. (i) Images of the transfected cells in each well per field of view. (ii) FRET signals in each well is indicated by the colour bar on the right corresponding to the GFP donor lifetime measured in picoseconds (ps), with a transition from blue to red from low to high FRET signals. The positions of each well are labelled A-H on the left and 1-12 below. The RASSF members are labelled 1-10 above the grids.

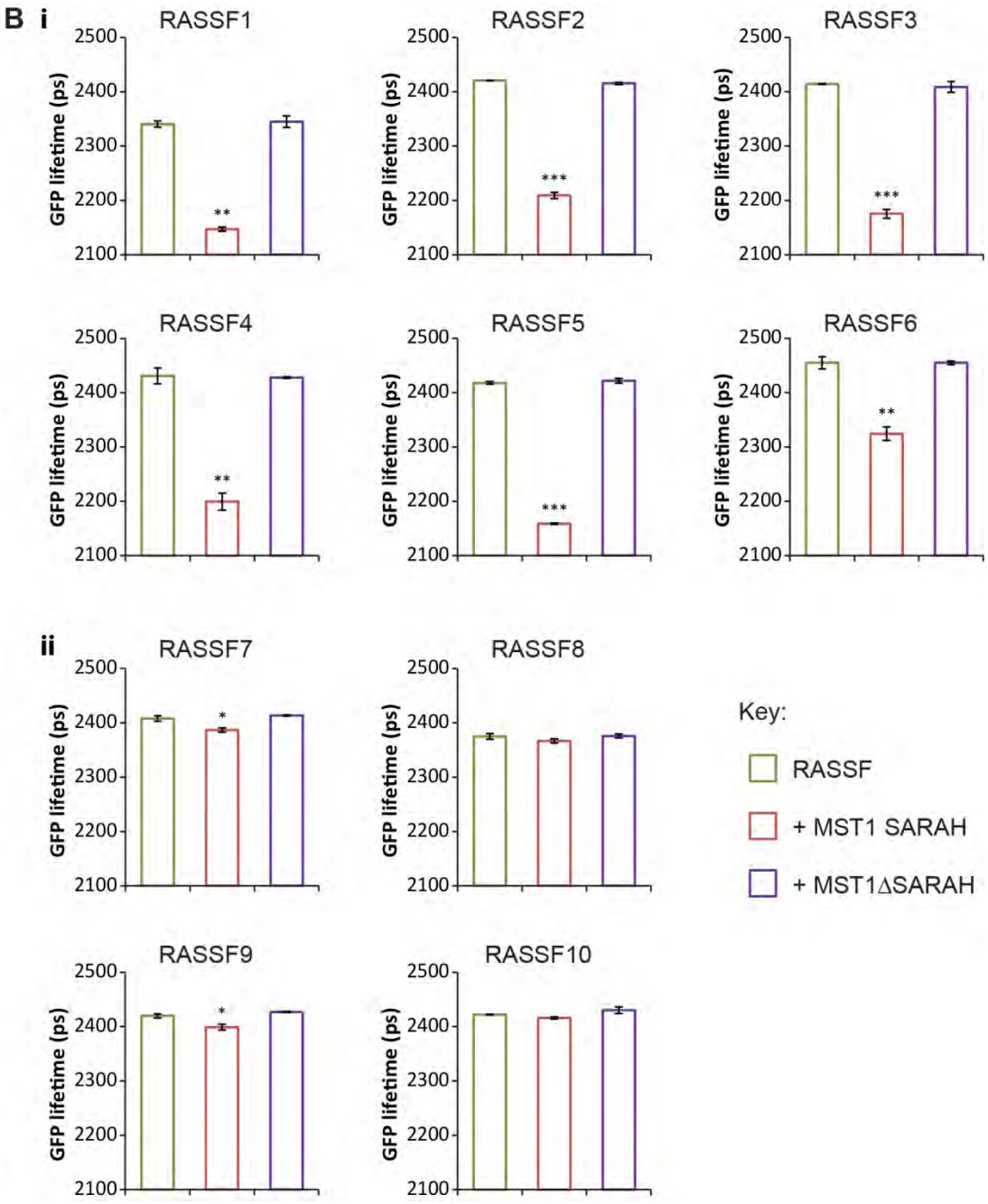

(B) Bar graphs showing the GFP lifetime changes per condition for (i) the classical RASSF1-6 and (ii) the N-terminal RASSF7-10. The bars are colour-coded for each condition, indicated in the key. The GFP lifetimes were calculated as an average per well and error bars are the standard deviations. P-values were calculated against both negative controls using the Student's t-test and are indicated as follows: $p \leq 0.05$ (*), $p \leq 0.01$ (**) and $p \leq 0.001$ (***). Only $p \leq 0.01$ is considered significant to take into account the occasional non-specific FRET in this study.

donor lifetime due to the lack of interaction. The decrease in the GFP donor lifetime, i.e. increase in FRET signal, is evident in the plate maps containing images of the cells (Figure 4.8Ai) or the FRET colour indicator (Figure 4.8Aii). This indicates the close proximity of the donor and acceptor fluorophores, hence, confirming the interaction between MST1 SARAH and RASSF1-6 (Figure 4.8Bi). In contrast, the changes observed for RASSF7-10 were minimal and statistically insignificant when taking into account the occasional occurrence of non-specific FRET signals, indicating no interaction between MST1 SARAH and the N-terminal RASSF members (Figure 4.8Bii).

We next compared the interaction between the full length RASSF proteins and full length MST1 or its isolated SARAH domain. In this set of experiment, cells expressing only GFP-RASSF and co-expressing GFP-RASSF and the fluorophore mCherry served as the negative controls. A clear decrease in the GFP donor lifetime was observed for RASSF1-6 co-expressed with both full length MST1 and MST1 SARAH, which is consistent with our first set of data (Figure 4.9A). However, this change was significantly greater for the isolated MST1 SARAH domain, which is likely due to the shorter donor-acceptor distance in the absence of the MST1 kinase region rather than stronger binding to the isolated SARAH domain under cellular conditions. Whereas, the changes in the FRET signals for RASSF7-10 were statistically insignificant (Figure 4.9B).

4.2.3.2. Potentially different binding affinities amongst the classical RASSFs

Interestingly, when we compared the two studies of RASSF interactions with the isolated MST1 SARAH domain, we noticed the strength of the FRET signals varied and somewhat followed the pattern of the SARAH domain sequence homologies (section 4.2.1). This could be an indication of their different binding affinities, with stronger FRET signals signifying higher affinities. RASSF3 and RASSF5 consistently showed the strongest FRET signals (Figure 4.10A), whilst RASSF1 displayed different signal intensities between the two experiments. However, its averaged signal was similar to RASSF2 and RASSF4, with RASSF6 showing the weakest FRET signal compared to the rest of the classical RASSF members. These interactions were also confirmed *in vitro* for the classical RASSF members alongside full length MST1 (Figure 4.10Bi) and appeared to follow the general pattern of binding affinities at least with the isolated MST1 SARAH domain (Figure 4.10Bii).

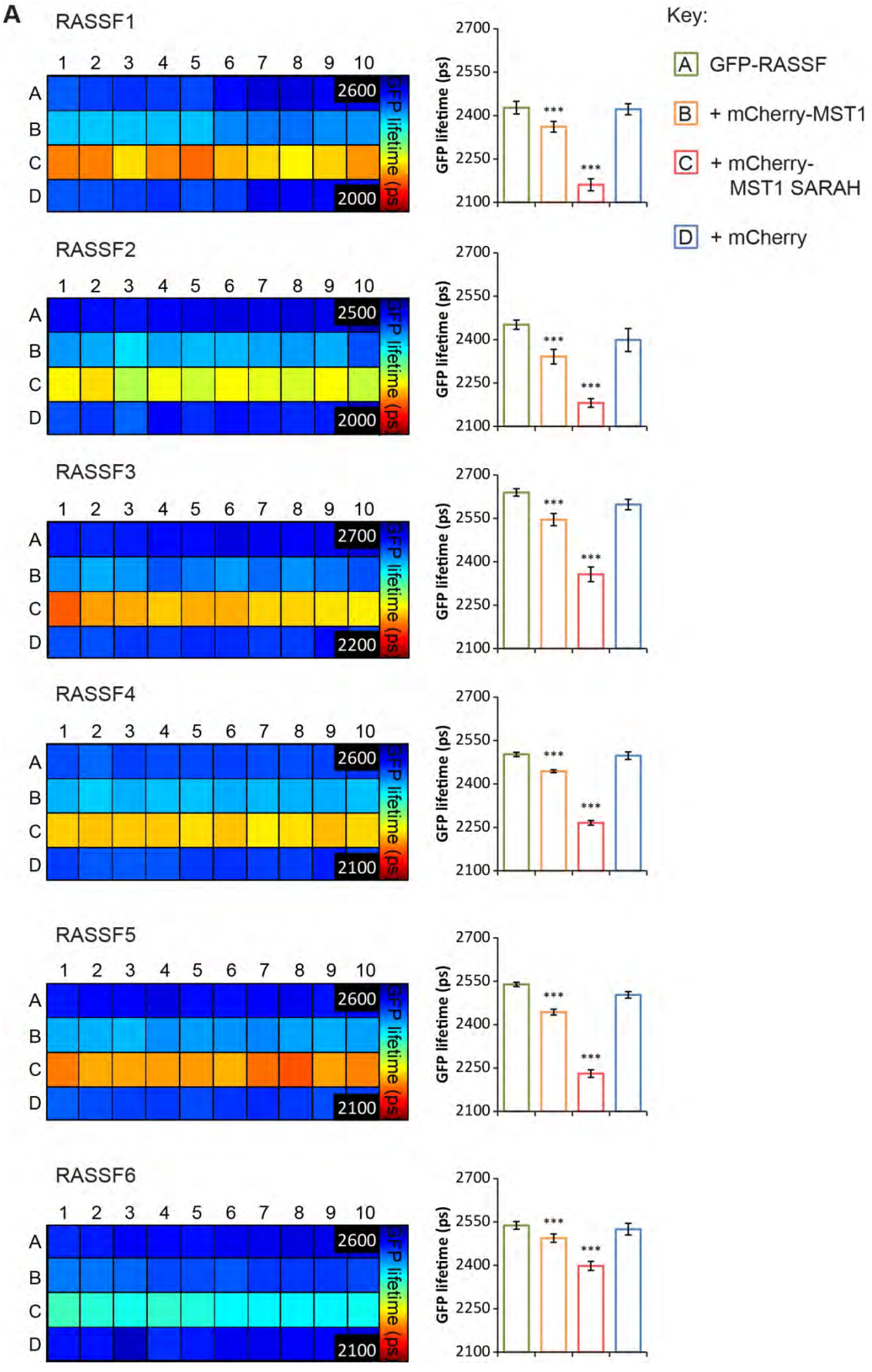
A
RASSF1
1 2 3 4 5 6 7 8 9 10
A
B
C
D
2600
2000
GFP lifetime (ps)
GFP lifetime (ps)
2700
2550
2400
2250
2100
***
***
Key:
A GFP-RASSF
B + mCherry-MST1
C + mCherry-MST1 SARAH
D + mCherry
RASSF2
2500
2000
RASSF3
2700
2200
RASSF4
2600
2100
RASSF5
2600
2100
RASSF6
2600
2100

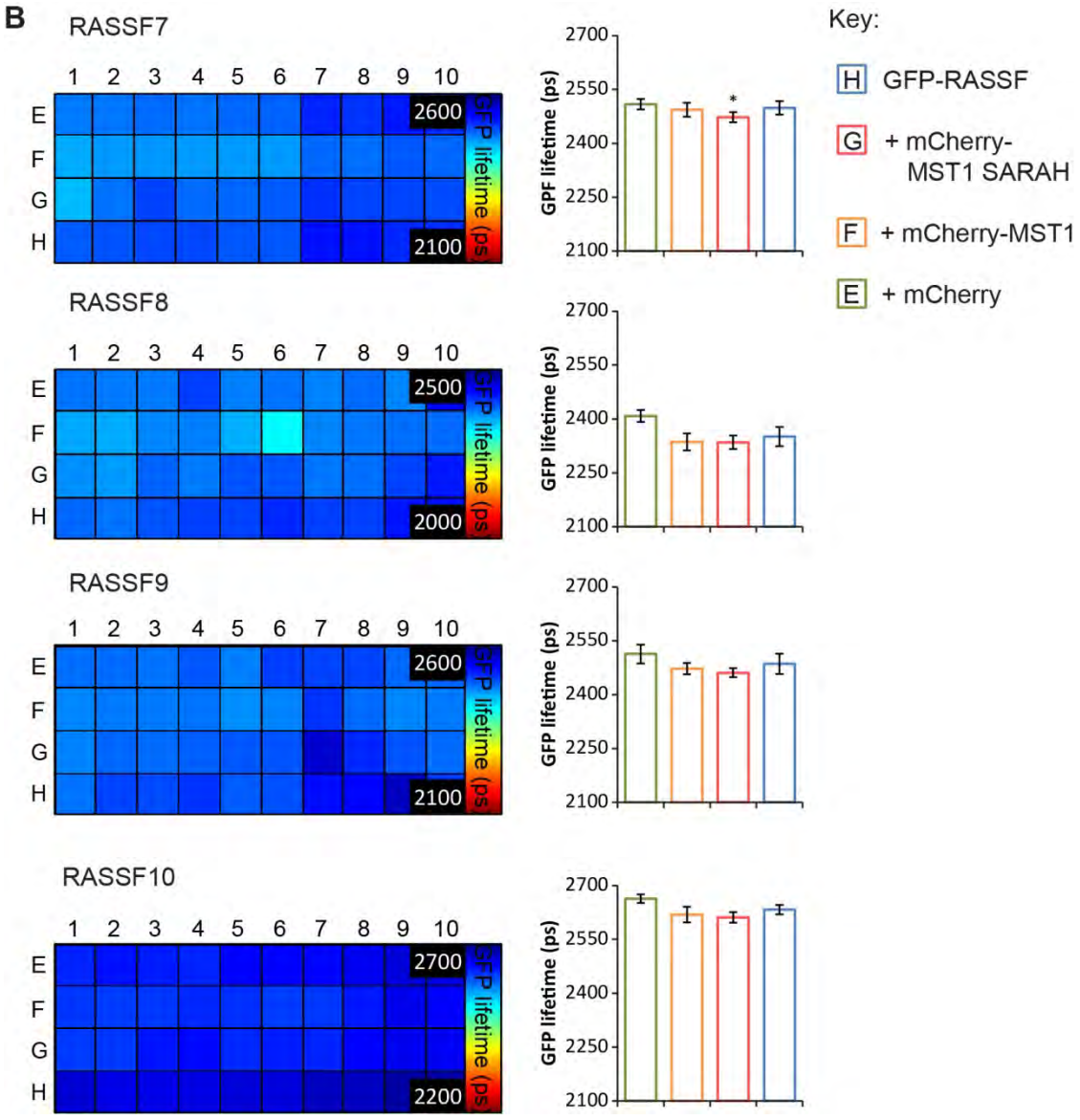

Figure 4.9 FRET studies comparing the interaction between RASSF and full length MST1 or its isolated SARAH domain

(A) Plate maps (left) and bar graphs (right) showing the GFP lifetime changes per condition for the classical RASSF1-6.

(B) Plate maps (left) and bar graphs (right) showing the GFP lifetime changes per condition for the N-terminal RASSF7-10.

An additional negative control, mCherry was used. The positions of each well are labelled A-H and 1-10. The corresponding wells, conditions and coloured bars in the graphs are indicated in the key. The GFP lifetimes, errors and p-values were calculated and indicated as described in Figure 4.8. Image acquisitions and data processing were performed by Dr Anca Margineanu as described in section 2.6.3.

Figure 4.10 Comparison of binding affinities amongst the classical RASSF members

(A) Graphical representation of the different FRET signals of each RASSF member, measured as a change in the GFP donor lifetimes from two separate studies. The changes were calculated using measurements from the isolated MST1 SARAH domain and the negative controls with mCherry-MST1ΔSARAH or mCherry only, and the error bars are the combined standard deviations (see Figure 4.8 and 4.9).

(B) (i) Co-IP assay showing interactions between the classical RASSF1-6 and full length MST1 K59R (left) or its isolated SARAH domain (right). This is representative of the results from three separate experiments and the controls are shown below. (ii) Quantification of the bands using ImageJ. The relative intensity of RASSF1 was set at 1 and used as a reference point (colour-filled bars). The error bars are standard deviations and p-values were calculated and indicated as described in Figure 4.8B.

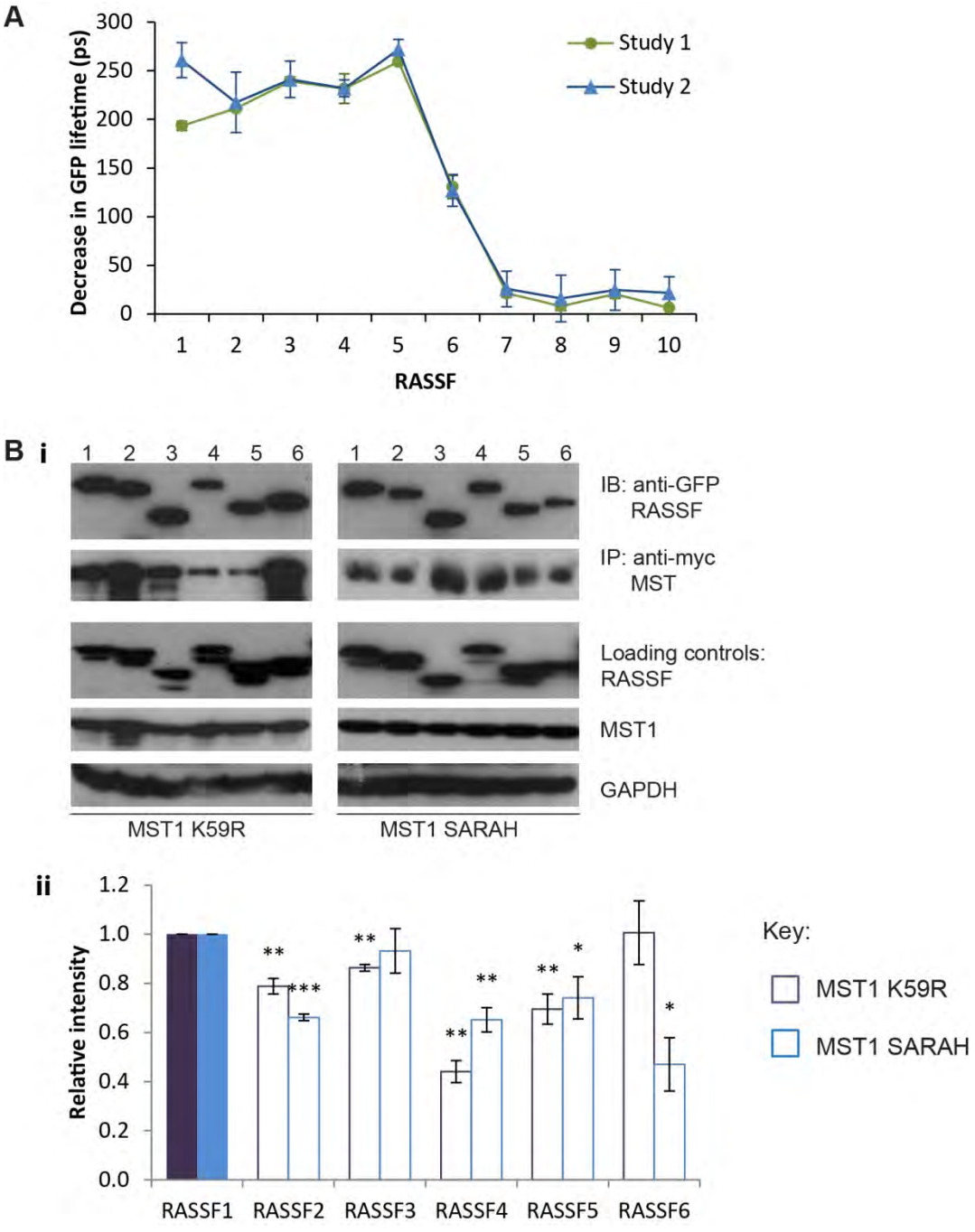
A
Decrease in GFP lifetime (ps)
300
250
200
150
100
50
0
1 2 3 4 5 6 7 8 9 10
RASSF
Study 1
Study 2
B i
1 2 3 4 5 6
1 2 3 4 5 6
IB: anti-GFP
RASSF
IP: anti-myc
MST
Loading controls:
RASSF
MST1
GAPDH
MST1 K59R
MST1 SARAH
ii
Relative intensity
1.2
1.0
0.8
0.6
0.4
0.2
0.0
RASSF1 RASSF2 RASSF3 RASSF4 RASSF5 RASSF6
Key:
MST1 K59R
MST1 SARAH

Without purified proteins, it is difficult to properly assess and compare binding affinities using the *in vitro* approach, thus quantitative FRET experiments were used in this study. However, further double exponential analysis of the FRET data, to take into account the different acceptor and donor intensities, is required to confirm our observations and more accurately quantify the binding affinities.

4.2.3.3. KRasV12 enhances dimerisation between RASSF and MST1

Previous studies have indicated an increase in MST1 activation upon forming a ternary complex with RASSF5 and activated Ras (Khokhlatchev et al., 2002, Praskova et al., 2004), which could be due to enhanced interaction between the two SARAH domains upon Ras association. Therefore, we compared the interaction of the RASSF proteins with MST1 both in the absence and presence of KRasV12 (Figure 4.11A).

Consistent with our initial observations, the preliminary data showed an increase in FRET signal when MST1 was co-expressed with RASSF1-6 (Figure 4.11Bi). Moreover, this signal was enhanced to different degrees upon the addition of activated KRas for all six classical RASSF members. Again, minimal changes were detected for RASSF7-10 (Figure 4.11Bii). In order to validate the effects of activated KRas on the interaction between MST1 and the classical RASSF proteins, additional controls could be used in future studies, including wild-type or inactivated KRas.

4.3. Discussion

Although the six RASSF SARAH domain models were generated using the MST1 SARAH domain template, a comparison between our RASSF5 SARAH domain model and the recent crystal structure of the murine RASSF5 SARAH domain shows that our predictions of the dimer interface and critical residues were accurate (Figure 4.12A, B). The main interacting helix H2 in both structures is also well superposed and has good structural correspondence (Figure 4.12C). The key interacting residues from MST1 correspond to those identified in the RASSF5 SARAH domain (L224, L228, L231, I239, Y246), with the addition of L253 and L257 (Figure 4.1C and 4.12A) (Makbul et al., 2013). As highlighted in section 4.2.1, these non-polar residues are highly conserved, including the two additional residues specifically involved in the RASSF SARAH

Figure 4.11 FRET studies indicating enhanced heterodimerisation by KRasV12

(A) Plate map showing the GFP lifetime changes from the interactions between GFP-RASSF1-10 and mCherry-MST1 in the absence and presence of activated KRasV12. The map and FRET intensity colour bar are labelled as in Figure 4.8A. Image acquisitions and data processing were performed by Dr Anca Margineanu as described in section 2.6.3.

(B) Bar graphs showing the GFP lifetime changes per condition for (i) the classical RASSF1-6 and (ii) the N-terminal RASSF7-10. The bars are colour-coded for each condition as indicated in the key. The GFP lifetimes, errors and p-values were calculated and presented as in Figure 4.8B.

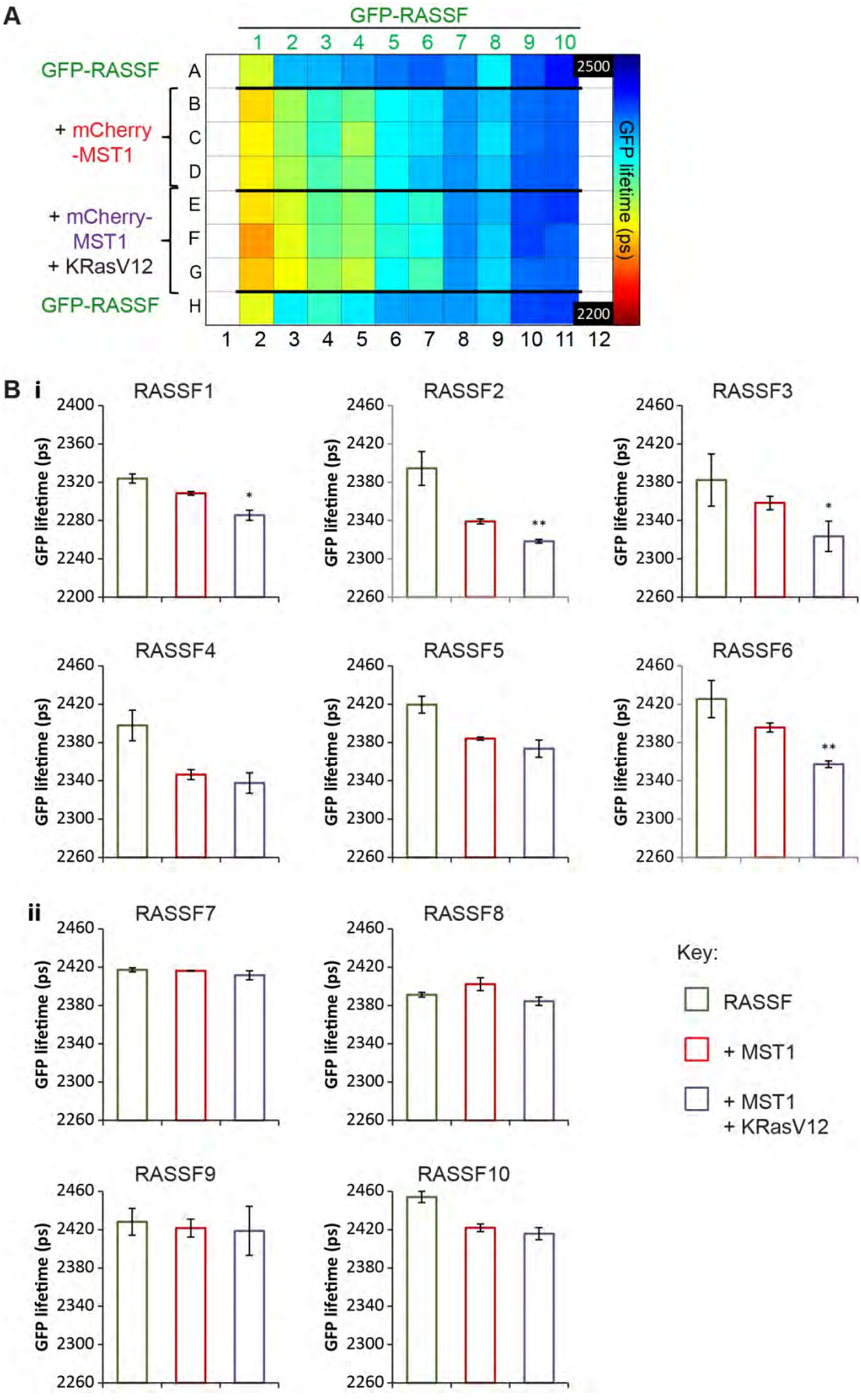
A
GFP-RASSF
1 2 3 4 5 6 7 8 9 10
GFP-RASSF
A
B
C
D
E
F
G
H
+ mCherry -MST1
+ mCherry-MST1 + KRasV12
GFP-RASSF
2500
2200
GFP lifetime (ps)
1 2 3 4 5 6 7 8 9 10 11 12
B i
RASSF1
RASSF2
RASSF3
RASSF4
RASSF5
RASSF6
ii
RASSF7
RASSF8
RASSF9
RASSF10
GFP lifetime (ps)
Key:
RASSF
+ MST1
+ MST1 + KRasV12

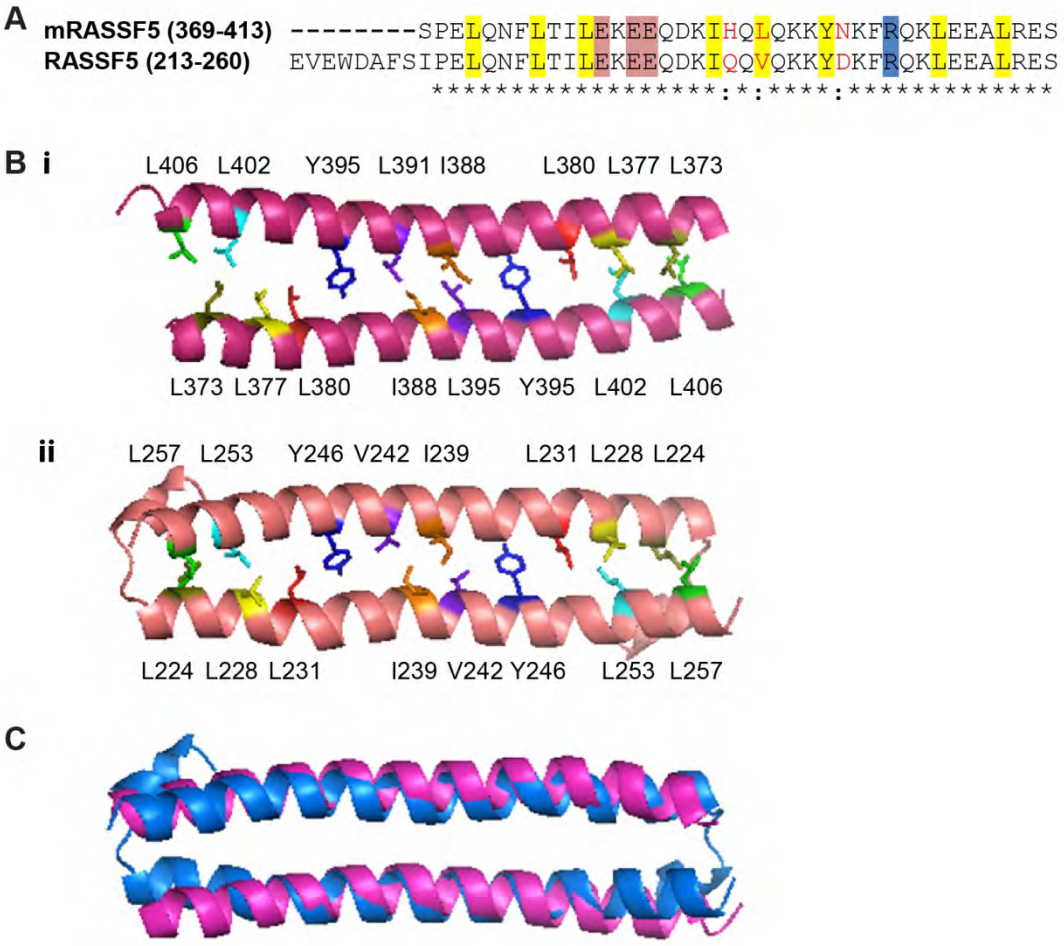

Figure 4.12 Comparison of the RASSF5 SARAH domain crystal structure and our homology model

(A) Sequence alignment of the SARAH domain of murine RASSF5 crystal structure and human RASSF5 used for homology modelling. Fully conserved residues are marked by asterisks (*) and highly conserved residues by colons (:) and shown in red text. Conserved hydrophobic residues involved in the dimer interface are highlighted in yellow, acidic residues in red and basic residues in blue.

(B) The homodimer structure of the RASSF5 SARAH domain. (i) Ribbon representation of the murine RASSF5 SARAH homodimer (PDB: 2YMY). The N-terminal helix, H1 is not crystallised. (ii) Ribbon representation of the human RASSF5 SARAH domain homodimer model. Side chains of the key hydrophobic residues are labelled and shown in colours corresponding to the same positions in both structures.

(C) Superposition of the crystallographic structure of murine RASSF5 SARAH (magenta) and human RASSF5 SARAH homology model (blue).

homodimerisation. In addition, our predictions of polar interactions between the stretch of acidic residues present in the RASSF SARAH domain and the highly conserved arginine residue aligning to R470 in MST1 (R250 in RASSF5) are confirmed by the RASSF5 structural studies. Specifically, E232, E234 and E235 of RASSF5 are involved in polar interactions at the dimer interface and these residues are well conserved across the classical RASSF members (Figure 4.3). These similarities between the RASSF5 structure and our homology models demonstrate the high quality of our *in silico* data and predictions.

Our *in vitro* and intracellular observations are also consistent with the *in silico* predictions of the SARAH domain-mediated interactions and confirm previous studies showing interactions between the classical RASSF members with either MST1 or MST2 (Eckfeld et al., 2004, Ikeda et al., 2009, Khokhlatchev et al., 2002, Praskova et al., 2004). All six classical RASSF members formed homotypic or heterotypic interactions with RASSF5 or the MST kinases, whereas the N-terminal RASSF7, 8, 9 and 10 that lack the SARAH domain failed to dimerise with either protein *in vitro* (see sections 4.2.2.2 and 4.2.2.3). This is reinforced by the intracellular FRET data showing interactions between MST1 and RASSF1-6, but not RASSF7-10 (see section 4.2.3.1). We can infer from these data that the SARAH domain is required for homodimerisation and heterodimerisation, whereas the predicted coiled-coil motif is insufficient to facilitate such interactions. Interestingly, our preliminary FRET data also indicate a tendency of activated KRas to enhance heterodimerisation between RASSF and MST1, although not all are statistically significant (see section 4.2.3.3). In contrast to reports in the literature (Khokhlatchev et al., 2002, Praskova et al., 2004), RASSF5 did not show any significant increase in MST1 binding in the presence of KRasV12. These observations involving KRas remain to be confirmed by further studies, thus the role of activated Ras in heterodimerisation between RASSF and MST remains an open question.

It is worth noting that these interactions were independent of the MST kinase activity, which supports an earlier study showing that the kinase activity was not required for the heterodimerisation between RASSF2 and the MST kinases (Cooper et al., 2009). Furthermore, this is consistent with previous observations of initial inhibition of the MST kinase activation by RASSF1 and RASSF5 before its eventual activation upon Ras binding and membrane localisation (Praskova et al., 2004). Taken together, the

RASSF proteins appear to bind MST kinases in their inactive form and subsequently facilitate their activation via additional interactions and signals.

In terms of the different dimer propensities, our observations are in contrast to what has been shown in literature (section 4.2.2.3). Hwang et al. (2007) reported free RASSF5 SARAH domain tetramers in solution, whereas we only observed homodimers and monomers for the isolated RASSF5 and MST1 SARAH domain proteins. Contrary to their observation of a higher propensity for heterodimerisation, this heterodimer was never present under a full *in vitro* setting, but only under cellular conditions in our studies. In contrast, we observed a mixture of homodimers and monomers in their native states, with a higher proportion of the latter. There are several plausible explanations for these observations. First, the isolated SARAH domain proteins could exist as natural homodimers. These homodimers could also consist of relatively high affinity interactions, thus could not readily dissociate under experimental conditions to allow for the formation of heterodimers. Furthermore, the monomers present in solution could be partially unfolded or denatured, hence inactive and unable to form heterodimers. On the contrary, a comparison between the *in vitro* pull-down and the co-IP using cell lysates containing pre-formed complexes indicates that the SARAH domain alone is sufficient to facilitate heterodimerisation under cellular conditions, but not under complete *in vitro* settings. It also highlights the possible differential preferences for homotypic and heterotypic interactions under different experimental conditions, whereby heterodimerisation may not be preferred in some instances and may also require specific conditions and factors found only in cellular systems.

The most remarkable discovery from our FRET data was the pattern of signal intensities of the RASSF proteins. Although the monoexponentially analysed FRET measurements are not definitive, they do provide an initial picture of the potential variations in binding affinities for the RASSF SARAH domains, which mirror their sequence homologies described in section 4.2.1. While the sequence homology scores vary, the phylogenetic tree indicates that the RASSF SARAH domains most similar to MST1 are RASSF1, 3 and 5. Coincidentally, RASSF3 and RASSF5 also appeared to be the strongest binders to MST1. This is followed by RASSF1, 2 and 4, with RASSF6 being the weakest. RASSF1 is the anomaly as it displayed a similar affinity to RASSF2 and RASSF4, despite their low homology identities and being grouped separately in the phylogenetic tree (Figure 4.2). This could be due to other more specific features in their

dimerisation interfaces that are not accounted for here. Conversely, the weak binding affinity between RASSF6 and MST1 could be due to a lack of specific key residues at its dimer interface given that it is the most divergent member amongst the classical RASSF members. Furthermore, this is in spite of its similar sequence identity score to MST1 compared to RASSF4 and RASSF5. These observations highlight the importance of specific residues in determining protein-protein interactions and their affinities. Additionally, the residues required for heterodimerisation may be different from those needed for homotypic interactions.

Interestingly, our observations are also in agreement with a previous study on using evolutionary distances in phylogenetic trees to predict protein-protein interactions with an accuracy of >66% (Pazos and Valencia, 2001). This is based on the foundation that proteins grouped together in a phylogenetic tree usually face similar selection pressures, thus they co-evolve, which is an indication of possible interacting partners. Furthermore, higher similarities could imply stronger interactions and vice versa, a pattern that was observed in this study as RASSF3 and RASSF5 fit into the former category, whilst RASSF2, 4 and 6 are in the latter category.

Overall, these new observations suggest that all the classical RASSF members can be involved in MST signalling regulation and they may have some overlapping functions. However, their different binding affinities for MST1 could also mean that the MST kinases are preferentially regulated by the higher affinity binders, whereas those RASSF members with lower binding affinities could compensate for the loss of the former under pathological circumstances. The SARAH domain of WW45 has previously been shown to form heterodimers with MST1 and MST2, and it also forms an indirect complex with RASSF6 via MST2 (Hwang et al., 2007, Ikeda et al., 2009). However, not much is known about its interaction with the remaining RASSF members. Given its significant role as a scaffolding protein for the MST kinases in Hippo signalling, further studies on its interaction with the all ten members of the RASSF family in the presence and absence of MST1 or MST2 would also provide more insight into the underlying molecular mechanisms of Hippo signalling regulation.

The predicted coiled-coil motifs do not appear to facilitate heterodimerisation with other RASSF members or the MST kinases. Although they cannot dimerise specifically with the SARAH domain, it is possible that they could homodimerise or

preferentially interact with other proteins and domains. For example, the RASSF7 coiled-coil was recently shown to bind microtubules in *Xenopus* (personal communication with Tulay Gulsen from Dr Andrew Chalmer's laboratory), which implicates it in cytoskeleton organisation and possibly cell cycle regulation. There have been no other studies on the RASSF coiled-coil motifs, thus they remain to be further investigated and characterised.

5 Mutations in the SARAH domain

5.1. Introduction

The SARAH domain, its structure and functions have been described in detail for MST1 and RASSF5 in Chapter 4. Although the homodimeric structures have been solved for MST1 and RASSF5 (Hwang et al., 2007, Makbul et al., 2013), and many studies have reported interactions between different classical RASSF1-6 and MST1 or MST2 (Table 1.3), there are few that focus on the importance of specific residues required for heterodimerisation.

The MST1 SARAH domain remains the most well studied in terms of its molecular interactions. Its NMR structure highlighted the importance of the network of aliphatic side chains in hydrophobic interactions, which are the main driving force for dimerisation (Hwang et al., 2007). In particular, L444 was highlighted as the key structural residue that contacts both helices in the homodimer and is completely buried with <1% solvent accessible surface area. Thus, a non-conservative mutation at this position could potentially disrupt the dimer. This hypothesis is supported by previous studies using a L444P point mutant that showed impaired homodimerisation, but still maintained its ability to heterodimerise with RASSF5 (Khokhlatchev et al., 2002, Praskova et al., 2004). However, reports on the biological effects due to a lack of homodimerisation are conflicting. Creasy et al. (1996) reported no effect on the MST1 activity, whereas Praskova et al. (2004) showed a lack of MST1 activity.

Besides heterodimerisation with MST kinases, the RASSF5C SARAH domain was recently shown to also bind SKAP1, a protein involved in T cell activation (Raab et al., 2011). The study also tested the effect of the mutation at the same position in RASSF5C, L224A, which impaired SKAP1 binding but did not have any effect on its heterodimerisation with MST1. This point mutation essentially maintains the helical structure and the physico-chemical properties of the residue in that position, thus may have little effect on dimerisation with MST1. Conversely, SKAP1 may interact differently with the SARAH domain at the molecular level, therefore is affected by this specific mutation.

Studies using a specific point mutant in the RASSF1 SARAH domain have also been performed. A mutation in a different conserved position, L308P aligning to L451 on MST1 and L231 on RASSF5C, both of which are part of the hydrophobic network, also impairs heterodimerisation with MST1 and MST2 (Del Re et al., 2010, Donninger et al., 2011). Consequently, this prevents the activation of MST1, which supports previous observations carried out using the dimer deficient MST1 L444P mutant (Del Re et al., 2010, Donninger et al., 2011, Praskova et al., 2004). Furthermore, the RASSF1 mutant is also defective in inducing the phosphorylation and activation of YAP, its nuclear localisation and binding to p73, which are components of the Hippo signalling network (Donninger et al., 2011). Interestingly, this mutation has no effect on RASSF1 heterodimerisation with the Sav SARAH domain, and is able to activate p73 via Sav independent of the canonical Hippo pathway (Donninger et al., 2011). These observations highlight the possibility of differential molecular interactions between the structurally similar SARAH domains, therefore, allowing them to compensate for one another in some instances.

Although structures for the MST1 and RASSF5 SARAH domain homodimers are now available, information on the underlying molecular mechanisms of interaction, especially for heterodimers remains scarce. Furthermore, the lack of structural information on the SARAH heterodimers and of a comparative analysis of the SARAH domain homodimers and heterodimers limits our understanding on the molecular mechanisms of their functions. The aim of this study was to generate structural models of the SARAH heterodimers, compare homodimer and heterodimer interfaces, and the effects of specific point mutations on these interactions. Our data suggest a higher propensity for heterodimer formation, with hydrophobic interactions and specific conserved non-polar residues, and to a lesser extent, electrostatic interactions and some charged residues playing an important role in dimerisation.

5.2. Results

5.2.1. Modelling SARAH domain heterodimers

The structural models of SARAH domain heterodimers between MST1 and each classical RASSF1-6 were built as described in section 2.8. Although the RASSF SARAH

domains share a higher sequence similarity amongst themselves, we decided not to rebuild our homodimeric homology models using the recent crystal structure of the RASSF5 SARAH domain. Instead, we used monomers from our homodimeric homology models based on the NMR structure of the MST1 homodimer (see section 4.2.1). Theoretically, these should have their side chains more optimally positioned to interact with a MST1 monomer to form a heterodimer. This approach should help to minimise erroneous results from the rigid body docking strategy as a result of its limitation in dealing with the large degrees of flexibility in protein-protein interactions.

The heterodimer models for each MST1/RASSF combination shown here are from the top of their ranked lists (Figure 5.1). They have the most favourable surface complementarities, electrostatic and desolvation free energies. Additionally, they also have the best scores from the clustering analysis whereby a 9Å Cα (central carbon atom of each amino acid residue) rms radius was used to find clusters with the most "neighbours". These "neighbours" should include atomic partners of side chains via all possible forces of interaction, including non-covalent bonds, such as hydrogen bonds, ionic bonds, van der Waals forces and hydrophobic interactions, all of which should be within 4.5Å (Lodish et al., 2000, Samanta et al., 2002).

The analytical output of these models is summarised in Table 5.1. The interface sizes shown were calculated from the ASA values as described in section 2.8. Residues that showed ≥10% change in ASA (ΔASA) upon dimerisation are considered part of the dimerisation interface and their side chains are highlighted in Figure 5.1. An increase in atomic partners is correlated with lower ASA, thus an increase in ΔASA and interface areas.

It is evident that the contact interface involves mainly the side chains and non-polar residues for all six heterodimers. There is also a small degree of polar or charged interaction between the highlighted acidic and basic residues. The polar interfaces make up 17.4-19.2% of the total interface for RASSF1-5, with RASSF6 having the smallest absolute as well as proportion of polar interface. The acidic residues involved are mostly Glu, with the occasional Asp, whilst the basic residues are a mixture of Lys and Arg. It is interesting to note that in all the heterodimers, there is at least one conserved Arg involved in the interface from the RASSF monomer except RASSF6 (Figure 5.1F).

A RASSF1

MST1 (433-480) YEFLKSWTVEDLQKRLLALDPMMEQEIEEIRQKYQSKRQPILDAIEAK

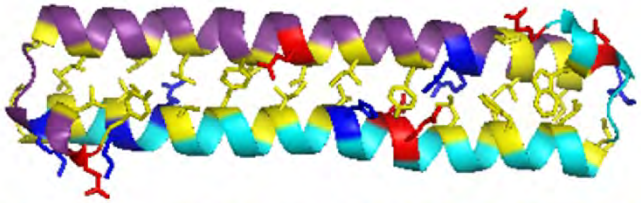

RASSF1 (290-337) EVNWDAFSMPELHNFLRILQREEEEHLRQILQKYSYCRQKIQEALHAC

B RASSF2

MST1 (433-480) YEFLKSWTVEDLQKRLLALDPMMEQEIEEIRQKYQSKRQPILDAIEAK

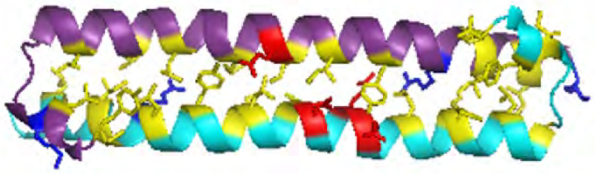

RASSF2 (272-319) VAQYIKFEMPVLKSFIQKLQEEEDREVKKLMRKYTVLRLMIRQRLEEI

C RASSF3

MST1 (433-480) YEFLKSWTVEDLQKRLLALDPMMEQEIEEIRQKYQSKRQPILDAIEAK

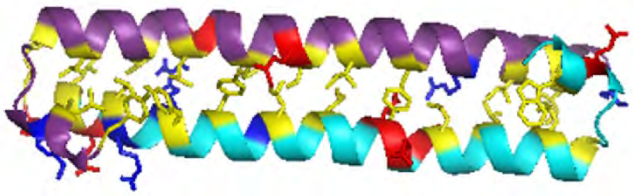

RASSF3 (187-234) IGEWEAFSLPELQNFLRILDKEEDEQLQNLKRRYTAYRQKLEEALREV

D RASSF4

MST1 (433-480) YEFLKSWTVEDLQKRLLALDPMMEQEIEEIRQKYQSKRQPILDAIEAK

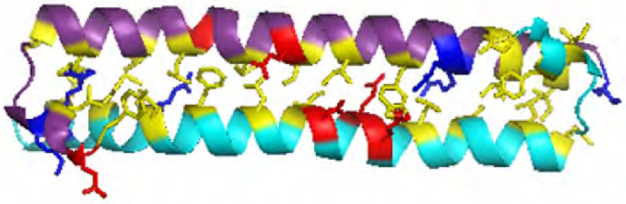

RASSF4 (270-317) VAQYIKFEMPVLDSFVEKLKEEEERETIKLTMKFQALRLTMLQRLEQL

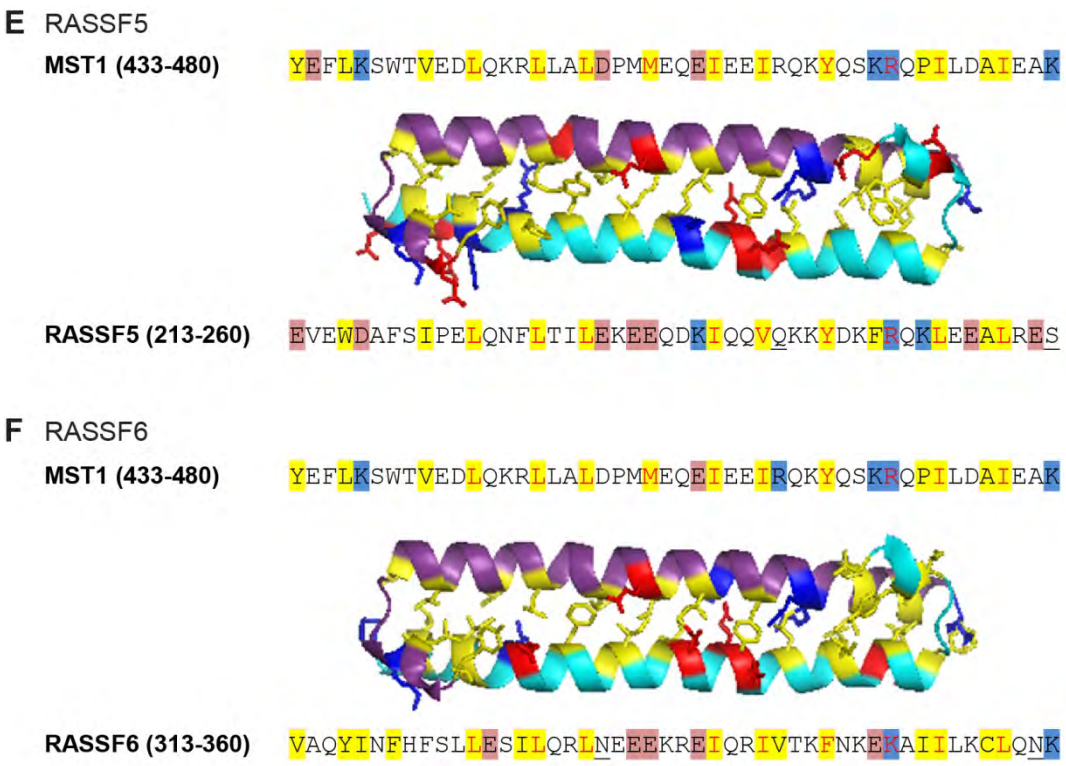

Figure 5.1 Heterodimer models of the MST1 and RASSF SARAH domain

(A-F) RASSF1-6 heterodimers models generated by Dr Delphine Flatters and Dr Fernando Rodriguez-Lima as described in section 2.8. The structure of the MST1 monomer is in purple and the RASSF monomer in cyan. Non-polar (yellow), acidic (red) and basic (blue) side chains of residues involved in the heterodimeric interface are shown. The sequences for the MST1 and RASSF SARAH domain are shown above and below the structural model respectively. The MST1 monomer is in the same orientation of the sequence, whist the RASSF monomer is in the reverse orientation. The side chains shown in the structures are also highlighted in the sequences using the same colour scheme. Residues in conserved positions are shown in red text and polar residues involved in the interface are underlined.

Table 5.1 Interface sizes of the SARAH heterodimer models

The interface sizes (in $Å^2$) were calculated using naccess for the best SARAH heterodimer model of each RASSF with MST1.

MST1 with:	Total	Side chain	Main chain	Non-polar	Polar
RASSF1	2844.6	2733.1	111.6	2350.6	494.1
RASSF2	2933.6	2808.9	124.6	2426.5	507.1
RASSF3	2767.7	2684.2	83.5	2235.5	532.2
RASSF4	2843.2	2731.5	111.7	2296.2	547.1
RASSF5	2820.9	2717.3	103.5	2278.6	542.2
RASSF6	2988.4	2889.5	98.9	2502.1	486.3

Table 5.2 Comparison of the interface sizes between SARAH domain homodimers and heterodimers

The interface sizes (in $Å^2$) were calculated using naccess for each SARAH homodimer structure, homology models and heterodimeric models.

	Total		Non-polar		Polar	
	Homodimer	Heterodimer	Homodimer	Heterodimer	Homodimer	Heterodimer
MST1 (2JO8)	2869.8	-	2430.6	-	439.2	-
RASSF1	2629.6	2844.6	2179.6	2350.6	450	494.1
RASSF2	2683.9	2933.6	2170.8	2426.5	513	507.1
RASSF3	2586.7	2767.7	2150.5	2235.5	436.2	532.2
RASSF4	2789.7	2843.2	2193.1	2296.2	596.6	547.1
RASSF5	2698.7	2820.9	2101.1	2278.6	597.5	542.2
RASSF6	2643.1	2988.4	2246.5	2502.1	396.6	486.3

The total interface and non-polar interface areas are largely similar for RASSF1-5 heterodimers with MST1. However, the MST1/RASSF6 heterodimer has a surprisingly larger total interface, whilst its larger non-polar interface area is due to the smaller contribution from polar residues. Essentially, all the conserved non-polar residues are involved in hydrophobic interactions in all six models. Interestingly, the MST1/RASSF1 heterodimeric interface also involves two Cys residues (Figure 5.1A), whilst the rest involves one or two polar residues, such as Asn, Gln, Ser and Thr (Figure 5.1B-F).

Overall, there are no major differences in the heterodimer models and interfaces with the exception of RASSF6, which has a larger total interface area and a much smaller polar interface compared to the rest of the classical RASSF members.

5.2.2. Comparison of SARAH domain homodimers and heterodimers

Next, we compared the SARAH heterodimer models with the homodimer homology models from Chapter 4.

5.2.2.1. Comparison of the homodimeric and heterodimeric structures

The structures of the SARAH homodimers and heterodimers for MST1 and RASSF1-6 are largely similar (Figure 5.2). All residues in the conserved positions described in Chapter 4 contribute to both the homodimeric and heterodimeric interfaces of all the models. However, the distinction between the homodimers and heterodimers, as well as amongst the six heterodimers, lies in the involvement of several specific residues in their dimeric interfaces.

A general comparison of the interface residues for the MST1 SARAH homodimer and its heterodimers with the classical RASSF members (Figure 5.2A) shows variation in several residues. These are mainly charged residues E434, D452, K469 and D475 and the non-polar P472. Interface residues are those showing ≥10% ΔASA as described in section 5.2.1. D475 is consistently absent from all the heterodimeric interfaces, whilst residues that contribute to the MST1 homodimeric interface but not to selected heterodimeric interfaces include D452, K469 and P472 (Figure 5.2B). E434 is an addition to the heterodimeric interface with RASSF1 and RASSF5 (Figure 5.2Bi, v).

A MST1 homodimer (433-480)

Homodimer YEFLKSWTVEDLQKRLLALDPMMEQEIEEIRQKYQSKRQPILDAIEAK
Heterodimer YEFLKSWTVEDLQKRLLALDPMMEQEIEEIRQKYQSKRQPILDAIEAK

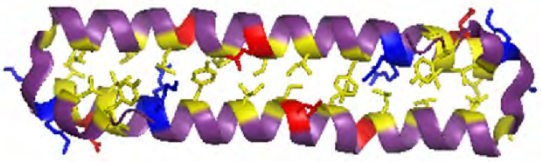

B i RASSF1 (290-337)

Homodimer Heterodimer

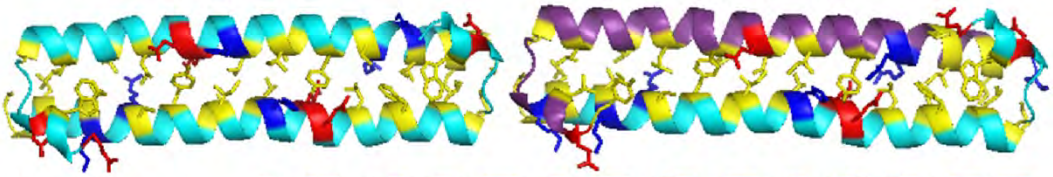

Homodimer EVNWDAFSMPELHNFLRILQREEEEHLRQILQKYSYCRQKIQEALHAC
Heterodimer EVNWDAFSMPELHNFLRILQREEEEHLRQILQKYSYCRQKIQEALHAC

ii RASSF2 (272-319)

Homodimer Heterodimer

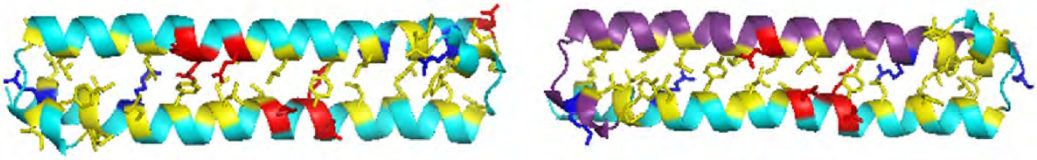

Homodimer VAQYIKFEMPVLKSFIQKLQEEEDREVKKLMRKYTVLRLMIRQRLEEI
Heterodimer VAQYIKFEMPVLKSFIQKLQEEEDREVKKLMRKYTVLRLMIRQRLEEI

iii RASSF3 (187-234)

Homodimer Heterodimer

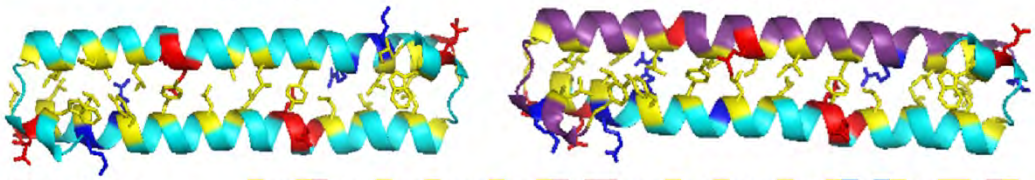

Homodimer IGEWEAFSLPELQNFLRILDKEEDEQLQNLKRRYTAYRQKLEEALREV
Heterodimer IGEWEAFSLPELQNFLRILDKEEDEQLQNLKRRYTAYRQKLEEALREV

iv RASSF4 (270-317)

Homodimer Heterodimer

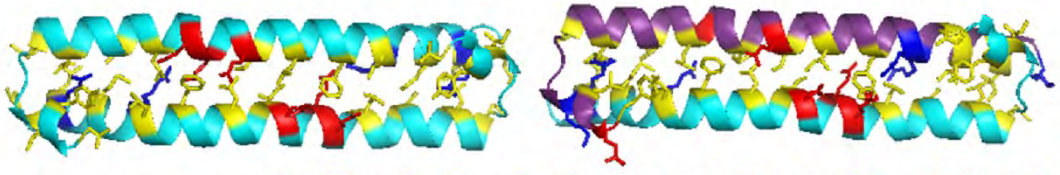

Homodimer VAQYIKFEMPVLDSFVEKLKEEEEREIIKLTMKFQALRLTMLQRLEQL
Heterodimer VAQYIKFEMPVLDSFVEKLKEEEEREIIKLTMKFQALRLTMLQRLEQL

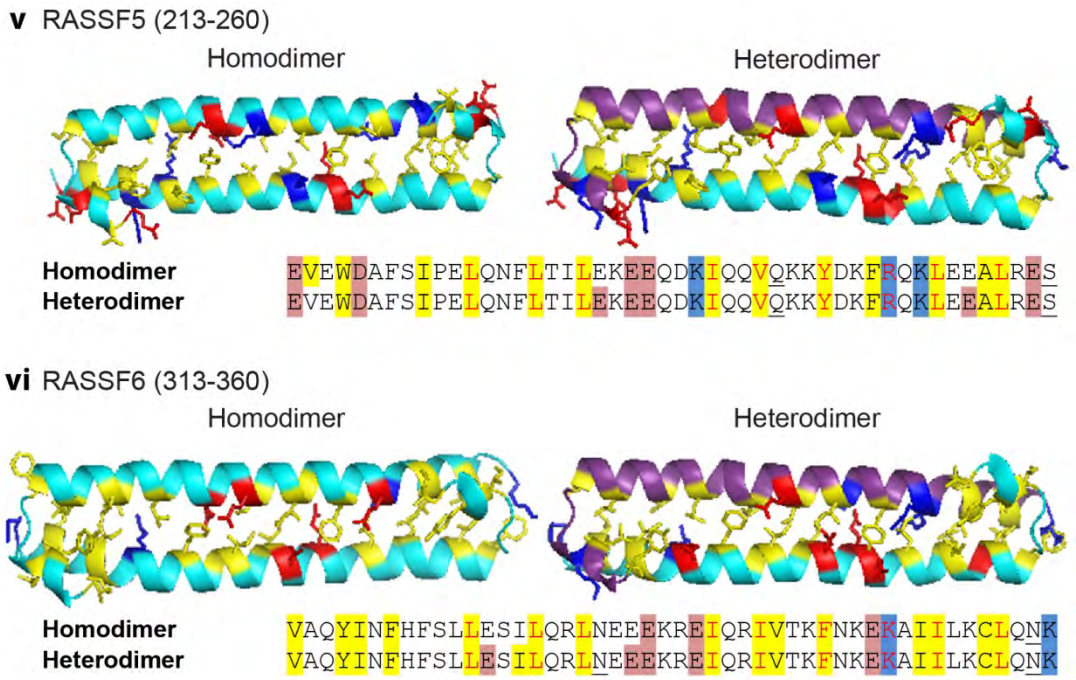

Figure 5.2 Comparison of the SARAH domain homodimers and heterodimers

(A) The MST1 SARAH homodimer structure is shown in purple. All interacting side chains in the homodimeric interface are shown and coloured as described in Figure 5.1. The SARAH domain sequence is shown above in the same orientation as the top monomer chain. Residues involved in the interface of the MST1 homodimer and its heterodimer with RASSF1-6 are highlighted in the corresponding colours to the structure. Changes in residue involvement in the heterodimeric interface are underlined.

(B) RASSF1-6 SARAH domain homodimer homology models (left) and heterodimer models with MST1 (right). MST1 monomer is shown in purple in the same orientation as the sequence in (A). RASSF monomers are shown in cyan and the bottom monomer is in the reverse orientation to the corresponding RASSF sequence shown below each model. Side chains of all interacting residues are shown in the models and highlighted in the sequence as described in (A). Residues in conserved positions are shown in red text and polar residues involved in the interface are underlined.

The residues from the RASSF monomers contributing to the dimeric interfaces are largely similar. There are no changes from RASSF1, whilst the variations in the remaining RASSF heterodimers are commonly addition of the aromatic residue Phe (Figure 5.2Bii), polar residues Gln, Ser and Thr (Figure 5.2Bii, iv) or charged residues Lys and Glu (Figure 5.2Biii, v, vi).

5.2.2.2. Comparison of the interfaces sizes of the dimeric models

The same parameters were used for the interface analysis of the homodimer models and these are summarised in comparison to the heterodimer analysis in Table 5.2. The main chain and side chain interface areas are not shown here as they are largely unchanged in proportion to the total interface areas in both types of dimers.

Similar to the heterodimers, the homodimer contact interfaces mainly involve side chains and non-polar residues. However, the total interface area for the heterodimers is noticeably larger than the homodimers, especially for the MST1/RASSF6 heterodimer, whereas the increase in the MST1/RASSF4 interface size is minimal. Naturally, this is accompanied by an increase in the non-polar interface areas by different magnitudes across the six heterodimers. These increases are the result of larger ΔASA for most of the existing interface residues and additional residues not involved in the homodimer interfaces (data not shown). Conversely, the minor differences in ΔASA between the RASSF4 homodimer and heterodimer interface residues are reflected by the minimal changes between the two interface areas.

The changes in the polar interface sizes are more varied, with an increase from homodimer to heterodimer for RASSF1, 3 and 6, and a small decrease for RASSF2, 4 and 5. Most of these changes are minor (<10%), with the most significant increases observed for the RASSF3 and RASSF6 heterodimer with MST1. However, the polar interface of RASSF6 remains the smallest in absolute terms as well as in proportion for both its homodimer and heterodimer models.

It is also noteworthy that the interface area of the MST1 SARAH homodimer is larger than all six RASSF homodimers and more similar to the heterodimeric interface sizes. Furthermore, its non-polar interface area is also larger than most of the non-polar interfaces for the heterodimeric models, except for RASSF6.

5.2.3. Effects of mutations in the SARAH domain on dimerisation

To test the importance of specific residues in the SARAH domain for homodimerisation and heterodimerisation, we generated specific single and double point mutants in MST1, RASSF1 and RASSF5, and performed co-IP experiments using cell lysates as described in section 2.6.2. MST1 and these two RASSF members were chosen for the mutational studies as either their SARAH domain structures or functions are well characterised. Existing literature on the MST1 L444P, RASSF1 L308P and RASSF5 L224A mutants are used as benchmarks and allow for comparison with our studies (Del Re et al., 2010, Donninger et al., 2011, Praskova et al., 2004, Raab et al., 2011).

5.2.3.1. Mutations in the MST1 SARAH domain

The three main residues in the MST1 SARAH domain, L444, L448 and L451 were mutated to Pro (Figure 5.3A). Single point mutants at each of these positions were generated, as well as all three possible combinations of double point mutants.

The mutants in their full length form were tested in comparison to the positive control, wild-type MST1, for binding to RASSF5. All six mutants retained their ability to heterodimerise with RASSF5 (Figure 5.3Bi). However, the signals detected for the double point mutants L444P/L451P and L448P/L451P were statistically weaker compared to the wild-type and the other mutants (Figure 5.3Bii).

In contrast, when wild-type MST1 and its mutants were tested for binding to the kinase-dead MST1 K59R, only the wild-type positive control was detected (Figure 5.3Ci). Very weak signals were detected for the single point mutants L444P, L448P and L451P and all three double point mutants were barely detectable (Figure 5.3Cii).

To confirm the true positives, we also performed a set of negative control co-IP in the absence of myc-tagged proteins (Figure 5.3D). Weak non-specific binding was detected for the single mutants L444P and L451P, and double mutant L444P/L451P, and a stronger signal for double mutant L448P/L451P. When these observations are taken into account, the signals detected for binding to MST1 can be discounted, indicating all six mutants lost their ability to homodimerise (Figure 5.3C). However, they retained the ability to heterodimerise with RASSF5, with possibly a reduced affinity by the double mutant L448P/L451P due to its slightly stronger non-specific binding effect (Figure 5.3B).

Figure 5.3 Effects of mutations in the MST1 SARAH domain on dimerisation

(A) The SARAH domain sequence of MST1. Main interacting non-polar (yellow), acidic (red) and basic (blue) residues are highlighted. The three positions in which mutations were introduced are marked by asterisks (*).

(B) (i) Co-IP assay to show heterodimerisation between myc-RASSF5Δ41 and wild-type (WT) GFP-MST1 and its three single and three double point mutants: L444P, L448P, L451P, L444P/L448P, L444/L451P and L448P/L451P. The loading controls and GAPDH endogenous controls are shown below. (ii) Quantification of the bands in terms of relative intensity to the WT control.

(C) Co-IP assay to show homodimerisation between myc-MST1 K59R and wild-type (WT) GFP-MST1 and its six mutants as described in (B). The loading controls are shown below. (ii) Quantification of the bands in terms of relative intensity to the WT control.

(D) Co-IP assay of the negative controls. A simultaneous negative control was performed using cell lysates containing only GFP-MST1 or its mutants. The loading controls are shown below.

All co-IP assays (B-D) were repeated three times and a representative is shown here. The bands were quantified using ImageJ. The relative intensity of the WT control was always set at 1 and used as a reference point. The error bars are standard deviations, p-values were calculated using the Student's t-test and indicated as follows: $p \leq 0.05$ (*), $p \leq 0.01$ (**) and $p \leq 0.001$ (***).

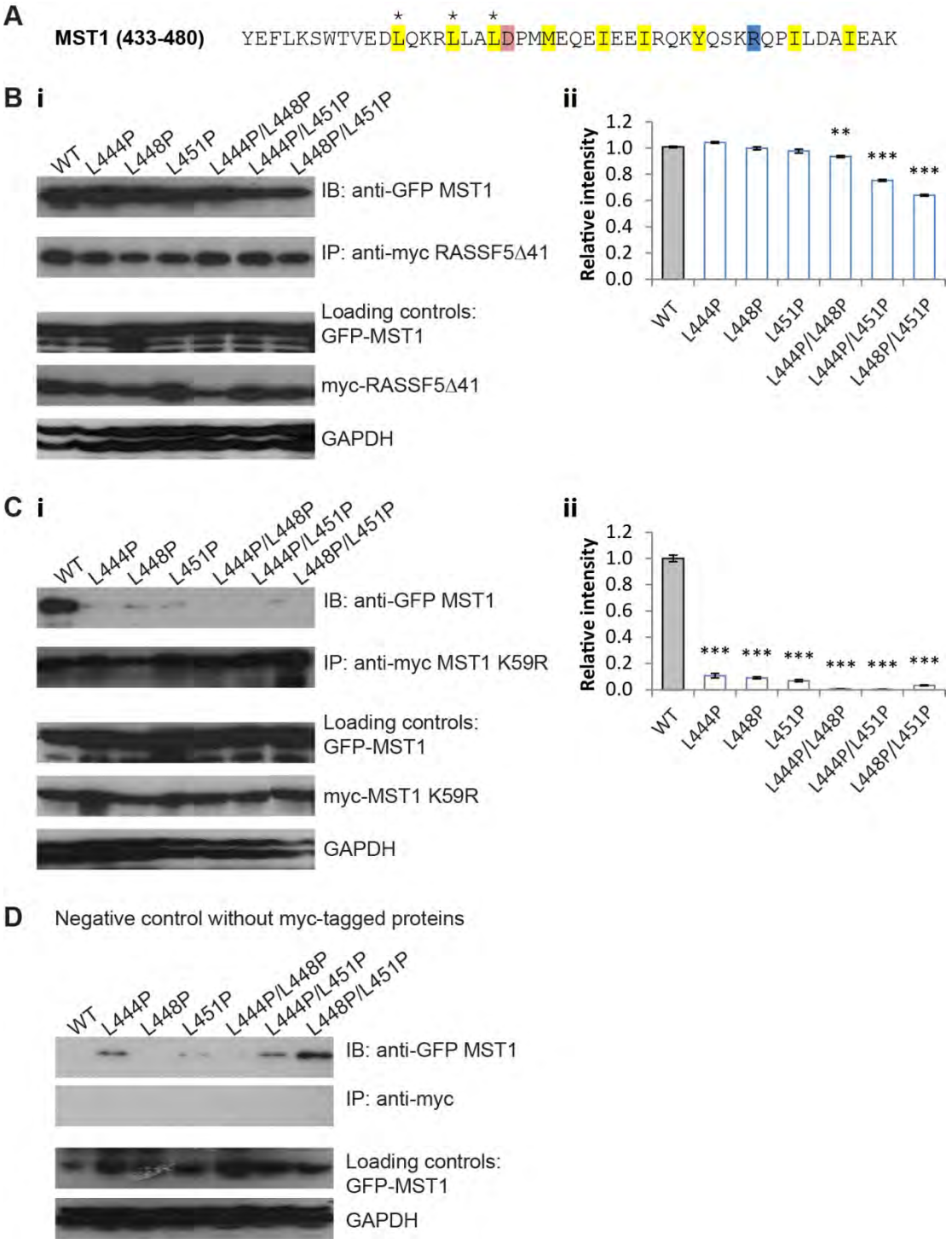
A
MST1 (433-480)
YEFLKSWTVEDLQKRLLALDPMMEQEIEEIRQKYQSKRQPILDAIEAK
B i
WT
L444P
L448P
L451P
L444P/L448P
L444P/L451P
L448P/L451P
IB: anti-GFP MST1
IP: anti-myc RASSF5Δ41
Loading controls: GFP-MST1
myc-RASSF5Δ41
GAPDH
ii
Relative intensity
1.2
1.0
0.8
0.6
0.4
0.2
0.0
**
***
***
C i
IB: anti-GFP MST1
IP: anti-myc MST1 K59R
Loading controls: GFP-MST1
myc-MST1 K59R
GAPDH
ii
***
D
Negative control without myc-tagged proteins
IB: anti-GFP MST1
IP: anti-myc
Loading controls: GFP-MST1
GAPDH

5.2.3.2. Mutations in the RASSF1 SARAH domain

For RASSF1, we mutated the three Leu residues, aligning to the same positions as those in MST1, to Pro: L301, L305 and L308 (Figure 5.4A). Again, three single point mutants and three double point mutants were generated.

Similar to the experiments in section 5.2.3.1, wild-type RASSF1 was used as a positive control for the co-IP experiments. When co-expressed with RASSF5, a strong signal was detected only for the positive control, a very weak signal was detected for single point mutant L301P, whereas the remaining five mutants failed to bind RASSF5 (Figure 5.4B). Likewise, only wild-type RASSF1 showed strong binding to MST1 (Figure 5.4C). Very weak signals were detected for all three single point mutants. However, the signal for L301P was slightly stronger in comparison to L305P and L308P, as well as to its interaction with RASSF5 (Figure 5.4Bii, Cii). Conversely, none of the double point mutants were detected. The negative control experiments, in which none of the wild-type or mutants showed non-specific binding, confirmed that the interactions detected were not false positives (Figure 5.4D).

We also performed intracellular FRET studies for the RASSF1 point mutants as described in section 2.6.3. Due to time constraint, we only tested the three single point mutants due to their very weak detection in the *in vitro* studies (Figure 5.5A). Wild-type RASSF1 showed a significant decrease in GFP donor lifetime (Figure 5.5Bi), whereas the changes in the FRET signals for the three mutants are statistically insignificant (Figure 5.5Bii-iv), indicating a lack of interaction between the mutants and MST1 SARAH.

5.2.3.3. Mutations in the RASSF5 SARAH domain

As with MST1 and RASSF1, three single and three double point mutants were generated for RASSF5. The three residues mutated in the RASSF5 SARAH domain were L224, L228 and L231, which align to the same conserved positions (Figure 5.6A).

Wild-type RASSF5 was used as the positive control against the six mutants. All three RASSF5 single point mutants co-immunoprecipitated at similar levels with myc-tagged RASSF5 (Figure 5.6B), thus retaining their ability to homodimerise. However, quantification of the bands showed that there were slight statistically significant

Figure 5.4 Effects of mutations in the RASSF1 SARAH domain on dimerisation

(A) The SARAH domain sequence of RASSF1. Main interacting non-polar (yellow), acidic (red) and basic (blue) residues are highlighted. The three positions in which mutations were introduced are marked by asterisks (*).

(B) Co-IP assay to show heterodimerisation between myc-RASSF5Δ41 and wild-type (WT) GFP-RASSF1 and its three single and three double point mutants: L301P, L305P, L308P, L301P/L305P, L301/L308P and L305P/L308P. The loading controls and GAPDH endogenous controls are shown below. (ii) Quantification of the bands in terms of relative intensity to the WT control.

(C) Co-IP assay to show heterodimerisation between myc-MST1 K59R and wild-type (WT) GFP-RASSF1 and its six mutants as described in (B). The loading controls are shown below. (ii) Quantification of the bands in terms of relative intensity to the WT control.

(D) Co-IP assay of the negative controls. A simultaneous negative control was performed using cell lysates containing only GFP-RASSF1 or its mutants. The loading controls are shown below.

All co-IP assays (B-D) were repeated three times and a representative is shown here. The quantification of the bands and calculation of p-values are as described in Figure 5.3.

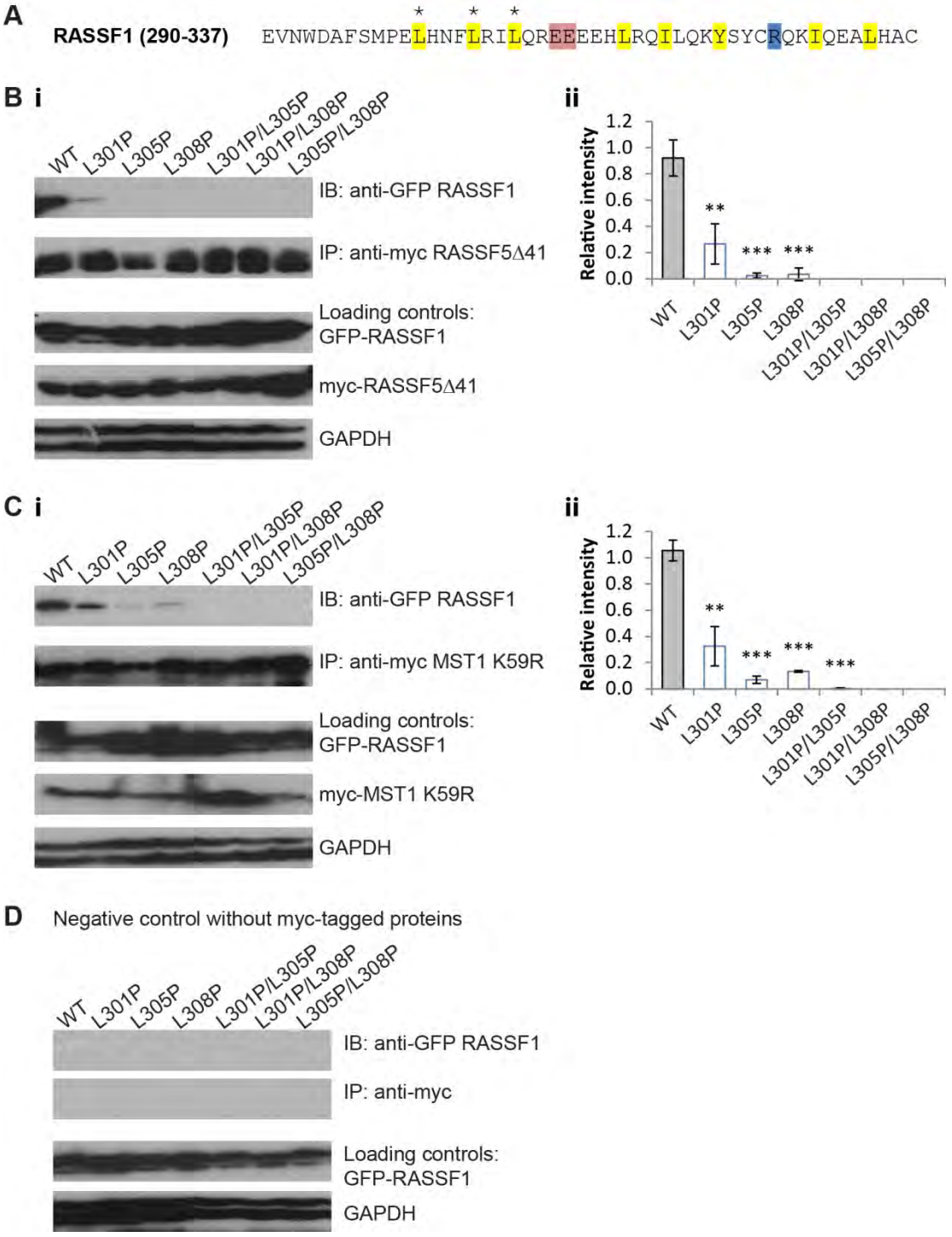
A
RASSF1 (290-337)
EVNWDAFSMPELHNFLRILQREEEEHLRQILQKYSYCRQKIQEALHAC
B i
WT
L301P
L305P
L308P
L301P/L305P
L301P/L308P
L305P/L308P
IB: anti-GFP RASSF1
IP: anti-myc RASSF5Δ41
Loading controls: GFP-RASSF1
myc-RASSF5Δ41
GAPDH
ii
Relative intensity
1.2
1.0
0.8
0.6
0.4
0.2
0.0
**
***
***
C i
IB: anti-GFP RASSF1
IP: anti-myc MST1 K59R
Loading controls: GFP-RASSF1
myc-MST1 K59R
GAPDH
D
Negative control without myc-tagged proteins
IB: anti-GFP RASSF1
IP: anti-myc
Loading controls: GFP-RASSF1
GAPDH

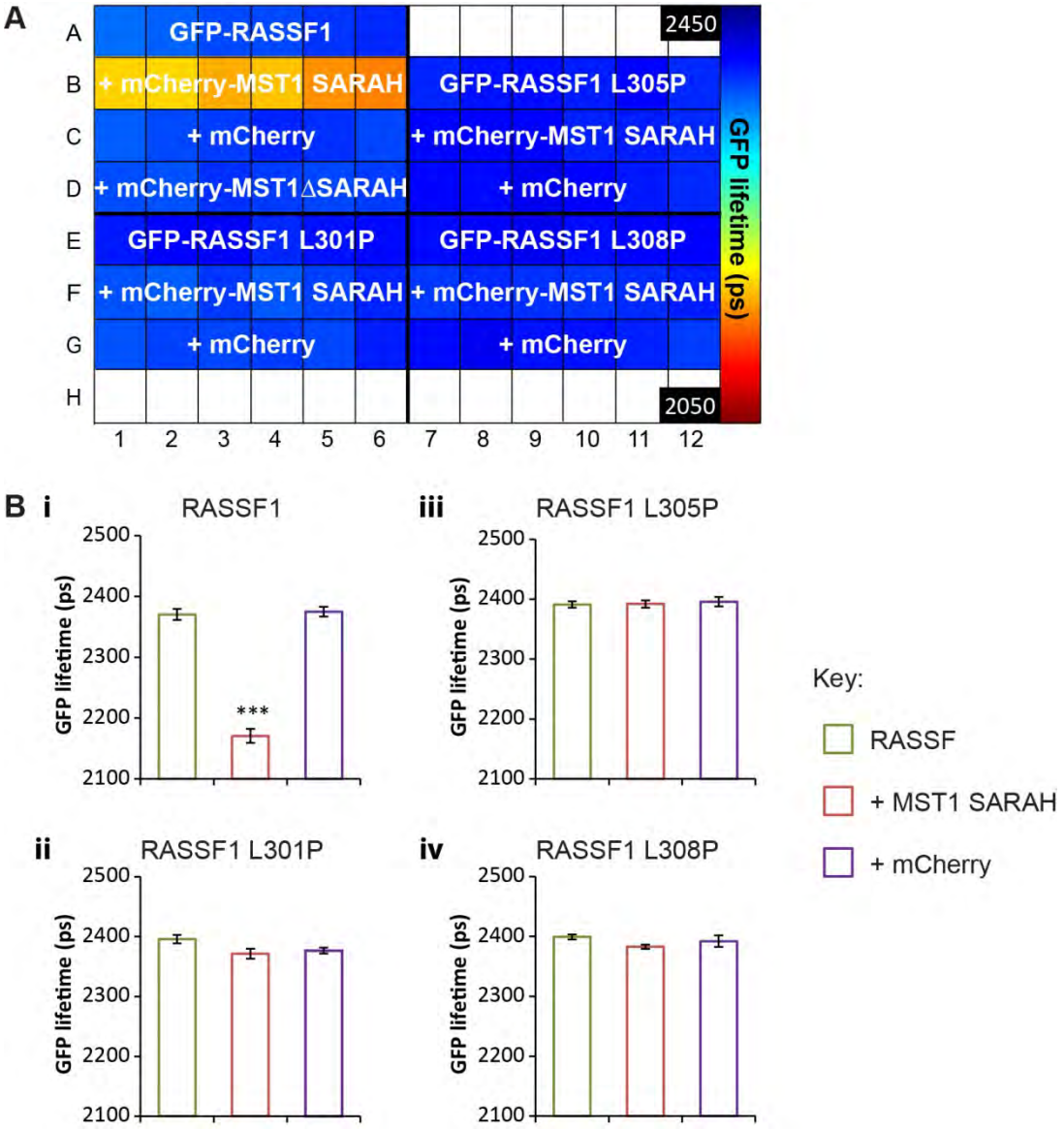

Figure 5.5 FRET studies on RASSF1 mutants and the MST1 SARAH domain

(A) Plate map of the 96-well plate setup for GFP-RASSF1 WT and its single point mutants with mCherry-MST1 SARAH or the negative controls mCherry and mCherry-MST1ΔSARAH. The wells and FRET signal are indicated as described in Figure 4.8. Image acquisitions and data processing were performed by Dr Anca Margineanu as described in section 2.6.3.

(B) Bar graphs showing the GFP lifetime changes per condition for (i) WT RASSF1 and (ii-iv) its three single point mutants. The GFP lifetimes were calculated as an average per well and error bars are standard deviations. P-values were calculated against the negative control mCherry using the Student's t-test and are indicated as follows: $p \leq 0.05$ (*), $p \leq 0.01$ (**) and $p \leq 0.001$ (***).

differences between the wild-type and the L228P and L231P mutants (Figure 5.6Bii). Conversely, for the double mutants, L224P/L228P and L228P/L231P were detected at lower levels, whilst L224P/L228P was not detected (Figure 5.6Bii). Similarly, in the co-IP assay for heterodimerisation with MST1, the signals detected for all six mutants were of a similar pattern to the homodimerisation assay above (Figure 5.6C). The negative control experiments confirmed that all the bands detected were not the result of non-specific binding (Figure 5.6D).

Intracellular FRET studies were also carried out for the three RASSF5 single point mutants (Figure 5.7A). Statistically significant increases in FRET signals were detected for wild-type RASSF5 as well as the three mutants tested (Figure 5.7B). However, the increase in FRET signals for the three mutants were clearly of a much smaller magnitude compared to the wild-type, which is an indication of a reduced binding affinity by the RASSF5 mutants.

5.2.3.4. Comparison of the effects of the RASSF1 and RASSF5 mutations

Based on the FRET data from sections 5.2.3.2 and 5.2.3.3, the changes in GFP donor lifetimes were calculated for the wild-type and mutants of both RASSF1 and RASSF5 (Figure 5.8A). As expected, both wild-type constructs showed the largest decrease in GFP lifetime, i.e. increase in FRET signal. All three RASSF1 mutants showed almost undetectable FRET signals, whereas this varies for the same mutations in RASSF5, with L228P producing the smallest increase in FRET signal, whilst L224P and L231P were less potent in inhibiting dimerisation. Overall, mutations of identical residues aligning to the same positions in RASSF1 (Figure 5.8B) appear to be more detrimental to heterodimerisation compared to RASSF5.

5.3. Discussion

The analytical outcome of both homodimeric and heterodimeric models places strong emphasis on side chain interactions and non-polar residues, which supports previous structural studies on the MST1 and RASSF5 SARAH domain (Hwang et al., 2007, Makbul et al., 2013). Furthermore, it suggests that the hydrophobic network plays a significant role not only in homodimerisation, but also in heterodimerisation, as the non-polar interface dominates all SARAH dimer interfaces.

Figure 5.6 Effects of mutations in the RASSF5 SARAH domain on dimerisation

(A) The SARAH domain sequence of RASSF5. Main interacting non-polar (yellow), acidic (red) and basic (blue) residues are highlighted. The three positions in which mutations were introduced are marked by asterisks (*).

(B) Co-IP assay to show homodimerisation between myc-RASSF5Δ41 and wild-type (WT) GFP-RASSF5 and its three single and three double point mutants: L224P, L228P, L231P, L224P/L228P, L224/L231P and L228P/L231P. The loading controls and GAPDH endogenous controls are shown below. (ii) Quantification of the bands in terms of relative intensity to the WT control.

(C) Co-IP assay to show heterodimerisation between myc-MST1 K59R and wild-type (WT) GFP-RASSF5 and its six mutants as described in (B). The loading controls are shown below. (ii) Quantification of the bands in terms of relative intensity to the WT control.

(D) Co-IP assay of the negative controls. A simultaneous negative control was performed using cell lysates containing only GFP-RASSF5 or its mutants. The loading controls are shown below.

All co-IP assays (B-D) were repeated three times and a representative is shown here. The quantification of the bands and calculation of p-values are as described in Figure 5.3.

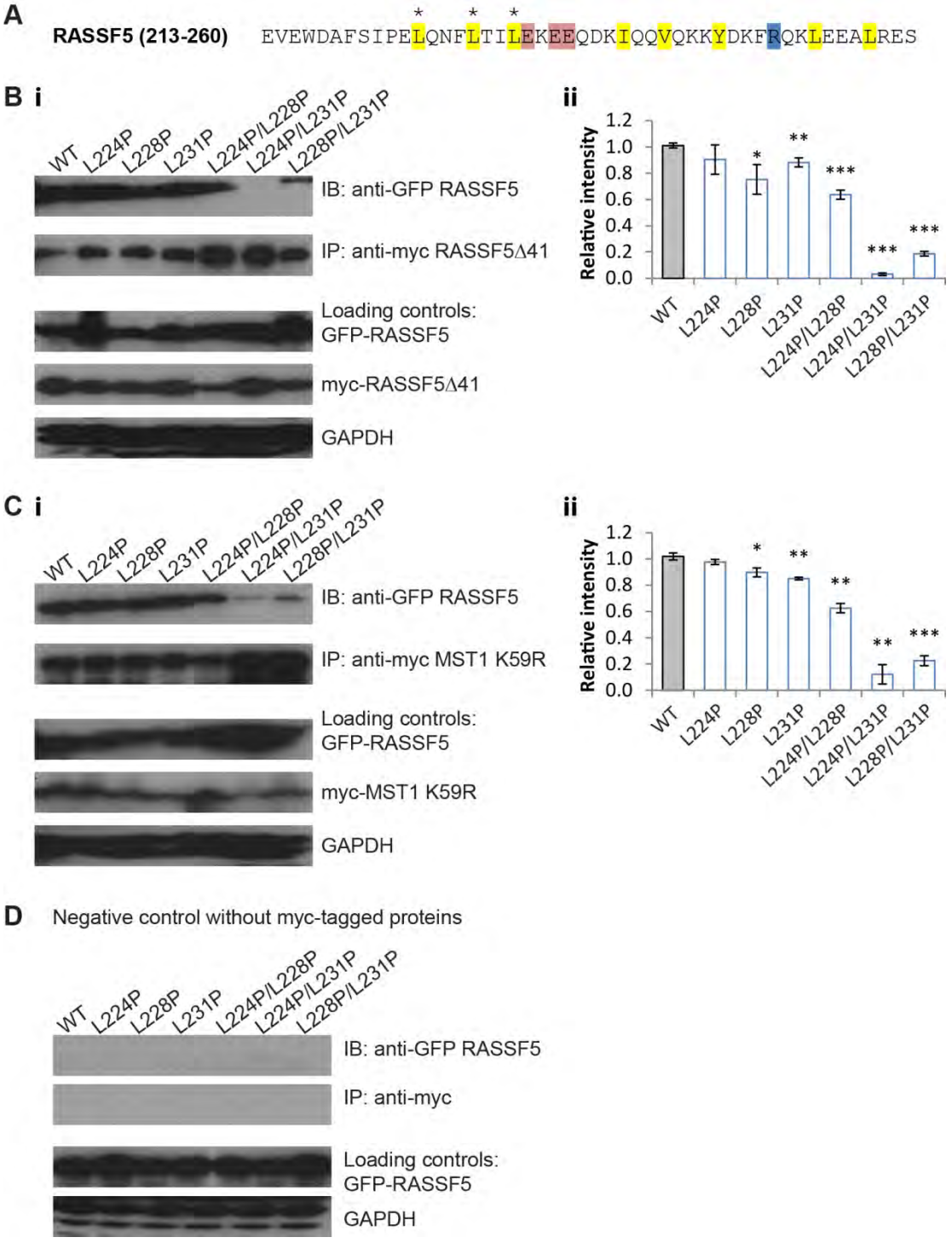
A
RASSF5 (213-260) EVEWDAFSIPELQNFLTILEKEEQDKIQQVQKKYDKFRQKLEEALRES
B i
WT
L224P
L228P
L231P
L224P/L228P
L224P/L231P
L228P/L231P
IB: anti-GFP RASSF5
IP: anti-myc RASSF5Δ41
Loading controls: GFP-RASSF5
myc-RASSF5Δ41
GAPDH
ii
Relative intensity
1.2
1.0
0.8
0.6
0.4
0.2
0.0
*
**
***
***
***
C i
WT
L224P
L228P
L231P
L224P/L228P
L224P/L231P
L228P/L231P
IB: anti-GFP RASSF5
IP: anti-myc MST1 K59R
Loading controls: GFP-RASSF5
myc-MST1 K59R
GAPDH
ii
Relative intensity
1.2
1.0
0.8
0.6
0.4
0.2
0.0
*
**
**
**
***
D
Negative control without myc-tagged proteins
WT
L224P
L228P
L231P
L224P/L228P
L224P/L231P
L228P/L231P
IB: anti-GFP RASSF5
IP: anti-myc
Loading controls: GFP-RASSF5
GAPDH

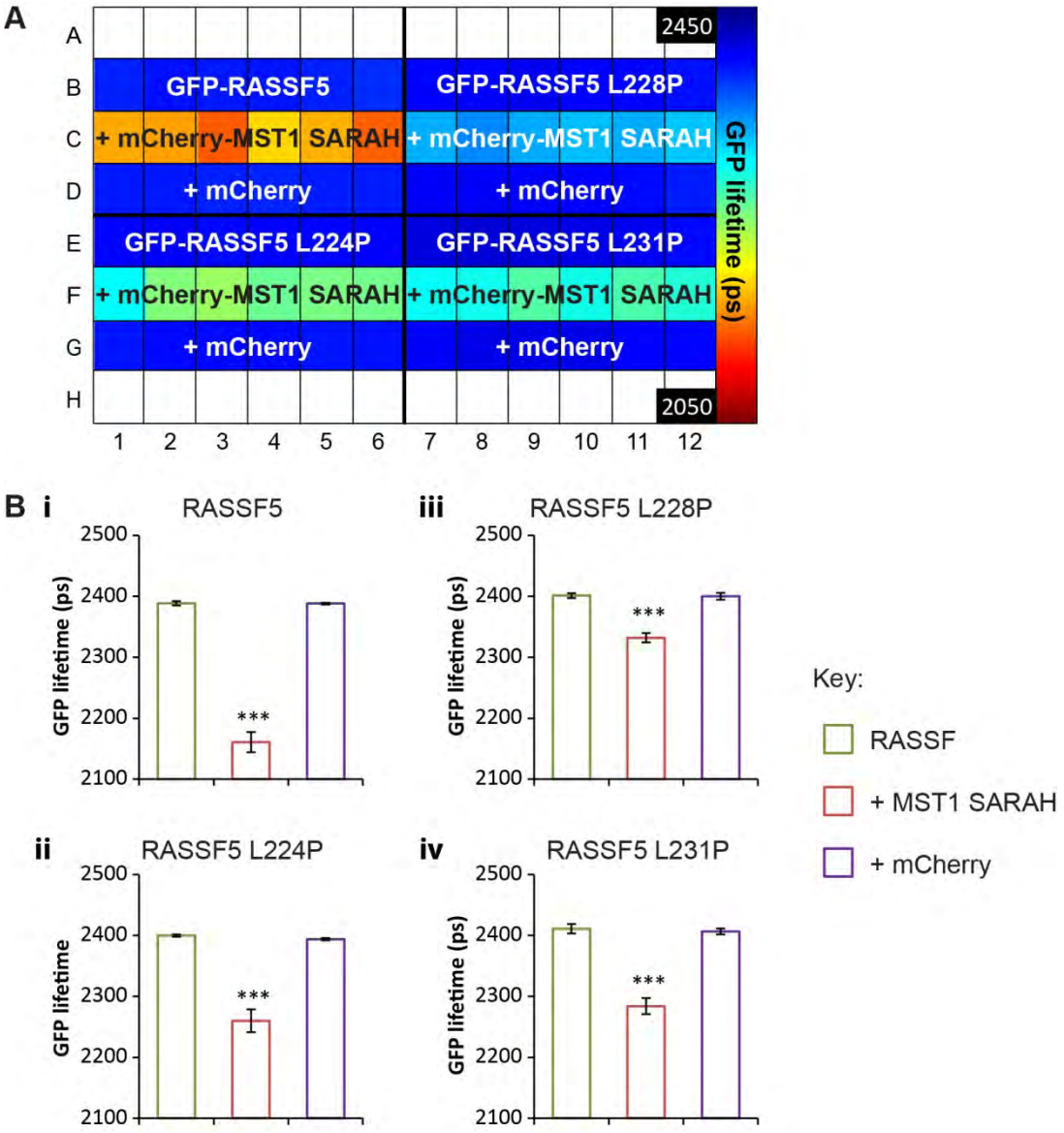

Figure 5.7 FRET studies on RASSF5 mutants and the MST1 SARAH domain

(A) Plate map of the 96-well plate setup for GFP-RASSF5 WT and its single point mutants with mCherry-MST1 SARAH or the negative control mCherry. The wells and FRET signal are indicated as described in Figure 4.8. Image acquisitions and data processing were performed by Dr Anca Margineanu as described in section 2.6.3.

(B) Bar graphs showing the GFP lifetime changes per condition for (i) WT RASSF5 and (ii-iv) its three single point mutants. The GFP lifetimes, errors and p-values were calculated and indicated as described in Figure 5.5B.

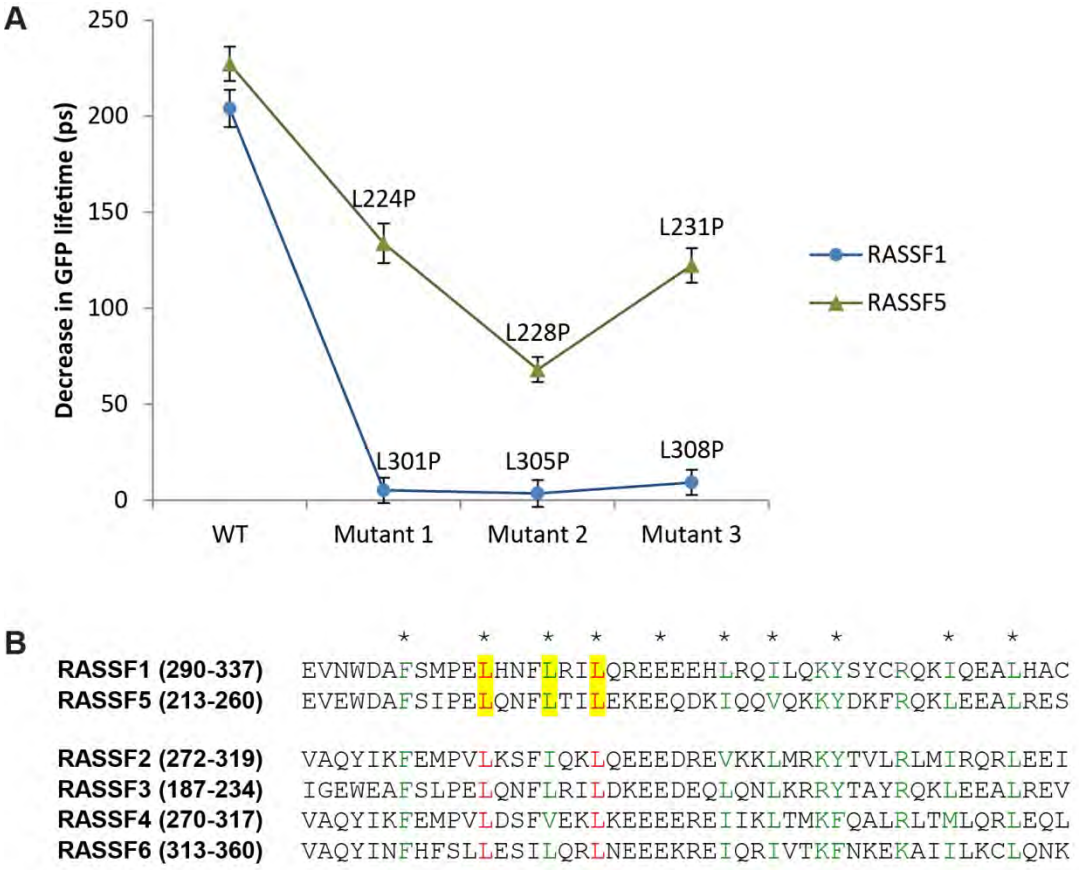

Figure 5.8 Comparison of the effects of the RASSF1 and RASSF5 mutations

(A) Graphical representation of the different FRET signals of the WT and single point mutants for RASSF1 and RASSF5. These were measured as a change in the GFP donor lifetimes and the error bars are the combined standard deviations (see Figure 5.5 and 5.7).

(B) Sequence alignments of the RASSF1-6 SARAH domains. Positions of the non-polar residues involved in interaction are marked by asterisks (*). Conserved residues in these positions are shown in red and similar residues in green. The residues mutated in RASSF1 and RASSF5 for this study are highlighted in yellow.

The globally larger interface area for heterodimers is an indication of more residues being involved at the interface or more interacting partners per residue. The latter is more likely as even when there are minimal changes in the interface residues, such as in the MST1/RASSF1 or RASSF4 heterodimer (Figure 5.2Bi, iv), interface areas remain greater for heterodimers. This is due to a larger ΔASA for each individual residue, which indicates more contacts are being made by these residues, hence stronger interactions. On the other hand, this interface enlargement could be due to the contribution from MST1, which has a globally larger interface compared to all the RASSF SARAH domains. Nonetheless, our *in silico* data are in agreement with previous studies highlighting the association between stronger protein interactions and larger interface areas, whereby larger ΔASA contribution means more hydrogen bonds, salt bridges and other forces of interaction (Jones and Thornton, 1995).

A previous study highlighted the natural preference for homodimers due to a higher affinity for self-attraction between two identical monomers with their identically aligned residues (Lukatsky et al., 2007). This is in agreement with our previous observation under complete *in vitro* experimental conditions (Chapter 4). However, this may be the opposite under cellular and physiological settings. Based on our *in silico* data and analyses, there is a high possibility that the SARAH domain has a greater propensity to heterodimerise due to the larger heterodimeric interface area and its correlation with stronger interactions. A higher heterodimer affinity in this case could also be due to the large degree of structural similarities between the different SARAH domains with the interacting side chains better orientated and tightly-packed in the heterodimeric structures (Figure 5.2B). The involvement of more aromatic residues (Phe, Trp, Tyr, His) in the heterodimeric interfaces probably contributes to the latter phenomenon. They are known to form strong hydrophobic interactions between bulky side chains, with parallel arrangements that create tighter packing with a better geometric fit (Yan et al., 2008).

There were two slight discrepancies between our *in vitro* and intracellular FRET observations for the interaction of MST1 with the RASSF mutants. The first was the RASSF1 mutants, where very weak interactions were detected *in vitro* but not in the FRET studies (Figure 5.4 and 5.5). This could be due to the much weaker binding affinity increasing the fluorophore donor-acceptor distances beyond the required 10 nm, thus FRET would not have been efficient enough for any changes to be detected even if the two proteins were interacting very weakly. The second discrepancy was the almost

equal or very small change in binding of the RASSF5 mutants to MST1 observed *in vitro* against the much reduced FRET signals in cells (Figure 5.6 and 5.7). The latter indicates that while binding still occurs, the affinities are definitely compromised by the mutations. This inconsistency could be due to the variable expression levels of the proteins in the *in vitro* assays. Thus, such techniques are adequate for detecting interactions but insufficient to discriminate between different binding affinities, whereas FRET is a much more sensitive approach. Nevertheless, the FRET data confirm that these mutations weaken the ability of RASSF1 and RASSF5 to heterodimerise, although to different extents; thus double mutations would completely eliminate dimerisation.

The different degrees of disruption to heterodimerisation caused by the RASSF1 and RASSF5 mutants (Figure 5.8) could be due to the variations in the specific residues involved in their individual heterodimeric interfaces, and the properties of the residues surrounding the mutated sites (Figure 5.1A, F). It is possible that the neighbouring residues in RASSF5, which are different from those in RASSF1, could compensate for the effects of the mutation, thus minimising the disruption. Alternatively, it could be the result of mutating the residues to Pro, which is known to introduce distortion to helices (Barlow and Thornton, 1988). This is observed in wild-type MST1, in which P453 and P472 cause a kink at their respective positions (Hwang et al., 2007). Thus, it is possible that introducing Pro into RASSF1 in those positions distorts the helical structure more severely than in RASSF5, resulting in an almost total loss of heterodimerisation, whereas RASSF5 still retains its ability to heterodimerise, albeit at a diminished level, which is in agreement with a previous report of a L224A mutant (Raab et al., 2011). It could also be that the Leu residues and hydrophobic interactions play a more critical role for RASSF1 heterodimerisation as opposed to RASSF5.

Interestingly, the MST1 mutants retain their ability to heterodimerise but not homodimerise (Figure 5.3B, C), thus helix distortion by Pro should not play a role in this case. This observation supports previous studies using the MST1 L444P mutant, which lost its affinity for homodimerisation but not heterodimerisation with RASSF5 (Khokhlatchev et al., 2002, Praskova et al., 2004). As described in Chapter 4, although the RASSF5 SARAH domain is structurally very similar to MST1, they are sequentially rather different with RASSF5 carrying a charged segment composed mainly of Asp, Glu and Lys residues. Consequently, heterodimeric interactions may be slightly different from homotypic interactions, whereby interactions between the charged residues could

compensate for the loss of some hydrophobic interactions. However, despite the *in vitro* data showing almost equal binding by the MST1 mutants to RASSF5, FRET studies would probably detect a reduction in binding affinities such as in the case of RASSF5.

Observations from our previous FRET experiments in section 4.2.3.2 suggest a potential heterodimer affinity with MST1 in the following order: RASSF3 and RASSF5 > RASSF4 > RASSF1 and RASSF2 >> RASSF6. The heterodimeric models here offer some plausible explanations for these differences. As the non-polar interface is a major feature and all the residues in the conserved positions are present, minor differences in the non-polar interfaces sizes amongst the heterodimers are unlikely to affect the dimerisation affinities. Conversely, we find a correlation between the affinity pattern and the proportion of the polar interface areas (Table 5.3). The potentially strongest binders, RASSF3 and RASSF5, have the largest proportional polar interface (19.2%). Although this is the same for RASSF4, it appeared to bind slightly weaker to MST1, which could be due to the fact that charged side chains make up only half of its polar interface, with the other half being polar uncharged side chains. This suggests that salt bridges formed between charged residues contribute more to stronger binding affinities compared to hydrogen bonds by polar uncharged side chains. The rest of the classical RASSF members 1, 2 and 6 follow a similar pattern. Therefore, whilst the hydrophobic network of non-polar residues plays an integral role in dimerisation and the maintenance of dimer stability (Hwang et al., 2007), the interactions between polar residues are likely also a strong contributing factor to the binding affinities.

It is also worth noting that despite the MST1/RASSF6 heterodimer having the smallest polar interface, the number of polar side chains involved is in fact similar to RASSF1 and RASSF2. However, the distinct difference lies in the residue aligning to R470 in MST1. Residues in this position are highly conserved in all other RASSF SARAH domains except for RASSF6, which carries a Lys (Figure 5.1F). Various studies have shown that Arg is superior to Lys in forming stronger salt bridges and maintaining protein stability due to the geometric properties of the Arg guanidinium group (Kumar and Nussinov, 1999, Musafia et al., 1995, Sokalingam et al., 2012). Thus, even with the largest total and non-polar interfaces, RASSF6 still has the weakest binding affinity for MST1. From these observations, we can infer that besides non-polar residues and

Table 5.3 Comparison of the SARAH heterodimer polar interfaces

The polar interfaces (in $Å^2$), their proportion to the total dimeric interfaces and the polar residues involved (in red) are shown for each RASSF heterodimer.

MST1 with:	Total	Polar	Polar/Total (%)	SARAH domain sequence
RASSF1	2844.6	494.1	17.4	EVNWDAFSMPELHNFLRILQREEEEHLRQILQKY SYCRQKIQEALHAC
RASSF2	2933.6	507.1	17.3	VAQYIKFEMPVLKSFIQKLQEEEDREVKKLMRKY TVLRLMIRQRLEEI
RASSF3	2767.7	532.2	19.2	IGEWEAFSLPELQNFLRILDKEEDEQLQNLKRRY TAYRQKLEEALREV
RASSF4	2843.2	547.1	19.2	VAQYIKFEMPVLDSFVEKLKEEEEREIIKLTMKF QALRLTMLQRLEQL
RASSF5	2820.9	542.2	19.2	EVEWDAFSIPELQNFLTILEKEEQDKIQQVQKKY DKFRQKLEEALRES
RASSF6	2988.4	486.3	16.3	VAQYINFHFSLLESILQRLNEEEKREIQRIVTKF NKEKAIILKCLQNK

hydrophobic interactions, the specificity of charged residues and the strength of their interactions also dictate the affinity of SARAH heterodimers.

Although we observed variations in the effect of all the mutations tested, the majority of them negatively affected dimerisation to different extents. These data could be used to predict the likelihood of the same mutations in disrupting the interactions of the other classical RASSF members. However, we do not know to what extent this effect will be for each individual RASSF member. Nevertheless, the residues mutated in this study are conserved within the family (Figure 5.8B), indicating that the residues and positions we have chosen are appropriate targets. Thus, similar residues could also play an important role in homodimerisation or heterodimerisation of the remaining RASSF members. Introducing mutations to these positions in other classical RASSF members may disrupt interaction. Moreover, any combination of double mutations to the residues highlighted in Figure 5.8B is highly likely to completely abolish dimerisation mediated by the SARAH domain.

In addition to predicting interactions, these mutational studies could also be very useful for future cellular or *in vivo* studies. Mutations that disrupt interaction could be used to assess the functions of the RASSF family under physiological conditions. Furthermore, they could provide further insights on functions that are dependent on homodimerisation or heterodimerisation via the SARAH domain.

6 Other potential interacting partners of the RASSF family

6.1. Introduction

Apart from the main interacting RA and SARAH domains, a few of the RASSF member have been shown to associate with other interacting partners via specific motifs present in their sequences. RASSF1 is the only member of the family that has been extensively studied and characterised in this aspect. Earlier studies have revealed its interaction with several key proteins in death and NFκB signalling, namely TNF-R1, MOAP1, DAPK and TBK1 (Baksh et al., 2005, Bialik et al., 2008, El-Kalla et al., 2010, Foley et al., 2008), whilst it could also be a potential phosphorylation target of DAPK (Shairaz Baksh, personal communication). These proteins consist of a variety of binding domains and motifs illustrated in Figure 6.1.

6.1.1. Proteins involved in death signalling

6.1.1.1. The RASSF/MOAP1/TNF-R1 complex

MOAP1 is a 40 kDa highly regulated pro-apoptotic protein, first identified in a yeast two-hybrid screen as a Bax-associating protein (Tan et al., 2001). It is ubiquitously expressed under normal cellular conditions but its expression levels are downregulated in a wide panel of human cancer tissues and cell lines (Law et al., 2012). Therefore, it has been suggested that the combined loss of MOAP1 and RASSF1 may be a common occurrence during carcinogenesis to deregulate the extrinsic death pathway. Similar to RASSF1, several single nucleotide polymorphisms (SNPs) have also been identified in MOAP1, with two of these observed in melanoma patients (P79S and A335D) (Wei et al., 2011). Although their biological consequences are yet to be determined, it has been speculated that these SNPs could impact phosphorylation patterns and RASSF1 association respectively.

TNF-R1 is a 55 kDa transmembrane protein that binds its ligand trimer via its Cys-rich TNFR domain (Figure 6.1B). This is followed by the recruitment of adaptor proteins to its cytoplasmic death domain, initiating a signalling cascade leading to cell death (described in section 1.2.3) (Locksley et al., 2001).

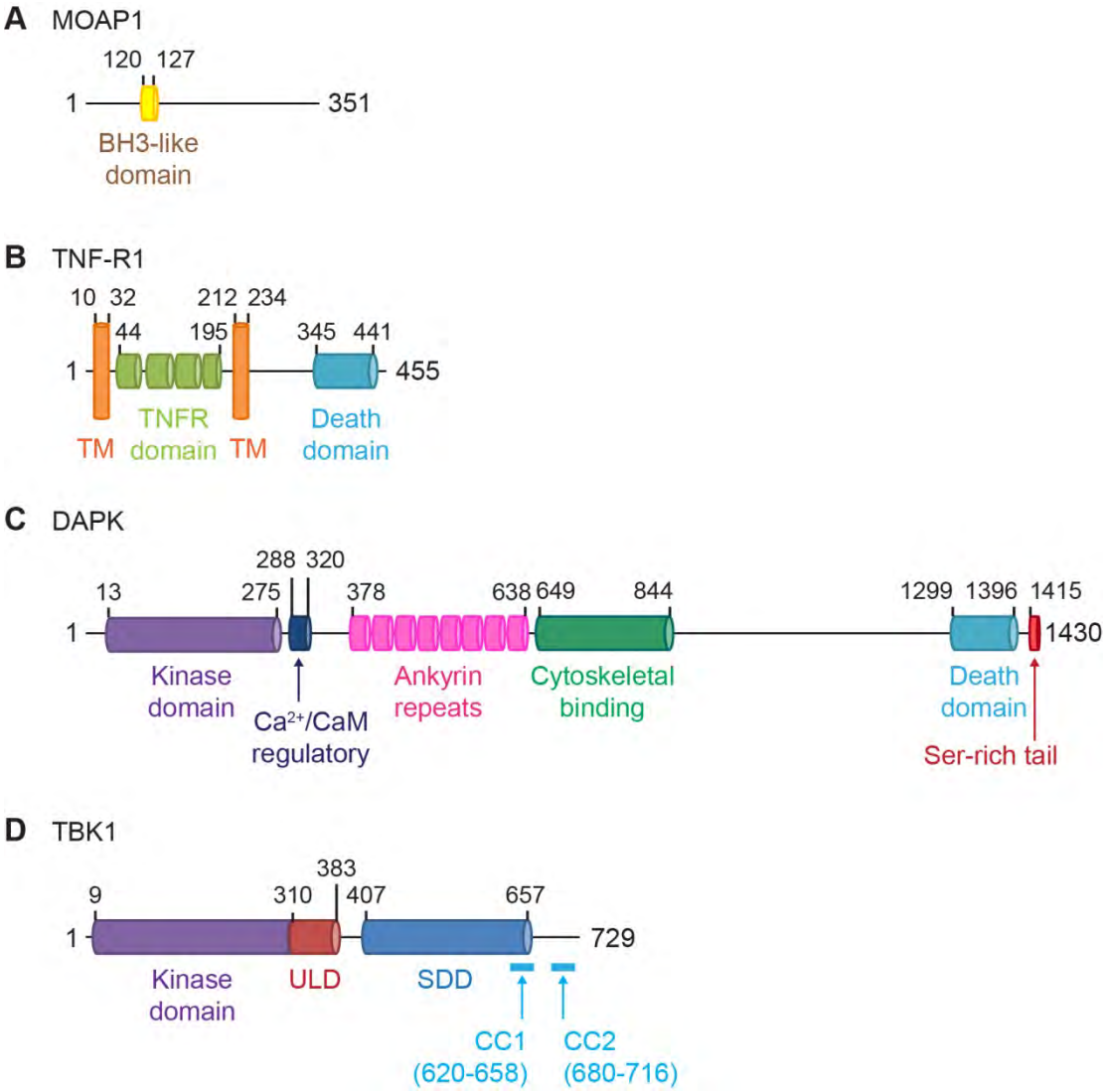

Figure 6.1 Schematic representations of the RASSF1 interacting proteins

(A-D) The length of each protein is indicated. The main structural features are labelled and the residue positions indicated above.

(BH3, Bcl2 homology domain 3; TM, transmembrane region; Ca^{2+}/CaM, calcium-activated calmodulin; ULD, ubiquitin-like domain; SDD, scaffold/ dimerisation domain; CC, coiled-coil)

The RASSF1/MOAP1/TNF-R1 complex has been extensively studied in recent years. RASSF1 and MOAP1 interact via a highly charged acidic segment in its SARAH domain (^{311}EEEEH) and a region of oppositely charged basic residues (^{201}EKRRR) in MOAP1 (Figure 6.2Ai, ii) (Baksh et al., 2005). Likewise, the complex between MOAP1 and TNF-R1 is mediated by a C-terminal segment of acidic residues (^{333}EAEEEEA) and a basic stretch in the death domain (^{408}TWRRR) respectively (Figure 6.2Ai, iii) (Foley et al., 2008). Whilst interactions with MOAP1 appear to be predominantly governed by electrostatic interactions, the interaction between RASSF1 and TNF-R1 is mediated by Cys and His residues of the zinc finger motifs within the RASSF1 C1 domain (Figure 6.2Aii) (Foley et al., 2008). RASSF1 and MOAP1 are mutually required to form a ternary complex with TNF-R1 and for their apoptotic function (Foley et al., 2008). At the same time, microtubule localisation of RASSF1 also plays an important role in accelerating TNF-R1 internalisation (El-Kalla et al., 2010). In its unbound form, MOAP1 is held in a "closed" conformation via intra-electrostatic interactions between (^{178}EEEF) and ^{202}KRRR (Baksh et al., 2005). The binding of RASSF1 triggers a conformational change in MOAP1 that exposes its BH3-like domain. This allows MOAP1 to bind Bax and induce its conformational change, enabling it to translocate to the mitochondria to cause MOMP, cytochrome c release and a signalling cascade resulting in cell death as described in section 1.2.3 (Figure 6.2B) (Law et al., 2012). Another study also revealed that ability of the RASSF1/TNF-R1 complex to promote MST activation and its subsequent apoptotic response, which suggests that this complex could be involved in multiple apoptotic pathways (Vichalkovski et al., 2008).

RASSF3 and RASSF6 have also been shown to interact with MOAP1, whilst RASSF5A interacted with TNF-R1; and these protein complexes are partly responsible for the pro-apoptotic effects of the three RASSF members (Allen et al., 2007, Ikeda et al., 2009, Kudo et al., 2012, Park et al., 2010). Interestingly, the interaction with MOAP1 could possibly occur via other regions in the RASSF protein as a truncated RASSF6 lacking the SARAH domain still bound to MOAP1 (Ikeda et al., 2009). However, the rest of the interactions have not been characterised and the underlying molecular mechanisms and specific interacting regions for these complexes are not known.

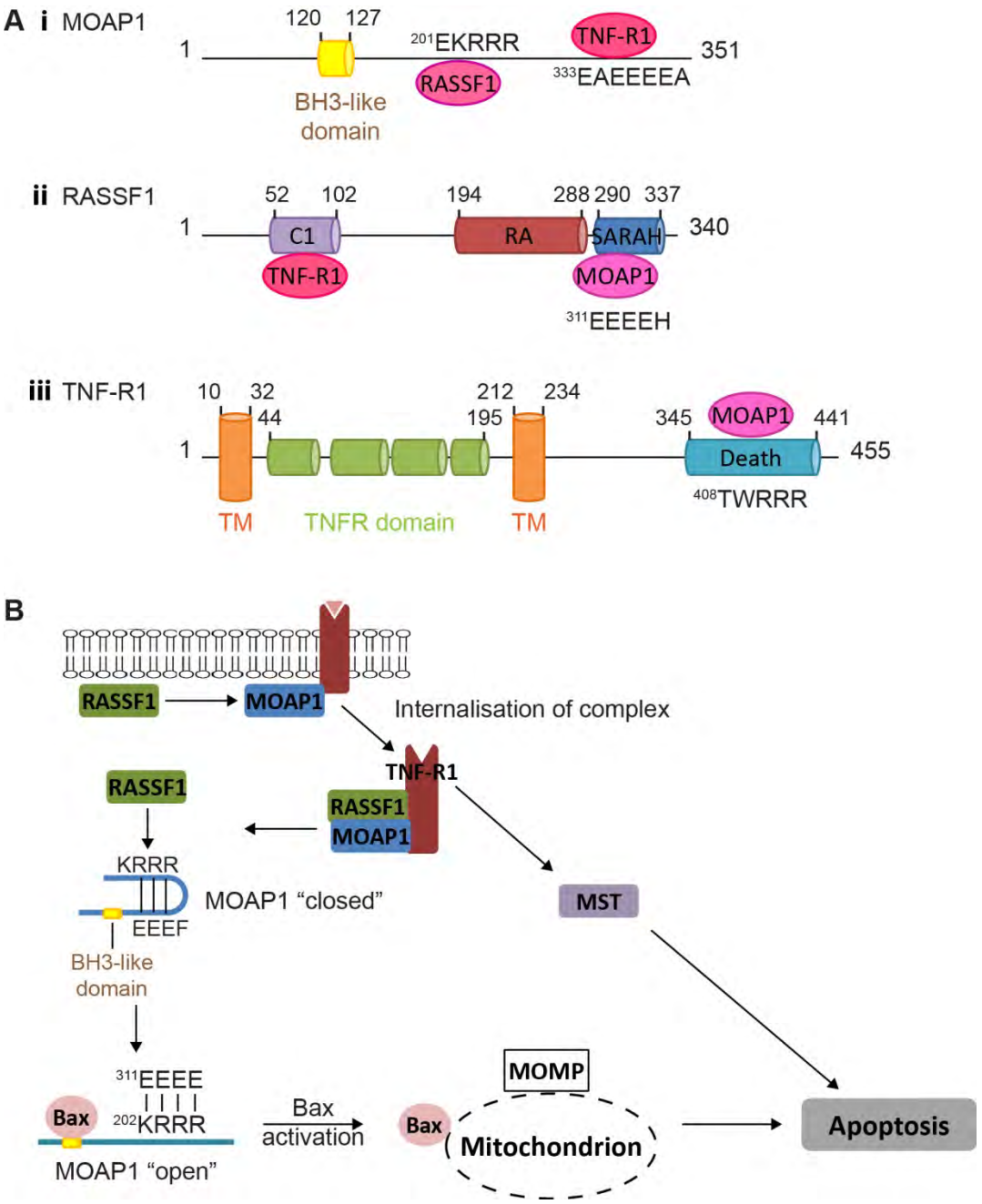

Figure 6.2 Key protein interactions in RASSF1-mediated death signalling

(A) Schematic representations of the proteins and their key regions involved in the RASSF1/MOAP1/TNF-R1 complex. In each schematic, interacting proteins are shown in pink and the sequences from the illustrated protein involved in interactions are shown. Adapted from Foley et al. (2008).

(B) The extrinsic signalling pathways involving the RASSF1/MOAP1/TNF-R1 complex. Adapted from Gordon et al. (2012) and Law et al. (2012).

6.1.1.2. Death-associated protein kinase (DAPK)

DAPK is a 160 kDa Ca^{2+}/CaM-regulated Ser/Thr kinase. It is known to induce cell death by multiple death signals and regulates both caspase-dependent apoptosis and caspase-independent autophagy depending on specific cell types and death signals (Bialik and Kimchi, 2006). In addition to its ability to sensitise cells to apoptotic signals, DAPK has been shown to suppress cellular transformation at early stages of tumour development and inhibit metastasis in mouse models (Bialik and Kimchi, 2006). As it is also quite frequently downregulated in a large variety of tumour types due to promoter hypermethylation, DAPK has been identified as a tumour suppressor. Intriguingly, epigenetic silencing of DAPK and RASSF1 are correlative events that are linked to poor prognosis of patients with NSCLC and malignant mesothelioma (Buckingham et al., 2010, Fischer et al., 2006).

DAPK consists of several key domains that are important for its functions (Figure 6.1C). Its activation is a two-step process: 1) binding of Ca^{2+}-activated CaM to the CaM regulatory domain releases DAPK autoinhibition and 2) dephosphorylation of S308 increases the affinity for CaM, thus promoting the kinase catalytic activity (Bialik and Kimchi, 2006). Additionally, the cytoskeletal binding domain facilitates its association with the actin cytoskeleton and the induction of membrane blebbing during apoptosis. The C-terminal death domain mediates interaction with Erk that activates DAPK, whilst the Ser-rich tail negatively regulates the functions of DAPK. Most importantly, its N-terminal kinase domain comprises two distinct clusters of acidic residues at the substrate-binding site that have been suggested to play a role in substrate recognition (Tereshko et al., 2001). Thus, though not always the case, many of its substrates possess two to three basic residues just N-terminal to the S/T phosphorylation sites to facilitate electrostatic interactions (Bialik and Kimchi, 2006). Interestingly, RASSF1 is able to bind DAPK (Shairaz Baksh, personal communication), and a high throughput proteomics screen also identified two potential phosphorylation sites within the RASSF1 RA domain (^{193}GRGTSVRRRTSFYLPK) (Gordon et al., 2012).

DAPK is activated by a wide variety of stimuli. Although most studies highlight the regulatory roles of DAPK in cell death signalling, it has been shown to have broader functions through its interaction with and regulation of the actin and microtubule cytoskeleton (Bialik and Kimchi, 2006, Harrison et al., 2008, Wu et al., 2011). Despite

the diverse functions of DAPK, few binding proteins have been identified for DAPK. Recent studies showed that DAPK is also able to inhibit TNFα-dependent NFκB activity and its targeted gene expression to cause cell cycle arrest and apoptosis (Wu et al., 2013, Yoo et al., 2012). The signalling network involving DAPK is outlined in Figure 6.3.

6.1.2. TANK-binding kinase (TBK1)

TBK1 is an 83 kDa Ser/Thr kinase and a non-canonical IKK along with its highly similar counterpart IKKε. It is a key node protein in multiple signalling pathways and is a critical inducer of the interferon (IFN) and NFκB signalling cascades (Figure 6.4) (Shen and Hahn, 2011). Stimuli and receptors that activate TBK1 include viral nucleic acids, LPS, and interleukins, TLR3, TLR4 and different IL-R's respectively. The primary functions of TBK1 are antiviral and antibacterial innate immune response, inflammation, autophagy, proliferation and growth (Helgason et al., 2013).

TBK1 carries several distinct domains shown in Figure 6.1D. The predicted CC2 is required for its binding to adaptor proteins TANK, Sintbad and NAP1, which are mutually exclusive (Goncalves et al., 2011). This in turn leads to different subcellular localisation of TBK1, which is crucial for its activation and substrate specificity (Helgason et al., 2013). The recent structure of TBK1 also showed that all three of its major domains, the kinase domain (KD), ULD and SDD form a tripartite complex and homodimer that positions the kinase active sites away from one another (Tu et al., 2013). Thus, activation of TBK1 occurs in a biphasic reaction, whereby the lag phase relies on the "activation loop-swap" mechanism in the local cluster of TBK1 molecules for the initial phosphorylation event, followed by a second phase of rapid trans-autophosphorylation (Ma et al., 2012). In addition to dimerisation, K63 polyubiquitination on conserved K30 and K401 is required for the activating phosphorylation of S172 in the TBK1 kinase activation loop (Tu et al., 2013).

Due to its broad spectrum of functions, TBK1 has been linked to the pathophysiology of various diseases, making it a potential therapeutic target (Niederberger et al., 2013). Of note, it has been shown to facilitate tumourigenesis and is highly expressed in several cancers (Shen and Hahn, 2011). Although its primary functions are mediated mainly by NFκB signalling, TBK1 is able to phosphorylate and activate Akt and drive pro-survival signals in lung cancer cells harbouring *KRAS*

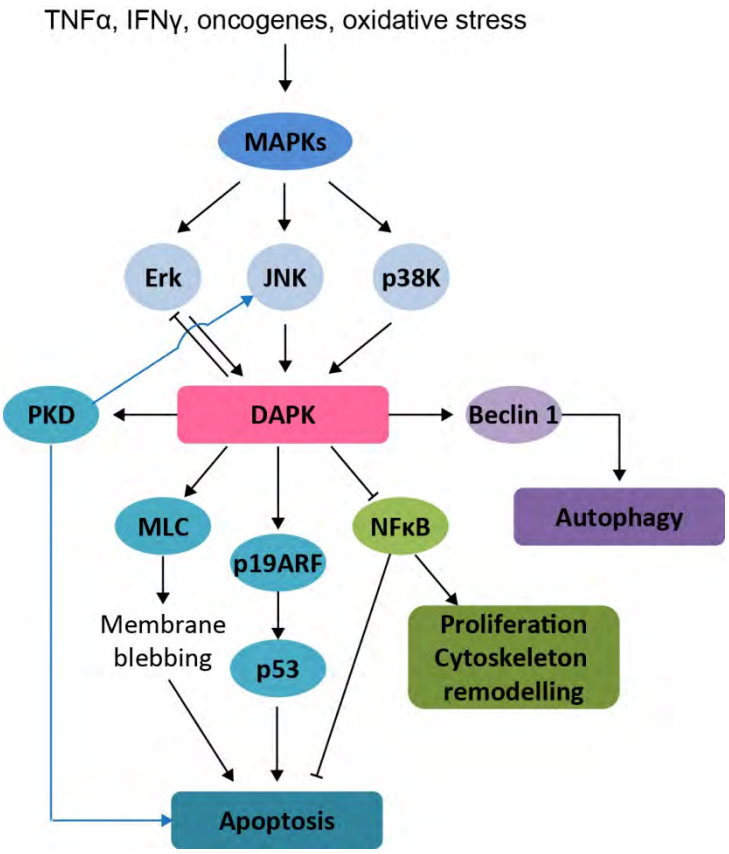

Figure 6.3 Illustration of the DAPK signalling cascade

DAPK signalling is initiated by various external stimuli to the cell, including inflammatory cytokines such as TNFα and IFNγ, oncogenes and oxidative stress. This leads to changes in apoptosis, autophagy and cell proliferation. Blue lines indicate JNK-mediated apoptosis via PKD activation by DAPK. Adapted from Rennier and Ji (2013).

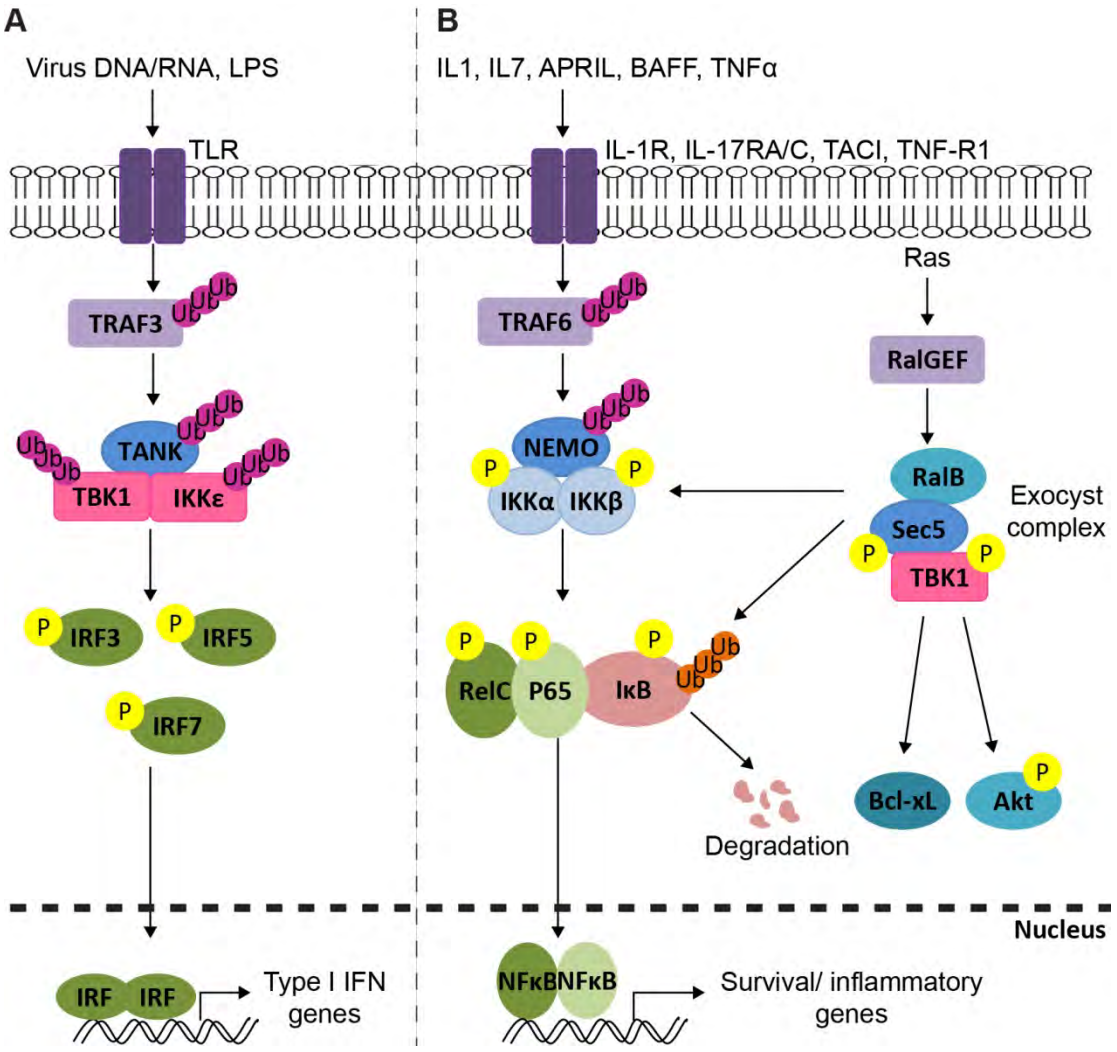

Figure 6.4 Illustration of NFκB signalling involving TBK1

(A) Non-cell autonomous TBK1/IKKε signalling. Viruses and bacterial toxin LPS engage TLR to initiate K63 polyubiquitination of TRAF3, recruitment and activation of TBK1/IKKε/TANK, IRF and IFN target genes.

(B) Cell autonomous TBK1 signalling. Stimuli activate the canonical NFκB signalling cascade. Ras activation leads to the formation of an exocyst complex of RalB/Sec5/TBK1. TBK1 mediates phosphorylation of multiple effectors, including Sec5, IKKβ and IκB, which leads to the activation of Bcl-xL, Akt and NFκB pro-survival signalling. Adapted from Helgason et al. (2013) and Shen and Hahn (2011).

(APRIL, a proliferation-inducing ligand; BAFF, B-cell activating factor; IFN, interferon; IL, interleukins; IRF, interferon response factors; TACI, TNF receptor superfamily member 13B; TLR, toll-like receptor; TRAF, TNF receptor-associated factor)

mutations, and is also activated by Ras GTPase RalB in cancers (Figure 6.4) (Helgason et al., 2013, Kim et al., 2013). Additionally, TBK1 has been shown to form a complex with TNF-R1 and upregulates anti-apoptotic genes in a NFκB-dependent manner upon TNFα stimulation (Delhase et al., 2012, Kuai et al., 2004). Current studies suggest crosstalk between Ras, TNF-R1 and NFκB signalling are likely to play an important role in the TBK1-driven immune response, inflammation and oncogenesis.

Recently, an interaction screen has identified TBK1 as a RASSF1 binding partner (Shairaz Baksh and Gerd Pfeifer, personal communication). However, there is little sequence conservation around the TBK1 phosphorylation sites, thus it is difficult to predict whether RASSF1 is a target substrate or simply an adaptor for TBK1. The molecular mechanisms behind the interaction between RASSF1 and TBK1 are also not known.

It is evident that MOAP1, TNF-R1, DAPK and TBK1 share some similar key functions, such as caspase-dependent cell death and other NFκB-driven activities. Furthermore, crosstalk between different signalling pathways appears to influence some of these functions. Given that the RASSF family members are relatively well conserved, it is possible that other RASSF members could also interact with these proteins, and may act as an adaptor or a phosphorylation substrate that adds another layer of regulation to these pathways. The aim of this study was to assess and compare the interactions of the RASSF family with these key proteins in cell death and NFkB signalling, and the effects of different stimuli on these interactions. Here, we observe differences in binding to the four interacting partners tested amongst the ten RASSF members, as well as in the absence and presence of different stimuli.

6.2. Results

6.2.1. Interaction between MOAP1 and the RASSF family

We first studied the interaction of the RASSF family with MOAP1. Figure 6.5Ai shows the three charged regions in MOAP1, referred to as R1-3, that are known to form either intra- or inter-electrostatic interactions as described in section 6.1.1.1. Based on existing reports on MOAP1-R2 (Figure 6.5Ai) being the basic segment that interacts with the

Figure 6.5 Interaction between the RASSF family and MOAP1

(A) Potential regions of interaction for (i) MOAP1 and (ii-iii) RASSF family members. The three regions in MOAP1 are referred to as R1-3. Acidic residues are shown in red, basic residues in blue and polar residues in green. Fully conserved residues are marked with asterisks (*) and weakly similar residues with periods (.).

(B) (i) Co-IP assay to show interaction between GFP-RASSF1-10 and myc-MOAP1 with and without TNFα-stimulation. This is representative of the results from three separate experiments. The loading controls are shown below. (ii) Quantification of the bands using ImageJ. The relative intensity of the stimulated binding by RASSF1 was set at 1 and used as a reference point. The error bars are standard deviations. P-values were calculated using the Student's t-test to compare unstimulated and TNFα-stimulated binding for each individual RASSF and indicated as follows: $p \leq 0.05$ (*), $p \leq 0.01$ (**) and $p \leq 0.001$ (***).

A i 3 regions in MOAP1 for potential electrostatic interaction:

MOAP1-R1 (178-181) EEEF
MOAP1-R2 (201-205) EKRRR
MOAP1-R3 (336-340) EEEEA

ii Charged regions in classical RASSF:

RASSF1 (310-315) REEEEH
RASSF2 (291-296) QEEEDR
RASSF3 (207-212) KEEDEQ
RASSF4 (289-294) KEEEER
RASSF5 (233-238) KEEQDK
RASSF6 (332-337) NEEEKR
.**. .

iii Charged regions in N-terminal RASSF:

RASSF8 (202-207) LEEEIV
RASSF8 (220-225) IEEEEF
RASSF8 (287-292) NEEEVK
RASSF10 (441-448) RRRRRQRR

B i

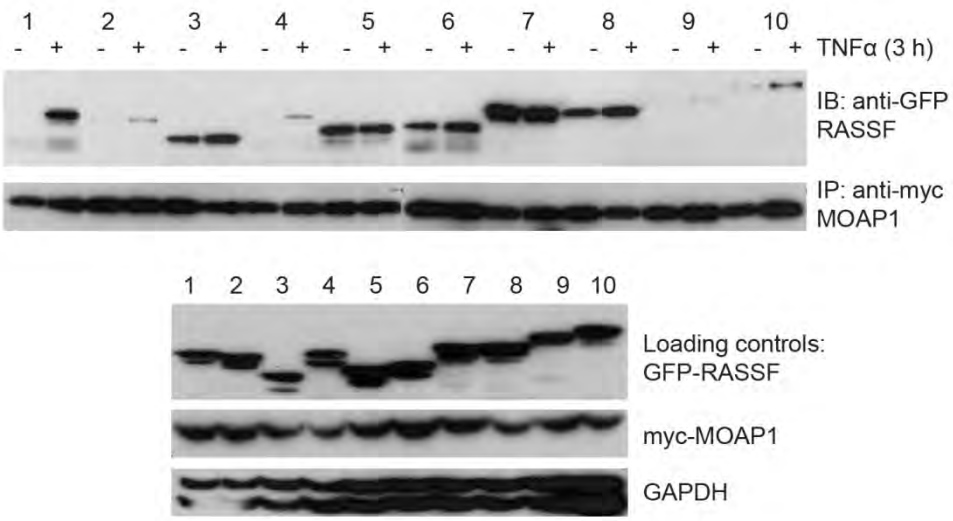

ii

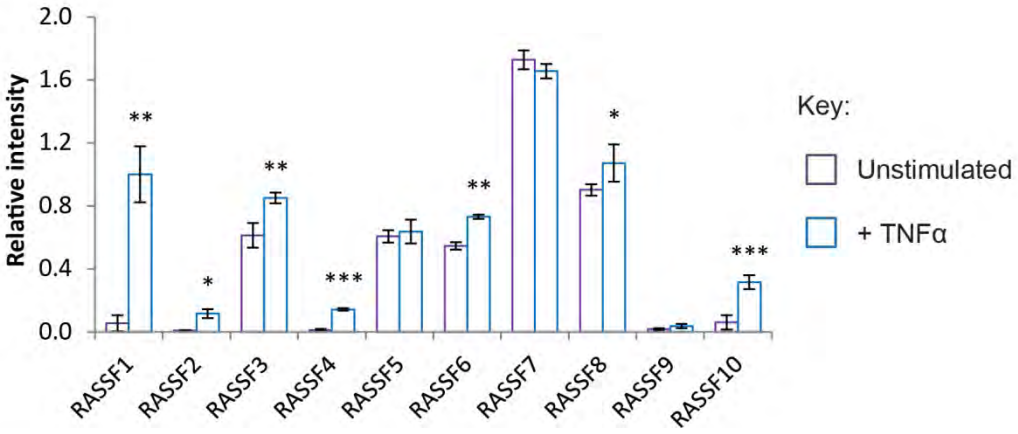

acidic residues in RASSF1, we performed multiple sequence alignments for this region in the classical RASSF members. As expected, as this region is part of the SARAH domain described in Chapter 4, the acidic residues are well-conserved across all six classical RASSF members (Figure 6.5Aii). However, the occurrence of charged segments are more variable in the N-terminal RASSF members. These are not present in RASSF7 and RASSF9. RASSF8 carries three different segments of acidic residues, whereas a long stretch of basic residues is found in RASSF10 (Figure 6.5Aiii). This basic region in RASSF10 could be involved in charged interaction with MOAP1 given that TNF-R1 is known to interact with MOAP1 via its segment of basic residues.

On the basis that interaction between the RASSF proteins and MOAP1 is mediated by electrostatic interactions, it would seem that all RASSF members except RASSF7 and RASSF9 are capable of binding MOAP1. To validate these predictions, we performed a series of co-IP using unstimulated and TNFα-stimulated cell lysates containing myc-MOAP1 and GFP-RASSF (Figure 6.5Bi). RASSF1 served as a positive control for stimulation-dependent binding. All six classical RASSF members were detected in the TNFα-stimulated immunoprecipitates. However, signals for RASSF2 and RASSF4 were very weak in comparison. Furthermore, RASSF3, 5 and 6 were also detected in the unstimulated immunoprecipitates, although signals for RASSF3 and RASSF6 were significantly higher for their stimulated interaction (Figure 6.5Bii). For the N-terminal RASSF members, RASSF8 and RASSF10 showed binding as expected. Conversely, the RASSF7 binding detected was unexpected and independent of stimulation. However, this could also be a case of non-specific binding, which has been demonstrated in section 4.2.2.2. These observations suggest stimulation-dependent binding for RASSF1, 2, 4 and 10, whereas RASSF3, 5, 6 and 8 appeared to bind MOAP1 in the absence of TNFα, with enhanced interaction for RASSF3, 6 and 8 upon cytokine stimulation.

6.2.2. Interaction between TNF-R1 and the RASSF family

We next focused on TNF-R1, the second component in the RASSF1 complex involved in extrinsic cell death. The zinc finger sequence within the C1 domain of RASSF1 and the residues required for its association to TNF-R1 are shown in Figure 6.6A. The C1 domain is absent in all other RASSF members except RASSF5A, which was not used in this study. Sequence alignments also did not show any similarities between other RASSF

Figure 6.6 Interaction between the RASSF family and TNF-R1

(A) Sequence of the RASSF1 C1 domain. Cys and His residues involved in interaction are highlighted in yellow and blue respectively.

(B) Schematic outline of the co-IP assay using co-transfected cell lysates containing pre-formed complexes. Endogenous TNF-R1 was immunoprecipitated as described in section 2.6.2.

(C) (i) Co-IP assay to show interaction between GFP-RASSF1-10 and TNF-R1 in the presence of MOAP1 with and without TNFα-stimulation. This is representative of the results from two separate experiments. The loading controls are shown below. (ii) Quantification of the bands using ImageJ. The error bars are standard deviations. The relative intensities and p-values were calculated and indicated as described in Figure 6.5B.

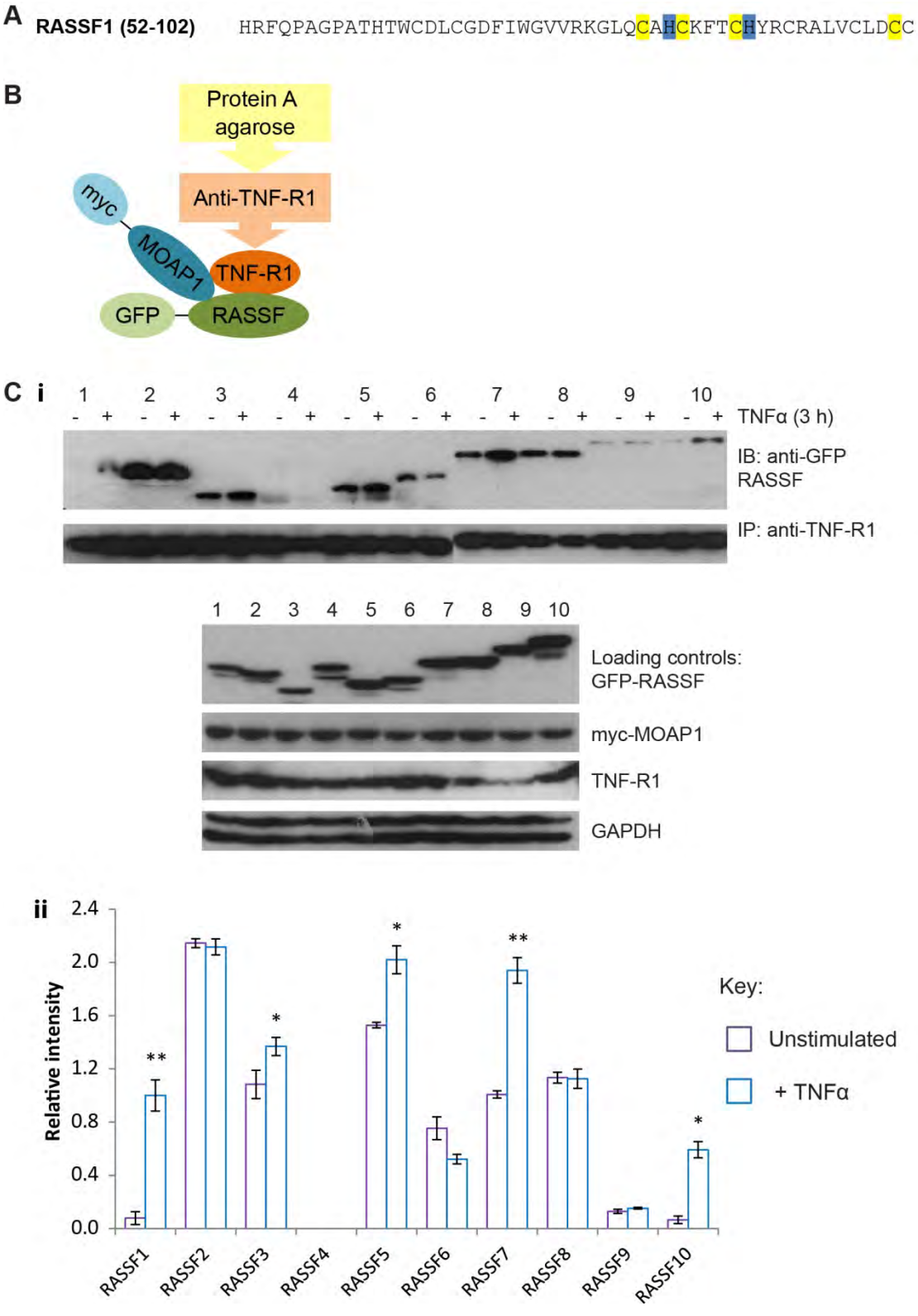
A
RASSF1 (52-102)
HRFQPAGPATHTWCDLCGDFIWGVVRKGLQCAHCKFTCHYRCRALVCLDCC
B
Protein A agarose
Anti-TNF-R1
myc
MOAP1
TNF-R1
GFP
RASSF
C i
1 2 3 4 5 6 7 8 9 10
- + - + - + - + - + - + - + - + - + - +
TNFα (3 h)
IB: anti-GFP RASSF
IP: anti-TNF-R1
1 2 3 4 5 6 7 8 9 10
Loading controls: GFP-RASSF
myc-MOAP1
TNF-R1
GAPDH
ii
Relative intensity
2.4
2.0
1.6
1.2
0.8
0.4
0.0
**
*
*
*
**
*
RASSF1
RASSF2
RASSF3
RASSF4
RASSF5
RASSF6
RASSF7
RASSF8
RASSF9
RASSF10
Key:
Unstimulated
+ TNFα

members and this region in RASSF1 (data not shown), therefore their interaction with TNF-R1 can only be determined experimentally.

As a previous report showed that interaction between RASSF1 and TNF-R1 required the presence of MOAP1 (Foley et al., 2008), we immunoprecipitated endogenous TNF-R1 from unstimulated and TNFα-stimulated cell lysates containing both myc-MOAP1 and GFP-RASSF (Figure 6.6B). The TNFα-stimulated interaction by RASSF1 was again used as a positive control. For the remaining classical RASSF members, both unstimulated and TNFα-stimulated interaction by RASSF2, 3, 5 and 6 were detected, and no signals of either were detected for RASSF4 (Figure 6.6Ci). Similar to their interactions with MOAP1, RASSF7, 8 and 10 from the N-terminal RASSF subgroup showed binding to TNF-R1. However, only the RASSF10 interaction appeared TNFα-dependent, whilst RASSF3 and surprisingly, RASSF5 and RASSF7, may form a constitutive complex with TNF-R1, where interaction could be enhanced upon stimulation (Figure 6.6Cii).

6.2.3. Interaction between DAPK and the RASSF family

There are two known consensus sequences for substrate recognition and binding to the DAPK kinase active site (Figure 6.7A) (Harrison et al., 2008, Velentza et al., 2001). However, the first full motif is not found in any of the RASSF proteins. Therefore, we performed a search for potential Ser/Thr phosphorylation sites in all ten RASSF members that fit the minimum RxxS/T consensus. Each RASSF member contains at least one such predicted site and these sites vary in their confidence scores (Table 6.1). They also do not appear to be positionally conserved within the RASSF family. Interestingly, the second motif identified from MAP1B is largely conserved at different C-terminal regions of RASSF1 and RASSF5 (Figure 6.7Aii). As the conservation of these consensus sequences are variable in the RASSF family, the presence of such motifs is not definitive of their recognition and binding by the DAPK active site, which have to be confirmed empirically.

A set of co-IPs was performed using unstimulated and TNFα-stimulated cell lysates containing overexpressed HA-DAPK and GFP-RASSF (Figure 6.7B). All classical RASSF members (1, 2, 4, 5 and 6) except for RASSF3 were detected in the immunoprecipitates, whilst RASSF7, 8 and 10 from the N-terminal RASSFs were also

Table 6.1 Predicted DAPK Ser/Thr phosphorylation sites for RASSF proteins

NetPhos 2.0 server (http://www.cbs.dtu.dk/services/NetPhos/) (Blom et al., 1999) was used to predict the phosphorylation sites. Those shown below carry the minimum consensus sequence required for DAPK phosphorylation: RxxS/T. Arg residues at the conserved position are in blue and Ser/Thr phosphorylation sites are underlined and numbered. The scores for the predictions are between 0 and 1, with 0.500 set as the minimum threshold. Higher scores indicate a higher level of confidence for a true phosphorylation site.

RASSF	Predicted phosphorylation site	Score
1	VRPV^{175}SVPSS	0.980
	GRGT^{197}SVRRR	0.990
	RRRT^{203}SFYLP	0.993
	VRRR^{202}TSFYL	0.850
2	VRIN^{197}STMTT	0.664
3	PRTD^{177}TLSFV	0.872
	KRRY^{221}TAYRQ	0.868
4	PRRP^{90}SCPLK	0.956
	VRVN^{194}STMTT	0.737
5	IRPQ^{107}SIYDA	0.997
6	YRTM^{155}SEAAL	0.614
	VRVN^{207}SNMRT	0.992
	QRIV^{312}TKFNK	0.516
7	GRPS^{97}SDSCP	0.990
	AREE^{327}SLLGA	0.730
8	ERPT^{90}SDSVA	0.996
	IRLQ^{174}TEKLQ	0.936
9	NRSP^{19}TKDMD	0.781
	KRTT^{49}SADVI	0.952
	QRVF^{403}SNYTN	0.992
10	SRRT^{27}TCSDV	0.990
	RRLG^{54}SAGDP	0.996
	ERVR^{392}TQLST	0.748

Figure 6.7 Interaction between the RASSF family and DAPK

(A) The DAPK phosphorylation consensus sequences from (i) computational analysis using docked peptide substrates (Velentza et al., 2001) and (ii) a DAPK binding protein, MAP1B (Harrison et al., 2008). The regions in RASSF1 and RASSF5 aligning to this sequence are shown. Fully conserved residues are in red and marked by asterisks (*) and partly conserved residues are in green.

(B) Schematic outline of the co-IP assay using co-transfected cell lysates containing HA-DAPK and GFP-RASSF as described in section 2.6.2.

(C) (i) Co-IP assay to show interaction between GFP-RASSF1-10 and HA-DAPK with and without TNFα-stimulation. This is representative of the results from two separate experiments. The controls are shown below. (ii) Quantification of the bands using ImageJ. The error bars are standard deviations. The relative intensities and p-values were calculated and indicated as described in Figure 6.5B.

A i DAPK phosphorylation consensus sequence:

(R/K) (R/K) (R/K) xxRxx **(S/T)**

ii DAPK kinase core binding consensus sequence:

	EEHLRRxxG
RASSF1 (313-321)	EEHLRQILQ
RASSF5 (254-262)	EEALRESQG
	** **

B

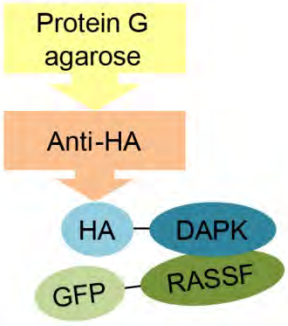

C i

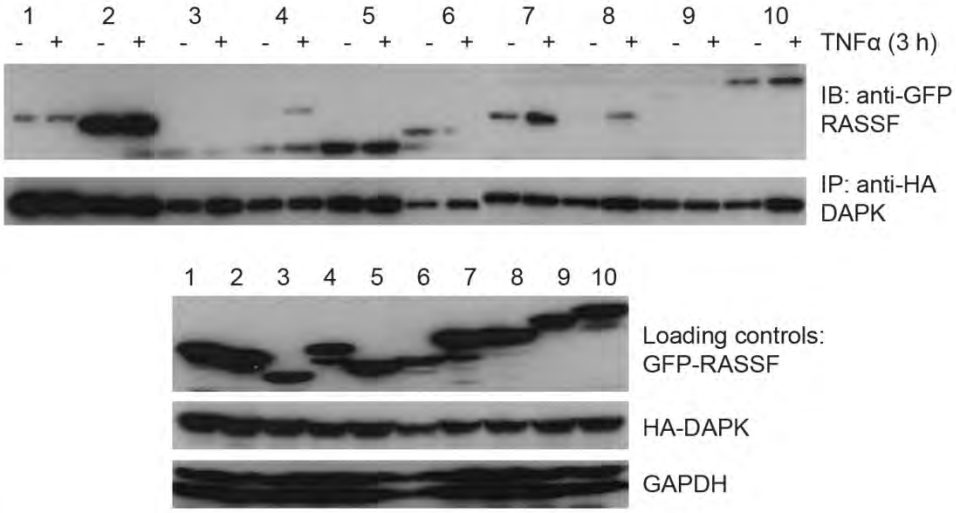

ii

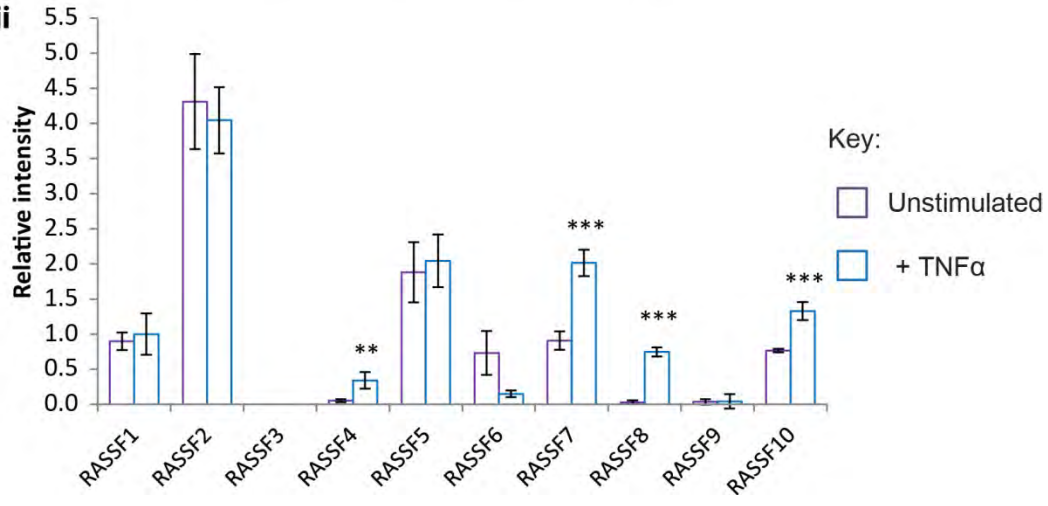

detected (Figure 6.7Ci). It is worth noting that the bands for RASSF5 overlapped with those for the immunoglobulin chains, thus RASSF5 binding may actually be weaker than observed. In addition, the difference in unstimulated and stimulated binding observed for RASSF1 and RASSF6 is more likely due to an inconsistency in exposure rather than a difference in binding. Overall, RASSF1, 2, 5 and 6 appeared to bind at their same respective levels regardless of stimulation, whilst RASSF4, 7, 8 and 10 showed statistically significant TNFα-dependent binding to DAPK (Figure 6.7Cii).

6.2.4. Interaction between TBK1 and the RASSF family

Interactions between the RASSF family and TBK1 were determined experimentally due to a lack of consensus sequence for substrate binding and recognition by TBK1 and data on regions of interaction for TBK1 and the RASSF proteins. As previous studies have shown TBK1 activation upon LPS treatment and association with TNF-R1 upon TNFα stimulation (Shen and Hahn, 2011), we used unstimulated, TNFα- or LPS-stimulated cell lysates containing GFP-RASSF for co-IP. Endogenous TBK1 was immunoprecipitated as shown in Figure 6.8A.

Low levels of RASSF1, 5 and 7 were detected in the unstimulated immunoprecipitates, whilst RASSF8 and RASSF10 appeared to bind TBK1 constitutively with high affinities (Figure 6.8Bi). Interestingly, RASSF1 and RASSF7 were the only members showing TNFα-stimulated binding to TBK1. Conversely, all six classical RASSF members, as well as RASSF7 and RASSF9, showed LPS-stimulated binding to TBK1. Quantification of the signals showed statistically significant differences between unstimulated and these stimulated interactions (Figure 6.8Bii). Furthermore, the interactions between RASSF1 or RASSF7 and TBK1 induced by the two different stimuli are significantly different. Overall, LPS appeared as the preferred, as well as stronger inducer of interaction between the RASSF proteins and TBK1.

6.3. Discussion

Given that this study focuses on MOAP1, TNF-R1, DAPK and TBK1 due to their known interactions with RASSF1, we set out to address a few main questions: 1) can other RASSF members also associate with these proteins, 2) are these interactions stimulation-

Figure 6.8 Interaction between the RASSF family and TBK1

(A) Schematic outline of the co-IP assay using transfected cell lysates containing GFP-RASSF. Endogenous TBK1 was immunoprecipitated as described in section 2.6.2.

(B) (i) Co-IP assay to show interaction between GFP-RASSF1-10 and TBK1 with and without TNFα- or LPS-stimulation. This is representative of the results from two separate experiments. The controls are shown below. (ii) Quantification of the bands using ImageJ. The relative intensity of LPS-stimulated binding by RASSF1 was set at 1 and used as a reference point. The error bars are standard deviations. P-values were calculated and indicated as described in Figure 6.5B, to compare unstimulated and TNFα- or LPS-stimulated (black), as well as TNFα- and LPS-stimulated interactions (red, brackets).

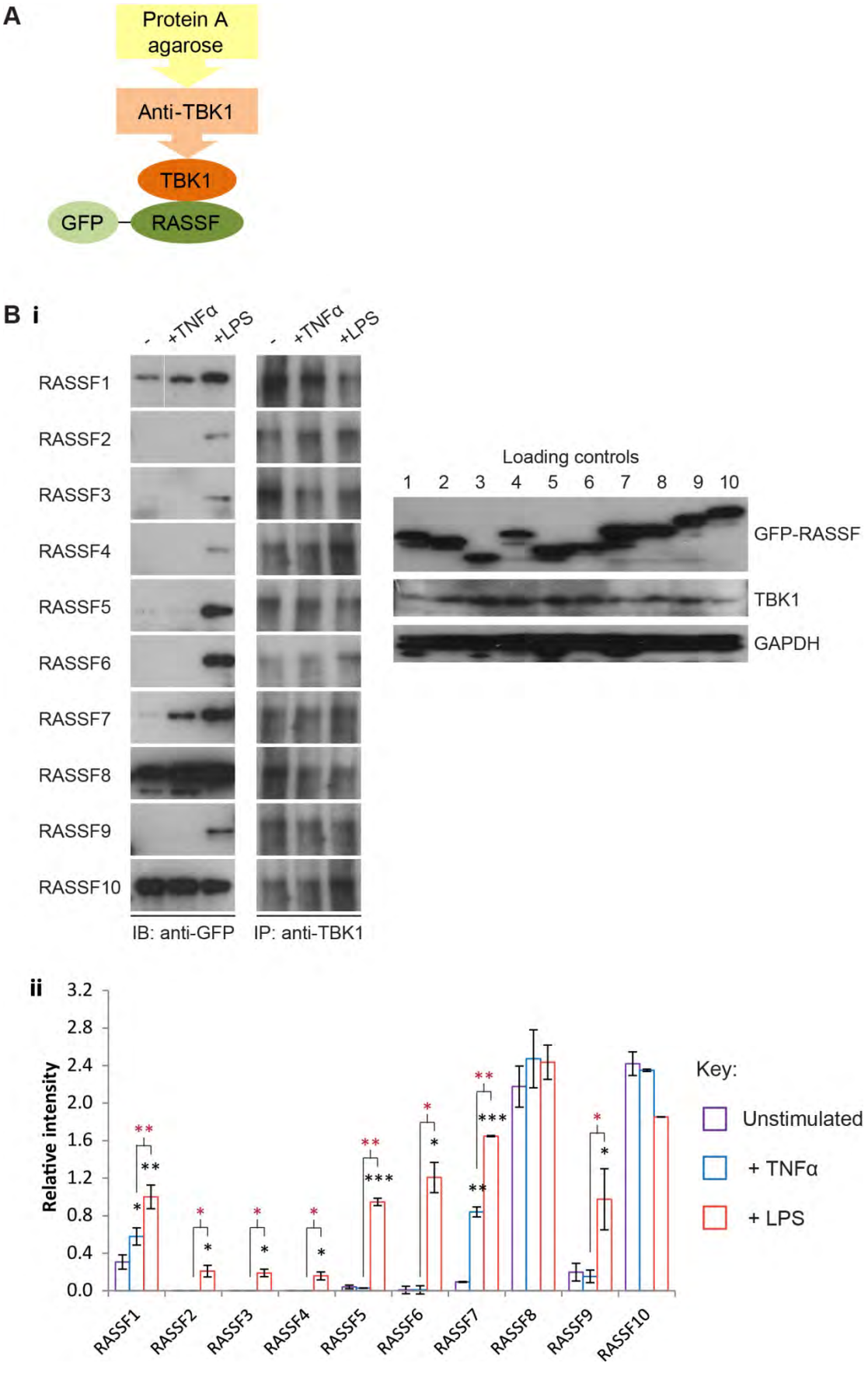
A
Protein A agarose
Anti-TBK1
TBK1
GFP
RASSF
B i
- +TNFα +LPS - +TNFα +LPS
RASSF1
RASSF2
RASSF3
RASSF4
RASSF5
RASSF6
RASSF7
RASSF8
RASSF9
RASSF10
IB: anti-GFP
IP: anti-TBK1
Loading controls
1 2 3 4 5 6 7 8 9 10
GFP-RASSF
TBK1
GAPDH
ii
Relative intensity
3.2
2.8
2.4
2.0
1.6
1.2
0.8
0.4
0.0
Key:
Unstimulated
+ TNFα
+ LPS
RASSF1
RASSF2
RASSF3
RASSF4
RASSF5
RASSF6
RASSF7
RASSF8
RASSF9
RASSF10

dependent and 3) are they mediated by the same domains and motifs identified for RASSF1?

As unstimulated interactions were observed in several instances, it is important to take into account the possibility of non-specific binding as a result of overexpression of these proteins of interest. Therefore, most of the observed constitutive interactions could be an artefact that is obscuring true stimulation-dependent binding. Since most interactions were significantly enhanced upon stimulation, they are highly likely stimulation-dependent, albeit of a potentially lower affinity, if these non-specific backgrounds were subtracted. The observed interactions accounting for potential non-specific binding are summarised in Table 6.2.

Whilst binding was observed between some RASSF members and MOAP1, TNF-R1 and DAPK (Table 6.2), it is difficult to draw any conclusions due to non-specific interactions and artefacts. Further studies are required to consolidate more data to confirm these potentially new regulatory interactions. In contrast, TBK1 has displayed the clearest and most consistent stimulation-dependent interactions with eight of the ten RASSF members, with very few artefacts.

TBK1 is known to form complexes with a large variety of interacting partners, most notably with distinct scaffolding proteins that are mutually exclusive and appear to localise TBK1 to different subcellular compartments (Helgason et al., 2013). As the RASSF family is famously known for its role as an adaptor, it could also act as a scaffolding protein for TBK1, and perhaps regulate the localisation and functions of TBK1 via its association with Ras GTPases or the cytoskeleton network. Mutational analysis has shown that similar to TNF-R1 binding, the RASSF1 zinc finger is also important for its interaction with TBK1 (Shairaz Baksh, personal communication). However, the TBK1 binding region may not be limited to the zinc finger as several polymorphisms in its ATM kinase phosphorylation motif and C-terminus also abolished association with TBK1. As some of these motifs are absent in the other RASSF members, TBK1 interaction is likely to involve other regions of the RASSF proteins. Taken together with previous observations of a TBK1/TNF-R1 complex (Kuai et al., 2004), interactions between some RASSF members and TBK1 could be linked to TNF-R1 and those that displayed differential binding patterns to TBK1 and TNF-R1 could have different regulatory roles.

Table 6.2 Summary of interactions between the RASSF family and proteins of interest

Interaction with:	MOAP1	TNF-R1	DAPK	TBK1
RASSF1	Induced	Induced	Constitutive (potential artefact)	TNFα-, LPS-induced
RASSF2	Induced	Constitutive (potential artefact)	Constitutive (potential artefact)	LPS-induced
RASSF3	Constitutive (potential artefact), obscured induction	Constitutive (potential artefact), obscured induction	None observed	LPS-induced
RASSF4	Induced	None observed	Induced	LPS-induced
RASSF5	Constitutive (potential artefact)	Constitutive (potential artefact), obscured induction	Constitutive (potential artefact)	LPS-induced
RASSF6	Constitutive (potential artefact), obscured induction	Constitutive (potential artefact)	Constitutive (potential artefact)	LPS-induced
RASSF7	Constitutive (potential artefact), could be induced	Constitutive (potential artefact), obscured induction	Constitutive (potential artefact), obscured induction	TNFα-, LPS-induced
RASSF8	Constitutive (potential artefact), obscured induction	Constitutive (potential artefact)	Induced	Constitutive (potential artefact), could be induced
RASSF9	None observed	Artefact	None observed	LPS-induced
RASSF10	Induced	Induced	Constitutive (potential artefact), obscured induction	Constitutive (potential artefact)

Interestingly, most of the RASSF family appear to bind TBK1 in a stimulation-dependent manner with the exception of RASSF10, whereas RASSF8 interaction could be inducible but is possibly obscured by a high level of non-specific binding (Table 6.2). Conversely, RASSF1 and RASSF7 were inducible by both TNFα and LPS, whilst the remaining interactions were solely dependent upon LPS stimulation (Table 6.2). However, in contrast to the high levels of clear LPS-stimulated binding by RASSF5 and RASSF6, interactions between TBK1 and RASSF2, 3, 4 or 9 could be TNFα-induced but were undetectable due to extremely low levels. These observations suggest the involvement of these selected RASSF members in TNFα- or LPS-activated NFκB signalling. Given that TBK1 is oncogenic, whereas the RASSF family is mostly anti-tumourigenic, it would be of interest to elucidate the regulatory roles of the RASSF/TBK1 complexes and determine whether the RASSF proteins could inhibit the TBK1 oncogenic functions. As different RASSF members also showed different levels of binding upon stimulation, the weaker binders, such as RASSF2, 3 and 4, could have a lesser impact on regulation. In contrast, as RASSF7 has displayed some pro-growth and anti-apoptotic properties (Recino et al., 2010), its association with TBK1 may help to promote tumour formation.

This study serves as a gateway for further investigation on the molecular mechanisms behind the interactions between the RASSF family and the four proteins of interest, the crosstalk between signalling pathways and their regulation. Foley et al. (2008) have shown that the RASSF1 homodimer dissociates upon death signal stimulation, allowing it to bind MOAP1 and TNF-R1. It would be interesting to assess how TNFα stimulation affects other RASSF dimers and likewise, how dimerisation affects other RASSF interactions. Furthermore, El-Kalla et al. (2010) showed that microtubule localisation of RASSF1 is required for its interaction with TNF-R1. Interestingly, RASSF5 and RASSF7 are associated with microtubules (Bee et al., 2010, Moshnikova et al., 2006, Recino et al., 2010, Sherwood et al., 2008), thus microtubule localisation could also be involved in the regulation of some of these interactions. Most importantly, identification of the specific residues and regions involved in the various interactions may provide more insight into the regulatory role of the RASSF family as an adaptor or a substrate for the kinases.

More than half the RASSF family interacts with MOAP1, TNF-R1, DAPK and TBK1, which is indicative of their involvement in the regulation of apoptosis and NFκB

signalling pathways. They may also have overlapping downstream functions and biological effects that could be compensatory in a pathological setting. The majority of the family are likely pro-apoptotic and anti-proliferative via cell cycle arrests, whereas RASSF7 could be anti-apoptotic, which has been previously demonstrated (Takahashi et al., 2011). As DAPK and TBK1 are also linked to autophagy (Bialik and Kimchi, 2006, Helgason et al., 2013), their interactions with the RASSF members, especially those capable of microtubule association, could also implicate them in this pathway.

Notably, our *in vitro* data are the most conclusive for TBK1, showing new stimulation-dependent interactions between TBK1 and the RASSF family, with some striking differences between TNFα and LPS stimulation. As shown in Figure 6.4, LPS activates the non-cell autonomous immune response, whilst TNFα induces cell autonomous responses in the form of inflammatory, pro-survival and anti-apoptotic gene expression (Shen and Hahn, 2011). Thus, the LPS-stimulated interactions of various RASSF members specifically implicate them in non-cell autonomous immune response. Furthermore, RASSF1 and RASSF7, that are inducible by both stimuli, could simultaneously regulate both types of immune responses and cell growth, which also suggests the presence of crosstalk between different NFκB signalling pathways. This essentially links the RASSF family to the regulation of both inflammation and tumourigenesis via NFκB, which has been a growing topic of interest (Ben-Neriah and Karin, 2011). Further studies determining the specific roles of each interacting RASSF member in NFκB signalling may provide a greater understanding of the regulation or deregulation of this signalling network in cancer and other diseases.

7 Conclusions and future perspectives

The main aims of this project were to characterise and compare the RA and SARAH domains of the RASSF family members and their interactions with several important binding partners using *in silico* predictions as well as *in vitro* and cellular assays. This is the first comprehensive comparison of the ten RASSF members and their interactions with different binding partners, which are summarised in Figure 7.1. The results will be discussed here with the aim of clarifying existing literature, highlighting new findings and further studies required to address outstanding questions. Finally, the implications of these interactions on the regulatory roles of the RASSF family will be discussed.

7.1. Ras interactions

Although our *in silico* predictions and *in vitro* observations did not fully complement each other, both approaches are equally important in the study of the RA domain and its binding characteristics in different RASSF members. The Ras specificity and binding affinities of the RASSF family vary despite certain shared conserved residues and the overall predicted architecture (Figure 3.6, 3.7 and 3.9). Some of our findings support earlier reports of Ras binding by selected RASSF members, namely RASSF1, 4, 5, 6 and 7 (see Table 1.2, Figure 7.1). We also identify a new Ras effector in the form of RASSF3 and show that the N-terminal RASSF7 is a more promiscuous Ras effector than previously reported (Takahashi et al., 2011). Overall, there is a clear difference in binding affinities between RASSF5, the most potent Ras binder, and the remaining RASSF members. Furthermore, this study confirms previous observations that not all predicted RA domains are capable of Ras interaction (Bunney et al., 2006, Wohlgemuth et al., 2005), which has to be determined empirically.

As Ras interaction may be influenced by many factors and conditions, negative detection of binding in this study should not rule out interaction with other types of Ras GTPases. Moreover, it is not known whether lipid modification of the Ras CAAX motif may account for some discrepancies between our *in vitro* data and the reported literature, particularly for RASSF2 (Clark et al., 2012, Vos et al., 2003a), for which we did not observe any interaction. Further studies are required to test more members of the Ras

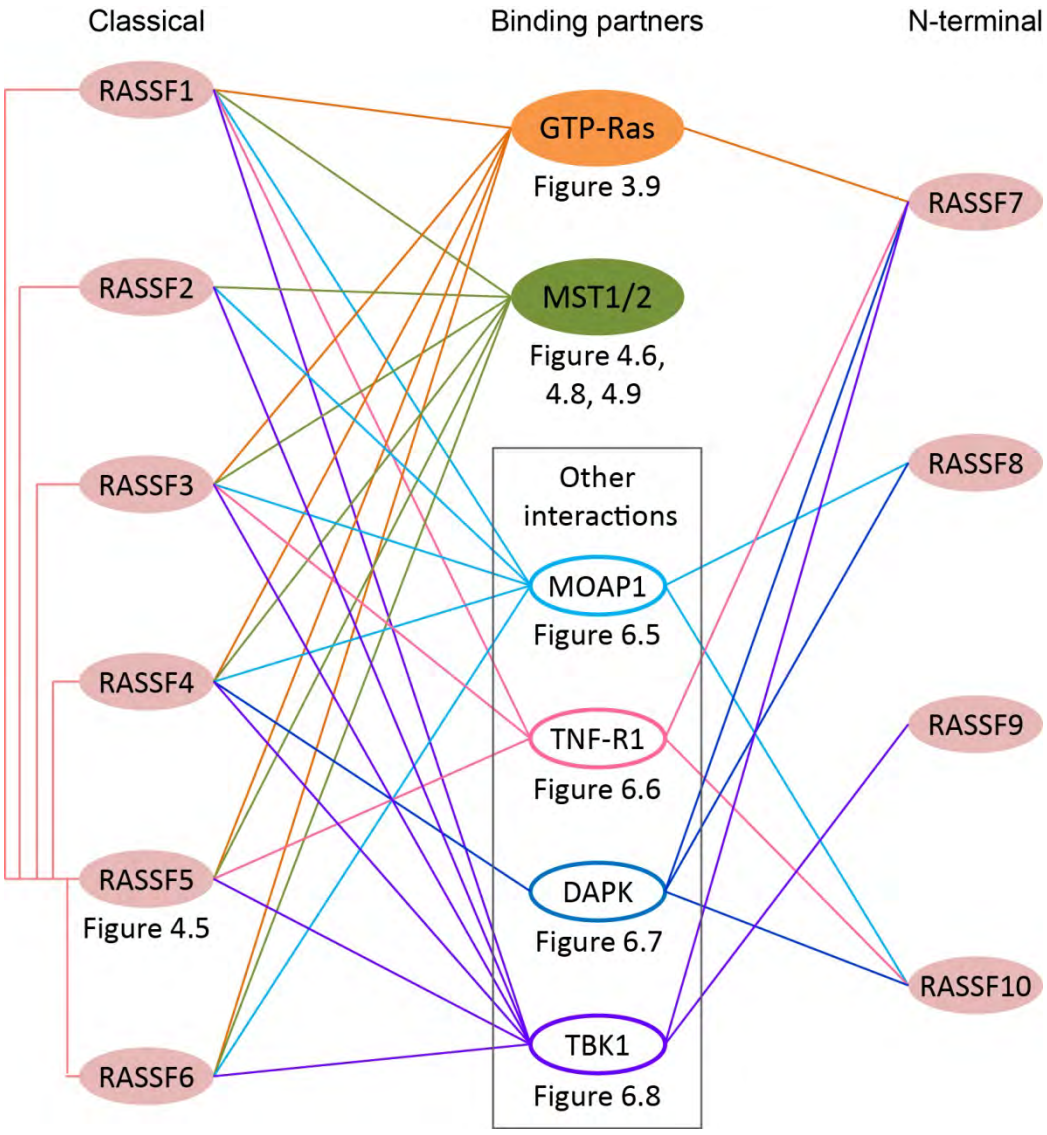

Figure 7.1 Summary of the RASSF interactions

The ten RASSF members are split into the classical members (left) and N-terminal members (right). The binding partners are shown in the middle, with reference to the figures showing their interactions. Only confirmed interactions are shown here with lines in colours corresponding to the respective binding partners. Other potential interactions are summarised in Table 6.2.

superfamily and compare interactions between unmodified and lipid modified Ras. Although the difficulty in expressing the RA domains in their isolated form presents a major hurdle in the study of Ras interaction, the *in silico* models could be used to select key residues for mutational studies, including those in the N-terminal subdomain of the classical RASSFs. These may provide valuable information on the molecular mechanisms specifically regulating Ras interaction with the RASSF RA domains, as well as Ras selectivity and binding affinities that may dictate the downstream functions of each RASSF member.

7.2. RASSF homodimers and interactions with MST kinases

The SARAH domain is highly conserved both in its key residues and structure, however the predicted coiled-coil motifs are more variable (see Chapter 4). Our data confirm that the SARAH domain in the classical RASSF1-6 mediates dimerisation. We also report for the first time that the coiled-coils do not interact with the SARAH domain as none of the N-terminal RASSF7-10 dimerised with RASSF5 or MST1/2 (Figure 7.1). Further studies are required to probe for other potential interactions mediated by the coiled-coils.

Our observations of SARAH-mediated dimerisation support existing reports on different dimeric interactions of the classical RASSF members (Table 1.3). The structural similarity of different SARAH domains suggests other homodimers and heterodimer combinations within the RASSF family are possible. We also identify several key interacting residues, including a few conserved non-polar residues, from our *in silico* models and mutational studies (Figure 5.2-5.7), reinforcing the observations from the MST1 and RASSF5 SARAH domain structures (Hwang et al., 2007, Makbul et al., 2013). Our FRET studies highlight the potential differences in heterodimerisation affinities despite the highly similar SARAH domains (Figure 4.10). Although hydrophobic interactions play a key role in dimerisation, specific charged residues and electrostatic interactions may contribute to binding affinities (Table 5.3). Furthermore, the SARAH domain may have a higher affinity to heterodimerise, which could potentially be enhanced by Ras binding (Figure 4.11), thereby supporting earlier studies wherein activated Ras increased MST1 activation via RASSF5 (Khokhlatchev et al., 2002, Praskova et al., 2004).

More advanced FRET analysis could be used to quantify and compare the binding affinities of the different SARAH homodimers and heterodimers. This may provide an indication of the more dominant RASSF members in MST1-mediated apoptosis, which may be in a constitutive complex with MST1, whereas weaker binders may exist as homodimers that could be redundant under normal physiological conditions. Further FRET and biochemical studies could be used to address the effects of Ras on dimerisation and MST1 activities, while fluorescent microscopy could also be used to study the cellular localisation of RASSF and MST1 as a result of Ras interaction. These would offer more insight into the pro-apoptotic regulation by Ras and MST1. More extensive mutational studies could provide further details on the molecular mechanisms behind SARAH-mediated dimerisation. Moreover, these mutations could be used for cellular and *in vivo* studies, such as knock-in mice, to assess the importance of each RASSF member and establish their downstream signalling events.

7.3. Other interactions of the RASSF family

One of the major tumour suppressive functions of the RASSF family lies in its pro-apoptotic regulation, which has mostly been associated with the MST kinases (see Chapter 1). While apoptotic regulation by the RASSF1/MOAP1/TNF-R1 complex is also well-documented (Baksh et al., 2005, El-Kalla et al., 2010, Foley et al., 2008), preliminary studies have identified new RASSF1 interacting partners, DAPK and TBK1, which are involved in apoptosis, autophagy and NFκB signalling (Bialik and Kimchi, 2006, Helgason et al., 2013).

Although we probed RASSF interactions with MOAP1, TNF-R1, DAPK and TBK1 (Figure 7.1), we did not consolidate enough data for the first three interacting partners to the point of conclusion. Several of these interactions remain ambiguous and require further studies for clarification. Nevertheless, our interaction data on TBK1 are the most conclusive, showing distinct stimulation-dependent binding to various RASSF members. Previous studies have implicated RASSF1, 2 and 6 in NFκB signalling (Allen et al., 2007, Del Re et al., 2010, Song et al., 2010), but the exact mechanism of regulation is not known. TBK1 could provide a link between the RASSF family and NFκB signalling. With such striking differences between TNFα- and LPS-induced

binding between the RASSF family and TBK1 (Figure 6.8), each RASSF member could be involved in different NFκB pathways. They could either regulate non-cell autonomous immune response or cell autonomous inflammation, apoptosis and proliferation (Figure 6.4), although crosstalk between pathways may be possible given that RASSF1 and RASSF7 are inducible by both stimuli, as discussed in section 6.3.

Mutational and biochemical studies are required to elucidate the comprehensive molecular mechanisms underpinning these interactions. Additionally, cellular functional studies using kinase inhibitors, RNAi gene silencing and interaction mutants, could be used to determine the role of each RASSF member in the regulation of apoptosis, autophagy, cell cycle and immune response. These additional studies could contribute to building a more detailed signalling network involving these common proteins.

7.4. Towards new interactions and functions

To date, RASSF1 and RASSF5 are the best characterised tumour suppressors within the family. However, recent studies are gradually unravelling the interactions and regulatory roles of the remaining RASSF members, pointing towards a trend in probing for new interactions of the family. Using our experimental system, we have revealed more novel interactions for each RASSF member that carry different implications for their functional roles.

The majority of the RASSF members are potential tumour suppressors, with the exception of RASSF7, whose role remains ambiguous. Functional studies have consolidated their tumour suppressor functions primarily through the regulation of apoptosis, cytoskeleton stability and the cell cycle. These are accomplished via some well-known pathways, such as Hippo, extrinsic death and Raf/Mek/Erk signalling, and the more novel Wnt and NFκB signalling pathways (see Chapter 1). Our studies implicate a growing list of RASSF members in NFκB signalling, which may play a prominent role in the anti-tumourigenic functions of the RASSF family. Furthermore, these new interactions also suggest a wider biological role for the RASSF family, including immune response and autophagy. Further studies exploring other potential roles of the RASSF members both *in vitro* and *in vivo* will help to build a more complete picture of the RASSF family.

Acknowledgements

First, I would like to thank my supervisor, Matilda Katan, for giving me the opportunity to pursue my PhD in her lab. I am very grateful for the supervision and support she has given me the last four years.

I am also grateful to the collaborators who have contributed to this project. These include Fernando Rodrigues-Lima and Delphine Flatters who provided invaluable assistance on protein modelling, Konstantinos Thalassinos and Jun Yan for their help with mass spectrometry, Shairaz Baksh who provided constructs and ideas for probing for other RASSF interactions, and Anca Margineanu and the Photonics Group at Imperial College who assisted in carrying out the FRET/FLIM experiments and analysis. I would also like to thank Cancer Research UK for funding this project.

Of course, I must thank every member of the Molecular Mechanisms of Signalling Team for their help, advice and encouragement over the last four years. Tom, who always has a solution to all my experimental problems, has been a constant source of advice and ideas. Marta was my tissue culture and western blot "go-to" advisor and gym buddy. Corine was the expert on all things protein-related (we also share a love for Harry Potter). Also, thanks to Sean who was always willing to help with my microscope-related issues and Chris who kept the lab running smoothly. Everyone in the team (past and present) and our colleagues in Darwin Room 115 were always friendly, helpful and happy to chat about anything, making my time at ICR and UCL such a memorable one.

Thank you to all my friends, especially Angela, Jun and Lu, with whom I share a special bond through our undergraduate and PhD days, and the countless dinners and cake sessions. Thank you to Fiona for her boundless optimism and encouragement. Special thanks to Michael, Ernest and Roderick, for always being there in times of need and for never failing to make me laugh.

Last but not least, thank you to my family, for their emotional support throughout and for their belief in me.

Publications

Chan JJ, Flatters D, Rodrigues-Lima F, Yan J, Thalassinos K, Katan M. Comparative analysis of interactions of RASSF1-10. Adv Biol Regul 2013;53:190-201.

Chan JJ, Katan M. PLCε and the RASSF family in tumour suppression and other functions. Adv Biol Regul 2013;53:258-79.

Margineanu A, Chan JJ, Kelly DR, Warren SC, Flatters D, Kumar S, Katan M, Dunsby CW, French PMW. Screening for protein-protein interactions using Förster resonance energy transfer (FRET) and fluorescence lifetime imaging microscopy (FLIM). [Manuscript in preparation]

References

Akino K, Toyota M, Suzuki H, Mita H, Sasaki Y, Ohe-Toyota M, et al. The Ras Effector RASSF2 Is a Novel Tumor-Suppressor Gene in Human Colorectal Cancer. Gastroenterology 2005;129:156-69.

Alibhai D, Kelly DJ, Warren S, Kumar S, Margineau A, Serwa RA, et al. Automated fluorescence lifetime imaging plate reader and its application to Forster resonant energy transfer readout of Gag protein aggregation. J Biophotonics 2013;6:398-408.

Allen NP, Donninger H, Vos MD, Eckfeld K, Hesson L, Gordon L, et al. RASSF6 is a novel member of the RASSF family of tumor suppressors. Oncogene 2007;26:6203-11.

Amin N, Vincan E. The Wnt signaling pathways and cell adhesion. Front Biosci 2012;17:784-804.

Anand R, Kim A-Y, Brent M, Marmorstein R. Biochemical analysis of MST1 kinase: elucidation of a C-terminal regulatory region. Biochemistry 2008;47:6719-26.

Aoyama Y, Avruch J, Zhang XF. Nore1 inhibits tumor cell growth independent of Ras or the MST1/2 kinases. Oncogene 2004;23:3426-33.

Avruch J, Praskova M, Ortiz‐Vega S, Liu M, Zhang XF. Nore1 and RASSF1 Regulation of Cell Proliferation and of the MST1/2 Kinases. Methods Enzymol 2006;407:290-310.

Avruch J, Zhou D, Fitamant J, Bardeesy N, Mou F, Barrufet LR. Protein kinases of the Hippo pathway: regulation and substrates. Semin Cell Dev Biol 2012;23:770-84.

Baksh S, Tommasi S, Fenton S, Yu VC, Martins LM, Pfeifer GP, et al. The tumor suppressor RASSF1A and MAP-1 link death receptor signaling to Bax conformational change and cell death. Mol Cell 2005;18:637-50.

Barlow DJ, Thornton JM. Helix geometry in proteins. J Mol Biol 1988;201:601-19.

Bee C, Moshnikova A, Mellor CD, Molloy JE, Koryakina Y, Stieglitz B, et al. Growth and tumor suppressor NORE1A is a regulatory node between Ras signaling and microtubule nucleation. J Biol Chem 2010;285:16258-66.

Ben-Neriah Y, Karin M. Inflammation meets cancer, with NF-kappaB as the matchmaker. Nat Immunol 2011;12:715-23.

Bialik S, Kimchi A. The death-associated protein kinases: structure, function, and beyond. Annu Rev Biochem 2006;75:189-210.

Bialik S, Berissi H, Kimchi A. A high throughput proteomics screen identifies novel substrates of death-associated protein kinase. Mol Cell Proteomics 2008;7:1089-98.

Blom N, Gammeltoft S, Brunak S. Sequence and structure-based prediction of eukaryotic protein phosphorylation sites. J Mol Biol 1999;294:1351-62.

Bric A, Miething C, Bialucha CU, Scuoppo C, Zender L, Krasnitz A, et al. Functional identification of tumor-suppressor genes through an in vivo RNA interference screen in a mouse lymphoma model. Cancer Cell 2009;16:324-35.

Buckingham L, Penfield Faber L, Kim A, Liptay M, Barger C, Basu S, et al. PTEN, RASSF1 and DAPK site-specific hypermethylation and outcome in surgically treated stage I and II nonsmall cell lung cancer patients. Int J Cancer 2010;126:1630-9.

Bunney TD, Harris R, Gandarillas NL, Josephs MB, Roe SM, Sorli SC, et al. Structural and mechanistic insights into ras association domains of phospholipase C epsilon. Mol Cell 2006;21:495-507.

Calvisi DF, Donninger H, Vos MD, Birrer MJ, Gordon L, Leaner V, et al. NORE1A tumor suppressor candidate modulates p21CIP1 via p53. Cancer Res 2009;69:4629-37.

Calvisi DF, Evert M, Dombrowski F. Pathogenetic and Prognostic Significance of Inactivation of RASSF Proteins in Human Hepatocellular Carcinoma. Mol Biol Int 2012;2012:849874.

Chen L, Johnson RC, Milgram SL. P-CIP1, a novel protein that interacts with the cytosolic domain of peptidylglycine alpha-amidating monooxygenase, is associated with endosomes. J Biol Chem 1998;273:33524-32.

Chow LS, Lo KW, Kwong J, Wong AY, Huang DP. Aberrant methylation of RASSF4/AD037 in nasopharyngeal carcinoma. Oncol Rep 2004;12:781-7.

Ciani B, Bjelic S, Honnappa S, Jawhari H, Jaussi R, Payapilly A, et al. Molecular basis of coiled-coil oligomerization-state specificity. Proc Natl Acad Sci U S A 2010;107:19850-5.

Clark J, Freeman J, Donninger H. Loss of RASSF2 Enhances Tumorigencity of Lung Cancer Cells and Confers Resistance to Chemotherapy. Mol Biol Int 2012;2012:705948.

Clevers H. Axin and hepatocellular carcinomas. Nat Genet 2000;24:206-8.

Clevers H, Nusse R. Wnt/beta-catenin signaling and disease. Cell 2012;149:1192-205.

Comeau SR, Gatchell DW, Vajda S, Camacho CJ. ClusPro: an automated docking and discrimination method for the prediction of protein complexes. Bioinformatics 2004;20:45-50.

Constantinescu Aruxandei D, Makbul C, Koturenkiene A, Ludemann MB, Herrmann C. Dimerization-induced folding of MST1 SARAH and the influence of the intrinsically unstructured inhibitory domain: low thermodynamic stability of monomer. Biochemistry 2011;50:10990-1000.

Cooper WN, Hesson LB, Matallanas D, Dallol A, von Kriegsheim A, Ward R, et al. RASSF2 associates with and stabilizes the proapoptotic kinase MST2. Oncogene 2009;28:2988-98.

Courtois G, Gilmore TD. Mutations in the NF-kappaB signaling pathway: implications for human disease. Oncogene 2006;25:6831-43.

Cox AD, Der CJ. The dark side of Ras: regulation of apoptosis. Oncogene 2003;22:8999-9006.

Cox AD, Der CJ. Ras history: The saga continues. Small GTPases 2010;1:2-27.

Creasy CL, Ambrose DM, Chernoff J. The Ste20-like Protein Kinase, Mst1, Dimerizes and Contains an Inhibitory Domain. J Biol Chem 1996;271:21049-53.

Dallol A, Agathanggelou A, Tommasi S, Pfeifer GP, Maher ER, Latif F. Involvement of the RASSF1A tumor suppressor gene in controlling cell migration. Cancer Res 2005;65:7653-9.

Dallol A, Hesson LB, Matallanas D, Cooper WN, O'Neill E, Maher ER, et al. RAN GTPase is a RASSF1A effector involved in controlling microtubule organization. Curr Biol 2009;19:1227-32.

Dammann R, Li C, Yoon JH, Chin PL, Bates S, Pfeifer GP. Epigenetic inactivation of a RAS association domain family protein from the lung tumour suppressor locus 3p21.3. Nat Genet 2000;25:315-9.

Dansranjavin T, Wagenlehner F, Gattenloehner S, Steger K, Weidner W, Dammann R, et al. Epigenetic down regulation of RASSF10 and its possible clinical implication in prostate carcinoma. Prostate 2012;72:1550-8.

Del Re DP, Matsuda T, Zhai P, Gao S, Clark GJ, Van Der Weyden L, et al. Proapoptotic Rassf1A/Mst1 signaling in cardiac fibroblasts is protective against pressure overload in mice. J Clin Invest 2010;120:3555-67.

Delhase M, Kim SY, Lee H, Naiki-Ito A, Chen Y, Ahn ER, et al. TANK-binding kinase 1 (TBK1) controls cell survival through PAI-2/serpinB2 and transglutaminase 2. Proc Natl Acad Sci U S A 2012;109:E177-86.

Dittfeld C, Richter AM, Steinmann K, Klagge-Ulonska A, Dammann RH. The SARAH Domain of RASSF1A and Its Tumor Suppressor Function. Mol Biol Int 2012;2012:196715.

Djos A, Martinsson T, Kogner P, Carén H. The RASSF gene family members RASSF5, RASSF6 and RASSF7 show frequent DNA methylation in neuroblastoma. Mol Cancer 2012;13:40.

Donninger H, Hesson L, Vos M, Beebe K, Gordon L, Sidransky D, et al. The Ras effector RASSF2 controls the PAR-4 tumor suppressor. Mol Cell Biol 2010;30:2608-20.

Donninger H, Barnoud T, Nelson N, Kassler S, Clark J, Cummins TD, et al. RASSF1A and the rs2073498 Cancer Associated SNP. Front Oncol 2011;1:54.

Downward J. Targeting RAS signalling pathways in cancer therapy. Nat Rev Cancer 2003;3:11-22.

Eckfeld K, Hesson L, Vos MD, Bieche I, Latif F, Clark GJ. RASSF4/AD037 is a potential ras effector/tumor suppressor of the RASSF family. Cancer Res 2004;64:8688-93.

El-Kalla M, Onyskiw C, Baksh S. Functional importance of RASSF1A microtubule localization and polymorphisms. Oncogene 2010;29:5729-40.

Eswar N, Webb B, Marti-Renom MA, Madhusudhan MS, Eramian D, Shen MY, et al. Comparative protein structure modeling using Modeller. Curr Protoc Bioinformatics 2006;Chapter 5:Unit 5.6.

Falvella FS, Manenti G, Spinola M, Pignatiello C, Conti B, Pastorino U, et al. Identification of RASSF8 as a candidate lung tumor suppressor gene. Oncogene 2006;25:3934-8.

Fausti F, Di Agostino S, Sacconi A, Strano S, Blandino G. Hippo and rassf1a Pathways: A Growing Affair. Mol Biol Int 2012;2012:307628.

Fischer A, Hekman M, Kuhlmann J, Rubio I, Wiese S, Rapp UR. B- and C-RAF display essential differences in their binding to Ras: the isotype-specific N terminus of B-RAF facilitates Ras binding. J Biol Chem 2007;282:26503-16.

Fischer JR, Ohnmacht U, Rieger N, Zemaitis M, Stoffregen C, Kostrzewa M, et al. Promoter methylation of RASSF1A, RARbeta and DAPK predict poor prognosis of patients with malignant mesothelioma. Lung Cancer 2006;54:109-16.

Foley CJ, Freedman H, Choo SL, Onyskiw C, Fu NY, Yu VC, et al. Dynamics of RASSF1A/MOAP-1 association with death receptors. Mol Cell Biol 2008;28:4520-35.

Fujita H, Fukuhara S, Sakurai A, Yamagishi A, Kamioka Y, Nakaoka Y, et al. Local activation of Rap1 contributes to directional vascular endothelial cell migration accompanied by extension of microtubules on which RAPL, a Rap1-associating molecule, localizes. J Biol Chem 2005;280:5022-31.

Gao B, Xie XJ, Huang C, Shames DS, Chen TT, Lewis CM, et al. RASSF1A polymorphism A133S is associated with early onset breast cancer in BRCA1/2 mutation carriers. Cancer Res 2008;68:22-5.

Gilmore TD. Introduction to NF-kappaB: players, pathways, perspectives. Oncogene 2006;25:6680-4.

Goncalves A, Burckstummer T, Dixit E, Scheicher R, Gorna MW, Karayel E, et al. Functional dissection of the TBK1 molecular network. PLoS One 2011;6:e23971.

Gordon M, El-Kalla M, Baksh S. RASSF1 Polymorphisms in Cancer. Mol Biol Int 2012;2012:365213.

Guerrero-Setas D, Perez-Janices N, Blanco-Fernandez L, Ojer A, Cambra K, Berdasco M, et al. RASSF2 hypermethylation is present and related to shorter survival in squamous cervical cancer. Mod Pathol 2013;26:1111-22.

Guo C, Tommasi S, Liu L, Yee JK, Dammann R, Pfeifer GP. RASSF1A is part of a complex similar to the Drosophila Hippo/Salvador/Lats tumor-suppressor network. Curr Biol 2007;17:700-5.

Guo C, Zhang X, Pfeifer GP. The tumor suppressor RASSF1A prevents dephosphorylation of the mammalian STE20-like kinases MST1 and MST2. J Biol Chem 2011;286:6253-61.

Hanahan D, Weinberg R. The hallmarks of cancer. Cell 2000;100:57-70.

Hancock JF. Ras proteins: different signals from different locations. Nat Rev Mol Cell Biol 2003;4:373-84.

Harjes E, Harjes S, Wohlgemuth S, Muller KH, Krieger E, Herrmann C, et al. GTP-Ras disrupts the intramolecular complex of C1 and RA domains of Nore1. Structure 2006;14:881-8.

Harrison B, Kraus M, Burch L, Stevens C, Craig A, Gordon-Weeks P, et al. DAPK-1 binding to a linear peptide motif in MAP1B stimulates autophagy and membrane blebbing. J Biol Chem 2008;283:9999-10014.

Harvey KF, Zhang X, Thomas DM. The Hippo pathway and human cancer. Nat Rev Cancer 2013;13:246-57.

Helgason E, Phung QT, Dueber EC. Recent insights into the complexity of Tank-binding kinase 1 signaling networks: the emerging role of cellular localization in the activation and substrate specificity of TBK1. FEBS Lett 2013;587:1230-7.

Herrmann C. Ras-effector interactions: after one decade. Curr Opin Struct Biol 2003;13:122-9.

Hesson LB, Wilson R, Morton D, Adams C, Walker M, Maher ER, et al. CpG island promoter hypermethylation of a novel Ras-effector gene RASSF2A is an early event in colon carcinogenesis and correlates inversely with K-ras mutations. Oncogene 2005;24:3987-94.

Hesson LB, Dunwell TL, Cooper WN, Catchpoole D, Brini AT, Chiaramonte R, et al. The novel RASSF6 and RASSF10 candidate tumour suppressor genes are frequently epigenetically inactivated in childhood leukaemias. Mol Cancer 2009;8:42.

Hill VK, Underhill-Day N, Krex D, Robel K, Sangan CB, Summersgill HR, et al. Epigenetic inactivation of the RASSF10 candidate tumor suppressor gene is a frequent and an early event in gliomagenesis. Oncogene 2011;30:978-89.

Hitomi J, Christofferson DE, Ng A, Yao J, Degterev A, Xavier RJ, et al. Identification of a Molecular Signaling Network that Regulates a Cellular Necrotic Cell Death Pathway. Cell 2008;135:1311-23.

Huang L, Hofer F, Martin GS, Kim SH. Structural basis for the interaction of Ras with RalGDS. Nat Struct Biol 1998;5:422-6.

Hwang E, Ryu KS, Paakkonen K, Guntert P, Cheong HK, Lim DS, et al. Structural insight into dimeric interaction of the SARAH domains from Mst1 and RASSF family proteins in the apoptosis pathway. Proc Natl Acad Sci U S A 2007;104:9236-41.

Ikeda M, Hirabayashi S, Fujiwara N, Mori H, Kawata A, Iida J, et al. Ras-association domain family protein 6 induces apoptosis via both caspase-dependent and caspase-independent pathways. Exp Cell Res 2007;313:1484-95.

Ikeda M, Kawata A, Nishikawa M, Tateishi Y, Yamaguchi M, Nakagawa K, et al. Hippo pathway-dependent and -independent roles of RASSF6. Sci Signal 2009;2:ra59.

Jacquemart IC, Springs AEB, Chen WENY. Rassf3 is responsible in part for resistance to mammary tumor development in neu transgenic mice. Int J Oncol 2009;34:517-28.

Jares-Erijman EA, Jovin TM. Imaging molecular interactions in living cells by FRET microscopy. Curr Opin Chem Biol 2006;10:409-16.

Jones S, Thornton JM. Protein-protein interactions: a review of protein dimer structures. Prog Biophys Mol Biol 1995;63:31-65.

Kalhammer G, Bähler M, Schmitz F, Jöckel J, Block C. Ras-binding domains: predicting function versus folding. FEBS Lett 1997;414:599-602.

Karnoub AE, Weinberg RA. Ras oncogenes: split personalities. Nat Rev Mol Cell Biol 2008;9:517-31.

Katagiri K, Maeda A, Shimonaka M, Kinashi T. RAPL, a Rap1-binding molecule that mediates Rap1-induced adhesion through spatial regulation of LFA-1. Nat Immunol 2003;4:741-8.

Katagiri K, Ohnishi N, Kabashima K, Iyoda T, Takeda N, Shinkai Y, et al. Crucial functions of the Rap1 effector molecule RAPL in lymphocyte and dendritic cell trafficking. Nat Immunol 2004;5:1045-51.

Katagiri K, Imamura M, Kinashi T. Spatiotemporal regulation of the kinase Mst1 by binding protein RAPL is critical for lymphocyte polarity and adhesion. Nat Immunol 2006;7:919-28.

Katagiri K, Ueda Y, Tomiyama T, Yasuda K, Toda Y, Ikehara S, et al. Deficiency of Rap1-binding protein RAPL causes lymphoproliferative disorders through mislocalization of p27kip1. Immunity 2011;34:24-38.

Khokhlatchev A, Rabizadeh S, Xavier R, Nedwidek M, Chen T, Zhang X-f, et al. Identification of a novel Ras-regulated proapoptotic pathway. Curr Biol 2002;12:253-65.

Khosravi-Far R, Esposti MD. Death receptor signals to mitochondria. Cancer Biol Ther 2004;3:1051-7.

Kiel C, Selzer T, Shaul Y, Schreiber G, Herrmann C. Electrostatically optimized Ras-binding Ral guanine dissociation stimulator mutants increase the rate of association by stabilizing the encounter complex. Proc Natl Acad Sci U S A 2004;101:9223-8.

Kiel C, Foglierini M, Kuemmerer N, Beltrao P, Serrano L. A genome-wide Ras-effector interaction network. J Mol Biol 2007;370:1020-32.

Kiel C, Beltrao P, Serrano L. Analyzing protein interaction networks using structural information. Annu Rev Biochem 2008;77:415-41.

Kim JY, Welsh EA, Oguz U, Fang B, Bai Y, Kinose F, et al. Dissection of TBK1 signaling via phosphoproteomics in lung cancer cells. Proc Natl Acad Sci U S A 2013;110:12414-9.

Kitagawa D, Kajiho H, Negishi T, Ur aS, Watanabe T, Wada T, et al. Release of RASSF1C from the nucleus by Daxx degradation links DNA damage and SAPK/JNK activation. EMBO J 2006;25:3286-97.

Kozakov D, Hall DR, Beglov D, Brenke R, Comeau SR, Shen Y, et al. Achieving reliability and high accuracy in automated protein docking: ClusPro, PIPER, SDU, and stability analysis in CAPRI rounds 13-19. Proteins 2010;78:3124-30.

Kuai J, Wooters J, Hall JP, Rao VR, Nickbarg E, Li B, et al. NAK is recruited to the TNFR1 complex in a TNFalpha-dependent manner and mediates the production of RANTES: identification of endogenous TNFR-interacting proteins by a proteomic approach. J Biol Chem 2004;279:53266-71.

Kudo T, Ikeda M, Nishikawa M, Yang Z, Ohno K, Nakagawa K, et al. The RASSF3 candidate tumor suppressor induces apoptosis and G1-S cell-cycle arrest via p53. Cancer Res 2012;72:2901-11.

Kumar S, Nussinov R. Salt bridge stability in monomeric proteins. J Mol Biol 1999;293:1241-55.

Kumar S, Alibhai D, Margineanu A, Laine R, Kennedy G, McGinty J, et al. FLIM FRET technology for drug discovery: automated multiwell-plate high-content analysis, multiplexed readouts and application in situ. Chemphyschem 2011;12:609-26.

Kumari G, Mahalingam S. Extracellular signal-regulated kinase 2 (ERK-2) mediated phosphorylation regulates nucleo-cytoplasmic shuttling and cell growth control of Ras-associated tumor suppressor protein, RASSF2. Exp Cell Res 2009;315:2775-90.

Kumari G, Singhal PK, Suryaraja R, Mahalingam S. Functional interaction of the Ras effector RASSF5 with the tyrosine kinase Lck: critical role in nucleocytoplasmic transport and cell cycle regulation. J Mol Biol 2010;397:89-109.

Laemmli UK. Cleavage of structural proteins during the assembly of the head of bacteriophage T4. Nature 1970;227:680-5.

Lammi L, Arte S, Somer M, Jarvinen H, Lahermo P, Thesleff I, et al. Mutations in AXIN2 cause familial tooth agenesis and predispose to colorectal cancer. Am J Hum Genet 2004;74:1043-50.

Lamouille S, Derynck R. Oncogene and tumour suppressor: the two faces of SnoN. EMBO J 2009;28:3459-60.

Langton PF, Colombani J, Chan EH, Wepf A, Gstaiger M, Tapon N. The dASPP-dRASSF8 complex regulates cell-cell adhesion during Drosophila retinal morphogenesis. Curr Biol 2009;19:1969-78.

Laskowski RA, MacArthur MW, Moss DS, Thornton JM. PROCHECK: a program to check the stereochemical quality of protein structures. J Appl Crystallogr 1993;26:283-91.

Law J, Yu VC, Baksh S. Modulator of Apoptosis 1: A Highly Regulated RASSF1A-Interacting BH3-Like Protein. Mol Biol Int 2012;2012:536802.

Lee CK, Lee JH, Lee MG, Jeong SI, Ha TK, Kang MJ, et al. Epigenetic inactivation of the NORE1 gene correlates with malignant progression of colorectal tumors. BMC Cancer 2010;10:577.

Lee CM, Yang P, Chen LC, Chen CC, Wu SC, Cheng HY, et al. A novel role of RASSF9 in maintaining epidermal homeostasis. PLoS One 2011;6:e17867.

Lee D, Park SJ, Sung KS, Park J, Lee SB, Park SY, et al. Mdm2 associates with Ras effector NORE1 to induce the degradation of oncoprotein HIPK1. EMBO Rep 2012;13:163-9.

Liu G, Yin B, Song YS. Methylation and protein expression of RASSF2 in prostate cancer. Zhonghua Nan Ke Xue 2013;19:107-10.

Liu L, Baier K, Dammann R, Pfeifer GP. The tumor suppressor RASSF1A does not interact with Cdc20, an activator of the anaphase-promoting complex. Cell Cycle 2007;6:1663-65.

Lock FE, Underhill-Day N, Dunwell T, Matallanas D, Cooper W, Hesson L, et al. The RASSF8 candidate tumor suppressor inhibits cell growth and regulates the Wnt and NF-kappaB signaling pathways. Oncogene 2010;29:4307-16.

Locksley RM, Killeen N, Lenardo MJ. The TNF and TNF Receptor Superfamilies: Integrating Mammalian Biology. Cell 2001;104:487-501.

Lodish H, Berk A, Zipursky S, Matsudaira P, Baltimore D, Darnell J. Molecular Cell Biology. 4th ed. New York: W. H. Freeman; 2000.

Lukatsky DB, Shakhnovich BE, Mintseris J, Shakhnovich EI. Structural similarity enhances interaction propensity of proteins. J Mol Biol 2007;365:1596-606.

Lupas A. Coiled coils: new structures and new functions. Trends Biochem Sci 1996;21:375-82.

Ma X, Helgason E, Phung QT, Quan CL, Iyer RS, Lee MW, et al. Molecular basis of Tank-binding kinase 1 activation by transautophosphorylation. Proc Natl Acad Sci U S A 2012;109:9378-83.

Macheiner D, Heller G, Kappel S, Bichler C, Stattner S, Ziegler B, et al. NORE1B, a candidate tumor suppressor, is epigenetically silenced in human hepatocellular carcinoma. J Hepatol 2006;45:81-9.

Macheiner D, Gauglhofer C, Rodgarkia-Dara C, Grusch M, Brachner A, Bichler C, et al. NORE1B is a putative tumor suppressor in hepatocarcinogenesis and may act via RASSF1A. Cancer Res 2009;69:235-42.

Macindoe G, Mavridis L, Venkatraman V, Devignes MD, Ritchie DW. HexServer: an FFT-based protein docking server powered by graphics processors. Nucleic Acids Res 2010;38:W445-9.

Magee T, Seabra MC. Fatty acylation and prenylation of proteins: what's hot in fat. Curr Opin Cell Biol 2005;17:190-6.

Makbul C, Constantinescu Aruxandei D, Hofmann E, Schwarz D, Wolf E, Herrmann C. Structural and thermodynamic characterization of Nore1-SARAH: a small, helical module important in signal transduction networks. Biochemistry 2013;52:1045-54.

Malpeli G, Amato E, Dandrea M, Fumagalli C, Debattisti V, Boninsegna L, et al. Methylation-associated down-regulation of RASSF1A and up-regulation of RASSF1C in pancreatic endocrine tumors. BMC Cancer 2011;11:351.

Malumbres M, Barbacid M. RAS oncogenes: the first 30 years. Nat Rev Cancer 2003;3:459-65.

Marblestone JG, Edavettal SC, Lim Y, Lim P, Zuo X, Butt TR. Comparison of SUMO fusion technology with traditional gene fusion systems: enhanced expression and solubility with SUMO. Protein Sci 2006;15:182-9.

Matallanas D, Romano D, Yee K, Meissl K, Kucerova L, Piazzolla D, et al. RASSF1A elicits apoptosis through an MST2 pathway directing proapoptotic transcription by the p73 tumor suppressor protein. Mol Cell 2007;27:962-75.

Matallanas D, Romano D, Hamilton G, Kolch W, Neill EO. A Hippo in the ointment. Cell Cycle 2008;7:879-84.

Miertzschke M, Stanley P, Bunney TD, Rodrigues-Lima F, Hogg N, Katan M. Characterization of interactions of adapter protein RAPL/Nore1B with RAP GTPases and their role in T cell migration. J Biol Chem 2007;282:30629-42.

Moon RT, Kohn AD, De Ferrari GV, Kaykas A. WNT and beta-catenin signalling: diseases and therapies. Nat Rev Genet 2004;5:691-701.

Moshnikova A, Frye J, Shay JW, Minna JD, Khokhlatchev AV. The growth and tumor suppressor NORE1A is a cytoskeletal protein that suppresses growth by inhibition of the ERK pathway. J Biol Chem 2006;281:8143-52.

Moshnikova A, Kuznetsov S, Khokhlatchev AV. Interaction of the growth and tumour suppressor NORE1A with microtubules is not required for its growth-suppressive function. BMC Res Notes 2008;1:13.

Moutevelis E, Woolfson DN. A periodic table of coiled-coil protein structures. J Mol Biol 2009;385:726-32.

Musafia B, Buchner V, Arad D. Complex Salt Bridges in Proteins: Statistical Analysis of Structure and Function. J Mol Biol 1995;254:761-70.

Nassar N, Horn G, Herrmann C, Block C, Janknecht R, Wittinghofer A. Ras/Rap effector specificity determined by charge reversal. Nat Struct Biol 1996;3:723-29.

Negrini S, Prada I, D'Alessandro R, Meldolesi J. REST: an oncogene or a tumor suppressor? Trends Cell Biol 2013;23:289-95.

Niederberger E, Moser CV, Kynast KL, Geisslinger G. The Non-Canonical IkappaB Kinases IKKepsilon and TBK1 as Potential Targets for the Development of Novel Therapeutic Drugs. Curr Mol Med 2013;13:1089-97.

Nusse R. Wnt signaling and stem cell control. Cell Res 2008;18:523-7.

O'Neill EE, Matallanas D, Kolch W. Mammalian sterile 20-like kinases in tumor suppression: an emerging pathway. Cancer Res 2005;65:5485-7.

Oceandy D, Pickard A, Prehar S, Zi M, Mohamed TM, Stanley PJ, et al. Tumor suppressor Ras-association domain family 1 isoform A is a novel regulator of cardiac hypertrophy. Circulation 2009;120:607-16.

Oh HJ, Lee KK, Song SJ, Jin MS, Song MS, Lee JH, et al. Role of the tumor suppressor RASSF1A in Mst1-mediated apoptosis. Cancer Res 2006;66:2562-9.

Oleksiewicz U, Liloglou T, Tasopoulou KM, Daskoulidou N, Bryan J, Gosney JR, et al. Cytoglobin has bimodal: tumour suppressor and oncogene functions in lung cancer cell lines. Hum Mol Genet 2013;22:3207-17.

Ortiz-Vega S, Khokhlatchev A, Nedwidek M, Zhang X-f, Dammann R, Pfeifer GP, et al. The putative tumor suppressor RASSF1A homodimerizes and heterodimerizes with the Ras-GTP binding protein Nore1. Oncogene 2002;21:1381-90.

Pacold ME, Suire S, Perisic O, Lara-Gonzalez S, Davis CT, Walker EH, et al. Crystal structure and functional analysis of Ras binding to its effector phosphoinositide 3-kinase gamma. Cell 2000;103:931-43.

Park J, Kang SI, Lee SY, Zhang XF, Kim MS, Beers LF, et al. Tumor suppressor ras association domain family 5 (RASSF5/NORE1) mediates death receptor ligand-induced apoptosis. J Biol Chem 2010;285:35029-38.

Park SJ, Lee D, Choi CY, Ryu SY. Induction of apoptosis by NORE1A in a manner dependent on its nuclear export. Biochem Biophys Res Commun 2008;368:56-61.

Pazos F, Valencia A. Similarity of phylogenetic trees as indicator of protein-protein interaction. Protein Eng 2001;14:609-14.

Peng H, Liu H, Zhao S, Wu J, Fan J, Liao J. Silencing of RASSF3 by DNA hypermethylation is associated with tumorigenesis in somatotroph adenomas. PLoS One 2013;8:e59024.

Perkins ND. Integrating cell-signalling pathways with NF-kappaB and IKK function. Nat Rev Mol Cell Biol 2007;8:49-62.

Pfeifer GP, Dammann R. Methylation of the tumor suppressor gene RASSF1A in human tumors. Biochemistry 2005;70:576-83.

Pierce AM, Schneider-Broussard R, Gimenez-Conti IB, Russell JL, Conti CJ, Johnson DG. E2F1 has both oncogenic and tumor-suppressive properties in a transgenic model. Mol Cell Biol 1999;19:6408-14.

Polesello C, Huelsmann S, Brown NH, Tapon N. The Drosophila RASSF homolog antagonizes the hippo pathway. Curr Biol 2006;16:2459-65.

Praskova M, Khoklatchev A, Ortiz-Vega S, Avruch J. Regulation of the MST1 kinase by autophosphorylation, by the growth inhibitory proteins, RASSF1 and NORE1, and by Ras. Biochem J 2004;381:453-62.

Pringle SD, Giles K, Wildgoose JL, Williams JP, Slade SE, Thalassinos K, et al. An investigation of the mobility separation of some peptide and protein ions using a new hybrid quadrupole/travelling wave IMS/oa-ToF instrument. Int J Mass Spectrom 2007;261:1-12.

Pylayeva-Gupta Y, Grabocka E, Bar-Sagi D. RAS oncogenes: weaving a tumorigenic web. Nat Rev Cancer 2011;11:761-74.

Raab M, Wang H, Lu Y, Smith X, Wu Z, Strebhardt K, et al. T cell receptor "inside-out" pathway via signaling module SKAP1-RapL regulates T cell motility and interactions in lymph nodes. Immunity 2010;32:541-56.

Raab M, Smith X, Matthess Y, Strebhardt K, Rudd CE. SKAP1 protein PH domain determines RapL membrane localization and Rap1 protein complex formation for T cell receptor (TCR) activation of LFA-1. J Biol Chem 2011;286:29663-70.

Radu M, Chernoff J. The DeMSTification of mammalian Ste20 kinases. Curr Biol 2009;19:R421-5.

Recino A, Sherwood V, Flaxman A, Cooper WN, Latif F, Ward A, et al. Human RASSF7 regulates the microtubule cytoskeleton and is required for spindle formation, Aurora B activation and chromosomal congression during mitosis. Biochem J 2010;430:207-13.

Reeves M, Baldwin M, Aragon R, Baldwin S, Chen S, Li X, et al. RASSF1C modulates the expression of a stem cell renewal gene, PIWIL1. BMC Res Notes 2012;16:239.

Reeves ME, Baldwin SW, Baldwin ML, Chen ST, Moretz JM, Aragon RJ, et al. Ras-association domain family 1C protein promotes breast cancer cell migration and attenuates apoptosis. BMC Cancer 2010;10:562.

Rennier K, Ji JY. The role of death-associated protein kinase (DAPK) in endothelial apoptosis under fluid shear stress. Life Sci 2013;93:194-200.

Ribeiro PS, Josue F, Wepf A, Wehr MC, Rinner O, Kelly G, et al. Combined functional genomic and proteomic approaches identify a PP2A complex as a negative regulator of Hippo signaling. Mol Cell 2010;39:521-34.

Richter AM, Pfeifer GP, Dammann RH. The RASSF proteins in cancer; from epigenetic silencing to functional characterization. Biochim Biophys Acta 2009;1796:114-28.

Richter AM, Walesch SK, Wurl P, Taubert H, Dammann RH. The tumor suppressor RASSF10 is upregulated upon contact inhibition and frequently epigenetically silenced in cancer. Oncogenesis 2012;1:e18.

Ritchie DW, Kemp GJ. Protein docking using spherical polar Fourier correlations. Proteins 2000;39:178-94.

Rodriguez-Viciana P, Sabatier C, McCormick F. Signaling specificity by Ras family GTPases is determined by the full spectrum of effectors they regulate. Mol Cell Biol 2004;24:4943-54.

Rong R, Jin W, Zhang J, Sheikh MS, Huang Y. Tumor suppressor RASSF1A is a microtubule-binding protein that stabilizes microtubules and induces G2/M arrest. Oncogene 2004;23:8216-30.

Rong R, Jiang LY, Sheikh MS, Huang Y. Mitotic kinase Aurora-A phosphorylates RASSF1A and modulates RASSF1A-mediated microtubule interaction and M-phase cell cycle regulation. Oncogene 2007;26:7700-8.

Samanta U, Bahadur RP, Chakrabarti P. Quantifying the accessible surface area of protein residues in their local environment. Protein Eng 2002;15:659-67.

Sanada Y, Kumoto T, Suehiro H, Nishimura F, Kato N, Hata Y, et al. RASSF6 expression in adipocytes is down-regulated by interaction with macrophages. PLoS One 2013;8:e61931.

Saucedo LJ, Edgar BA. Filling out the Hippo pathway. Nat Rev Mol Cell Biol 2007;8:613-21.

Schagdarsurengin U, Seidel C, Ulbrich EJ, Kolbl H, Dittmer J, Dammann R. A polymorphism at codon 133 of the tumor suppressor RASSF1A is associated with tumorous alteration of the breast. Int J Oncol 2005;27:185-91.

Schagdarsurengin U, Richter A, Wöhler C, Dammann R. Frequent epigenetic inactivation of RASSF10 in thyroid cancer. Epigenetics 2009;4:571-6.

Schagdarsurengin U, Richter AM, Hornung J, Lange C, Steinmann K, Dammann RH. Frequent epigenetic inactivation of RASSF2 in thyroid cancer and functional consequences. Mol Cancer 2010;9:264.

Scheel H, Hofmann K. A novel inter action motif, SARAH, connects three classes of tumor suppressor. Curr Biol 2003;13:R899-R900.

Scrace SF, O'Neill E. RASSF Signalling and DNA Damage: Monitoring the Integrity of the Genome? Mol Biol Int 2012;2012:141732.

Shen RR, Hahn WC. Emerging roles for the non-canonical IKKs in cancer. Oncogene 2011;30:631-41.

Sherwood V, Manbodh R, Sheppard C, Chalmers AD. RASSF7 is a member of a new family of RAS association domain-containing proteins and is required for completing mitosis. Mol Biol Cell 2008;19:1772-82.

Sherwood V, Recino A, Jeffries A, Ward A, Chalmers AD. The N-terminal RASSF family: a new group of Ras-association-domain-containing proteins, with emerging links to cancer formation. Biochem J 2010;425:303-11.

Sokalingam S, Raghunathan G, Soundrarajan N, Lee S-G. A Study on the Effect of Surface Lysine to Arginine Mutagenesis on Protein Stability and Structure Using Green Fluorescent Protein. PLoS One 2012;7:e40410.

Song H, Oh S, Oh HJ, Lim DS. Role of the tumor suppressor RASSF2 in regulation of MST1 kinase activity. Biochem Biophys Res Commun 2010;391:969-73.

Song H, Kim H, Lee K, Lee DH, Kim TS, Song JY, et al. Ablation of Rassf2 induces bone defects and subsequent haematopoietic anomalies in mice. EMBO J 2012;31:1147-59.

Song MS, Song SJ, Ayad NG, Chang JS, Lee JH, Hong HK, et al. The tumour suppressor RASSF1A regulates mitosis by inhibiting the APC-Cdc20 complex. Nat Cell Biol 2004;6:129-37.

Song MS, Song SJ, Kim SJ, Nakayama K, Nakayama KI, Lim DS. Skp2 regulates the antiproliferative function of the tumor suppressor RASSF1A via ubiquitin-mediated degradation at the G1-S transition. Oncogene 2008;27:3176-85.

Song SJ, Song MS, Kim SJ, Kim SY, Kwon SH, Kim JG, et al. Aurora A regulates prometaphase progression by inhibiting the ability of RASSF1A to suppress APC-Cdc20 activity. Cancer Res 2009;69:2314-23.

Stang S, Bottorff D, Stone JC. Interaction of activated Ras with Raf-1 alone may be sufficient for transformation of rat2 cells. Mol Cell Biol 1997;17:3047-55.

Stieglitz B, Bee C, Schwarz D, Yildiz O, Moshnikova A, Khokhlatchev A, et al. Novel type of Ras effector interaction established between tumour suppressor NORE1A and Ras switch II. EMBO J 2008;27:1995-2005.

Suryaraja R, Anitha M, Anbarasu K, Kumari G, Mahalingam S. The E3 ubiquitin ligase Itch regulates tumor suppressor protein RASSF5/NORE1 stability in an acetylation-dependent manner. Cell Death Dis 2013;4:e565.

Tait SW, Green DR. Mitochondria and cell death: outer membrane permeabilization and beyond. Nat Rev Mol Cell Biol 2010;11:621-32.

Takahashi S, Ebihara A, Kajiho H, Kontani K, Nishina H, Katada T. RASSF7 negatively regulates pro-apoptotic JNK signaling by inhibiting the activity of phosphorylated-MKK7. Cell Death Differ 2011;18:645-55.

Tan KO, Tan KM, Chan SL, Yee KS, Bevort M, Ang KC, et al. MAP-1, a novel proapoptotic protein containing a BH3-like motif that associates with Bax through its Bcl-2 homology domains. J Biol Chem 2001;276:2802-7.

Tereshko V, Teplova M, Brunzelle J, Watterson DM, Egli M. Crystal structures of the catalytic domain of human protein kinase associated with apoptosis and tumor suppression. Nat Struct Biol 2001;8:899-907.

Thaler S, Hahnel PS, Schad A, Dammann R, Schuler M. RASSF1A mediates p21Cip1/Waf1-dependent cell cycle arrest and senescence through modulation of the Raf-MEK-ERK pathway and inhibition of Akt. Cancer Res 2009;69:1748-57.

Tommasi S, Dammann R, Jin S-g, Zhang X-f, Avruch J. RASSF3 and NORE1: identification and cloning of two human homologues of the putative tumor suppressor gene RASSF1. Oncogene 2002;21:2713-20.

Towbin H, Staehelin T, Gordon J. Electrophoretic transfer of proteins from polyacrylamide gels to nitrocellulose sheets: procedure and some applications. Proc Natl Acad Sci U S A 1979;76:4350-4.

Tu D, Zhu Z, Zhou AY, Yun CH, Lee KE, Toms AV, et al. Structure and ubiquitination-dependent activation of TANK-binding kinase 1. Cell Rep 2013;3:747-58.

Underhill-Day N, Hill V, Latif F. N-terminal RASSF family: RASSF7-RASSF10. Epigenetics 2011;6:284-92.

van der Weyden L, Adams DJ. The Ras-association domain family (RASSF) members and their role in human tumourigenesis. Biochim Biophys Acta 2007;1776:58-85.

Vavvas D, Li X, Avruch J, Zhang XF. Identification of Nore1 as a Potential Ras Effector. J Biol Chem 1998;273:5439-42.

Velentza AV, Schumacher AM, Weiss C, Egli M, Watterson DM. A protein kinase associated with apoptosis and tumor suppression: structure, activity, and discovery of peptide substrates. J Biol Chem 2001;276:38956-65.

Verma SK, Ganesan TS, Kishore U, Parker PJ. The tumor suppressor RASSF1A is a novel effector of small G protein Rap1A. Protein Cell 2011;2:237-49.

Vichalkovski A, Gresko E, Cornils H, Hergovich A, Schmitz D, Hemmings BA. NDR kinase is activated by RASSF1A/MST1 in response to Fas receptor stimulation and promotes apoptosis. Curr Biol 2008;18:1889-95.

Vos MD, Ellis CA, Bell A, Birrer MJ, Clark GJ. Ras uses the novel tumor suppressor RASSF1 as an effector to mediate apoptosis. J Biol Chem 2000;275:35669-72.

Vos MD, Ellis CA, Elam C, Ulku AS, Taylor BJ, Clark GJ. RASSF2 is a novel K-Ras-specific effector and potential tumor suppressor. J Biol Chem 2003a;278:28045-51.

Vos MD, Martinez A, Ellis CA, Vallecorsa T, Clark GJ. The pro-apoptotic Ras effector Nore1 may serve as a Ras-regulated tumor suppressor in the lung. J Biol Chem 2003b;278:21938-43.

Vos MD, Dallol A, Eckfeld K, Allen NP, Donninger H, Hesson LB, et al. The RASSF1A tumor suppressor activates Bax via MOAP-1. J Biol Chem 2006;281:4557-63.

Warren SC, Margineanu A, Alibhai D, Kelly DJ, Talbot C, Alexandrov Y, et al. Rapid global fitting of large fluorescence lifetime imaging microscopy datasets. PLoS One 2013;8:e70687.

Webster MT, Rozycka M, Sara E, Davis E, Smalley M, Young N, et al. Sequence variants of the axin gene in breast, colon, and other cancers: an analysis of mutations that interfere with GSK3 binding. Genes Chromosomes Cancer 2000;28:443-53.

Wei X, Walia V, Lin JC, Teer JK, Prickett TD, Gartner J, et al. Exome sequencing identifies GRIN2A as frequently mutated in melanoma. Nat Genet 2011;43:442-6.

Wei Z, Chen X, Chen J, Wang W, Xu X, Cai Q. RASSF10 is epigenetically silenced and functions as a tumor suppressor in gastric cancer. Biochem Biophys Res Commun 2013;432:632-7.

Weitzel JN, Kasperczyk A, Mohan C, Krontiris TG. The HRAS1 gene cluster: Two upstream regions recognizing transcripts and a third encoding a gene with a leucine zipper domain. Genomics 1992;14:309-19.

Welcsh PL, Lee MK, Gonzalez-Hernandez RM, Black DJ, Mahadevappa M, Swisher EM, et al. BRCA1 transcriptionally regulates genes involved in breast tumorigenesis. Proc Natl Acad Sci U S A 2002;99:7560-5.

Wen Y, Wang Q, Zhou C, Yan D, Qiu G, Yang C, et al. Decreased expression of RASSF6 is a novel independent prognostic marker of a worse outcome in gastric cancer patients after curative surgery. Ann Surg Oncol 2011;18:3858-67.

Wennerberg K, Rossman KL, Der CJ. The Ras superfamily at a glance. J Cell Sci 2005;118:843-6.

Wittinghofer A, Pai EF. The structure of Ras protein: a model for a universal molecular switch. Trends Biochem Sci 1991;16:382-7.

Wittinghofer A, Nassar N. How Ras-related proteins talk to their effectors. Trends Biochem Sci 1996;21:488-91.

Wohlgemuth S, Kiel C, Kramer A, Serrano L, Wittinghofer F, Herrmann C. Recognizing and defining true Ras binding domains I: biochemical analysis. J Mol Biol 2005;348:741-58.

Wu B, Yao H, Wang S, Xu R. DAPK1 modulates a curcumin-induced G2/M arrest and apoptosis by regulating STAT3, NF-kappaB, and caspase-3 activation. Biochem Biophys Res Commun 2013;434:75-80.

Wu PR, Tsai PI, Chen GC, Chou HJ, Huang YP, Chen YH, et al. DAPK activates MARK1/2 to regulate microtubule assembly, neuronal differentiation, and tau toxicity. Cell Death Differ 2011;18:1507-20.

Yan C, Wu F, Jernigan RL, Dobbs D, Honavar V. Characterization of protein-protein interfaces. Protein J 2008;27:59-70.

Yoo HJ, Byun HJ, Kim BR, Lee KH, Park SY, Rho SB. DAPk1 inhibits NF-kappaB activation through TNF-alpha and INF-gamma-induced apoptosis. Cell Signal 2012;24:1471-7.

Zhou X, Li TT, Feng X, Hsiang E, Xiong Y, Guan KL, et al. Targeted polyubiquitylation of RASSF1C by the Mule and SCFbeta-TrCP ligases in response to DNA damage. Biochem J 2012;441:227-36.